Rheological Properties of Partially Denatured Whey Proteins

by

ZHUO ZHANG

B.Sc., M.Sc. (Food Science)

A thesis submitted for the degree of

DOCTOR of PHILOSOPHY (Food Science)

Heriot Watt University
School of Life Sciences
Food Science Department
Edinburgh
September 2014

Abstract

As one of the sources for food materials, whey protein concentrates (WPC) are widely processed such as by heat treatment for different application purposes, one of which is to produce protein-based fat replacers. Those fat replacers benefit from high nutritive value and generally recognized as safe (GRAS) status of whey proteins, and moreover, the heat-induced denaturation and aggregations of these proteins provide the desired texture and mouthfeel to the low-fat food systems. Two fat replacers, i.e., Simplesse and Hiprotal60 serial products, have been comprehensively characterized in this research with various techniques. The scope of this study extended from the molecular structure of the heat-induced denatured whey proteins (β-lactoglobulins) to the flowing and rheological behaviour of the protein aggregates.

From the characterization of the fat replacer materials, molecular dynamics (MD) computer simulations were also performed on β-lactoglobulin proteins, which are the major proteins in WPC. It has been predicted that the β-lactoglobulin molecule lost α-helices and β-barrels during heat-induced unfolding, and the four solvent inaccessible cysteine (Cys) residues (Cys^{66}, Cys^{106}, Cys^{119} and Cys^{121}) exposed to the molecular surface. Such changes contributed to the protein-protein interactions and aggregations through –SH/S-S exchange interactions. Denatured proteins were also found to have weak ability to form hydrogen bonds with hydrated water molecules, but the hydrogen bonds between those hydrated water molecules were improved by protein unfolding, which decreased the repulsions due to hydration shells between protein molecules. As for the materials, the microparticulated proteins, Simplesse, were found to be particles with a median diameter, D[0.5] = 1.72 ± 0.04 μm, which is larger than the WPC (Lacprodan87) with D[0.5] = 0.48 ± 0.04 μm. As for the partially denatured proteins, i.e., Hiprotal60 products, values of D[0.5] ranged from 5.484 ± 0.001 μm and 3.296 ± 0.001 μm for Hiprotal60 and Hiprotal60-TS0709, respectively, to around 17 μm for both of

Hiprotal60-TS0710 and Hiprotal60-TS0712, depending upon the degree of the protein aggregations. The structures of different protein aggregates were also visualized through ESEM, where small particles were found to form separate aggregates while those larger ones were observed to have more continuous structures. However, there was no disulphide bond present in those protein based fat replacers as indicated by the results of normal and reduced SDS-PAGE and thus, the aggregates were formed and stabilized by non-bonded interactions, mainly hydrophobic interactions, between those denatured protein molecules.

From the flowing properties, all the protein-based fat replacers and WPC in aqueous solutions exhibited exponential increases in apparent viscosity at 100 s^{-1} with protein concentrations from 6% to 21% because of hydrodynamic and protein-protein interactions. Higher exponential dependence of viscosity on protein concentrations was observed for protein-based fat replacers, suggesting stronger interactions between those modified protein molecules. According to the shear thinning and thixotropic analyses, Simplesse required more protein molecules to aggregate for a given increases in viscosity than WPC, while for Hiprotal60 products, the flowing behavior changed with the extent of the protein denaturation and aggregations. Compared with WPC and other protein-based fat replacers, Hiprotal60-TS0710 and Hiprotal60-TS0712 with largest aggregates had the best structuring properties with the lowest concentration requirement for increased viscosity and the strongest network structures with the largest viscosities.

From the oscillation tests, intermolecular or interfloc interactions were found in Simplesse as indicated by the solid-like behaviour of this material at high concentrations. Hiprotal60 and Hiprotal60-TS0709 behaved as viscoelatic liquid, and the Cox-Merz rule was valid for such samples, indicating the absence of a network formed by these protein molecules or aggregates. Because of their small values of storage moduli (G'), the rheological properties of Simplesse and Hiprotal60 and Hiprotal60-0709 were believed to result from colloidal crystal structures of the protein molecules and their flocs. The lattice-like structures of these colloidal crystals were mainly stabilized by electrostatic repulsions

between the proteins. Hiprotal60-TS0710 and Hiprotal60-TS0712, were found to form strong gels with self-similar or fractal structures at high concentrations. The polymeric chains were densely packed in the gels as revealed by large values of fractal dimensions (≈ 2.3) of the self-similar networks. By adjusting the pH to the pI (≈ 4.5) of the whey proteins, all the protein-based fat replacers exhibited cold-setting gelation behaviour. Fractal structures were found in the acid-induced gels formed by Simplesse but not in those from Hiprotal60 or Hiprotal60-0709. It has been observed that the protein molecules and flocs pack more densely at pI than at natural pH as indicated by the fractal dimensions of acid-induced cold gels formed by Simplesse (≈ 2.3) and Hiprotal60-0710 and Hiprotal60-0712 (≈ 2.4).

From the rheological tests of sol-emulsion systems, emulsion droplets were found to affect the rheological properties of the protein-based fat replacers. Emulsion droplets disrupted the interactions of Simplesse as indicated by decreased elasticity, but the viscosity increased due to more hydrodynamic interactions. Due to their larger particle sizes, Hiprotal60 and Hiprotal60-TS0709 induced flocculation of the droplets, which was improved by shearing treatments. Droplet flocculation was also induced by Hiprotal60-TS0710 and Hiprotal60-TS0712, but there was no shear-improving effect. This can be attributed to the large viscosity of the continuous phase in such systems. There was no active filling effect of protein-coated droplets on the gelling behaviour of Hiprotal60-TS0710 and Hiprotal60-TS0712, indicating that thermal denaturation of the protein layers of the droplets played an important role in their active filling effects on protein gels.

Acknowledgement

I would like to thank Dr. Stephen Euston for his guidance and patience during the period of my PhD studies. I have learned so much from you leading me to an impressive “silicon world”. My appreciation is also extended to Dr. Lydia Campbell who has generously provided me with experimental samples, technical details and suggestions for this research. I would like to extend my appreciation to Dr. Arrighi Valeria who has provided me with some facilities and answers to a lot of questions in chemistry, helping me understand the project better. Also, I would like to thank my committee members Dr. Rammile Ettelaie and Dr. Alex Speers for their kind patience, assistance and suggestions for my dissertation. There are also numerous appreciations to all staff members especially Ms. Vicky Goodfellow, Mr. Robert Rennie, and Dr. Julien Lachamp for their warm help in my research.

I would also like to thank all the PhD students, MSc students and exchanged students who are working or had worked in my lab. All of you are my good colleagues and close friends.

I am appreciative of the financial assistance I have received through the Heriot-Watt University Life Science/Physical Sciences Interface Theme.

Last but not least, I would like to thank all my friends and family, especially to my parents, who have provided me love and support for the past 32 years.

Declaration

I, Zhuo Zhang, hereby declare that I am the author of this thesis. All the work described in this thesis is my own, except where stated in the text. The work presented here has not been previously used in an application for a higher degree. All the sources of information are acknowledged by means of references.

_____

Zhuo Zhang

ACADEMIC REGISTRY-Research Thesis Submission

Name*:*	ZHUO ZHANG		
School/PGI:	School of Life Sciences		
Version:	Final	Degree Sought (Award **and** Subject area)	PhD (*Food Science*)

Declaration

In accordance with the appropriate regulations I hereby submit my thesis and I declare that:

1) the thesis embodies the results of my own work and has been composed by myself
2) where appropriate, I have made acknowledgement of the work of others and have made reference to work carried out in collaboration with other persons
3) the thesis is the correct version of the thesis for submission and is the same version as any electronic versions submitted*.
4) my thesis for the award referred to, deposited in the Heriot-Watt University Library, should be made available for loan or photocopying and be available via the Institutional Repository, subject to such conditions as the Librarian may require
5) I understand that as a student of the University I am required to abide by the Regulations of the University and to conform to its discipline.

* *Please note that it is the responsibility of the candidate to ensure that the correct version of the thesis is submitted.*

Signature of Candidate*:*		Date:	

Submission

Submitted By *(name in capitals):*	ZHUO ZHANG
Signature of Individual Submitting:	
Date Submitted:	

For Completion in the Student Service Centre (SSC)

Received in the SSC by (*name in capitals*):			
Method of Submission (*Handed in to SSC; posted through internal/external mail*):			
E-thesis Submitted (mandatory for final theses)			
Signature:		Date:	

Table of Content

Table of Figures

List of Tables

1 Introduction

One of the 'holy grails' of food research is to manufacture products with reduced or even no fat, which benefit humans, especially those with obesity problems. There are various foods with low fat content available in supermarkets nowadays, and their competitive prices and improved healthy benefits have increased their market share with potential for further extension (Sandrou & Arvanitoyannis, 2000). However, the uptake of low-fat food could be increased if they had better organoleptic properties (Sandrou & Arvanitoyannis, 2000). Therefore, research effort is required to improve the texture, mouthfeel and taste of foods with low fat contents for their long-term consumer acceptance. For such purposes, food scientists have turned to the so-called fat replacers, which generally refers to substances added into food systems to substitute triglycericides and provide lower fat and calorie contents (Sandrou & Arvanitoyannis, 2000).

1.1 Fat replacers

There are various methods to manufacture fat replacers in the food industry. For instance, Olestra is produced by chemical reactions between sugars and fatty acids, while Simplesse is a microparticulate protein product in the form of particles with round shapes and small particle sizes derived from proteins (Sandrou & Arvanitoyannis, 2000). Those products from lipids are classified as lipid-based fat substitutes, in which fatty acids are esterified with carbohydrates or alkyl glycoside to limit the digestion and absorption of these materials in human bodies (Sandrou & Arvanitoyannis, 2000). Additionally, carbohydrates and proteins are also used to produce fat replacers and these products are usually labeled as starch-based and protein-based fat mimetics according to their source materials (Sandrou & Arvanitoyannis, 2000). Starch-based fat replacers are essentially modified starches by hydrolyzation or substitution (Sandrou & Arvanitoyannis, 2000). Association of water molecules with these modified carbohydrates plays an important role in the functionalities of those products. The

modified starches interact with water in such a way that the starch-based fat replacers provide a very similar mouthfeel to fat in the low fat foods (Yackel & Cox, 1992). Protein-based fat mimetics are usually proteins modified by heat treatment (Gaull, 1991). These products provide low-fat foods with similar mouthfeel and texture as their full-fat counterparts through modified hydration properties. Examples of such products are Simplesse and Hiprotal60.

1.2 Whey proteins as a source for fat replacers

Of the available proteins, the bovine milk whey proteins are of special interest for the production of protein-based fat mimetics. First of all, whey proteins are components in bovine milk and byproducts from cheese, allowing them to take the advantages of abundance, high nutritive value and generally recognized as safe (GRAS) status as food ingredients and additives (Bryant & McClements, 1998; Harper, 2004; Ikeda & Morris, 2002; Madureira, Pereira, Gomes, Pintado, & Xavier Malcata, 2007; Séverina & Xia, 2005). Moreover, improved functional properties through modifying their molecular structures also extend the applications of whey proteins in the food industry. Modified whey proteins have been used as gelling agents, emulsifiers, texture modifiers, thickening agents and foaming agents for foods.

There have been a variety of techniques reported to effectively modify the molecular structure of whey proteins effectively, such as genetically, chemically, enzymatically and physically (Barbut & Foegeding, 1993; Hongsprabhas & Barbut, 1997; Kinsella & Whitehead, 1988; McClements & Keogh, 1995; Mulvihill & Kinsella, 1988; Van Camp, Messens, Clément, & Huyghebaert, 1997). However, some of the techniques are too expensive for large-scale manufactures and some others are not GRAS, and therefore, modifications through simple physical treatments, for example heat-denaturation, are preferred in food industry (Bryant & McClements, 1998).

1.3 Heat-induced denatured whey proteins

There are a number of functional properties of whey proteins that can be improved through heat treatments. One of the most important functionalities of heat denatured

whey proteins is their ability to aggregate and form gels, which act as a matrix for entrapping water, lipids and other food components, thus improving the textural properties of food products (Foegeding, Vardhanabhuti, & Yang, 2011; Hudson, Daubert, & Foegeding, 2000; Jeurnink & De Kruif, 1993; Kinsella & Whitehead, 1988; Lizarraga, De Piante Vicin, González, Rubiolo, & Santiago, 2006; Resch & Daubert, 2002). It has been found that the polypeptide chains of whey proteins are unfolded during heat-induced denaturation, with the interior non-polar regions and sulfhydryl groups exposed to the solvent accessible surfaces, and thus there are increased attractions between molecules, mainly due to hydrophobic interactions and possible disulphide bonds, resulting in protein aggregation (Elofsson, Dejmek, Paulsson, & Burling, 1997; Ju & Kilara, 1998). Heat-induced denatured whey proteins have also been reported to gel at room temperature at low ionic strength (McClements & Keogh, 1995). Such cold-setting gelation could be of great value in the food industry, since it meets the thickening requirement for some special foods not suitable for heat processing. Milk proteins are also very good emulsifiers and have been widely used to stabilize emulsions in the food industry (Dickinson, 1998, 2001, 2012). Dickinson and Chen (1999) found that droplets coated by whey proteins aggregated with other non-absorbed whey protein molecules in the water phase, and acted as active fillers for the heat-set gels. Such functionality makes whey proteins very important ingredients for the food, pharmacy and cosmetic industries, where emulsions and gels are commonly used in the products (Lorenzo, Zaritzky, & Califano, 2013).

1.4 About this dissertation

In this dissertation, the protein-based partially denatured fat mimetics are studied and compared to microparticulated WPC, such as Simplesse. The research extends from the molecular structure of denatured whey proteins (β-lactoglobulin) and characterization of particle structure in aqueous dispersions (Chapter 5) to the rheological functionalities of those fat replacers in different environments (Chapter 6, 7 and 8). The main techniques applied in this research, i.e., rheology and molecular dynamic (MD) computer simulations are briefly introduced in Chapter 2 and 3, where a discussion of the fundamentals of each methodology is given, respectively. Chapter 4

briefly introduces the specific methodologies used for the experimental and modeling parts of the research, and describes the general principles. More detailed methodologies are given at the start of each of the result chapters.

1.5 References

Barbut, S., & Foegeding, E.A. (1993). Ca^{2+}-induced gelation of pre-heated whey protein isolate. *Journal of Food Science, 58*(4), 867-871.

Bryant, C.M., & McClements, D.J. (1998). Molecular basis of protein functionality with special consideration of cold-set gels derived from heat-denatured whey. *Trends in Food Science & Technology, 9*(4), 143-151.

Dickinson, E. (1998). Proteins at interfaces and in emulsions: Stability, rheology and interactions. *Journal of the Chemical Society, Faraday Transactions, 94*(12), 1657-1669.

Dickinson, E. (2001). Milk protein interfacial layers and the relationship to emulsion stability and rheology. *Colloids and Surfaces B: Biointerfaces, 20*(197-210).

Dickinson, E. (2012). Emulsion gels: The structuring of soft solids with protein-stabilized oil droplets. *Food Hydrocolloids, 2012*, 224-241.

Dickinson, E., & Chen, J. (1999). Heat-set whey protein emulsion gels: Role of active and inactive filler particles. *Journal of Dispersion Science and Technology, 20*(1&2), 197-213.

Elofsson, C., Dejmek, P., Paulsson, M., & Burling, H. (1997). Characterization of a cold-gelling whey protein concentrate. *International Dairy Journal, 7*(8-9), 601-608.

Foegeding, E.A., Vardhanabhuti, B., & Yang, X. (2011). Dairy Systems. In I. T. Norton, F. Spyropoulos & P. Cox (Eds.), *Practical food rheology: An interpretive approach*: Wiley-Blackwell.

Gaull, G.E. (1991). Role of micro-particulated protein fat substitutes in food and nutrition. *Annals of the New York Academy of Sciences, 623*(1), 350-355.

Harper, W.J., & American Dairy Products Institute. (2004). *Biological properties of whey components : a review : update 2004*. Elmhurst, IL, US: American Dairy Products Institute.

Hongsprabhas, P., & Barbut, S. (1997). Protein and salt effects on Ca^{2+}-induced cold gelation of whey protein isolate. *Journal of Food Science, 62*(2), 382-385.

Hudson, H.M., Daubert, C.R., & Foegeding, E.A. (2000). Rheological and physical properties of derivitized whey protein isolate powders. *Journal of Agricultural and Food Chemistry, 48*(8), 3112-3119.

Ikeda, S., & Morris, V.J. (2002). Fine-stranded and particulate aggregates of heat-denatured whey proteins visualized by atomic force microscopy. *Biomacromolecules, 3*(2), 382-389.

Jeurnink, T.J.M., & De Kruif, K.G. (1993). Changes in milk on heating: viscosity measurements. *Journal of Dairy Research, 60*, 130-150.

Ju, Z.Y., & Kilara, A. (1998). Textural properties of cold-set gels induced from

heat-denatured whey protein isolates. *Journal of Food Science, 63*(2), 288-292.

Kinsella, J.E., & Whitehead, D.M. (1988). Proteins in whey: Chemical, physical, and functional properties. *Advances in Food and Nutrition Research, 33*, 343-438.

Lizarraga, M.S., De Piante Vicin, D., González, R., Rubiolo, A., & Santiago, L.G. (2006). Rheological behaviour of whey protein concentrate and λ-carrageenan aqueous mixtures. *Food Hydrocolloids, 20*(5), 740-748.

Lorenzo, G., Zaritzky, N., & Califano, A. (2013). Rheological analysis of emulsion-filled gels based on high acyl gellan gum. *Food Hydrocolloids, 30*, 672-680.

Madureira, A.R., Pereira, C.I., Gomes, A.M.P., Pintado, M.E., & Xavier Malcata, F. (2007). Bovine whey proteins - Overview on their main biological properties. *Food Research International, 40*(10), 1197-1211.

McClements, D.J., & Keogh, M.K. (1995). Physical properties of cold-setting gels formed from heat-denatured whey protein isolate. *Journal of the Science of Food and Agriculture, 69*(1), 7-14.

Mulvihill, D.M., & Kinsella, J.E. (1988). Gelation of β-lactoglobulin: Effects of sodium chloride and calcium chloride on the rheological and structural properties of gels. *Journal of Food Science, 53*(1), 231-236.

Resch, J.J., & Daubert, C.R. (2002). Rheological and physicochemical properties of derivatized whey protein concentrate powders. *International Journal of Food Properties, 5*(2), 419-434.

Séverina, S., & Xia, W. . (2005). Milk biologically active components as nutraceuticals: Review. *Critical Reviews in Food Science and Nutrition, 45*(7-8), 645-656.

Sandrou, D.K., & Arvanitoyannis, I.S. (2000). Low-fat/calorie foods: Current state and perspectives. *Critical Reviews in Food Science and Nutrition, 40*(5), 427-447.

Van Camp, J., Messens, W., Clément, J., & Huyghebaert, A. (1997). Influence of ph and calcium chloride on the high-pressure-induced aggregation of a whey protein concentrate. *Journal of Agricultural and Food Chemistry, 45*(5), 1600-1607.

Yackel, W.C., & Cox, C. (1992). Application of starch- based fat replacers. *Food Technology, 6*, 146-148.

2 Rheology

When Heraclitus said ‘everything flows’, he was perhaps just expressing his thoughts in philosophy, and had no idea that he had actually pointed out the fundamentals of one of the most pivotal subjects that would draw a lot of attention from physicists and chemists working in the field of food, cosmetics and materials 2500 years after his time. Rheology is the study of the flow and deformation of matter (Barnes, Hutton, & Walters, 1989; Goodwin & Hughes, 2008; Morrison, 2001; Rao, 2007). Commonly, ideal solids and ideal liquids are distinguished through the stresses applied for deformations and flows, i.e., stresses on the former are proportional to the deformations (strains) while those on the latter are related to the flow speed (shear rates). It is well known that the response of simple solids and liquids to a stress is well described in terms of Hooke’s law of elasticity and Newton’s law of viscosity, respectively. However, most practical systems, such as polymers, particulate dispersions and emulsions are beyond such simplicity and turn out to exhibit complex behaviour. In such cases, either Hooke’s law of elasticity or Newton’s law of viscosity loses its validity to explain the flow properties of those complex materials and other models are required to describe the behaviour (Barnes et al., 1989). Fortunately, many different kinds of rheometers are available nowadays allowing the most complicated flow behavior to be characterized accurately and precisely. In addition to the flow properties, the microscopic structure of matter based on its macroscopic flow responses to shear stresses.

2.1 Viscosity and elasticity

Matter will deform under an external force, which is due to microscopic displacement of its particles or atoms relative to each other (Morrison, 2001). Such a displacement is described as strain, γ. The concept of strain can be described by a simple parallel plate model, as illustrated in Figure 2.1. When the moving plate is subjected to an external shear force, F, it will move at a velocity of u. The strain, γ,

shear rate, $\dot{\gamma}$, and shear stress, σ, are then defined as

$$\gamma = \frac{\mathbf{d}\,x}{h}$$
$$\dot{\gamma} = \frac{u}{h}$$
$$\sigma = \frac{F}{A}$$

where A is the area of the interface of the moving plate and the sample inside, and $\mathbf{d}x$ and h are depicted in Figure 2.1.

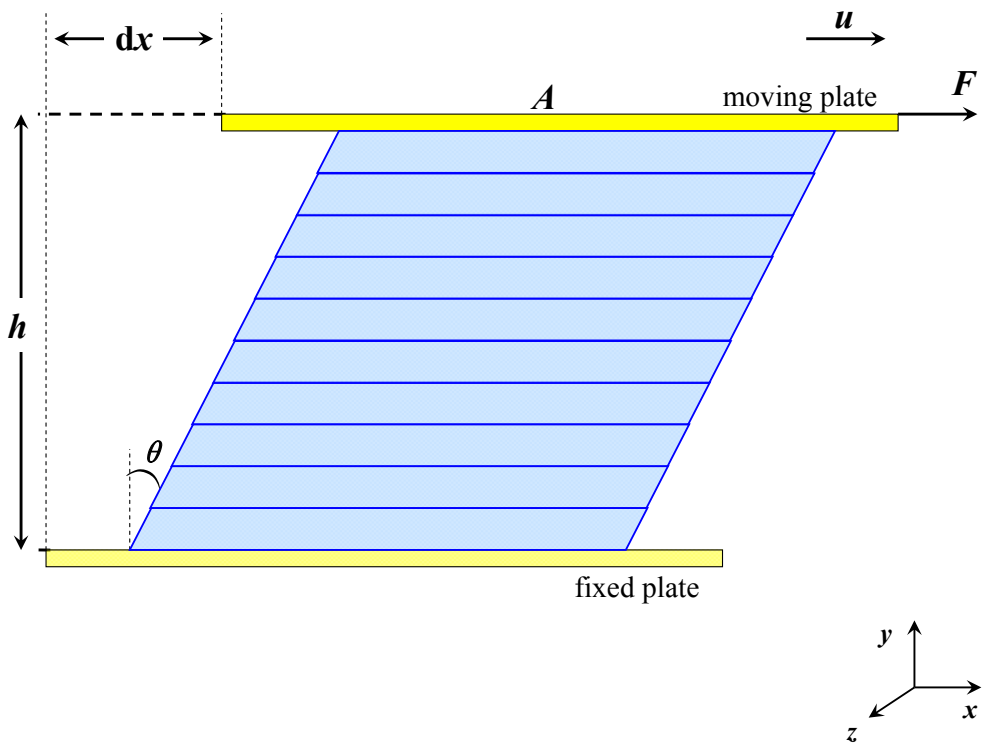

Figure 2.1 Illustration of a parallel plate model.

When liquid flows under an exerted external stress, σ, its constituent particles exhibit a resistance to such flow, which manifests itself as the viscosity (Barnes, 2000; Barnes et al., 1989; Macosko, 1994). Viscosity, η, is simply defined in terms of the stress, σ, applied to the sample and the resultant shear rate, $\dot{\gamma}$, as (Barnes, 2000; Barnes et al., 1989; Goodwin & Hughes, 2008; Macosko, 1994; Morrison, 2001; Rao, 2007):

$$\eta = \frac{\sigma}{\dot{\gamma}}, \tag{2.1}$$

Hooke's law for elastic solids defines strain as the change in the angle (θ in Figure 2.1) of a solid (Goodwin & Hughes, 2008). Since the deformation is relatively small in solids or otherwise the structure will be broken down, the strain is estimated as $\theta \approx \mathbf{tan}\,\theta = \mathbf{d}\,x/h = \gamma$ (θ is in radius) and thus, the elastic modulus is calculated as (Goodwin & Hughes, 2008; Morrison, 2001):

$$G = \frac{\sigma}{\gamma} \tag{2.2}$$

2.2 Normal stress differences

Figure 2.1 is a 2-D representation of a 3-D solid. In practice, the situation is more complex because there is more than one direction that the force can be applied to the solid. If Figure 2.1 is considered as a cube, the force for each face can be applied in three directions, i.e., along the *x*, *y* and *z* axes. According to the definition of stress in Figure 2.1, the stress actually represents σ_{yx}, where the subscript $_{yx}$ indicates that a force F_{yx} in the $_x$ direction is applied on the $_y$ plane or face of the cube ($_y$ indicates the outwardly pointing normal to the plane/face). Accordingly, there will be a total of nine stresses that can be applied to the cube, three (*x*, *y*, *z*) for each of the three planes/faces (both *x*, both *y* and both *z* faces are only counted once). This can be represented in a total stress tensor as

$$\Pi = \begin{bmatrix} p+\sigma_{xx} & \sigma_{xy} & \sigma_{xz} \\ \sigma_{yx} & p+\sigma_{yy} & \sigma_{yz} \\ \sigma_{zx} & \sigma_{zy} & p+\sigma_{zz} \end{bmatrix}_{xyz} \tag{2.3}$$

where *p* is the hydrostatic pressure (Morrison, 2001). Considering Figure 2.1, the only external force F_{yx} is applied on the $_y$ plane in the $_x$ direction and the shear flow is symmetric, it follows that there are no shear components in the z-direction or on the z-face and so $\sigma_{xz} = \sigma_{zx} = \sigma_{yz} = \sigma_{zy} = 0$ and $\sigma_{xy} = \sigma_{yx} = \sigma$, according to Newton's third law (Morrison, 2001). Thus, the total stress tensor is simplified to

$$\Pi = \begin{bmatrix} p+\sigma_{xx} & \sigma & 0 \\ \sigma & p+\sigma_{yy} & 0 \\ 0 & 0 & p+\sigma_{zz} \end{bmatrix}_{xyz} \tag{2.4}$$

where σ_{xx}, σ_{yy} and σ_{zz} are the extra normal stresses. The hydrostatic pressure is determined by boundary conditions and the extra normal stresses are determined by the deformation (Macosko, 1994). Practically, it is impossible to separate the contributions from the hydrostatic pressure and the extra normal stresses, and therefore, the latter are measured as two normal stress differences, N_1 and N_2 so that the influence of the hydrostatic pressure p is removed (Jeffrey & Acrivos, 1976; Macosko, 1994; Morrison, 2001; Rao, 2007):

$$N_1 = \Pi_{xx} - \Pi_{yy} = \sigma_{xx} - \sigma_{yy} \tag{2.5}$$

$$N_2 = \Pi_{yy} - \Pi_{zz} = \sigma_{yy} - \sigma_{zz} \tag{2.6}$$

The first and second normal stress coefficients, Ψ_1 and Ψ_2 are used to describe the flow behavior of the fluid (Barnes et al., 1989; Morrison, 2001; Rao, 2007) and are defined as

$$\Psi_1 = \frac{N_1}{\dot{\gamma}^2} = \frac{\sigma_{xx} - \sigma_{yy}}{\dot{\gamma}^2} \tag{2.7}$$

$$\Psi_2 = \frac{N_2}{\dot{\gamma}^2} = \frac{\sigma_{yy} - \sigma_{zz}}{\dot{\gamma}^2} \tag{2.8}$$

It has been widely reported that values of Ψ_1 are positive and relatively large, while those of Ψ_2 small and negative (Ψ_2 is about only 10% of the value of Ψ_1 for most polymers) (Macosko, 1994; Morrison, 2001; Rao, 2007).

It has been suggested that anisotropy of the structure of the materials in fluids under shearing generates the normal stresses and the differences between them (Barnes et al., 1989). In aqueous polymer solutions, for instance, the shapes of the polymeric molecules tend to minimize the interfacial free-energy of the system (Barnes et al., 1989). Once such shapes are deformed by shearing effects, from spheres to ellipsoids for example, stored stresses are generated that act to retain the previous shapes (Barnes et al., 1989). Since the external stress is applied in the x direction, the shape of a polymeric molecule is deformed mainly in the x directions and accordingly in the y and

z directions, which results in large extra normal stress, σ_{xx}, in the x direction and smaller ones (σ_{yy} and σ_{zz}) in the y and z directions. Therefore, a large value of Ψ_1 and a small value of Ψ_2 are observed (Barnes et al., 1989; Macosko, 1994; Morrison, 2001; Rao, 2007).

2.3 Yield stress

In some materials it is reported that there is little or no flow or deformation observed until a minimum stress is exceeded. Such a stress is referred to as a yield stress and such materials are referred to as plastic (Barnes et al., 1989; Macosko, 1994; Matveenko & Kirsanov, 2011; Morrison, 2001; Rao, 2007). Particles are assumed to connect with each other and form a framework in plastic materials which are destroyed by stresses higher than the yield point, and therefore, the yield stress is considered as a result of phase transition from solid to liquid (Markovitz, 1985; Matveenko & Kirsanov, 2011). Barnes and Walters (1985) argued that the observations of yield stress were due to extremely high viscosity of the materials and limitation of the instrument used for measurements. It is reasonable to believe that everything is found to flow at extremely low shear stresses given that the observation time is long enough and the measurement is sensitive enough (Barnes & Walters, 1985; Goodwin & Hughes, 2008; Macosko, 1994). However, it is difficult to wait for years or even decades to achieve a rheological experiment, although some researchers are doing that (Edgeworth, Dalton, & Parnell, 1984). Astarita (1990) proposed the engineering reality of yield stress, providing a solution to the argument. Nowadays, the concept of yield stress is still being used and discussed for microscopic information on materials even though its existence is doubted (Goodwin & Hughes, 2008; Macosko, 1994).

2.4 Newtonian and Non-Newtonian behaviors

2.4.1 Newtonian behavior

Liquids are generally classified into Newtonian and non-Newtonian fluids according to the shear rate and time dependence of viscosity. A Newtonian fluid is

defined as fluid with a constant viscosity that is independent of shear rate and shear time (Barnes et al., 1989; Goodwin & Hughes, 2008; Morrison, 2001). Water for instance, behaves as a Newtonian fluid under some conditions. In addition, another property of Newtonian fluids is that there are no normal stress differences (Barnes et al., 1989; Jeffrey & Acrivos, 1976; Morrison, 2001), which distinguishes Newtonian fluids from Boger fluids, elastic fluids displaying a constant viscosity but non-zero normal stress values (James, 2009).

2.4.2 Shear dependence

With the development of advanced viscometers, more complicated fluids, such as colloidal suspensions and polymeric solutions were investigated at larger range of shear rates, and departure from Newtonian behavior for almost all such materials were observed (Macosko, 1994; Rao, 2007). For the vast majority of materials, especially protein dispersions, shear-thinning behavior was observed, where the viscosity of a material was found to decrease with an increase in the shear rate (Barnes et al., 1989; Goodwin & Hughes, 2008; Macosko, 1994; Morrison, 2001; Rao, 2007; M. A. Tung, 1978). Shear-thinning behavior has been observed for most non-Newtonian foods, such as many salad dressings and some concentrated fruit juices and has been considered to originate from breakdown of structural units in these foods (Rao, 2007). There could be a lot of reasons causing such phenomenon. Substances, such as proteins, in systems, especially solutions, might form clusters and flocs that are broken down under high shear stresses/rates, which reduces hydrodynamic forces and frictions between those materials. Therefore, the viscosity of the solution containing smaller solutes is found to decrease. Moreover, polymeric molecules are randomly oriented and entangled in dispersions at rest to attain maximum entropy. However, such random orientations and entanglements are disrupted by shearing effects which align the polymeric molecules, and therefore, decreased viscosity of the system is observed because of a reduced extent of entanglements (M. A. Tung, 1978). Besides, removal of the solvation layers of solvated dispersions also accounts for shear-thinning behaviors. By progressively removing the solvated solvent molecules that have lower mobility than the bulk ones,

shearing effects reduce the gyration radii of aggregates and the interactions between the aggregates and solvent molecules, and thus lower the viscosity (M. A. Tung, 1978). Typical shear-thinning behaviors are commonly characterized by two Newtonian plateaus with constant viscosities at extremely low and high shear rates, respectively, and a shear-thinning region in the middle (Barnes et al., 1989; Goodwin & Hughes, 2008; Morrison, 2001; Rao, 2007; M. A. Tung, 1978). According to the origin of shear-thinning behavior, complete disruption of the fluid structure, such as alignment of polymeric molecules and removal of solvation layers, is achieved under extremely high shear rate, and therefore a low constant viscosity is observed (Matveenko & Kirsanov, 2011; M. A. Tung, 1978). Since the maximal destruction of materials needs large values of stress and is only confirmed at infinite shear rates, the constant infinite shear viscosity is seldom obtained in usual viscometric measurements (Matveenko & Kirsanov, 2011). In contrast, microstructures of a system are not disrupted by ultralow shear effects and a constant viscosity due to the friction between aggregates and solvent molecules is observed (M. A. Tung, 1978). For the materials exhibiting shear-thinning behavior, such constant viscosity at ultralow shear rates, referred to as zero shear viscosity, η_0, is used as Newtonian viscosity (Barnes et al., 1989; Jeffrey & Acrivos, 1976; Morrison, 2001; Rao, 2007).

In contrast to shear-thinning behavior, some materials exhibit stronger resistance to flow under shearing effects, which is referred to as shear-thickening behavior (Barnes et al., 1989; Goodwin & Hughes, 2008; Morrison, 2001; Rao, 2007). Shearing-thickening behavior has been observed in starch gelatinization (Bagley & Christianson, 1982; Dail & Steffe, 1990a, 1990b; Okechukwu & Rao, 1995; Rao, 2007). Rearrangement of the spatial distribution of the particles in a material due to shearing effects accounts for the increase in the resistance to flow (Barnes et al., 1989). Barnes (1989) proposed that viscosity is increased by a shear-induced transition from a two-dimensional arrangement of the system to a three dimensional one, which has been demonstrated by the existence of transient clusters in shear-thickening suspensions under high shear rates (Goodwin & Hughes, 2008; Hillman & Mannan, 2006; Maranzano & Wagner, 2002). Since the transient clusters increase the volume fraction of the dispersed phase, therefore “dilatancy” is also used to refer to

shear-thickening behavior (Barnes et al., 1989; Goodwin & Hughes, 2008; Morrison, 2001; Rao, 2007). It should be noted that the shear-thickening behavior of most materials starts at high shear rates and seldom lasts for more than one decade of shear rates (Barnes, 1989; Barnes et al., 1989), while a region of shear-thinning behavior at lower shear rates is commonly observed before shear thickening (Barnes et al., 1989).

2.4.3 Time dependence

There is another shear-thinning behaviour to be noted, where the viscosity decreases with time under steady shear stresses (Barnes et al., 1989; Macosko, 1994; Mewis, 1979). Such a time-dependent decrease in viscosity is defined as thixotropy and the effect is reversible when the flow is decreased or arrested (Barnes et al., 1989; Mewis & Wagner, 2009). Similarly, reversible time-dependent shear-thickening behaviour is defined as anti-thixotropy or rheopexy (Barnes et al., 1989; Mewis & Wagner, 2009; Morrison, 2001). Such time-dependent effects are believed to result from alteration in the structure of the material under stresses. The interactions between molecules or particles in thixotropic system are broken by the hydrodynamic forces caused by shear, and recovery of the interactions take place when the system is out of shear (Barnes et al., 1989; Dullaet & Mewis, 2005; Macosko, 1994; Mewis, 1979; Mewis & Wagner, 2009). It is found that the recovery of the structure of thixotropic materials occurs slowly instead of immediately (Dullaet & Mewis, 2005; Mewis, 1979; Mewis & Wagner, 2009), and thus, hysteresis loops are observed experimentally, of which the area is considered as a measure of the degree of thixotropy of the material (Mewis, 1979). Besides the hysteresis loops, stepwise changes in shear rate or shear stress are also applied in thixotropy studies, where sudden changes in shear stresses follow a steady shearing state (Dullaet & Mewis, 2005; Mewis & Wagner, 2009). In such experiment, time and shear rate are taken as two separated parameters and it is possible to vary them independently (Dullaet & Mewis, 2005; Mewis & Wagner, 2009).

2.5 Viscoelasticity

2.5.1 Relaxation behaviour and Deborah number

Generally, the behaviour of a material is classified as fluid or solid in terms of experimental observations, of which the results depend on the timescale of the observations (Goodwin & Hughes, 2008). Accordingly, the common classifications of most materials based on experience are considered as the result of observations with reasonable timescale. Pitch, for instance, is considered as a solid in daily life. However, being observed over a long time (e.g., 8.0 years), it is seen to flow like a fluid (Edgeworth et al., 1984). It is common sense that a material deforms when an external stress is applied to it (Barnes et al., 1989; Goodwin & Hughes, 2008; Macosko, 1994; Morrison, 2001). The stress dissipates immediately for liquids as they flow, while it is maintained for solids to keep the applied strain constant (Macosko, 1994). However, such stress is found to decay with time because of the diffusive motion of the microstructural elements, and this decay and the time of the decay are defined as relaxation behaviour and relaxation time, τ, respectively (Macosko, 1994). It should be emphasized here that such relaxation behaviour exists in all materials but with various relaxation times (Barnes et al., 1989; Barnes & Walters, 1985; Edgeworth et al., 1984; Macosko, 1994).

According to the concept of relaxation, a material is found to flow if the observation time is so long compared with its relaxation time that the microstructural elements diffuse completely to relax the strain. Otherwise, a solid behaviour is observed (Barnes et al., 1989; Edgeworth et al., 1984; Goodwin & Hughes, 2008; Macosko, 1994). From such a point of view, the Deborah number, De, is introduced as the ratio of relaxation time, τ, to the observation time, t.

$$De = \frac{\tau}{t} \tag{2.9}$$

From the value of the Deborah number, the time dependence of the flow behaviour of a material is illustrated. A material is defined as a solid with $De \gg 1$ and it displays a liquid-like behaviout with $De \ll 1$ (Barnes et al., 1989; Goodwin & Hughes, 2008; Macosko, 1994; Morrison, 2001). A more complicated behaviour often

observed for complex materials, especially for polymers, with *De* is of the order of 1, where the relaxation behaviour is observed during the experiment, is considered as a combination of liquid-like and solid-like behaviours, and is known as viscoelasticity (Barnes et al., 1989; Goodwin & Hughes, 2008; Macosko, 1994).

2.5.2 Viscoelastic models

As indicated by the term 'viscoelasticity', viscolastic materials possess both elastic and viscous properties. That is, some energy will be stored by the system (elasticity) while the rest will be dissipated through viscous flows when an external stress or strain is applied to a material. Practically, such behaviour is often described by a Hooken spring and a dashpot filled with Newtonian oil, respectively (Barnes, 2000; Barnes et al., 1989; Goodwin & Hughes, 2008; Macosko, 1994). Accordingly, viscoelastic models are proposed as combinations of Hooken springs and Newtonian dashpots (Barnes et al., 1989; Goodwin & Hughes, 2008; Macosko, 1994).

The simplest viscoelastic models consist of a Hooken spring with a constant elastic modulus, G, and a Newtonian dashpot with a constant viscosity, η (Barnes, 2000; Barnes et al., 1989; Goodwin & Hughes, 2008; Macosko, 1994). Viscoelastic models are described according to the pattern of the connection of the spring with the dashpot. A Maxwell model consists of a spring and a dashpot in series, while a Kelvin-Voigt model is obtained when they are in parallel, as illustrated in Figure 2.2 (Barnes et al., 1989; Goodwin & Hughes, 2008; Macosko, 1994).

In terms of Maxwell and Kelvin-Voigt models, the viscoelastic behaviour of a system is described based on the constant modulus, G, of the spring and the constant viscosity, η, of the dashpot (Barnes et al., 1989; Goodwin & Hughes, 2008; Macosko, 1994). In order to obtain the characteristics of viscoelasticity, a stress relaxation experiment on such systems is of great practice, where a constant strain is applied and held on the system by an external stress, and the time dependence of the stress is observed (Goodwin & Hughes, 2008; Macosko, 1994). Experimentally, the stress is observed to decay with time for viscoelastic models (Goodwin & Hughes, 2008; Macosko, 1994).

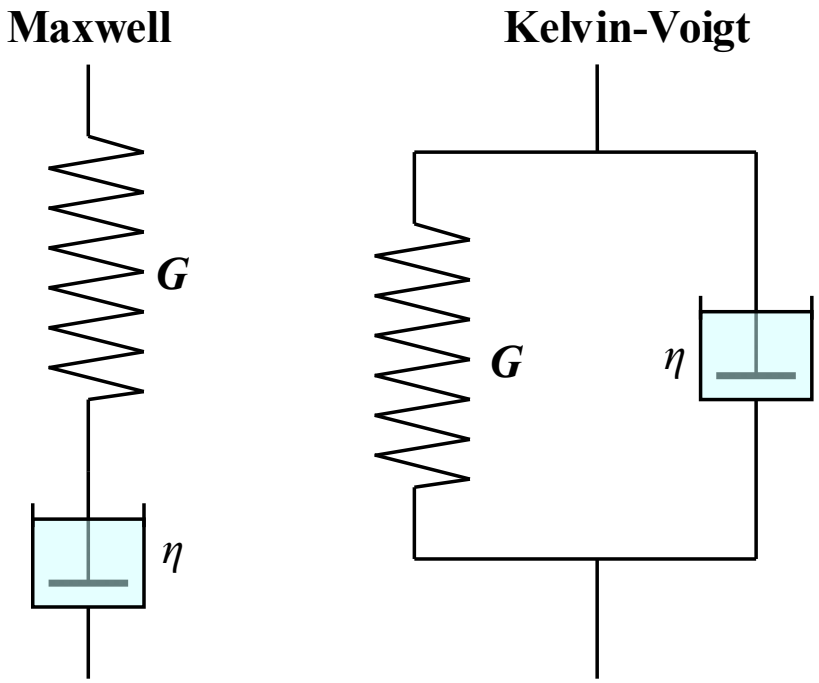

Figure 2.2 Illustration of Maxwell and Kelvin-Voigt models.

As illustrated in Figure 2.2, it is the shear rate, $\dot{\gamma}$, and the strain, γ, of the spring and the dashpot that are in accordance with linear addition for Maxwell and Kelvin-Voigt models, respectively, when external stresses are applied to these two systems (Barnes, 2000; Barnes et al., 1989; Goodwin & Hughes, 2008; Macosko, 1994). According to equations 2.1 and 2.2, the constitutive equations for the models are obtained (Goodwin & Hughes, 2008),

for Maxwell model

$$\dot{\gamma} = d\left(\frac{\sigma}{G}\right)\Big/dt + \frac{\sigma}{\eta} \tag{2.10}$$

for Kelvin-Voigt model

$$\sigma = G\cdot\gamma + \eta\cdot\dot{\gamma} \tag{2.11}$$

where G and η are the constant elastic modulus of the spring and the constant viscosity of the dashpot, respectively. It should be noted that in the stress relaxation experiment, the decay of the initial external stress, σ_0, is observed under a constant strain, γ_0, when

there is no further change in the strain of the whole system, and thus, $\dot{\gamma} = 0$, Accordingly, the decay of the stress, $\sigma(t)$, on the Maxwell model is obtained from equation 2.10,

$$\sigma(t) = \sigma_0 \cdot \mathbf{exp}\left(-\frac{t}{\eta/G}\right) \tag{2.12}$$

where t represents the time of observation. According to equation 2.2, the shear modulus, $G(t)$, is defined as the ratio of the instantaneous stress, $\sigma(t)$, to the constant strain, γ_0 (Goodwin & Hughes, 2008; Macosko, 1994),

$$G(t) = \frac{\sigma(t)}{\gamma_0} = G \cdot \mathbf{exp}\left(-\frac{t}{\eta/G}\right) \tag{2.13}$$

It should be noted that the shear modulus, $G(t)$, is dependent on the observation time while the elastic modulus, G, is a constant. The decay of the stress is due to the relaxation of the dashpot and thus the recovery of the spring in the Maxwell model, which induces smaller strain on the Hooken spring. However, the whole system is treated as a spring with a constant strain but different elastic modulus by the introduction of shear modulus, $G(t)$, and such varying 'elastic modulus', $G(t)$, reveals the transition from solid-like behaviour to liquid-like of a material and such a transition only depends on the properties of the material, i.e., G and η, and the observation time (Goodwin & Hughes, 2008; Macosko, 1994).

It is interesting to note that the shear modulus, $G(t)$, is independent of time according to equation 2.11 for the Kelvin-Voigt model, $G(t) = G$. Thus, the transition from solid to liquid of the system is invisible in the Kelvin-Voigt model during a stress relaxation time. Actually, such a model is preferred for the creep and recovery experiment, where the strain, $\gamma(t)$, of the system is observed under a constant stress, σ_0, as well as the recovery of the strain with the stress withdrawn (Barnes, 2000; Barnes et al., 1989; Gladwell, Rahalkar, & Richmond, 1985, 1986; Macosko, 1994; Morrison, 2001). In such experiments, the compliance, defined as the ratio of strain to the stress, $J(t) = \gamma(t)/\sigma_0$, is referred to, rather than the shear modulus, $G(t)$, as the characteristic parameter of viscoelastic behaviour. The details of the creep and recovery experiment are not discussed in this thesis.

Besides the shear modulus, $G(t)$, and the compliance, $J(t)$, the relaxation time, τ, is also considered as an important characteristic description of viscoelastic behaviour, which reveals the time scale of transition from the solid to liquid (Goodwin & Hughes, 2008; Macosko, 1994). For the simplest vicoelastic models, the relaxation time, τ, of the system is defined as the ratio of the viscosity of the dashpot, η, to the elasticity of the spring, G,

$$\tau = \frac{\eta}{G} \tag{2.14}$$

Therefore, the relaxation time of the system is a constant solely depending on the properties of the materials rather than the external stress. As a results, the shear modulus, $G(t)$, of the Maxwell model is obtained as

$$G(t) = \frac{\sigma(t)}{\gamma_0} = G \cdot \mathbf{exp}\left(-\frac{t}{\tau}\right) \tag{2.15}$$

It should be note that the relaxation time, τ, indicates the time spent by the system for its shear modulus, $G(t)$, to decay to the value of (G/e), but not to achieve the complete relaxation as $G(t) = 0$.

2.5.3 Linear viscoelasticity

As indicated in equation 2.15, the shear modulus, $G(t)$, depends on the material properties, G and τ, and the observation time, t, rather than the initial value of the external stress, σ_0, or strain, γ_0. According to equations 2.2 and 2.15, the strain of the system is found to depend linearly as the initial external stress, with a ratio of $G(0) = G$. For instance, the values of γ_0 are doubled when σ_0 doubled. Such linearity between strain and stress is defined as linear viscoelasticity (Barnes, 2000; Barnes et al., 1989; Goodwin & Hughes, 2008; Macosko, 1994; Morrison, 2001). Experimentally, the linear viscoelasticity is achieved at small values of strains and stresses, which guarantee that the spring is in the Hooken limit and the piston of the dashpot remains in the Newtonian oil, as demonstrated in Figure 2.2 (Goodwin & Hughes, 2008; Macosko, 1994). The linear viscoelasticity is an important concept in the rheology of viscoelastic materials and many experiment designs, such as relaxation, creep and

oscillation, apply small strains to study the response of the materials to external stresses in the linear region.

2.5.4 Small amplitude oscillatory shear

In order to obtain the viscoelastic properties of material, small strain experiments, for instance, relaxation, creep and recovery and oscillatory shear are widely performed, from which the results are related to each other through the shear modulus, $G(t)$, and thus the properties of the materials, i.e., G and η (Goodwin & Hughes, 2008; Macosko, 1994). Small strain experiments are applied to obtain rheological data over different time scales, and the oscillatory shear method is considered to provide adjustable time ranges, and therefore is widely used (Macosko, 1994).

In oscillatory shear, the sample is deformed sinusoidally with a radial frequency, ω, and an amplitude of the strain, γ_0, (Barnes, 2000; Barnes et al., 1989; Goodwin & Hughes, 2008; Macosko, 1994; Morrison, 2001). The instantaneous strain, $\gamma(t)$, and the instantaneous shear rate, $\dot{\gamma}(t)$, at a specific time, t, are obtained from

$$\gamma(t) = \gamma_0 \cdot \mathbf{sin}(\omega \cdot t) \tag{2.16}$$

$$\dot{\gamma}(t) = \frac{d\gamma(t)}{dt} = \omega \cdot \gamma_0 \cdot \mathbf{cos}(\omega \cdot t) \tag{2.17}$$

From equation 2.16 and 2.17, the instantaneous strain and the instantaneous shear rate are out of phase as illustrated in Figure 2.3. It has been found experimentally for viscoelastic materials that the instantaneous stress, $\sigma(t)$, oscillates sinusoidally with an amplitude of σ_0, and a phase difference of δ from the strain, as illustrated in Figure 2.3,

$$\sigma(t) = \sigma_0 \cdot \mathbf{sin}(\omega \cdot t + \delta) \tag{2.18}$$

where the phase difference angle, δ, is a characteristic parameter of the material (Goodwin & Hughes, 2008).

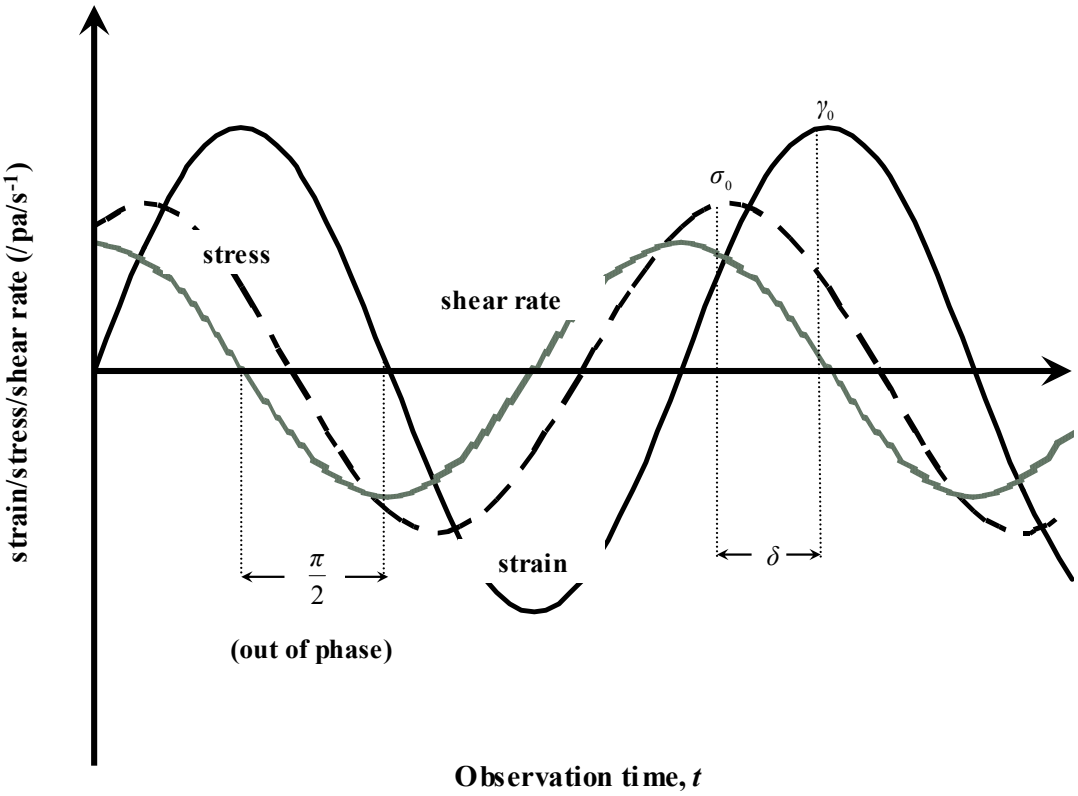

Figure 2.3 Illustration of oscillatory shear.

For the Kelvin-Voigt model (as shown in Figure 2.2), the instantaneous stress for the oscillatory shear is simply attributed to viscosity and elasticity of the material, which are directly related to instantaneous shear rate and instantaneous strain, respectively, according to equation 2.1 and 2.2.

$$\sigma(t) = \sigma(t)_{elastic} + \sigma(t)_{viscous} = G' \cdot \gamma(t) + \eta' \cdot \dot{\gamma}(t) \tag{2.19}$$

where *G'* and η' are defined as storage modulus and dynamic viscosity for oscillatory shear, respectively. In the analyses of oscillatory shear experiments, the loss modulus, *G"*, is used with the storage modulus, *G'*, instead of the dynamic viscosity, η', for consistency.

$$G'' = \omega \cdot \eta' \tag{2.20}$$

As the name indicates, the loss modulus actually measures the dissipation of energy due to the viscous flow of the material, for instance from the dashpot in Figure 2.2, while the storage modulus is a measure of the energy stored in the spring (Barnes, 2000; Barnes et al., 1989; Dhont & Nägele, 1998; Goodwin & Hughes, 2008; Macosko, 1994; Morrison, 2001).

According to 2.10 to 2.14 and trigonometry, the instantaneous stress, $\sigma(t)$, and the phase difference, δ, are found to be related with the storage modulus, *G'*, and the loss modulus, *G"* (Barnes, 2000; Barnes et al., 1989; Goodwin & Hughes, 2008; Macosko, 1994; Morrison, 2001).

$$\sigma(t) = \gamma_0 \cdot \sqrt{(G')^2 + (G'')^2} \cdot \mathbf{sin}(\omega \cdot t + \delta) \tag{2.21}$$

where

$$\mathbf{tan}\,\delta = \frac{G''}{G'} \tag{2.22}$$

and

$$\sqrt{(G')^2 + (G'')^2} = \frac{\sigma_0}{\gamma_0} \tag{2.23}$$

In terms of the above discussion that the loss modulus, *G"*, and the storage modulus, *G'*, indicate the viscous and the elastic behaviour of a material, respectively, the phase angle, δ, is used as a characteristic parameter to indicate the viscoelastic behaviour of a material, according to equation 2.22 (Barnes, 2000; Barnes et al., 1989; Goodwin & Hughes, 2008; Macosko, 1994; Morrison, 2001). As shown in Figure 2.2, it is obvious that the elasticity of the model is constant and only attributed to the spring in the Kelvin-Voigt model. Therefore, the storage modulus, *G'*, is simply determined by the constant elasticity of the system, i.e., *G'*=*G*, and would be used to examine the properties of materials. For instance, pure liquids are found to have a phase angle of 90^o with $G' = 0$ (i.e., there is no spring in the model), whilst a pure solid has a phase angle of 0^o due to no viscous response, i.e., $G'' = 0$ (Barnes, 2000; Barnes et al., 1989; Goodwin & Hughes, 2008; Macosko, 1994; Morrison, 2001). According to equation 2.23, the value of the expression $\sqrt{(G')^2 + (G'')^2}$ is determined by the amplitudes of the oscillatory stress, σ_0, and the oscillatory strain, γ_0, and is independent of the observation time, *t*. Therefore, this expression gives another characteristic parameter of the material, which is discussed below.

Due to the constant elasticity, Kelvin-Voigt model is employed for viscoelastic solids. As for viscoelastic liquids, the oscillatory responses are more complicated and the Maxwell model is applied. For matter that behaves as Maxwell model (as shown in

Figure 2.2), it is common to describe the complicated oscillatory response in terms of complex parameters, i.e., complex strain and complex stress. In physics, harmonic signals, for example, those in sinusoidal and cosinoidal forms, are often described with complex numbers in terms of Euler's formula (Andreescu & Andrica, 2006; Boas, 1983; Morrison, 2001; Ponnusamy & Silverman, 2006).

$$\mathbf{exp}\left(\pm i\cdot\theta\right)=\mathbf{cos}\,\theta\pm i\cdot\mathbf{sin}\,\theta \tag{2.24}$$

where i is the imaginary number with the value of $\sqrt{-1}$.

Therefore, the complex strain, $\gamma^*(t)$, and complex stress, $\sigma^*(t)$, are introduced as

$$\gamma^*\left(t\right)=-i\gamma_0\cdot\mathbf{exp}\left(i\cdot\omega t\right) \tag{2.25}$$

$$\sigma^*\left(t\right)=-i\sigma_0\cdot\mathbf{exp}\left[i\cdot\left(\omega t+\delta\right)\right] \tag{2.26}$$

where the values of instantaneous strain and stress are the real part of their complex counterparts, i.e., $\gamma\left(t\right)=\mathbf{Re}\left[\gamma^*\left(t\right)\right]$ and $\sigma\left(t\right)=\mathbf{Re}\left[\sigma^*\left(t\right)\right]$ (Boas, 1983; Goodwin & Hughes, 2008; Meyers & Chawla, 2009; Morrison, 2001). Thus, the complex shear rate, $\dot{\gamma}^*\left(t\right)$, is obtained,

$$\dot{\gamma}^*\left(t\right)=\frac{d\gamma^*\left(t\right)}{dt}=\omega\gamma_0\cdot\mathbf{exp}\left(i\cdot\omega t\right) \tag{2.27}$$

According to equation 2.10, the complex the complex shear rate, $\dot{\gamma}^*\left(t\right)$, is expressed as

$$\dot{\gamma}^*\left(t\right)=d\left[\frac{\sigma^*\left(t\right)}{G}\right]\Big/dt+\frac{\sigma^*\left(t\right)}{\eta} \tag{2.28}$$

and thus,

$$\frac{\dot{\gamma}^*\left(t\right)}{\sigma^*\left(t\right)}=\frac{1}{G}+\frac{1}{i\omega\eta} \tag{2.29}$$

Based on the concept of complex numbers, the complex modulus, G^*, of the material is defined as,

$$G^*=\frac{\sigma^*\left(t\right)}{\gamma^*\left(t\right)}=\frac{\sigma_0}{\gamma_0}\mathbf{exp}\left(i\cdot\delta\right) \tag{2.30}$$

From equation 2.22, 2.23 and 2.30 and Euler's formula, the complex modulus and the

storage and the loss moduli are related (Blom, Mellema, Lopulissa, & Reuvers, 1984; Goodwin & Hughes, 2008; Meyers & Chawla, 2009; Morrison, 2001).

$$G^* = G' + i \cdot G'' \tag{2.31}$$

Therefore, for the Maxwell model *G'* and *G''* are calculated as

$$G' = G\frac{(\omega\tau)^2}{1+(\omega\tau)^2} \tag{2.32}$$

and

$$G'' = G\frac{\omega\tau}{1+(\omega\tau)^2} \tag{2.33}$$

where τ is the relaxation time of the model and is defined in equation 2.14 ($\tau=\eta/G$). Furtherly, *G'* and *G''* are related,

$$G' = |G^*| \cdot \cos\delta \tag{2.34}$$

and

$$G'' = |G^*| \cdot \sin\delta \tag{2.35}$$

where

$$|G^*| = \sqrt{(G')^2 + (G'')^2} \tag{2.36}$$

is the magnitude of the complex modulus. The complex modulus, *G**, and its magnitude, $|G^*|$, are founded to be independent of the observation time according to equations 2.23 and 2.30, and thus, the complex modulus, *G**, as well as its magnitude, $|G^*|$, is used as a characteristic parameter for a material (Barnes, 2000; Barnes et al., 1989; Goodwin & Hughes, 2008; Macosko, 1994; Morrison, 2001).

Following the concept of equation 2.2, the complex modulus, *G**, gives the elasticity of a material under oscillatory shear since it is the ratio of the signal of the stress to that of the strain. However, it should be noted that *G** is a complex number and the imaginary part indicates out-of-phase properties (Boas, 1983; Goodwin & Hughes, 2008). Therefore, it is concluded that only *G'* accounts for the elastic behaviour of the material, and *G''* reveals the viscous response, which confines the concept in 2.19.

According to equation 2.30, the complex modulus, *G**, is the evaluation of the

complex stress in terms of the complex strain to obtain the elastic response of a material. Similarly, it is possible to obtain the viscous response through the complex stress and the complex shear rate, and thus, the complex viscosity, η^*, is introduced (Barnes, 2000; Barnes et al., 1989; Blom et al., 1984; Goodwin & Hughes, 2008; Macosko, 1994; Meyers & Chawla, 2009; Morrison, 2001).

$$\eta^* = \eta' + i \cdot \eta'' \tag{2.37}$$

where

$$\eta' = \frac{G''}{\omega} \tag{2.38}$$

and

$$\eta'' = \frac{G'}{\omega} \tag{2.39}$$

The dynamic viscosity, η' accounts for the viscous behaviour of a material as discussed in equations 2.19 and 2.20, while the out-of-phase component, η'', reveals the elasticity of a material. Similar to equation 2.36, the magnitude of the complex viscosity is calculated as

$$|\eta^*| = \sqrt{\left(\frac{G''}{\omega}\right)^2 + \left(\frac{G'}{\omega}\right)^2} \tag{2.40}$$

2.5.5 Frequency dependence and Cox-Merz rule

It has been discussed that the storage and loss moduli (G' and G'') are independent of observation time in oscillatory shear, but they are found to change with the frequency, ω, of oscillation (Barnes et al., 1989; Blom et al., 1984; Goodwin & Hughes, 2008; Macosko, 1994; Morrison, 2001). Actually, it is the oscillatory frequency that determines the timescale of the shear. At very low frequency, for instance, a long time ($\sim 1/\omega$) is spent to achieve the strain of γ_0, and thus, enough time is available for a material to relax the deformation. Therefore, the material behaves like a liquid. However, the time for relaxation is very short during oscillatory shear with high frequencies, and thus solid-like response to shear is observed (Barnes et al., 1989; Goodwin & Hughes, 2008; Macosko, 1994; Morrison, 2001). As a result, the

viscoelastic behaviour of a material, i.e., G', G'', δ, and thus G^* and η^*, are determined by the comparison of the relaxation time of a material with the available time for relaxation (~ $1/\omega$).

Experimentally, the viscoelastic behaviour of a material is determined from oscillatory shear with a range of frequencies. As discussed above, there is enough time for matter to relax the deformation at low frequencies and the material displays a liquid-like property. Therefore, elastic behaviour is barely observed, and according to equations 2.19 and 2.40, a relationship between the viscosity obtained from oscillatory shear and that from steady shear is established,

$$\left|\eta^*_{(\omega=\dot{\gamma})}\right| = \eta_{\dot{\gamma}} \tag{2.41}$$

which is an empirical relationship known as the Cox-Merz rule and is valid for many materials in the range of low and intermediate frequencies (Al-Hadithi, Barnes, & Waiters, 2002; Barnes et al., 1989; Cox & Merz, 1958; Gleissle & Hochstein, 2003; Goodwin & Hughes, 2008; Macosko, 1994; Morrison, 2001; Ohl & Gleissle, 1993; Sharma, Jaishankar, Wang, & McKinley, 2011). However, the Cox-Merz rule only holds for some materials but not for all (Barnes et al., 1989; Morrison, 2001; Rao, 2007). Since the major difference between oscillatory shear and steady shear resides in the strain of the shear, i.e., oscillatory shear is constrained in small strain from linear viscoelasticity, violations to the Cox-Merz rule indicates the effects of large strains on the structure of a material (Ikeda & Nishinari, 2000, 2001). For example, it is observed in many food systems, such as dairy systems, that $\left|\eta^*_{(\omega=\dot{\gamma})}\right|$ is greater than $\eta_{\dot{\gamma}}$, suggesting that the structure decays under the effects of large strain applied to the system in steady shear (Foegeding et al., 2011; Yaşar, Kahyaoglu, & Şahan, 2009).

2.6 Rheology of proteins

2.6.1 Hydrodynamic interactions

As indicated in Figure 2.4, addition of particles into a solvent alters the flow field and therefore increases the viscosity, η, of the system through interactions between the particles and the solvent (Macosko, 1994; Tadros, 1994). The Einstein equation

(Einstein, 1906, 1911) has been recognized as a classical model to express such effects in a dilute suspension, where the particles are far from each other so that the particle-particle interactions are negligible,

$$\eta = \eta_s \left(1 + 2.5\varphi\right) \tag{2.42}$$

where η_s is the viscosity of the solvent and φ is the volume fraction of the particles (Macosko, 1994; Tadros, 1994; Willenbacher & Georgieva, 2013). However, such a model is restricted to very dilute suspensions with $\varphi < 0.01$. As the volume fraction increases, however, the disturbed flow fields of different particles approach and overlap, leading to hydrodynamic interactions between particles (Macosko, 1994; Tadros, 1994; Taneda, 1979; Willenbacher & Georgieva, 2013), as shown in Figure 2.4. In such cases, higher-order terms in φ have to be introduced to account for the hydrodynamic interactions

$$\eta = \eta_s \left(1 + 2.5\varphi + 6.2\varphi^2 + k_3\varphi^3 + \cdots\right) \tag{2.43}$$

where the high orders correspond to pair and triple interactions and so on (Batchelor, 1977; Macosko, 1994; Tadros, 1994; Willenbacher & Georgieva, 2013). Besides the two equations 2.42 and 2.43, empirical models based on a phenomenological appoach have also been proposed, for example by Krieger and Dougherty (1959) and Quemada (1977), which provide more understanding for the viscosity of concentrated dispersions and suspensions.

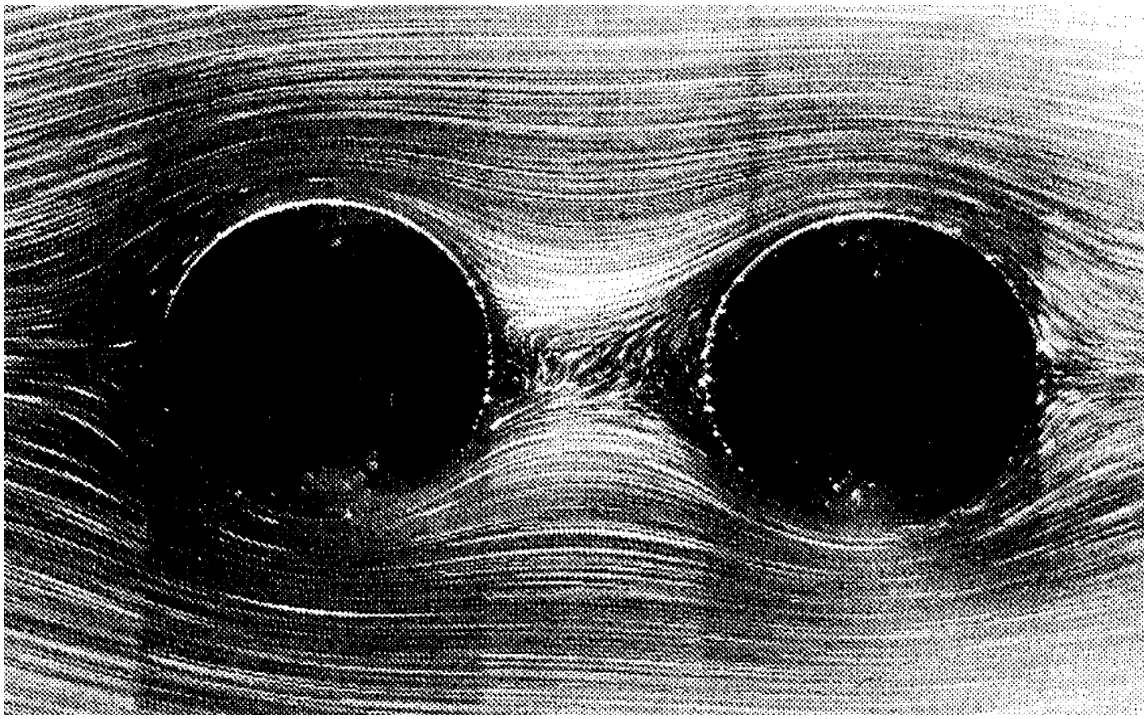

Figure 2.4 Streamline patterns around spheres (Taneda 1979).

However, it has to be stressed that the understanding of relationship of viscosity with hydrodynamic interactions are mainly based on the assumption of suspensions of hard spheres, where the particles are symmetric spheres and there is no interaction between the particles unless they contact with each other (Macosko, 1994; Willenbacher & Georgieva, 2013). Protein molecules are obviously more complicated particles than hard spheres due to their molecular asymmetry and intermolecular interactions. Therefore, more factors other than hydrodynamic interactions have to be taken into account for studies on the rheological properties of protein dispersions (Macosko, 1994; M. A. Tung, 1978).

2.6.2 Molecular orientation and Péclet number

Proteins, even those with globular structures, can not be considered as perfect spheres due to the molecular asymmetry. Therefore, molecular orientations of the proteins significantly affect the viscosity of the solutions. Orientation of protein molecules is determined by the hydrodynamic forces on proteins from solvents and the Brownian motions of the proteins themselves, of which the former aligns protein

molecules with the flow, while the latter favors the proteins to orient themselves randomly (Macosko, 1994; Willenbacher & Georgieva, 2013).

In order to evaluate the balance between hydrodynamic forces and Brownian motion, the Péclet number, *Pe*, is introduced, which compares the time scales of convective and Brownian motions (Goodwin & Hughes, 2008; Macosko, 1994; Willenbacher & Georgieva, 2013). According to the Stokes-Einstein equation, the diffusion coefficient, *D*, for a particle with a radius of *r* is calculated as

$$D = \frac{k_B T}{6\pi\eta r} \tag{2.44}$$

where k_B is the Boltzmann constant ($=1.38062\times10^{-23}$ J/K), T represents absolute temperature (in K), and η is the viscosity of the solution. It should be noted that the viscosity involved in calculating the diffusion coefficient is that for the solution but not the solvent, since the Péclet number relies on the diffusivity of an isolated particle in the system, which is also affected by neighboring particles other than the solvent (Goodwin & Hughes, 2008; Macosko, 1994; Willenbacher & Georgieva, 2013). As for calculating *Pe*, the characteristic distance for Brownian motions are the particle radius, *r*, while the characteristic time for flow is set as the reciprocal of the shear rate, $\dot{\gamma}$ (Goodwin & Hughes, 2008). Therefore, the characteristic times, $t_{Brownian}$ for Brownian motions and *t*, for the flows are given as

$$t_{Brownian} = \frac{r^2}{D} = \frac{6\pi\eta r^3}{k_B T} \tag{2.45}$$

and

$$t = \frac{1}{\dot{\gamma}} \tag{2.46}$$

Accordingly, the Péclet number, *Pe*, is expressed as

$$Pe = \frac{t_{Brownian}}{t} = \frac{6\pi r^3 \sigma}{k_B T} \tag{2.47}$$

where $\sigma = \eta \cdot \dot{\gamma}$ is the shear stress.

According to equation 2.42, time scales for Brownian-motion-induced randomization of the molecular orientations and flow-induced molecular alignments

are compared and the more significant effects are deduced. For instance, $Pe \gg 1$, indicates that randomization of orientations takes a much longer time than alignments for the proteins molecules, and thus, effects of molecular orientations on viscosity of protein solutions are negligible (Macosko, 1994; Willenbacher & Georgieva, 2013).

2.6.3 Protein-protein interactions

As indicated in Section 2.6.1, proteins can not be considered as hard spheres since there are several different interactions existing between the molecules, such as van der Waals and electrostatic interactions (Bryant & McClements, 1998; Damodaran, 1996b). The van der Waals interactions are attractive forces between dipoles in the molecules induced by the neighboring particles (Mahanty & Ninham, 1976). It is known that proteins will be charged when they are dispersed in a liquid with the pH different from their isoelectric point (pI), and thus, repulsive electrostatic interactions between the charged molecules arise (Bryant & McClements, 1998; Damodaran, 1996b). Besides these forces, repulsions are also exhibited between protein molecules due to steric overlaps of hydration shells and molecules (Bryant & McClements, 1998; Ikeda & Nishinari, 2000, 2001), while attractions are enhanced through hydrophobic interactions and disulphide bonds between proteins (Bryant & McClements, 1998; Damodaran, 1996b). The balance between protein-protein repulsions and attractions determines the rheological properties of protein dispersions. Some proteins, such as ovalbumin and bovine and rat serum albumins, have been found to exhibit solid-like mechanical properties, i.e., $G' > G''$, in aqueous solutions (Inoue & Matsumoto, 1994; Matsumoto & Chiba, 1990; Matsumoto, Chiba, & Inoue, 1992; Matsumoto & Inoue, 1992; Renard, Acxelos, Boué, & Lefebvre, 1996). It has been proposed that those protein particles arrange into a crystalline lattice due to strong repulsions between them and are considered as colloidal crystals (Ikeda & Nishinari, 2000, 2001). Based on the observations of bovine serum albumin solutions, those authors also explained that such colloidal crystals formed by proteins were actually stabilized by repulsions between hydration shells of the proteins rather than intermolecular electrostatic forces (Ikeda & Nishinari, 2000). For the case where attractions overcome the repulsive forces between

the proteins, for example the denatured proteins where hydrophobic attractions between the molecules significantly increase, protein molecules tend to aggregate and form gels, exhibiting complicated structures and rheological properties (Bryant & McClements, 1998; Damodaran, 1996b; Ikeda, Foegeding, & Hagiwara, 1999; Lefebvre, Renard, & Sanchez-Gimeno, 1998; Renard, Robert, Faucheron, & Sanchez, 1999; Stading & Hermansson, 1990).

2.6.4 Rheology of protein gels

Gels are a three dimensional network formed by molecules or particles that form during the transition of liquid to solid (Clark, 1996). Protein gels are of great scientific interests and commercial importance due to their unique flow behaviour and potentials for improving sensory properties, such as thick mouthfeel, for food products (Clark, 1996; van den Berg, Rosenberg, van Boekel, Rosenberg, & van de Velde, 2009). The phenomenon of gelation is commonly classified to be either physically-induced or chemically-induced (de Gennes, 1979; Goodwin & Hughes, 2008). Physically-induced gels are usually referred to as network structures formed through physical interactions, such as hydrophobic interactions and hydrogen bonds for proteins, while chemically-induced gels are stabilized though covalent bonds, for example disulphide bonds for proteins (de Gennes, 1979; Goodwin & Hughes, 2008). Protein gels are formed mainly through hydrophobic interactions, but some for instance those of β-lactoglobulins, contain disulphide bonds between protein molecules. Therefore, it is difficult to define protein gels as either physical or chemical. Actually, such classification of physical and chemical gels seems not so crucial after Miyoshi and Nishinari (1999) observed that the findings of Vilgis and Winter (1988) on the rheology of chemical gels also applied to physical gels.

Unlike liquid systems, where the viscosity is often the focus of their rheological properties, dynamic moduli, i.e., storage (*G'*) and loss (*G"*) moduli, are of more interests for gel systems, since the crosslinkage of the protein network increases both the elasticity (i.e., *G'*) and viscosity (given by *G"*) of the system (Clark, Kavanagh, & Ross-Murphy, 2001; Ikeda & Nishinari, 2001). Values of *G'* and *G"* reveal the state of

a system, i.e., whether it is liquid ($G'<G''$) or solid ($G'>G''$) (Barnes, 2000; Barnes et al., 1989; Goodwin & Hughes, 2008; Macosko, 1994; Morrison, 2001). As a result, a system with $G'=G''$ is considered to be neither liquid nor solid and is defined as a critical gel, where the network of the proteins occupies the total volume of the container (W. Hess, Vilgis, & Winter, 1988; Winter, 1987). Such a concept is widely used in gelation experiments, such as heat gelation of protein solutions, to define the gelation point of proteins, i.e., the G'-G'' crossover (Ikeda & Nishinari, 2001; Stading & Hermansson, 1990; C. M. Tung & Dynes, 1982).

Detailed information on the structure of a gel is also obtained through the values and frequency dependence of G' and G''. The elasticity reveals the strength of a gel since it is related to the degree of the crosslinking of the network (Xu, Inglett, Chen, & Liu, 2013). The frequency dependence of dynamic moduli is also employed to examine the structure of protein gels. It is found that G' is frequency independent for solids and thus, the strength of a gel, i.e., how close it is to a solid, can be evaluated through the frequency dependence of G' (Goodwin & Hughes, 2008; Macosko, 1994; Rao, 2007). Vilgis and Winter (1988) proposed the same power law frequency dependence of dynamic moduli, i.e., $G'\sim G''\sim\omega^n$, for chemical gels with self-similar or fractal structures, which is also found to be valid for physical and protein gels (Ikeda, 2003; Ikeda & Nishinari, 2001; Miyoshi & Nishinari, 1999). The fractal dimension, d_f, of a gel reveals the density of the particle arrangement in the network (Ikeda & Nishinari, 2001; Vilgis & Winter, 1988). The particles in a solid, for instance, are fully packed and give a d_f of 3.0, while critical gels have open structures, as indicated by the d_f of 2.0 (W. Hess et al., 1988; Vilgis & Winter, 1988; Winter & Chambon, 1986).

Structures of protein gels, even those formed by the same molecules, can be very different in structure due to the individual aggregation process involved (Ikeda et al., 1999; Stading & Hermansson, 1990; Stading, Langton, & Hermansson, 1993). Once the protein molecules start to aggregate, induced by heat for instance, clusters are formed through random aggregations of the molecules. However, the growth of such random structure could terminate when the clusters are large enough, and there is a possibility for the protein clusters to aggregate in some orientated pathways (Ikeda et al., 1999). In such cases, protein clusters form linear strand-like structures and then

connect and entangle with each other to form a coarse and open-space network with the fractal dimensions of 2.0 ~ 2.2 (Gimel, Durand, & Nicolai, 1994; Ikeda et al., 1999; Vreeker, Hoekstra, den Boer, & Agterof, 1992). For example, β-lactoglobulin has been found to form fine-standed gels at a pH far from the pI (> 6 or < 4), which possess smaller *G'* but less frequency dependence than the particulate type of gels formed at pH 4 ~ 6 (Stading & Hermansson, 1990).

2.7 References

Al-Hadithi, T.S.R., Barnes, H.A., & Waiters, K. (2002). The relationship between the linear (oscillatory) and nonlinear (steady-state) flow properties of a series of polymer and colloidal systems. *Colloid & Polymer Science, 270*(1), 40-46.

Andreescu, T., & Andrica, D. (2006). *Complex Numbers from A to. . . Z*. Boston, US: Birkhäuser.

Astarita, G. (1990). Letter to the Editor: The engineering reality of the yield stress. *Journal of Rheology, 34*(2), 275-277.

Bagley, E.B., & Christianson, D.D. (1982). Swelling capacity of starch and its relationship to suspension viscosity: effect of cooking time, temperature and concentration. *Journal of Texture Studies, 13*(1), 115-126.

Barnes, H.A. (1989). Shear thickening "Dilatancy" in suspensions of non aggregating solid particlesdispersed in Newtonian liquids. *Journal of Rheology, 33*(2), 329-366.

Barnes, H.A. (2000). *Handbook of elementary rheology*. Aberystwyth, UK: Cambrian Printers.

Barnes, H.A., Hutton, J.F., & Walters, K. (1989). *An introduction to rheology*. Amsterdam, The Netherlands: Elsevier.

Barnes, H.A., & Walters, K. (1985). The yield stress myth? *Rheologica Acta, 24*, 323-326.

Batchelor, G.K. (1977). The effect of Brownian motion on the bulk stress in a suspension of spherical particles. *Journal of Fluid Mechanics, 83*(1), 97-117.

Blom, C., Mellema, J. , Lopulissa, J.S., & Reuvers, A.J. (1984). Frequency dependent linear viscoelastic properties of ordered polystyrene latices. *Colloid & Polymer Science, 262*, 397-402.

Boas, M.L. (1983). *Mathematical Methods in the Physical Sciences* (2 ed.). US: John Wiley & Sons, Inc.

Bryant, C.M., & McClements, D.J. (1998). Molecular basis of protein functionality with special consideration of cold-set gels derived from heat-denatured whey. *Trends in Food Science & Technology, 9*(4), 143-151.

Clark, A.H. (1996). Biopolymer gels. *Current Opinion in Colloid & Interface Science, 1*(6), 712-717.

Clark, A.H., Kavanagh, G.M., & Ross-Murphy, S.B. (2001). Globular protein

gelation-theory and experiment. *Food Hydrocolloids, 15*(4-6), 383-400.
Cox, W.P., & Merz, E.H. (1958). Correlation of dynamic and steady flow viscosities. *Journal of Polymer Science, 28*(118), 619-622.
Dail, R.V., & Steffe, J.F. (1990a). Dilatancy in starch solutions under low acid aseptic processing conditions. *Journal of Food Science, 55*(6), 1764-1765.
Dail, R.V., & Steffe, J.F. (1990b). Rheological characterization of crosslinked waxy maize starch solutions under low acid aseptic processing conditions using tube viscometry techniques. *Journal of Food Science, 55*(6), 1660-1665.
Damodaran, S. (1996). Amino acids, peptides, and proteins. In O. R. Fennema (Ed.), *Food Chemistry* (3rd ed., pp. 321-429). New York, USA.: Marcel Dekker.
de Gennes, P.G. (1979). Gelation of polymer *Scaling Concepts in Polymer Physics* (pp. 128-162). New York.: Comell University, Ithaca.
Dhont, J.K.G., & Nägele, G. (1998). Critical viscoelastic behavior of colloids. *Physical Review E, 58*(6), 7710-7732.
Dullaet, K., & Mewis, J. (2005). Thixotropy: Build-up and breakdown curves during flow. *Journal of Rheology, 49*(6), 1213-1230.
Edgeworth, R., Dalton, B.J., & Parnell, T. (1984). The pitch drop experiment. *European Journal of Physics, 5*(4), 198-200.
Einstein, A. (1906). Eine neue Bestimmung der Moleküldimensionen. *Annalen der Physik, 324*(2), 289-306.
Einstein, A. (1911). Berichtigung zu meiner Arbeit: Eine neue Bestimmung der Moleküldimensionen. *Annalen der Physik, 339*(3), 591-592.
Foegeding, E.A., Vardhanabhuti, B., & Yang, X. (2011). Dairy Systems. In I. T. Norton, F. Spyropoulos & P. Cox (Eds.), *Practical food rheology: An interpretive approach*: Wiley-Blackwell.
Gimel, J.-C., Durand, D., & Nicolai, T. (1994). Structure and distribution of aggregates formed after heat-induced denaturation of globular proteins. *Macromolecules, 27*(2), 583-589.
Gladwell, N., Rahalkar, R.R., & Richmond, P. (1985). Creep/recovery behavior of oil-water emulsions: Influence of disperse phase concentration. *Journal of Food Science, 50*, 1477-1481.
Gladwell, N., Rahalkar, R.R., & Richmond, P. (1986). Influence of disperse phase concentration upon the viscoelastic behaviour of emulsions. *Rheologica Acta, 25*, 55-61.
Gleissle, W., & Hochstein, B. (2003). Validity of the Cox-Merz rule for concentrated suspensions. *Journal of Rheology, 47*(4), 897-910.
Goodwin, J.W., & Hughes, R.W. (2008). *Rheology for Chemists-An Introduction* (2 ed.). Cambridge, UK: The Royal Society of Chemistry.
Hess, W., Vilgis, T.A., & Winter, H.H. (1988). Dynamical critical behavior during chemical gelation and vulcanization. *Macromolecules, 21*(8), 2536–2542.
Hillman, S., & Mannan, S.H. (2006). Analysis of jamming networks in sheared suspensions. *Journal of Rheology, 50*(3), 239-258.
Ikeda, S. (2003). Heat-induced gelation of whey proteins observed by rheology, atomic force microscopy, and Raman scattering spectroscopy. *Food Hydrocolloids, 17*(4), 399-406.
Ikeda, S., Foegeding, E.A., & Hagiwara, T. (1999). Rheological study on the fractal

nature of the protein gel structure. *Langmuir, 15*(25), 8584-8589.
Ikeda, S., & Nishinari, K. (2000). Intermolecular forces in bovine serum albumin solutions exhibiting solidlike mechanical behaviors. *Biomacromolecules, 7*(4), 757-763.
Ikeda, S., & Nishinari, K. (2001). On solid-like rheological bahaviors of globular protein solutions. *Food Hydrocolloids, 15*, 401-406.
Inoue, H., & Matsumoto, T. (1994). Viscoelastic and SAXS studies of the structural transition in concentrated aqueous colloids of ovalbumin and serum albumins. *Journal of Rheology, 38*(4), 973-984.
James, D.F. (2009). Boger fluids. *Annual Review of Fluid Mechanics, 41*, 129-142.
Jeffrey, D.J., & Acrivos, A. (1976). The rheological properties of suspensions of rigid particles. *AIChE Journal, 22*(3), 417-432.
Krieger, I.M., & Dougherty, T.J. (1959). A mechanism for non-Newtonian flow in suspensions of rigid spheres. *Journal of Rheology, 3*(1), 137-152.
Lefebvre, J., Renard, D., & Sanchez-Gimeno, A.C. (1998). Structure and rheology of heat-set gels of globular proteins. *Rheologica Acta, 37*(4), 345-357.
Macosko, C.W. (1994). *Rheology: Principles, Measurements, and Applications*. New York, USA: Wiley-VCH, Inc.
Mahanty, J., & Ninham, B.W. (1976). *Dispersion Forces*. London, UK: Academic Press.
Maranzano, B.J., & Wagner, N.J. (2002). Flow-small angle neutron scattering measurements of colloidal dispersion microstructure evolution through the shear thickening transition. *Journal of Chemical Physics, 117*(22), 10291-10302.
Markovitz, H. (1985). Rheology: in the beginning. *Journal of Rheology, 29*(6), 777-798.
Matsumoto, T., & Chiba, J. (1990). Rheological and small-angle X-ray scattering investigations on the shape and ordered arrangement of native ovalbumin molecules in aqueous colloids. *Journal of the Chemical Society, Faraday Transactions, 86*(16), 2877-2882.
Matsumoto, T., Chiba, J., & Inoue, H. (1992). Effect of pH on colloidal properties of native ovalbumin aqueous systems. *Colloid and Polymer Science, 270*(7), 687-693.
Matsumoto, T., & Inoue, H. (1992). Application of the Yukawa potential to the auto-controlled mechanism of the ovalbumin molecule in aqueous systems. *Chemical Physics, 166*(1-2), 299-302.
Matveenko, V.N., & Kirsanov, E.A. (2011). The viscosity and structure of dispersed systems. *Moscow University Chemistry Bulletin, 66*(4), 199-228.
Mewis, J. (1979). Thixotropy - A general review. *Journal of Non-Newtonian Fluid Mechanics, 6*(1), 1-20.
Mewis, J., & Wagner, N.J. (2009). Thixotropy. *Advances in Colloid and Interface Science, 147-148*, 214-227.
Meyers, M.A., & Chawla, K.K. (2009). *Mechanical Behavior of Materials*. New York, US: Cambridge University Press.
Miyoshi, E., & Nishinari, K. (1999). Rheological and thermal properties near the sol-gel transition of gellan gum aqueous solutions. *Progress in Colloid and*

Polymer Science, 114, 68-82.

Morrison, F.A. (2001). *Understanding Rheology*. New York, USA: Oxford University Press, Inc.

Ohl, N., & Gleissle, W. (1993). The characterization of the steady-state shear and normal stress functions of highly concentrated suspensions formulated with viscoelastic liquids. *Journal of Rheology, 37*(2), 381-406.

Okechukwu, P.E., & Rao, M.A. (1995). Influence of granule size on viscosity of cornstarch suspension. *Journal of Texture Studies, 26*(5), 501-516.

Ponnusamy, S., & Silverman, H. (2006). *Complex Variables with Applications*. Boston, US: Birkhäuser.

Quemada, D. (1977). Rheology of concentrated disperse systems and minimum energy dissipation principle I. Viscosity-concentration relationship. *Rheologica Acta, 16*(1), 82-94.

Rao, M.A. (2007). *Rheology of Fluid and Semisolid Foods Principles and Applications*. New York, USA: Springer Science+Business Media.

Renard, D., Acxelos, M.A.V., Boué, F., & Lefebvre, J. (1996). Small angle neutron scattering and viscoelasticity study of the colloidal structure of aqueous solutions and gels of a globular proteins. *Journal de Chimie Physique, 93*, 998-1015.

Renard, D., Robert, P., Faucheron, S., & Sanchez, C. (1999). Rheological properties of mixed gels made of microparticulated whey proteins and b-lactoglobulin. *Colloids and Surfaces B: Biointerfaces, 12*, 113-121.

Sharma, V., Jaishankar, A., Wang, Y., & McKinley, G.H. (2011). Rheology of globular proteins: apparent yield stress, high shear rate viscosity and interfacial viscoelasticity of bovine serum albumin solutions. *Soft Matter, 7*, 5150-5160.

Stading, M., & Hermansson, A. (1990). Viscoelastic behaviour of b-lactoglobulin gel structures. *Food Hydrocolloids, 4*(2), 121-135.

Stading, M., Langton, M., & Hermansson, A. (1993). Microstructure and rheological behaviour of particulate b-lactoglobulin gels. *Food Hydrocolloids, 7*(3), 195-212.

Tadros, Th.F. (1994). Fundamental principles of emulsion rheology and their applications. *Colloids and Surfaces Physicochemical and Engineering Aspects, 91*, 39-55.

Taneda, S. (1979). Visualization of separating Stokes flows. *Journal of the Physical Society of Japan, 46*(6), 1935-1942.

Tung, C.M., & Dynes, P.J. (1982). Relationship between viscoelastic properties and gelation in thermosetting systems. *Journal of Applied Polymer Science, 27*, 569-574.

Tung, M.A. (1978). Rheology of protein dispersions. *Journal of Texture Studies, 9*(1-2), 3-31.

van den Berg, L., Rosenberg, Y., van Boekel, M.A.J.S., Rosenberg, M., & van de Velde, F. (2009). Microstructural features of composite whey protein/polysaccharide gels characterized at different length scales. *Food Hydrocolloids, 23*(5), 1288-1298.

Vilgis, T.A., & Winter, H.H. (1988). Mechanical self similarity of polymers during chemical gelation. *Colloid and Polymer Science, 266*(6), 494-500.

Vreeker, R., Hoekstra, L.L., den Boer, D.C., & Agterof, W.G.M. (1992). Fractal aggregation of whey proteins. *Food Hydrocolloids, 6*(5), 423-435.

Willenbacher, N., & Georgieva, K. (2013). Rheology of disperse systems. In U. Brocke, W. Meier & G. Wagner (Eds.), *Product Design and Engineering: Formulation of Gels and Pastes* (pp. 7-49). Weinheim, Germany: Wiley-VCH Verlag GmbH & Co.

Winter, H.H. (1987). Transient networks Evolution of rheology during chemical gelation. *Progress in Colloid & Polymer Science, 75*, 104-110.

Winter, H.H., & Chambon, F. (1986). Analysis of linear viscoelasticity of a crosslinking polymer at the gel point. *Journal of Rheology, 30*, 367-382.

Xu, J., Inglett, G.E., Chen, D., & Liu, S.X. (2013). Viscoelastic properties of oat b-glucan-rich aqueous dispersions. *Food Chemistry, 138*, 186-191.

Yaşar, K., Kahyaoglu, T., & Şahan, N. (2009). Dynamic rheological characterization of salep glucomannan/galactomannan-based milk beverages. *Food Hydrocolloids, 23* (5), 1305-1311.

3 Molecular dynamics computer simulations

Computers have improved considerably over the last 60 years. Computers have changed the world in many ways, one of which is the ability to tackle the scientific problems previously difficult to solve. For example, the properties of molecular materials could only be approximately predicted based on theories of intermolecular interactions due to the complex computations and lengthy calculations required. The development of computers allowed a new approach to be tried. Computer simulations were developed from the 1950's (Alder & Wainwright, 1957, 1959; Metropolis, Rosenbluth, Rosenbluth, Teller, & Teller, 1953) and are now employed widely in science and other research fields. There was a debate on whether computer simulations are theories or experiments in 1970's since they applied calculations and measurements on unreal systems but gave reproducible results with statistical errors. Haile (1997) proposed that computer simulations were forms of theory in order to avoid the risk of replacement of laboratory experiments by in-silico measurements. In practice, computer simulations are applied to test and improve the theories of intermolecular interactions through comparisons of simulations based on new theory with those of traditional theories or experiment results (Allen, 2004; Allen & Tildesley, 1987; Frenkel & Smit, 2002). Such methods are also involved in the measurements of properties of matter under difficult or impossible conditions, such as extreme temperatures or pressures (Allen, 2004).

Computer simulations can be achieved through several different methods, e.g., Monte Carlo, Brownian dynamic, Langevin dynamics and Molecular Dynamics, according to the way in which molecular positions, $\mathbf{q}^N$ are computed (Haile, 1997). Monte Carlo (MC) simulation, for instance, first carried out by Metropolis et al. (1953) is a purely stochastic method because $\mathbf{q}^N$ is randomly generated in this method (Haile, 1997; Leach, 2001). Molecular dynamics (MD) simulation, on the other hand, is deterministic, because the set of molecular positions are calculated through solving differential equations of motion and therefore connected in time (Haile, 1997; Leach,

2001).

3.1 Molecular mechanics and force fields

The Born-Oppenheimer approximation is considered as one of the most important foundations for the calculations of atomic and molecular interactions. In this, the rapid motion of electrons are averaged out and therefore, the Hamiltonian, $\mathscr{H}$, of a system containing N atoms is expressed as a function of the nuclear variables, i.e., the set of coordinates, $\mathbf{q}^N$ and their conjugate generalized momenta, $\mathbf{p}^N$,

$$\mathscr{H}\left(\mathbf{p}^N,\mathbf{q}^N\right)=\mathscr{K}\left(\mathbf{p}^N\right)+\mathscr{V}\left(\mathbf{q}^N\right) \tag{3.1}$$

where $\mathscr{K}$ and $\mathscr{V}$ represent kinetic energy and potential energy, respectively (Allen & Tildesley, 1987; Haile, 1997; Hoover, 1991). The kinetic energy, $\mathscr{K}$, which is a function of the momenta, $\mathbf{p}^N$, of the atoms, usually takes the form

$$\mathscr{K}\left(\mathbf{p}^N\right)=\sum_{i=1}^{N}\left|\mathbf{p}_i\right|^2/2m_i \tag{3.2}$$

where m_i represents the mass of the i-th atom in the system. However, more important to molecular dynamics is the potential energy, $\mathscr{V}$, where the intra- and intermolecular forces can be revealed, and thus, the equation of motion and time evolution of the system, as well as its mechanical properties, can be obtained (Allen & Tildesley, 1987; Haile, 1997; Hoover, 1991; Tuckerman, 2010).

Based on the Born-Oppenheimer approximation, force field methods, also know as molecular mechanics have been proposed, which allow computations of the potential of a system in terms of the coordinates of the atomic nuclei (Allen & Tildesley, 1987; González, 2011; Leach, 2001; Ponder & Case, 2003). The most commonly used protein force fields treat the atoms of a protein molecule as beads connected through elastic springs, and compute the potential of a system in terms of bonded and non-bonded interactions (González, 2011; Leach, 2001; Ponder & Case, 2003),

$$\begin{aligned}\mathscr{V}\left(\mathbf{q}^N\right)=&\sum_{\text{bonds}}\frac{k_b}{2}\left(b_i-b_{i,0}\right)^2+\sum_{\text{angles}}\frac{k_a}{2}\left(\theta_i-\theta_{i,0}\right)^2+\sum_{\text{torsions}}\frac{V_n}{2}\left[1+\mathbf{cos}\left(n\Phi-\delta\right)\right]\\&+\sum_{i=1}^{N}\sum_{j=i+1}^{N}\left\{4\varepsilon_{ij}\left[\left(\frac{\sigma_{ij}}{r_{ij}}\right)^{12}-\left(\frac{\sigma_{ij}}{r_{ij}}\right)^{6}\right]+\frac{z_i z_j}{4\pi\varepsilon_0 r_{ij}}\right\}\end{aligned} \tag{3.3}$$

where b, θ, Φ, r_{ij} denote the bond length, bond angle, dihedral angle and distance

between the *i*-th and *j*-th atoms, respectively, as illustrated in Figure 3.1, and the subscript $_0$, indicates the properties of the equilibrium state of the 'springs'. As shown in equation 3.3, the first three terms give the bonded interactions, i.e., bond stretching, angle bending and torsions, respectively, and the last term indicates the non-bonded interactions, i.e., the van der Waals interaction expressed by Lenard-Jones potential and the electrostatic interactions (González, 2011; Leach, 2001; Ponder & Case, 2003). It is clear that the dependence of potential energy on the distance between atoms, r_{ij}, is accessible once the other parameters are evaluated, which in practice is achieved through quantum mechanical calculations or by fitting to data obtained from experiments, such as neutron, X-ray, and electron diffraction, NMR, FTIR to name a few (González, 2011).

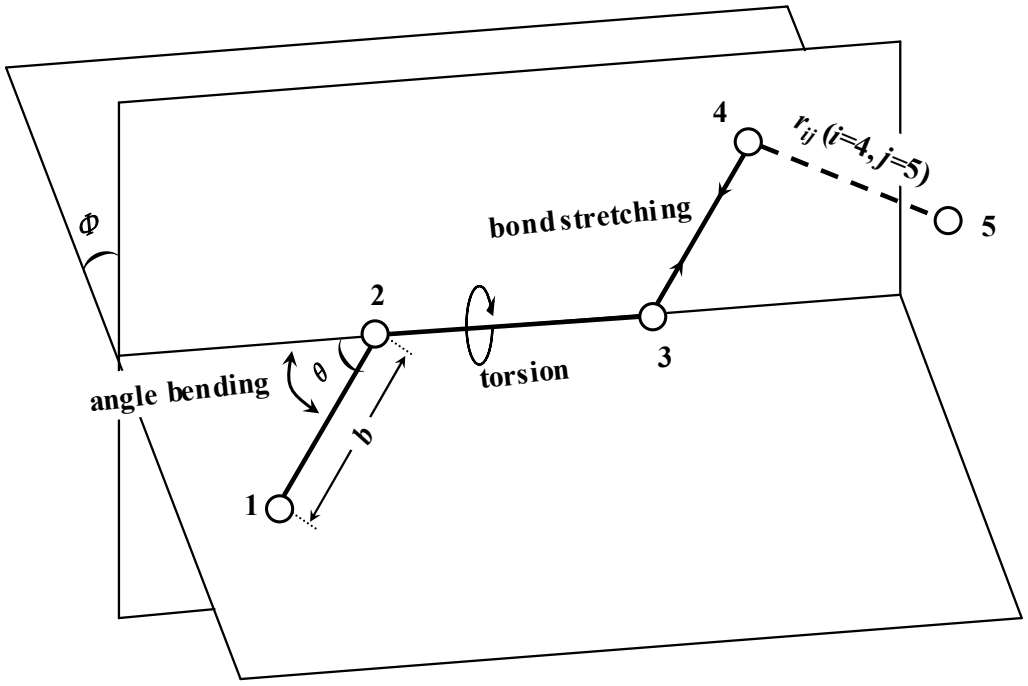

Figure 3.1 Illustration of molecular interactions.

With the availability of computers with increased speed, a number of efforts have been made to parameterize the factors in equation 3.3. Meanwhile, more effective methods for determining the potential energy other than equation 3.3 have been developed (González, 2011). Such efforts have provided more straightforward and

accessible force fields for computer simulations of molecules, ranging from small organic molecules to more complex biopolymers, such as proteins and nuclear acids (González, 2011; Ponder & Case, 2003). Currently, there are a number of force fields widely used in computer simulations of proteins, including AMBER, CHARMM, OPLS, and GROMOS. Detailed descriptions of these force fields are available from a number of sources e.g., Cornell et al. (1995), MacKerell et al. (1998), Jorgensen, Maxwell, and Tirado-Rives (1996), and Oostenbrink, Villa, Mark, and van Gunsteren (2004), respectively. It should be noted that none of the force fields would provide exact information on molecular interactions, but only good estimates that are close to experimental results, and therefore, efforts are still being made to improve the available force fields. Moreover, it is inadvisable to compare the performance of the existing force fields, since the results strongly depend on the simulated system and properties (González, 2011). Most of the time, a force field gives a good estimate for some interactions but less accurate information for others. For example, Paton and Goodman (2009) evaluated the interaction energies of 22 molecular complexes of small and medium size and 143 nuclear acid bases and amino acids using seven different force fields, including MM2, MM3, AMBER, OPLS, OPLS-AA, MMFF94, and MMFF94s, and compared the results with those obtained from high-level ab initio calculations. Their results indicated that all the potentials involved described electrostatic and van der Waals interactions quite accurately, but severely underestimated the magnitudes of hydrogen bonding interactions.

3.2 Periodic boundary condition and potential truncation

Since there are only a relatively small number of particles involved in computer simulations, the boundary effects become significant, and thus, the periodic boundaries are introduced (Allen, 2004; Allen & Tildesley, 1987; Leach, 2001). In the periodic boundary conditions, the central cell, for instance a cubic box, is replicated in all directions to form a periodic array. Thus, there are 8 neighboring replicas of the central box for a 2-dimensional example, as shown in Figure 3.2, while in 3 dimensions there are 26 images. As illustrated in Figure 3.2, all the replicas are exactly same as the central box, including the positions and velocities of the particles, and thus the image

of a molecule enters the box once the original one leaves from the opposite side, which guarantees the consistence of the total number of the particles in the box. As a result, a continuous system without boundary effects is obtained for modeling. Besides cubic boxes, periodic boundary conditions are also applied to other shapes, such as the rhombic dodecahedron (Wang & Krumhansl, 1972) and the truncated octahedron (Adams, 1979), which are more nearly spherical than cubes, and considered to be more useful for the simulations of matter with spatially isotropic structures, such as liquids (Allen & Tildesley, 1987).

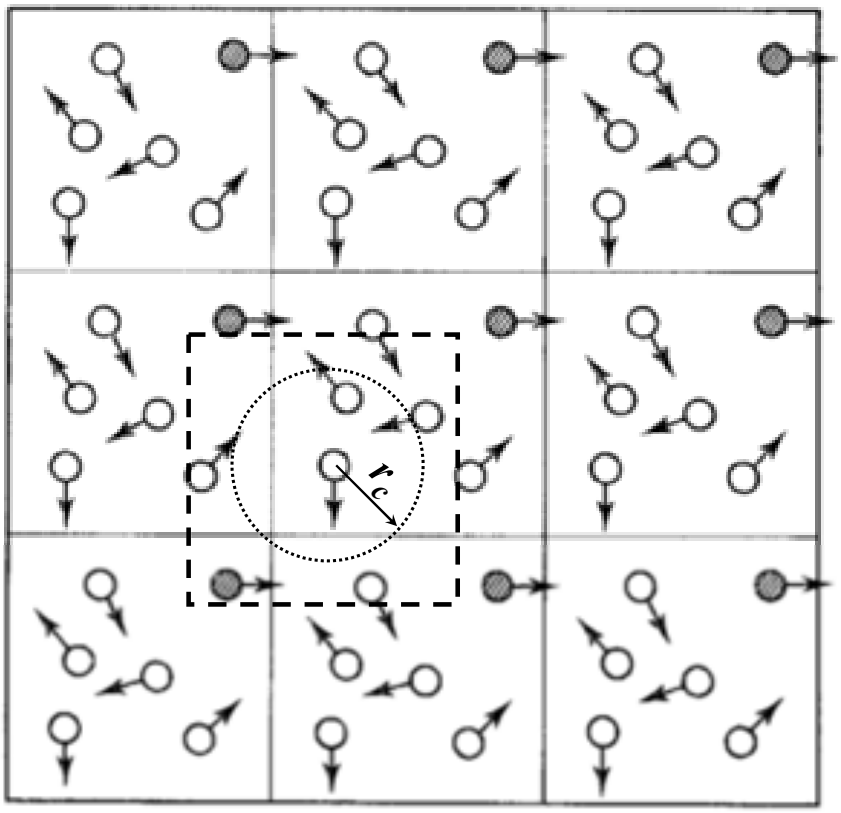

Figure 3.2 Illustration of periodic boundary conditions in 2 dimensions.

Calculations of the potentials and/or the forces of the particles in the system are the heart of the computer simulations, from which the trajectory of the system is obtained (Allen & Tildesley, 1987; Hoover, 1991). However, it is impossible to achieve for the system with periodic boundaries since such conditions extend the system to infinity. The solution is to approximate the potential energy through the minimum image convention, which restricts a particle to interact at most with just one image of every other particle in the system, as indicated by the dashed square in Figure 3.2

(Allen & Tildesley, 1987; Leach, 2001; Metropolis et al., 1953). Based on the minimum image convention, the calculations are further simplified through non-bonded cutoff (Allen & Tildesley, 1987; Leach, 2001). For the short-ranged potentials, such as the Lenard-Jones potential, the majority of the potentials, and thus the forces, results from the close neighbors of the particle of interest. Accordingly, a spherical cutoff with the radius of r_c is applied. As illustrated by the dashed circle in Figure 3.2, the pair potential is set to 0 when the distance between the particles exceeds r_c. It should be noted the magnitude of r_c is not allowed to be larger than half of the box length due to the minimum image convention. In order to save the computing time, the concept of the neighbor list is also introduced, which records the neighboring particles of a particular one in a list (Verlet, 1967). The region of those neighboring particles for the list is supposed to be larger than the cutoff. As a result, only the distance between the particular particle and those in the neighbor list is checked for every time step and the neighbor list is updated every 10 ~ 20 time steps (Leach, 2001).

It should be stressed here the potential cutoff concept is applied to cope with the short-ranged potentials that decays fast with distance but not for the long-ranged ones, such as electrostatic interactions. There are several algorithms for handling the long-ranged forces, for example the Ewald summation method (Allen & Tildesley, 1987; Leach, 2001), having been widely used in simulations for polar or charged systems, including proteins and DNA, which are not introduced here.

3.3 Statistical mechanics

It has been mentioned above that computer simulations deal with molecular interactions at atomic levels, and therefore, provide microscopic information on the system modeled. Statistical mechanics has to be involved for linking the microscopic information to the macroscopic properties (Chandler, 1987; Glazer & Wark, 2001; McQuarrie, 2000).

It is indicated in equation 3.1 that the Hamiltonian, $\mathscr{H}$, of a system depends on the set of the atomic momenta, $\mathbf{p}^N$, and coordinates, $\mathbf{q}^N$. Accordingly, a space with the coordinates of $\mathbf{p}^N$ and $\mathbf{q}^N$ can be defined, which is known as the phase space. The phase space is imagined to have $6N$ dimensions, i.e., 3 directions for momenta and

coordinates for the N atoms, respectively. As a result, each single point, $\mathbf{\Gamma}$, in this $6N$-dimensional phase space represents a system (Allen & Tildesley, 1987; Haile, 1997; Hoover, 1991). However, it is virtually impossible to obtain detailed information for a multi-body system, and the observed energy, i.e., $\mathscr{H}$, actually gives a constant-energy surface in the phase space for the system. Such a surface represents a collection of all possible states of the system with a constant energy, E, and is known as a (microcanonical) ensemble (Allen & Tildesley, 1987; Mandl, 1988; McQuarrie, 2000). According to Gibbs, an observed property, A_{obs}, represents the average of all the possible states of the system, i.e., the ensemble average, $<A(\mathbf{\Gamma})>_{ens}$ (Allen & Tildesley, 1987; Frenkel & Smit, 2002; McQuarrie, 2000). The ensembles are determined by the fixed microscopic parameters, such as the atom number (N), the system volume (V), the system temperature (T) and pressure (P), the system energy (E) and chemical potential (μ). There are four widely-used ensembles as listed in Table 3.1 (Allen & Tildesley, 1987; Mandl, 1988; McQuarrie, 2000).

Table 3.1 Common ensembles with their fixed macroscopic properties.

Ensemble	Fixed properties
Microcanonical	NVE
Canonical	NVT
Isothermal-isobaric	NPT
Grand canonical	μVT

Since there is no evidence to demonstrate that any one possible state of a system is more important than the others, those possible states for a system are postulated to occur with equal probability, which is known as the principle of equal a priori probabilities for an ensemble (Mandl, 1988; McQuarrie, 2000). In terms of such principle, it is possible to obtain the observed macroscopic property A_{obs}, from ensemble average, $<A(\mathbf{\Gamma})>_{ens}$, once the number of possible systems in an ensemble $\Omega(\mathbf{\Gamma})$ is known.

$$A_{obs} = \left\langle A(\mathbf{\Gamma}) \right\rangle_{ens} = \frac{\sum_{\Gamma} \Omega(\mathbf{\Gamma}) A(\mathbf{\Gamma})}{\sum_{\Gamma} \Omega(\mathbf{\Gamma})} \tag{3.4}$$

where $A(\boldsymbol{\Gamma})$ denotes an instantaneous value for a possible state of the system (Allen & Tildesley, 1987; Frenkel & Smit, 2002; McQuarrie, 2000).

Being considered as a fully-fledged subject, statistical mechanics has been comprehensively explained and widely utilized in physics and chemistry. There is only a brief introduction provided here to complete the introduction of computer simulation methods. There are many references introducing statistical mechanics in more detail, such as those from Chandler (1987) and Glazer and Wark (2001), while the work of McQuarrie (2000) is strongly recommended for a full understanding of statistical mechanics.

3.4 Monte Carlo simulations

In the Monte Carlo (MC) methods, configurations of the system are randomly generated according to the Boltzmann factor, $\mathbf{exp}\left\{-\mathscr{V}\left(\mathbf{q}^N\right)/k_BT\right\}$, where k_B and T denote the Boltzmann constant ($=1.38062\times10^{-23}$ J/K) and absolute temperature, respectively (Leach, 2001). Based on the initial system, a disturbance is applied, for instance, by randomly moving one atom or molecule or rotating one or more bonds, to generate a new configuration. The potential energy of the new configuration is then calculated through molecular mechanics methods. This potential energy is employed to determine whether the new configuration is possible. In the case of $\mathscr{V}_{new}\left(\mathbf{q}^N\right)<\mathscr{V}_{old}\left(\mathbf{q}^N\right)$, the new configuration is accepted. However, if the potential energy of the new configuration is found to increase from its predecessor, the Boltzmann factor is used to determine acceptance of the new configuration. The value of $\mathbf{exp}\left\{-\left[\mathscr{V}_{new}\left(\mathbf{q}^N\right)-\mathscr{V}_{old}\left(\mathbf{q}^N\right)\right]/k_BT\right\}$ is calculated and compared with a number, $\mathscr{R}$, randomly picked from 0 to 1. The new configuration will be rejected and generated again in the case of $\mathbf{exp}\left\{-\left[\mathscr{V}_{new}\left(\mathbf{q}^N\right)-\mathscr{V}_{old}\left(\mathbf{q}^N\right)\right]/k_BT\right\}<\mathscr{R}$. Otherwise the new configuration is accepted. An ensemble is approximated by repeating such procedure for a number of times, M times for example. Detailed studies of Monte Carlo methods have shown that the sequence of movements corresponds to a Markov chain of states (Hammersley & Handscomb, 1967). Markov chains, and hence MC simulations can be

shown to reach an equilibrium state after a sufficiently large number of steps regardless of the initial state of the system (Leach, 2001). Thus, once an MC simulation has reached equilibrium, any macroscopic property of the system, <*A*>, is obtained by simply averaging the values of all the configurations as illustrated in equation 3.4 (Leach, 2001).

$$\langle A \rangle = \frac{1}{M} \sum_{i=1}^{M} A_i \left(\mathbf{q}^N \right) \tag{3.5}$$

3.5 Molecular Dynamics

Unlike the MC methods, the molecular dynamics (MD) methods use a more straightforward concept for simulating the system. Experimentally, an observed property, A_{obs}, of a system are considered as the time average of the collection of the instantaneous properties, $A(\mathbf{\Gamma})$, for a long time (Allen & Tildesley, 1987; Frenkel & Smit, 2002). It is believed in statistical mechanics that a long-time trajectory of a system experiences the whole available surface in the phase space unless the system is trapped in some meta-stable states, which is known as the ergodic hypothesis (Frenkel & Smit, 2002; Haile, 1997; Hoover, 1991; McQuarrie, 2000). Therefore, results from the MD simulations are supposed to be the same as those from the MC methods provided the evolution time is long enough (Frenkel & Smit, 2002). Moreover, the former has the advantage over the latter in giving an access to time-dependent properties of the modeling system (Allen, 2004).

3.5.1 Hamiltonian dynamics

In the MD methods, the so called Hamiltonian dynamics is usually employed to solve the equations of the motion for the system because the Hamiltonian, $\mathscr{H}$, is not only a function of the momenta and coordinates, ($\mathbf{p}^N$, $\mathbf{q}^N$), of the atoms in the system, but also of the time, t (Allen & Tildesley, 1987; Haile, 1997; Tuckerman, 2010). Strictly, $\mathscr{H}$ is defined as

$$\mathscr{H}\left(\mathbf{p}^N, \mathbf{q}^N \right) = \sum_{i}^{N} \dot{\mathbf{q}}_i \mathbf{p}_i - \mathscr{L}\left(\mathbf{q}^N, \dot{\mathbf{q}}^N \right) \tag{3.6}$$

where $\mathscr{L}\left(\mathbf{q}^N, \dot{\mathbf{q}}^N \right)$ is the Lagrangian equation of motion defined as

$$\mathscr{L}\left(\mathbf{q}^N, \dot{\mathbf{q}}^N\right) = \mathscr{K}\left(\dot{\mathbf{q}}^N\right) - \mathscr{V}\left(\mathbf{q}^N\right) \tag{3.7}$$

with the kinetic energy $\mathscr{K}\left(\dot{\mathbf{q}}^N\right) = \sum_{i=1}^{N} m_i \left|\dot{\mathbf{q}}_i\right|^2 / 2$ according to classical mechanics. In the applications of the Hamiltonian formulation, forces are defined as vector quantities derived from a scalar function, as is the case in MD simulations, where the force acting on the *i*th atom (or molecule), $\mathbf{F}_i$, is derivable from the potential $\mathscr{V}$, i.e.,

$$\mathbf{F}_i = -\frac{\partial \mathscr{V}\left(\mathbf{q}^N\right)}{\partial \mathbf{q}_i} \tag{3.8}$$

Accordingly, the following equation can be obtained from the Lagrangian that

$$\frac{d}{dt}\left(\partial \mathscr{L} / \partial \dot{\mathbf{q}}_i\right) - \left(\partial \mathscr{L} / \partial \mathbf{q}_i\right) = 0 \tag{3.9}$$

since $\frac{d}{dt}\left(\partial \mathscr{L} / \partial \dot{\mathbf{q}}_i\right) = m_i \ddot{\mathbf{q}}_i = \mathbf{F}_i$ and $\partial \mathscr{L} / \partial \mathbf{q}_i = -\partial \mathscr{V} / \partial \mathbf{q}_i = \mathbf{F}_i$, where $\ddot{\mathbf{q}}_i$ is the acceleration (also expressed as **a**) of the *i*th atom (or molecule) according to Newton's second law. The momentum, $\mathbf{p}_i$, conjugate to the coordinate, $\mathbf{q}_i$, of the *i*th atom (or molecule) is defined as $\mathbf{p}_i = \partial \mathscr{L} / \partial \dot{\mathbf{q}}_i = m_i \dot{\mathbf{q}}_i$ from equation 3.9.

The Hamiltonian, $\mathscr{H}$, is usually used in molecular dynamics because as illustrated in equations 3.1 and 3.2, it is a function of coordinates, $\mathbf{q}^N$, and their conjugate momenta, $\mathbf{p}^N$, of the atoms in the system, and time, *t*. The time derivative of $\mathscr{H}$ is expressed as

$$\frac{d\mathscr{H}}{dt} = \sum_i \frac{\partial \mathscr{H}}{\partial \mathbf{p}_i} \cdot \dot{\mathbf{p}}_i + \sum_i \frac{\partial \mathscr{H}}{\partial \mathbf{q}_i} \cdot \dot{\mathbf{q}}_i + \frac{\partial \mathscr{H}}{\partial t} \tag{3.10}$$

According to equation 3.6,

$$\frac{\partial \mathscr{H}}{\partial \mathbf{p}_i} = \frac{\mathbf{p}_i}{m} = \dot{\mathbf{q}}_i \tag{3.11}$$

$$\frac{\partial \mathscr{H}}{\partial \mathbf{q}_i} = -\frac{\partial \mathscr{L}}{\partial \mathbf{q}_i} = -\frac{d}{dt}\left(\frac{\partial \mathscr{L}}{\partial \dot{\mathbf{q}}_i}\right) = -\dot{\mathbf{p}}_i \tag{3.12}$$

There is no explicit time dependence in $\mathscr{H}(\mathbf{p}^N, \mathbf{q}^N)$, i.e., $\partial \mathscr{H} / \partial t = 0$, and according to equation 3.10 to 3.12, it is found that

$$\frac{d\mathscr{H}}{dt} = \sum_i \frac{\partial \mathscr{H}}{\partial \mathbf{p}_i} \cdot \dot{\mathbf{p}}_i + \sum_i \frac{\partial \mathscr{H}}{\partial \mathbf{q}_i} \cdot \dot{\mathbf{q}}_i = 0 \tag{3.13}$$

In other words, the Hamiltonian, $\mathscr{H}$, is simply the total energy of the system as a

function of the momenta and positions of the atoms (Haile, 1997; Tuckerman, 2010). One of the great advantages of Hamilton's equations of motion, i.e., equations 3.11 and 3.12, is that they change the differential equations from second-order (as for Newton's second law) to first-order, which saves a lot of time for computing (Haile, 1997; Tuckerman, 2010). Moreover, the Hamiltonian, $\mathscr{H}$, is independent of time even for non-isolated systems as illustrated in equation 3.13.

3.5.2 Verlet algorithm

Equations 3.3 and 3.8 show that, the forces acting on each atom in the system are determined by its position and the positions of those atoms interacting with it. As a result, the continuous potentials between atoms couple the motions of all the atoms (or molecules) together, making it unfeasible to analytically solve such many-body problems (Leach, 2001). Under such circumstances, finite difference methods are applied to integrate the equations of motion, of which the Verlet algorithm proposed by Verlet (1967) is the most widely used for molecular dynamic simulations.

The basic assumption of a finite difference method is that the atomic positions, $\mathbf{q}$, and dynamic properties, i.e., velocity, $\dot{\mathbf{q}}$, and acceleration, $\ddot{\mathbf{q}}$, and so on, are approximated as Taylor series expansions

$$\mathbf{q}(t+\delta t)=\mathbf{q}(t)+\delta t\cdot\dot{\mathbf{q}}(t)+\frac{1}{2}\delta t^2\cdot\ddot{\mathbf{q}}(t)+\frac{1}{6}\delta t^3\cdot\dddot{\mathbf{q}}(t)+\frac{1}{24}\delta t^4\cdot\ddddot{\mathbf{q}}(t)+\cdots$$

$$\dot{\mathbf{q}}(t+\delta t)=\dot{\mathbf{q}}(t)+\delta t\cdot\ddot{\mathbf{q}}(t)+\frac{1}{2}\delta t^2\cdot\dddot{\mathbf{q}}(t)+\frac{1}{6}\delta t^3\cdot\ddddot{\mathbf{q}}(t)+\cdots$$

$$\ddot{\mathbf{q}}(t+\delta t)=\ddot{\mathbf{q}}(t)+\delta t\cdot\dddot{\mathbf{q}}(t)+\frac{1}{2}\delta t^2\cdot\ddddot{\mathbf{q}}(t)+\cdots$$

$$\dddot{\mathbf{q}}(t+\delta t)=\dddot{\mathbf{q}}(t)+\delta t\cdot\ddddot{\mathbf{q}}(t)+\cdots$$

$$\cdots$$

where δt represents the time step in the simulation after the time point, t. Based on the Taylor expansions, the Verlet algorithm approximates the positions at (t-δt) and (t+δt) as,

$$\mathbf{q}(t-\delta t)=\mathbf{q}(t)-\delta t\cdot\dot{\mathbf{q}}(t)+\frac{1}{2}\delta t^2\cdot\ddot{\mathbf{q}}(t)-\cdots$$

$$\mathbf{q}(t+\delta t)=\mathbf{q}(t)+\delta t\cdot\dot{\mathbf{q}}(t)+\frac{1}{2}\delta t^2\cdot\ddot{\mathbf{q}}(t)-\cdots$$

Therefore, by adding the two equations above, the new positions at (t+δt) can be approximated with the current positions and accelerations, $\mathbf{q}(t)$ and $\ddot{\mathbf{q}}(t)$, and the previous positions, $\mathbf{q}(t\text{-}\delta t)$, i.e.,

$$\mathbf{q}(t+\delta t) = 2\mathbf{q}(t) - \mathbf{q}(t-\delta t) + \delta t^2 \cdot \ddot{\mathbf{q}}(t) \tag{3.14}$$

While the velocity of the atoms, $\dot{\mathbf{q}}(t)$, is calculated as the average velocity between time (t-δt) and (t+δt)

$$\dot{\mathbf{q}}(t) = \frac{\mathbf{q}(t+\delta t) - \mathbf{q}(t-\delta t)}{2\delta t} \tag{3.15}$$

As indicated in equation 3.14, it is from $\mathbf{q}(t)$ and $\mathbf{q}(t\text{-}\delta t)$ that $\mathbf{q}(t\text{+}\delta t)$ can be calculated, which makes a problem for the first step since there is only one set of atomic coordinate, i.e., $\mathbf{q}(0)$. In practice, the positions $\mathbf{q}(\text{-}\delta t)$ is obtained from the Taylor series with the truncation after the first term, as shown in Figure 3.3 (Leach, 2001). The concept of the Verlet algorithm is explained in detail in Figure 3.3. This method is straightforward and has modest storage costs for computing. However, there are some drawbacks of the Verlet algorithm. One of the most important disadvantages of the Verlet algorithm is the loss of precision due to adding a small term, $[\delta t^2 \cdot \ddot{\mathbf{q}}(t)]$, to the difference of two large terms, i.e., $[2\mathbf{q}(t) - \mathbf{q}(t-\delta t)]$. Secondly, it is difficult to obtain the velocity in the Verlet algorithm, and $\dot{\mathbf{q}}(t)$ is inaccessible until the positions of the next time step, $\mathbf{q}(t+\delta t)$, is available (Leach, 2001). As a result, several modifications have been proposed to the Verlet algorithm.

The leap-frog algorithm was proposed by Hockney (1970), where the velocities at the time (t+δt/2) is firstly calculated and the positions at the time (t+δt) are then deduced

$$\dot{\mathbf{q}}(t+\delta t/2) = \dot{\mathbf{q}}(t-\delta t/2) + \delta t \cdot \ddot{\mathbf{q}}(t) \tag{3.16}$$

$$\mathbf{q}(t+\delta t) = \mathbf{q}(t) + \delta t \cdot \dot{\mathbf{q}}(t+\delta t/2) \tag{3.17}$$

As shown in equations 3.16 and 3.17, there is no explicit term involving the velocities at the time (t+δt), and they are calculated as the average of the velocities from (t-δt/2) to (t+δt/2)

$$\dot{\mathbf{q}}\left(t+\delta t\right)=\frac{\dot{\mathbf{q}}\left(t+\delta t/2\right)+\dot{\mathbf{q}}\left(t-\delta t/2\right)}{2} \tag{3.18}$$

Since there is no term obtained from the difference between two large numbers, the precision of the leap-frog algorithm is improved. However, as found in equations 3.16 and 3.17, the velocities and positions calculated from such algorithm are not synchronized, making it impossible to obtain the kinetic and potential energies simultaneously.

The velocity Verlet method is a modified form of the Verlet algorithm, where velocities, positions and accelerations are calculated at the same time step without loss of precision (Swope, Andersen, Berens, & Wilson, 1982). In this method, new positions are obtained following the Taylor series with a truncation at the second order, while the new velocities are calculated from the average of the current and new accelerations

$$\mathbf{q}\left(t+\delta t\right)=\mathbf{q}\left(t\right)+\delta t\cdot\dot{\mathbf{q}}\left(t\right)+\frac{\delta t^{2}\cdot\ddot{\mathbf{q}}\left(t\right)}{2} \tag{3.19}$$

$$\dot{\mathbf{q}}\left(\delta t\right)=\dot{\mathbf{q}}\left(0\right)+\delta t\cdot\frac{\left[\ddot{\mathbf{q}}\left(0\right)+\ddot{\mathbf{q}}\left(\delta t\right)\right]}{2} \tag{3.20}$$

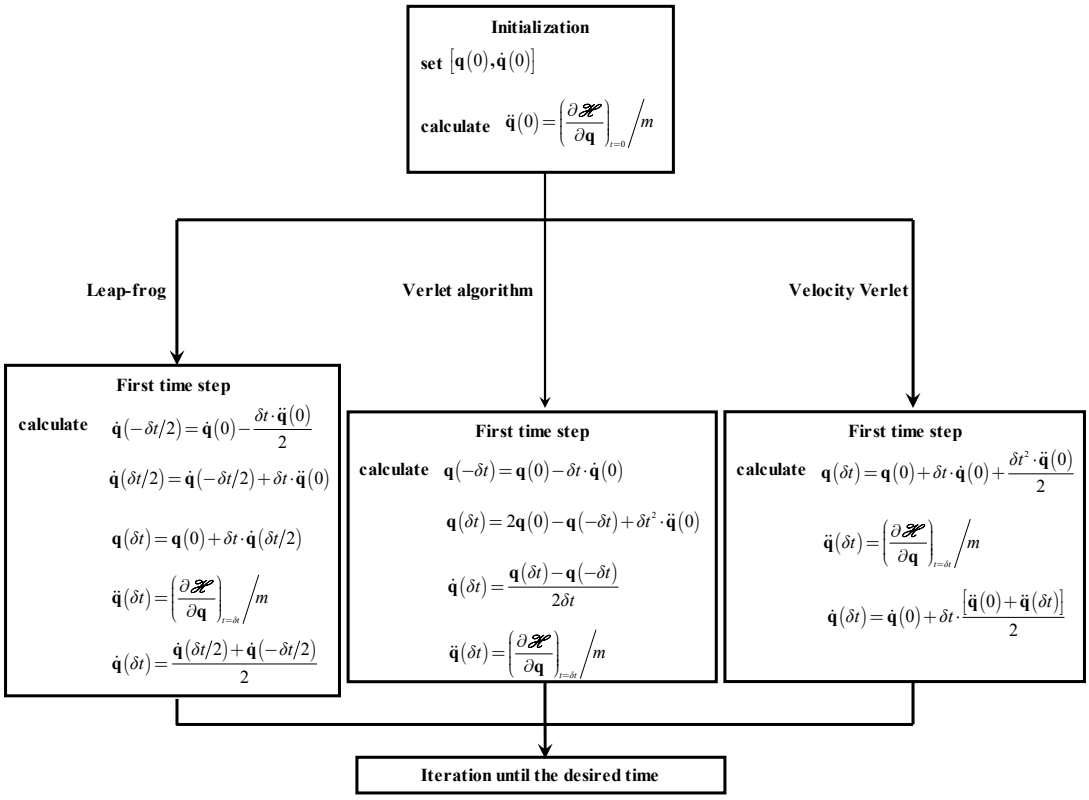

Figure 3.3 Procedure of a MD simulation with the Verlet algorithm and the modified methods.

Besides the finite difference methods, other strategies, such as the predictor-corrector integration methods, can also be found in some MD simulations, but are not discussed here. It is difficult to state which integration method is better than the others, since more accurate and precise results are usually at the expense of storage and time for computation. Nevertheless, there are still some factors providing suggestions on the choice of integration methods. The most important factor is considered as the energy conservation during the simulations (Leach, 2001). Fincham and Heyes (1982) concluded that the Verlet algorithm gave better energy conservation in simulations with longer time steps. Moreover, considering the synchronisation of velocities and positions, and self-starting properties, i.e., no term of time (t-δt) involved, the velocity Verlet method could be recommended. These integration algorithms have been successfully applied in computer modeling packages, for instance GROMACS, where the leap-frog and the velocity Verlet algorithms are commonly used.

3.5.3 Constraint dynamics

It is well known that the intramolecular bonds experience vibrations, including stretching and bending, altering the bond lengths and angles, respectively. Additionally, torsional motions of the bonds also exist, which change the dihedrals. Bond vibrations are of less importance than their torsional motions in determining the conformation of polyatomic molecules, such as proteins (Allen & Tildesley, 1987; B. Hess, Bekker, Berendsen, & Fraaije, 1997; Leach, 2001). However, the length of each time step of a molecular dynamics simulation is dictated by the bond vibrations rather than the torsional motions because of the high frequency of the former (Leach, 2001). Therefore, constraints are imposed on the molecules to fix the bond lengths and angles in classical molecular dynamics simulations so that the time step is increased without prejudiced accuracy (Allen & Tildesley, 1987; Leach, 2001).

Constraints are often categorized as holonomic and non-holonomic types, depending on the required conditions to be satisfied for the constraints along a trajectory (Allen & Tildesley, 1987; Leach, 2001; Tuckerman, 2010). For the holonomic constraints, the relationship of the particle positions and/or time is constrained, while the non-holonomic constraints restrict both the particle positions and velocities, as shown in equation 3.21 and 3.22, respectively,

$$g_k(\mathbf{q},t) = 0 \qquad k = 1,\ldots,N_C \tag{3.21}$$

$$g_k(\mathbf{q},\dot{\mathbf{q}}) = 0 \qquad k = 1,\ldots,N_C \tag{3.22}$$

where N_C represents the number of the constraints (Leach, 2001).

Generally, two types of forces are defined for the equations of motion for a constrained system. The normal forces, $\mathbf{F}_i$, on the atom, i, as introduced in equation 3.8, resulting from the intra- and intermolecular interactions and being calculated in terms on the potential energy. The second one is the constraint force, $\mathbf{F}_C$, which maintains the required conditions for the constrained system, and is expressed as

$$\mathbf{F}_{Ck} = \lambda_k \frac{\partial g_k}{\partial \mathbf{q}} \tag{3.23}$$

where λ_k is the Lagrange multiplier to determine for the k-th constraint (Allen, 2004;

Allen & Tildesley, 1987; B. Hess et al., 1997; Leach, 2001).

It is clear that the constraint is holonomic in the case of fixing the intramolecular bonds and for the two atoms *i* and *j* connected by a bond the conditions are required to be

$$\left|\mathbf{r}_{ij}\right|^2 = \left(\mathbf{q}_i - \mathbf{q}_j\right)^2 - d_{ij}^2 = 0 \tag{3.24}$$

where $\mathbf{r}_{ij}$ is distance between the two atoms *i* and *j*, and d_{ij} is the length of the bond connecting atom *i* and *j* with a prescribed value.

According to equations 3.14, 3.23 and 3.24, the Verlet algorithm for a constrained system is obtained as

$$\mathbf{q}_i\left(t+\delta t\right) = 2\mathbf{q}_i\left(t\right) - \mathbf{q}_i\left(t-\delta t\right) + \frac{\delta t^2}{m_i}\mathbf{F}_i\left(t\right) + \sum_k \frac{\lambda_k \delta t^2}{m_i}\mathbf{r}_{ij}\left(t\right) \tag{3.25}$$

where $\mathbf{F}_i$ is the normal force on atom *i* and calculated from equation 3.8. The last term on the right side represents the contribution from the constraints and is obtained from equations 3.23 and 3.24. Since equation 3.25 separates the contributions to the position of the atom *i* in to normal and constrained part, and there only one constraint between the atom *i* and *j*, i.e., the fixed bond length, it is rewritten as

$$\mathbf{q}_i^{con}\left(t+\delta t\right) = \mathbf{q}_i^{unc}\left(t+\delta t\right) + \frac{\lambda_{ij}\delta t^2}{m_i}\mathbf{r}_{ij}\left(t\right) \tag{3.26}$$

where the superscripts ^{con} and ^{unc} denote constrained and unconstrained, respectively. According to the Newton's third law, the constraint force acting on the atom *j* from *i* is of the same amplitude but opposite directions, and thus

$$\mathbf{q}_i^{con}\left(t+\delta t\right) = \mathbf{q}_i^{unc}\left(t+\delta t\right) - \frac{\lambda_{ij}\delta t^2}{m_i}\mathbf{r}_{ij}\left(t\right) \tag{3.27}$$

Combined with equation 3.24, it is possible to calculate the constrained positions of atoms *i* and *j* as well as the Lagrange multiplier, λ_{ij}, from equations 3.26 and 3.27. However, it is algebraicallty complicated to solve such equations, especially for polyatomic molecules containing a large number of atoms and constraints, and fortunately, some algorithms have been proposed to cope with this dilemma (Allen, 2004; Allen & Tildesley, 1987; B. Hess et al., 1997; Leach, 2001).

The SHAKE algorithm was proposed by Ryckaert, Ciccotti, and Berendsen (1977),

which considers and solves the constraints sequentially. Since the solutions for one constraint probably lead to violations against other constraints, the calculations have to be applied iteratively until all the constraints are satisfied within a tight tolerance, which means that the fluctuations caused from the SHAKE algorithm are smaller than those from the other sources, such a the potential cutoff. Another widely used algorithm, the LINear Constraint Solver (LINCS) was proposed by B. Hess et al. (1997), who projected the bonds on the directions of the original bonds. By setting the length of the projected images of the bonds, the authors managed to obtain the bonds with prescribed values. It should be noted that the new constrained positions are obtained from the old positions and the new unconstrained positions through either the SHAKE or the LINCS algorithm. However, the LINCS is 3 ~ 4 times faster than the SHAKE algorithm (B. Hess et al., 1997). Besides, since there is no iterative procedure in the LINCS, this algorithm is much easier to parallelize over several processors, which is of great help and importance for simulations of large molecules and make this algorithm widely used in simulation packages, such as GROMACS (B. Hess et al., 1997; B. Hess, Kutzner, van der Spoel, & Lindahl, 2008; van der Spoel et al., 2005).

3.5.4 Temperature and pressure coupling

In early MD studies, simulations were mainly performed in the microcanonical (*NVE*) ensemble, where the energy, *E*, of the system is fixed. However, canonical (*NVT*) ensembles are more essential in some systems, especially when the temperature-dependent behaviour of the system is of interests, such as unfolding of proteins. It was not until a practical way of controlling temperature was proposed by Andersen (1980) that simulations in the *NVT* ensemble were achieved, even though his method was not widely used (Bussi, Donadio, & Parrinello, 2007). Generally, temperature coupling is realized based on the definition of the kinetic temperature, $\mathscr{T}$, (McQuarrie, 2000; Moore, 1976)

$$\mathscr{T} = \frac{1}{3\left(N - N_c\right)} \sum_{i=1}^{N} \left|\mathbf{p}_i\right|^2 \Big/ m_i \tag{3.28}$$

where N_c is the number of internal constraints, i.e., fixed bond lengths and angles, in

the *N*-atom system (Allen & Tildesley, 1987). According to equation 3.28, the average of the kinetic temperature can be set to a target temperature, *T*, by adjusting the velocities, $\dot{\mathbf{q}}_i$, and thus, the momenta, $\mathbf{p}_i$, of the system.

There have been several methods proposed to achieve the adjustment of the velocities. Andersen (1980) performed a collision on a randomly selected particle in the system to transfer energies, but this method was not widely applied due to the introduction of discontinuous trajectories (Bussi et al., 2007). The most widely used methods are connecting the system with a thermostat, such as Berendsen, Postma, Van Gunsteren, Di Nola, and Haak (1984) and Bussi et al. (2007), or extend the system with a reservoir (Hoover, 1985; Nosé, 1984), of which the former is briefly introduced here because of the complexity of the latter.

In the Berendsen et al. (1984) method, the system is coupled with an external heat bath with the fixed desired temperature, T_{bath}. The velocities of the system are scaled at each step as the bath supplies or removes heat from the system, and the rate of change in temperature, $dT(t)/dt$, is proportional to the difference between the bath and system temperatures, T_{bath} and $T(t)$, respectively

$$\frac{dT(t)}{dt} = \frac{T_{\text{bath}} - T(t)}{\tau_T} \tag{3.29}$$

where τ_T is a coupling parameter determining the strength of the connection between the bath and the system. As a result, the Berendsen thermostat give an exponential decay of $T(t)$ towards T_{bath}, i.e., the desired temperature. As indicated in equation 3.28, the system temperature is proportional to the kinetic energy of the system, i.e., $\left|\dot{\mathbf{q}}_i\right|^2$, and thus, the rescaling factor, $\lambda_{\dot{\mathbf{q}}}$, used for generating new velocities, $\dot{\mathbf{q}}_i' = \lambda_{\dot{\mathbf{q}}}\dot{\mathbf{q}}_i$, at each step is obtained as

$$\lambda_{\dot{\mathbf{q}}}^2 = \frac{T(t) + \delta t \cdot dT(t)/dt}{T(t)} = 1 + \frac{\delta t}{\tau_T}\left[\frac{T_{\text{bath}}}{T(t)} - 1\right] \tag{3.30}$$

where it can be found the τ_T is inversely proportional to the strength of the connection between the bath and the system. The Berendsen thermostat is stable and simple and therefore is widely employed in MD simulations. However, there is no conserved quantity to indicate the canonical sampling in such method (Bussi et al., 2007). Bussi

et al. (2007) improved the Berendsen thermostat by a velocity-rescaling thermostat, where $\lambda_{\dot{\mathbf{q}}}$ is obtained from the target kinetic energy, K_t, which is drawn from the canonical equilibrium distribution and thus enforces canonical sampling. The single rescaling factor, $\lambda_{\dot{\mathbf{q}}}$, is used to rescale the velocities of all the atoms in the system, so that the bond lengths are intact. Moreover, the authors defined a conserved effective energy, $\tilde{H}(t)$, indicating the balance in the energy fluxes between the system and the thermostat, and proposed to measure the accuracy of canonical samplings with such conserved quantity.

In a similar way to the temperature coupling, pressure coupling is achieved through changing the volume, V, of the system, according to the relationship between the pressure P, and the volume, V,

$$\beta_T = -\frac{1}{V}\left(\frac{\partial V}{\partial P}\right)_T \tag{3.31}$$

where β_T is the isothermal compressibility coefficient of the system (Zhang & Scanlon, 2011). Analogous to the thermostat, in a barostat a coupling parameter, τ_P, the bath pressure, P_{bath}, and scaling factor for volume, λ_V, are introduced (Berendsen et al., 1984)

$$\frac{dP(t)}{dt} = \frac{P_{\text{bath}} - P(t)}{\tau_P} \tag{3.32}$$

and

$$\lambda_V = \frac{V(t) + \delta t \cdot dV(t)/dt}{V(t)} = 1 - \beta_T \frac{\delta t}{\tau_P}\left[P_{\text{bath}} - P(t)\right] \tag{3.33}$$

The volume of the system is rescaled through adjusting the coordinates of the atoms, i.e., $\mathbf{q}_i' = \lambda_V^{1/3}\mathbf{q}_i$.

Besides the Berendsen barostat, other strategies have been also proposed, such as the extended system methods (Andersen, 1980), and constraint methods (Evans & Morriss, 1983, 1984), which will not be discussed here. An alternative method with changes in the box shape as well as its size for pressure coupling is also widely used in MD simulations (Parrinello & Rahman, 1980, 1981).

3.6 Water molecule models

Since water is a very important component and solvent in life, it is usually involved in computer simulations, especially those for proteins and DNA. However, the molecular structure of water is so complex that it can only be described in the framework of quantum mechanics, which is not applicable for MD simulations (Bytnar, Kucaba-Piętal, & Walenta, 2009). Therefore, water models are introduced for simulations to simplify the water molecular structure and reproduce the experimental data. The potentials between water molecules, *a* and *b*, are calculated as the sum of the Lenard-Jones potential between the oxygen (O) atoms and the Columbic interactions between the two molecules

$$\mathscr{V}_{ab} = 4\varepsilon_0\left[\left(\frac{\sigma_0}{r_{\mathrm{OO}}}\right)^{12} - \left(\frac{\sigma_0}{r_{\mathrm{OO}}}\right)^{6}\right] + \sum_{ij}\frac{q_i q_j}{4\pi\varepsilon_0 r_{ij}} \tag{3.34}$$

where r_{OO} and r_{ij} denote the distances between the two O atoms and between different charges, respectively (Berendsen, Grigera, & Straatsma, 1987; Jorgensen, 1981; Jorgensen, Chandrasekhar, Madura, Impey, & Klein, 1983; Mahoney & Jorgensen, 2000).

Generally, the result of equations 3.34 is adjusted by selecting the geometric shapes of the water molecule models and the force field for the calculation. There are 4 geometrical shapes as shown in Figure 3.4 that are most frequent used for water molecule models (Bytnar et al., 2009). It is clear in Figure 3.4 that the shapes of water models vary depending on the distribution of the charges on the molecule. Type (a) represents a 3-site molecule where each atom is assigned the corresponding charge (1 positive for H and 2 negative for O, and therefore, the O atom contribute to both of the Lenard-Jones the Columbic interactions. As for the type (b) and (c), a dummy atom is created to take the negative charges and the atom O only responds for the Lenard-Jones potential in equation 3.34. Type (d) is a 5-site model with the negative charges split and forming a lone pair of electrons.

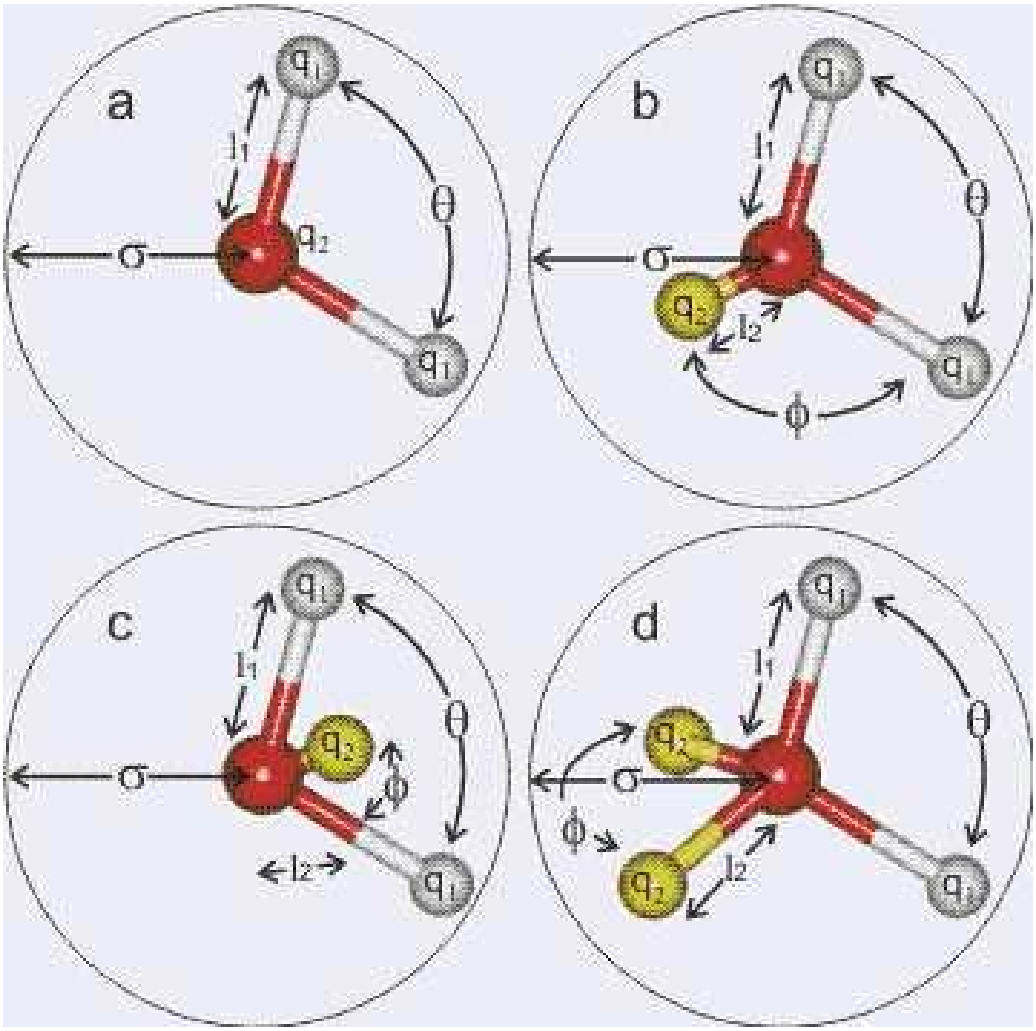

Figure 3.4 most frequent used geometrical shapes for water molecule models.

Based on the shapes, water molecule models can be categorized as 3-site, 4-site and 5-site. The most commonly used models SPC (Berendsen, Postma, van Gunsteren, & Hermans, 1981), SPC/E (Berendsen et al., 1987) and TIP3P (Jorgensen, 1981) are 3-site molecules, while TIP4P (Jorgensen et al., 1983) and TIP5P (Mahoney & Jorgensen, 2000) are 4-site and 5-site, respectively. The model parameters for these models are listed in Table 3.2. From those parameters, interactions, including Lenard-Jones potential and Columbic interactions as shown in equation 3.3 and 3.34, between water molecules and other substances could be obtained. Beside, physical properties of water could also be predicted and calculated based on equation 3.34 and those parameters for different water models.

Table 3.2 Parameters of different water molecule models (data from the corresponding reference)

Model	Type	σ (Å)	Lenard-Jones (kJ/mol)	l_1 (Å)	l_2 (Å)	q_1 (e)	q_2 (e)	θ°	φ°
SPC	**A**	3.16600	0.6500	1.0000	-	+0.4100	-0.8200	109.47	-
SPC/E	**A**	3.16600	0.6500	1.0000	-	+0.4238	-0.8476	109.47	-
TIP3P	**A**	3.15061	0.6364	0.9572	-	+0.4170	-0.8340	104.52	-
TIP4P	**C**	3.15365	0.6480	0.9572	0.06	+0.5200	-1.0400	104.25	52.26
TIP5P	**D**	3.12000	0.6694	0.9572	0.70	+0.2410	-0.2410	104.52	109.47

Besides different geometric shapes and parameters, the water molecule models were also developed in different force fields, i.e., the parameters for the Lenard-Jones potential in equation 3.34 are different. For instance, the SPC and SPC/E models were developed in GROMOS while TIP3P and TIP4P, and TIP5P were developed in AMBER and OPLS, respectively. Although developed in some specific force field, those models are often adopted to other force fields (van der Spoel, van Maaren, & Berendsen, 1998). Some studies have compared different water molecule models, but it is inadvisable to conclude one is superior to the others since no model available is able to reproduce all the properties of water with good accuracy (Mahoney & Jorgensen, 2000). Practically, water molecule models are selected depending on the force field and the consideration of computational cost and accuracy.

3.7 Applications of the MD simulations

Since 1977 when the first MD simulation was applied to a small protein in vacuum for 9.2 ps (McCammon, Gelin, & Karplus, 1977), such techniques have been widely used in studies on protein molecules, since they provide details of time dependent motions of individual atoms and thus give access to some special properties, such as pathway of protein folding (Zhou & Karplus, 1999) and lifetime of hydrogen bonds (Luzar & Chandler, 1996; van der Spoel, van Maaren, Larsson, & Tîmneanu, 2006). Nowadays, with the developments in computing power and improvements in potential functions, it is routine to run simulations on much larger proteins for longer time (up to 100 ns) in more complicated solvent (e.g., water and salt) at higher stability and accuracy (Karplus & Kuriyan, 2005; Mackerell Jr., 2004).

Bio-molecules, e.g., proteins, lipids and carbohydrates, play important roles in functionalities of food system and are of great interest for researchers who attempt to explain and improve the food properties. MD simulations are considered a powerful supplement to experiments in this field. The tertiary structures of the caseins, for instance, are difficult to experimentally determine since those proteins cannot be crystallized. Therefore, modeling techniques have been used and the conformations of α_{s1}-, β- and κ-casein were successfully accessed based on their primary and secondary structures (Kummosinski, Brown, & Farrell, 1991, 1993a, 1993b), which were found to be much looser structures than globular proteins. Besides predictions of protein conformations, MD simulations are also performed for structural changes during protein denaturation, especially for those globular proteins whose tertiary structures are available with high resolution from X-ray crystallography and NMR. Euston, Ur-Rehman, and Costello (2007) have simulated heat-induced unfolding of β-lactoglobulins and found the loss of α-helix and relative preservation of β-sheet structures, which were consistent with experimental observations (Belloque & Smith, 1998; Panick, Malessa, & Winter, 1999; Qi et al., 1997). Besides the molecular levels, MD simulations have also been used to explain phenomena in food systems. Protein absorption, for example, has been modeled and it has been concluded that α-helices unfolded much faster than β-sheet based on the simulations of absorption of peptide fragments to a solid surface (Raffaini & Ganazzoli, 2003, 2004).

3.8 References

Adams, D.J. (1979). Computer simulation of ionic systems: The distorting effects of the boundary conditions. *Chemical Physics Letters, 62*(2), 329-332.

Alder, B.J., & Wainwright, T.E. (1957). Phase transition for a hard sphere system. *Journal of Chemical Physics, 27*(5), 1208-1209.

Alder, B.J., & Wainwright, T.E. (1959). Studies in molecular dynamics. I. General method. *Journal of Chemical Physics, 31*(2), 459-466.

Allen, M.P. (2004). Introduction to molecular dynamics simulation. In D. Frenkel, N. Attig, K. Binder, H. Grubmüller & K. Kremer (Eds.), *Computational Soft Matter: From Synthetic Polymers to Proteins, Lecture Notes* (Vol. 23, pp. 1-28). Jülich, Germany: John von Neumann Institute for Computing.

Allen, M.P., & Tildesley, D.J. (1987). *Computer Simulation of Liquids*. UK: Oxford

University Press.
Andersen, H.C. (1980). Molecular dynamics simulations at constant pressure and/or temperature. *Journal of Chemical Physics, 72*(4), 2384-2393.
Belloque, J., & Smith, G.M. (1998). Thermal denaturation of β-lactoglobulin. A ^{1}H NMR study. *Journal of Agricultural & Food Chemistry, 46*(5), 1805-1813.
Berendsen, H.J.C., Grigera, J.R., & Straatsma, T.P. (1987). The missing term in effective pair potentials. *The Journal of Physical Chemistry, 91*(24), 6269-6271.
Berendsen, H.J.C., Postma, J.P.M., Van Gunsteren, W.F., Di Nola, A., & Haak, J.R. (1984). Molecular dynamics with coupling to an external bath. *Journal of Physical Chemistry, 81*(8), 3684-3690.
Berendsen, H.J.C., Postma, J.P.M., van Gunsteren, W.F., & Hermans, J. (1981). Interaction models for water in relation to protein hydration. In B. Pullman (Ed.), *Intermolecular Forces* (pp. 331-342). Dordrecht, Holland: D . Reidel Publishing Company.
Bussi, G., Donadio, D., & Parrinello, M. (2007). Canonical sampling through velocity rescaling. *Journal of Chemical Physics, 126*(1), 014101(014101-014107).
Bytnar, J., Kucaba-Piętal, A., & Walenta, Z. (2009). Effects of molecular water models on Molecular Dynamic simulation of nanoflows. *Proceedings in Applied Mathematics and Mechanics, 9*(1), 653-654.
Chandler, D. (1987). *Introduction to Modern Statistical Mechanics*. New York, USA: Oxford University Press.
Cornell, W.D., Cieplak, P., Bayly, C.I., Gould, I.R., Merz, K.M., Ferguson, D.M., et al. (1995). A second generation force field for the simulation of proteins, nucleic acids, and organic molecules. *Journal of The American Chemical Society, 117*(19), 5179-5197.
Euston, S.R., Ur-Rehman, S., & Costello, G. (2007). Denaturation and aggregation of b-lactoglobulin - a preliminary molecular dynamics study. *Food Hydrocolloids, 21*(7), 1081-1091.
Evans, D.J., & Morriss, G.P. (1983). The isothermal/isobaric molecular dynamics ensemble. *Physics Letters A, 98*(8-9), 433-436.
Evans, D.J., & Morriss, G.P. (1984). Non-Newtonian molecular dynamics. *Computer Physics Reports, 1*(6), 297-343.
Fincham, D., & Heyes, D.M. (1982). Integration algorithm in molecular dynamics. *CCP5 Quarterly, 6*, 4-10.
Frenkel, D., & Smit, B. (2002). *Understanding Molecular Simulation From Algorithms to Applications*. UK: Academic Press.
Glazer, A.M., & Wark, J.S. (2001). *Statistical Mechanics A Survival Guide*. New York, USA: Oxford University Press.
González, M.A. (2011). Force fields and molecular dynamics simulations. *Collection SFN, 12*, 169-200.
Haile, J.M. (1997). *Molecular Dynamics Simulation Elementary Methods* (Paperback ed.). United States: Jhon Wiley & Sons, Inc.
Hammersley, J.M., & Handscomb, D.C. (1967). *Monte Carlo Methods*. London, UK: Methuen & Co.
Hess, B., Bekker, H., Berendsen, H.J.C., & Fraaije, J.G.E.M. . (1997). LINCS: A linear

constraint solver for molecular simulations. *Journal of Computational Chemistry, 18*(12), 1463-1472.

Hess, B., Kutzner, C., van der Spoel, D., & Lindahl, E. (2008). Gromacs 4: Algorithms for highly efficient, load-balanced, and scalable molecular simulation. *Journal of Chemical Theory and Computation, 4*(3), 435-477.

Hockney, R.W. (1970). The potential calculation and some applications. *Methods in computational Physics, 9*, 136-211.

Hoover, W.G. (1985). Canonical dynamics: Equilibrium phase-space distribution. *Physical Review A31*, 1695-1697.

Hoover, W.G. (1991). *Computational Statistical Mechanics* (Vol. 11): Elsevier Science Ltd.

Jorgensen, W.L. (1981). Transferable intermolecular potential functions for water, alcohols, and ethers. Application to liquid water. *Journal of the American Chemical Society, 103*(2), 341-345.

Jorgensen, W.L., Chandrasekhar, J., Madura, J.D., Impey, R.W., & Klein, M.L. (1983). Comparison of simple potential functions for simulating liquid water. *The Journal of Chemical Physics, 79*(2), 926-935.

Jorgensen, W.L., Maxwell, D.S., & Tirado-Rives, J. (1996). Development and testing of the opls all-atom force field on conformational energetics and properties of organic liquids. *Journal of The American Chemical Society, 118*(45), 11225-11236.

Karplus, M, & Kuriyan, J. (2005). Molecular dynamics and protein function. *Proceedings of the National Academy of Sciences, 102*(19), 6679-6685.

Kummosinski, T.F., Brown, E.M., & Farrell, H.M. (1991). Three-dimensional molecular modeling of bovine caseins: alpha s1-casein. *Journal of Dairy Science, 74*(9), 2889-2895.

Kummosinski, T.F., Brown, E.M., & Farrell, H.M. (1993a). Three-dimensional molecular modeling of bovine caseins: A refined, energy-minimized kappa-casein structure. *Journal of Dairy Science, 76*(9), 2507-2520.

Kummosinski, T.F., Brown, E.M., & Farrell, H.M. (1993b). Three-dimensional molecular modeling of bovine caseins: An energy-minimized beta-casein structure. *Journal of Dairy Science, 76*(4), 931-945.

Leach, A.R. (2001). *Molecular Modelling Principles and Applications* (2 ed.). UK: Pearson Education Limited.

Luzar, A., & Chandler, D. (1996). Hydrogen-bond kinetics in liquid water. *Nature, 379*(4), 55-57.

MacKerell, Jr., A. D., Bashford, D., Bellott, M., Dunbrack, Jr., R.L., Evanseck, J.D., Field, M.J., Fischer, S., Gao, J., Guo, H., Ha, S., Joseph-McCarthy, D., Kuchnir, L., Kuczera, K., Lau, F.T.K., Mattos, C., Michnick, S., Ngo, T., Nguyen, D.T., Prodhom, B., Reiher, W.E., Roux, B., Schlenkrich, M., Smith, J.C., Stote, R., Straub, J., Watanabe, M., Wiórkiewicz-Kuczera, J., Yin, D., Karplus, M. (1998). All-atom empirical potential for molecular modeling and dynamics studies of proteins. *The Journal of Physical Chemistry B, 102*(18), 3586-3616.

Mackerell Jr., A.D. (2004). Empirical force fields for biological macromolecules: Overview and issues. *Journal of Computational Chemistry, 25*(13), 1584-1604.

Mahoney, M.W., & Jorgensen, W.L. (2000). A five-site model for liquid water and the

reproduction of the density anomaly by rigid, nonpolarizable potential functions. *Journal of Chemical Physics, 112*(20), 8910-8922.

Mandl, F. (1988). *Statistical Physics* (2 ed.). Cornwall, UK: JohnWiley & Sons.

McCammon, J.A., Gelin, B.R., & Karplus, M. (1977). Dynamics of folded proteins. *Nature, 267*, 585-590.

McQuarrie, D.A. (2000). *Statistical Mechanics*. USA: University Science Books.

Metropolis, N., Rosenbluth, A.W., Rosenbluth, M.N., Teller, A.H., & Teller, E. (1953). Equation of state calculations by fast computing machines. *Journal of Chemical Physics, 21*(6), 1087-1092.

Moore, W.J. (1976). *Physical Chemistry* (5th ed.). London, UK.: Longman Group Limited.

Nosé, S. (1984). A molecular dynamics method for simulation in the canonical ensemble. *Molecular Physics, 52*(2), 255-268.

Oostenbrink, C., Villa, A., Mark, A.E., & van Gunsteren, W.F. (2004). A biomolecular force field based on the free enthalpy of hydration and solvation: The GROMOS force-field parameter sets 53A5 and 53A6. *Journal of Computational Chemistry, 25*(13), 1656-1676.

Panick, G., Malessa, R., & Winter, R. (1999). Differences between the pressure- and temperature-induced denaturation and aggregation of beta-lactoglobulin A, B, and AB monitored by FT-IR spectroscopy and small-angle X-ray scattering. *Biochemistry, 38*(20), 6512-6519.

Parrinello, M., & Rahman, A. (1980). Crystal structure and pait potentials: a molecular dynamics study. *Physical Review Letters, 45*(14), 1196-1199.

Parrinello, M., & Rahman, A. (1981). Polymorphic transitions in single crystals: a new molecular dynamics method. *Journal of Applied Physics, 52*(12), 7182-7190.

Paton, R.S., & Goodman, J.M. (2009). Hydrogen bonding and pi-stacking: how reliable are force fields? A critical evaluation of force field descriptions of nonbonded interactions. *Journal of Chemical Information and Modeling, 49*(4), 944-955.

Ponder, J.W., & Case, D.A. (2003). Force fields for protein simulations. *Advances in Protein Chemistry, 66*, 27-85.

Qi, X.L., Holt, C., McNulty, D., Clarke, D.T., Brownlow, S., & Jones, G.R. (1997). Effect of temperature on the secondary structure of beta-lactoglobulin at ph 6.7, as determined by cd and ir spectroscopy: A test of the molten globule hypothesis. *Biochemical Journal, 324*(Pt 1), 341-346.

Raffaini, G., & Ganazzoli, F. (2003). Simulation study of the interaction of some albumin subdomains with a flat graphite surface. *Langmuir, 19*(8), 3403-3412.

Raffaini, G., & Ganazzoli, F. (2004). Molecular dynamics simulation of the adsorption of a fibronectin module on a graphite surface. *Langmuir, 20*(8), 3371-3378.

Ryckaert, J.P., Ciccotti, G., & Berendsen, H.J.C. (1977). Numerical integration of the cartesian equations of motion of a system with constraints: Molecular dynamics of n-alkanes. *Journal of Computational Physics, 23*(3), 321-341.

Swope, W.C., Andersen, H.C., Berens, P.H., & Wilson, K.R. (1982). A computer simulation method for the calculation of equillibrium constants for the formation of physical clusters of molecules: Application to small water clusters. *Journal of Chemical Physics, 76*, 637-649.

Tuckerman, M.E. (2010). *Statistical Mechanics: Theory and Molecular Simulation*. New York, USA: Oxford University Press.

van der Spoel, D., Lindahl, E., Hess, B., Groenhof, G., Mark, A.E., & Berendsen, H.J.C. (2005). Gromacs: Fast, flexible, and free. *Journal of Computational Chemistry, 26*(16), 1701-1718.

van der Spoel, D., van Maaren, P.J., & Berendsen, H.J.C. (1998). A systematic study of water models for molecular simulation: Derivation of water models optimized for use with a reaction field. *Journal of Chemical Physics, 108*(24), 10220-10230.

van der Spoel, D., van Maaren, P.J., Larsson, P., & Tîmneanu, N. (2006). Thermodynamics of hydrogen bonding in hydrophilic and hydrophobic media. *Journal of Physical Chemistry B, 110*(9), 4393-4398.

Verlet, L. (1967). Computer "experiments" on classical fluids. I. Thermodynamical properties of lennard-jones molecules. *Physical Review, 159*, 98-103.

Wang, S., & Krumhansl, J.A. (1972). Superposition assumption. II. High density fluid argon. *The Journal of Chemical Physics, 56*(9), 4287-4290.

Zhang, Z., & Scanlon, M.G. (2011). Solvent effects on the molecular structures of crude gliadins as revealed by density and ultrasound velocity measurements. *Journal of Cereal Science, 54*(2), 181-186.

Zhou, Y., & Karplus, M. (1999). Interpreting the folding kinetics of helical proteins. *Nature, 401*, 400-403.

4 Material and methods

A general discussion of the methodology used in this work follows. Specific details of individual experiment are included with the corresponding chapter.

4.1 Protein-based fat replacers

There are three kinds of protein products studied in this program, i.e., WPC, microparticulate proteins and partially denatured proteins, of which the former one was used as control and the latter two were examined as different protein-based fat replacers. Lacprodan87 (Arla Foods Ingredients, Denmark) was used as the WPC and Simplesse® 100[E] (CP Kelco UK Limited, UK) and a series of Hiprotal60 products (Friesland Foods, the Netherland) were microparticulate proteins and partially denatured proteins, respectively. All the samples are multi-component systems containing protein, carbohydrate and minerals, and the protein content of each sample was obtained from Kjeldahl method and product manuals as shown in Table 4.1. Simplesse is produced from an extreme shearing treatment on heat-induced aggregates of whey proteins (Gaull, 1991). Hiprotal60 is a commercial product, while Hiprotal60-TS0709, Hiprotal60-TS0710, and Hiprotal60-TS0712 are soluble aggregates of partially denatured WPC with different particle size manufactured on a pilot scale by Friesland Foods, the Netherlands. The particle sizes of the products are controlled through different heating treatments and pH environments as shown in Table 4.1. The samples have then been ultrafiltered to a standardized protein content and spray dried to a powder.

Table 4.1 Protein contents of samples and process conditions for Hiprotal60 products.

		Protein content (%)	Process conditions	
			Temperature (^{o}C)	pH
Lacprodan87		87	-	-
Simplesse		53	-	-
Hiprotal60	**Hiprotal60**	60	-	-
	-TS0709	60	72.5	6.4
	-TS0710	60	72.5	7.0
	-TS0712	60	74	7.0

For commercial reasons, the exact details of how the protein samples are made cannot be revealed, but general information that has already been patented can be discussed. Nandi Protein Ltd (Blackpool, UK) has patented a technology that allows control of the solubility, particle size and hence, functionality of protein products through monitoring of the free sulphydryl content of the proteins during the partial denaturation process. Figure 4.1 illustrates that the content of free sulphydryl can be used to reveal the heat-induced denaturation of whey proteins. Moreover, Nandi has also found a way to monitor free sulphydryl content of the proteins at-line, allowing the control on the particle size and functionality of manufactured partially denatured proteins. The exact methodology used is commercially sensitive. Through this technology, the partially denatured WPC's used in this study have been manufactured.

It is found from Figure 4.1, the free –SH content increases with heating to and then begins to decrease above some certain temperature (holding time not shown), i.e., there is a peak in the free –SH content during heating. It believed that disulphide bonds start to form above the maximum in free –SH. This maximum in free –SH corresponds closely to the denaturation temperature of the proteins (i.e., β-lactoglobulins). Below the peak in –SH, soluble protein powders can be made that have improved functional properties (not shown in Figure 4.1). Above the peak, however, the proteins start to lose their functional properties. By controlling the free –SH content during processing (using those temperatures smaller than the denaturation one, controlling holding time, pH, and monitoring free –SH content), the functional properties and degree of aggregation of the proteins can be controlled.

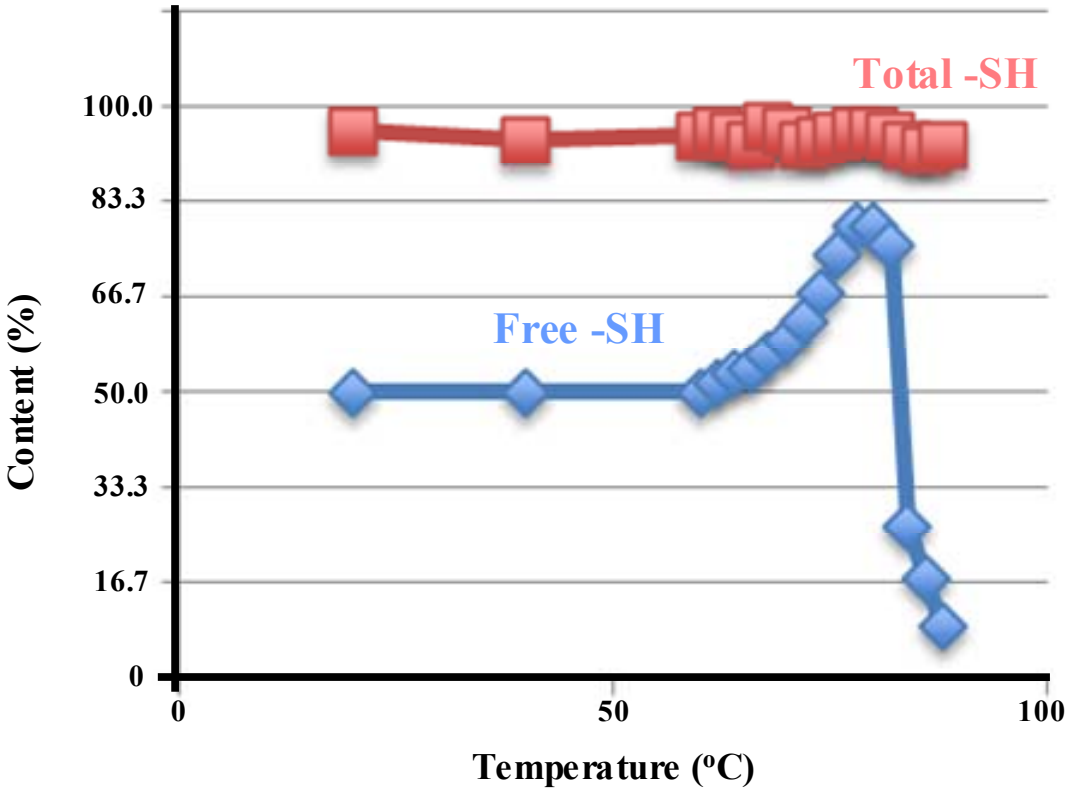

Figure 4.1 Denaturation of WPC with temperature as indicated by the content of free sulphydryl (Courtesy of Nandi Protein Ltd.).

4.2 Rheometry

All rheological measurements were performed using a Gemini advanced rheometer (Bohlin Instruments, UK), with a 4°/40 mm cone-and-plate geometry (Figure 4.2), and all the measurements were carried out at a temperature of 20 °C. The Gemini advanced rheometer can be operated by both strain control and stress control. The torque available for the rheometer ranges from 0.05 μNm to 200 mNm with a high resolution better than 1 nNm, making the instrument versatile for various applications for research purpose. A 4°/40 mm cone-and-plate geometry consists of a truncated rotating cone and a lower stationary plate, as shown schematically in Figure 4.2. The cone is cut off to avoid friction between the cone and the plate (Willenbacher & Georgieva, 2013). The gap angle θ is 4^{o} and the cone diameter is 40 mm, as indicated by the name 4°/40 mm. The gap $h(r)$ between the cone and plate increases linearly with the distance r from the rotation axis with a minimum value of h=0.150 mm, at the cone center,

$$h(r) = r\tan\theta$$

and the circumferential velocity $u(r)$is also an increasing function of r,

$$u(r) = r\omega$$

where ω is the angular velocity of the rotator. According to Section 2.1, shear rate of the rotating cone is calculated from $u(r)$ and $h(r)$ as,

$$\dot{\gamma} = \frac{du(r)}{dh(r)} = \frac{\omega}{\tan\theta} \approx \frac{\omega}{\theta}$$

where the approximation, $\theta \approx \tan\theta$, is valid for small values of θ, such as 4^{o}. It is obvious that the shear rate depends on neither h nor r and homogeneous shear conditions are established within the entire gap, which is considered an advantage of the cone-and-plate geometry (Willenbacher & Georgieva, 2013). The shear stress is calculated from the torque, M_D, on the cone,

$$\sigma = \frac{3M_D}{2\pi(D/2)^3}$$

In practice, liquid samples, i.e., protein dispersions, are loaded into the gap between the cone and the plate, and then the cone is set to the position for measurements, with the gap of 0.150 mm as shown in Figure 4.2. The excess samples were removed and the edge of the cone was covered by silicone oil (Sigma-Aldrich Co., UK) to protect moisture from evaporation. Results of rheological measurements were recorded and analyzed with the software Bohlin R6.50.5.7 (Bohlin Instruments, UK). Using the rheometer, viscosity of the liquid samples at constant and varying shear rates and viscoelastic properties, i.e., the storage modulus, *G'*, and the loss modulus, *G"*, are determined through viscometry and oscillation tests, which are introduced in the corresponding chapters, i.e., Chapter 6, Chapter 7, and Chapter 8.

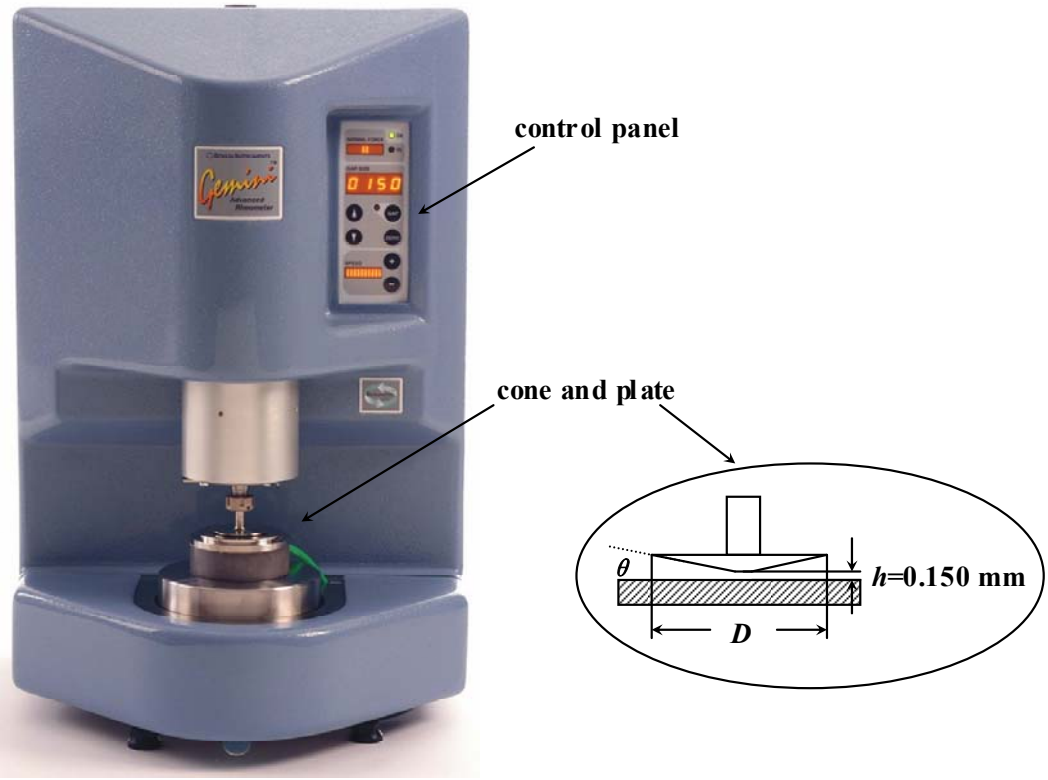

Figure 4.2 A Gemini advanced rheometer and a cone-and-plate geometry.

4.3 Molecular dynamics simulation

The molecular structure of β-lactoglobulin determined by X-ray diffraction was downloaded from the Protein Data Bank (a PDB file) with the code of 3BLG (Qin et al., 1998). The GROMACS 4.5 MD package (B. Hess et al., 2008) was used to perform the MD simulations on the molecule. The β-lactoglobulin molecule was inserted into a periodic cubic box with the sides 1.0 nm from the surface of the protein molecule in three coordinate directions and then filled with SPC water molecules (Berweger, van Gunsteren, & Müller-Plathe, 1995), giving a system containing 1 β-lactoglobulin molecule and 11486 water molecules. The simulations were performed in a GROMOS96 53A6 force field (Oostenbrink et al., 2004). It was found that the 3BLG molecule carried a net charge of -9e, and thus 9 Na^+ counter ions were added to neutralize the system. The energy of the neutralized system was minimized with a steepest descent algorithm. For all the simulations, electrostatic interactions were modeled with the particle mesh Ewald method with a cut-off of 1 nm (Darden, York, &

Pedersen, 1993; Essmann et al., 1995).

The 3BLG molecules were solvated in SPC water at 300 K and 500 K for 100 ns to obtain the conformations of native and unfolded molecules of the protein, respectively. From the trajectory of the unfolded molecule, five conformations with different molecular radii were selected and quenched to 300 K for 100 ns, respectively. For protein solvation (300 K) and unfolding (500 K) simulations, *NPT* ensembles were created by controlling temperature and pressure through a velocity-rescaling thermostat (Bussi et al., 2007) and a Parrinello-Rahman (Parrinello & Rahman, 1981) barostat, respectively. The scheme of the MD simulations on β-lactoglobulin is shown in Figure 4.3.

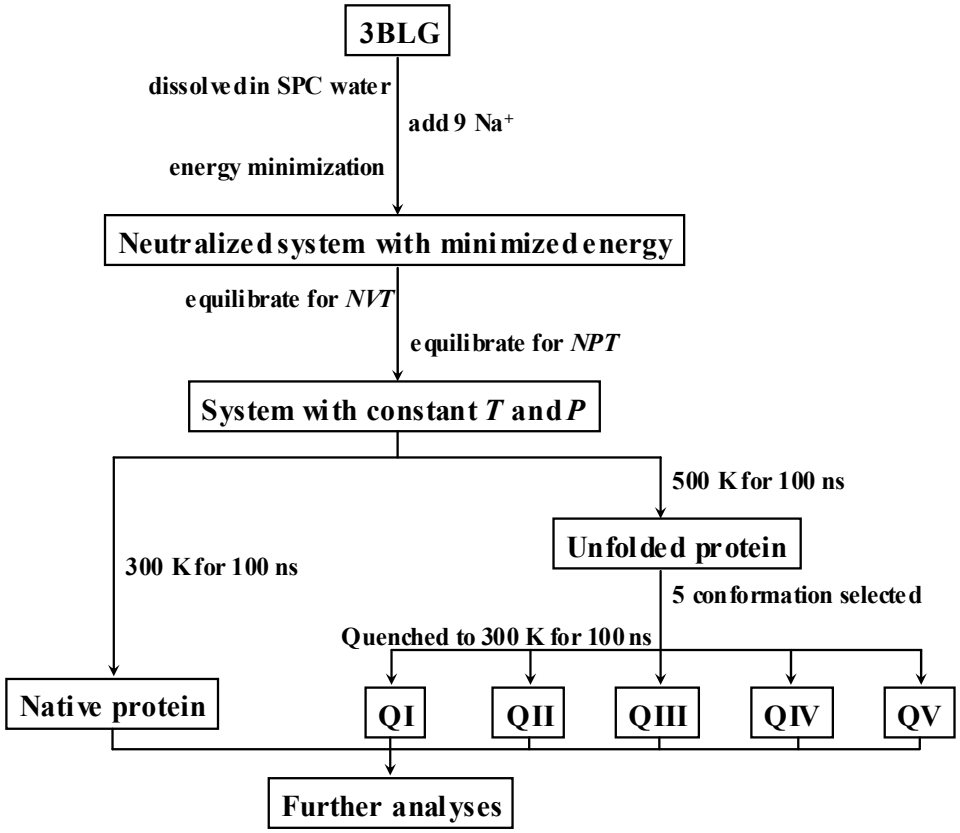

Figure 4.3 Scheme of MD simulations on β-lactoglobulin (3BLG).

The five conformations from unfolded 3BLG molecule were selected from plateaus of the root mean square deviation (RMSD) of the backbone of the unfolded molecule with respect to the native one (as shown in Section 5.3.1). RMSD is calculated from the atomic coordinates of the unfolded molecule, $\mathbf{q}_{it}$, and of the reference structure, i.e.,

the native 3BLG molecule, $\mathbf{q}_{i0}$,

$$\mathrm{RMSD} = \sum_{i}^{N} \left| \mathbf{q}_{it} - \mathbf{q}_{i0} \right|^{2}$$

Therefore, plateaus in RMSD indicate small fluctuations in the structure of the protein compared with the reference molecule. It should be noted that motions of the protein molecule in the system, including translations and rotations, will affect the coordinates of the atoms of the molecule, and therefore, GROMACS fits the motions of the unfolded and the reference proteins so that they have the same positions for center of mass and orientations.

At the end of the simulations, six different β-lactoglobulin molecules were obtained at 300 K, i.e., one native and five unfolded 3BLG molecules with different conformations. Free energy landscapes (FEL) (Maisuradze, Liwo, & Scheraga, 2009, 2010) were applied to find the representative structures, on which further analyses would be performed. For the FEL, two parameters, $X^{(1)}$and $X^{(2)}$, for instance RMSD and radius of gyration, are selected to distinguish the molecular conformations, i.e., the conformations of a protein are considered identical if $X_i^{(1)}$ and $X_i^{(2)}$ are the same. This is an approximation that is sufficiently accurate for free energy determination (Maisuradze et al., 2009, 2010). From the population of the conformations for each paired parameters, $P_i(X_i^{(1)}, X_i^{(2)})$, the thermodynamic potential is obtained,

$$\Psi_i\left(X_i^{(1)}, X_i^{(2)}\right) = -k_B T \ln P_i\left(X_i^{(1)}, X_i^{(2)}\right)$$

where k_B and T are the Boltzmann constant and the absolute temperature, respectively (Allen, 2004; McQuarrie, 2000). The Gibbs free energy, G_{Gibbs}, has been defined as the thermodynamic potential in the isothermal-isobaric (*NPT*) ensembles, and therefore, the FEL of the simulations provided the G_{Gibbs} as a function of a pair of structural parameters. In practice, the gyration radius and the root mean square deviation (RMSD) of the protein molecule are usually selected as those two parameters, i.e., $X^{(1)}$=gyration radius and $X^{(2)}$=RMSD (Maisuradze et al., 2010). Finally, the structure of each molecule was represented by the conformation with the lowest Gibbs free energy, and then further analyses were performed based on the 20 ns evolution of each representative structure.

The solvent accessible surface area was computed to obtain the hydrophobic, hydrophilic and total surfaces of a protein molecule, which revealed the degree of protein unfolding. The number of water molecules was counted as a function of the distance from the protein surface, where the thicknesses of the protein hydration shells were estimated as the distances for the troughs of the number of water molecules.

In the GROMACS package, hydrogen bonds (HB) are geometrically defined as being when the distance between the hydrogen (H) and the acceptor (A) is smaller than 0.35 nm and the angle donor-hydrogen-acceptor (ADH) is smaller than 30^{o}, as illustrated in Figure 4.4. According to the definition, the number of HB formed by hydration water molecules with other water molecules and the protein molecule were counted respectively for each representative protein structure. The protein-water and water-water HB forming abilities of the hydration water molecules, $A(\mathrm{HB})_{\text{protein-water}}$ and $A(\mathrm{HB})_{\text{water-water}}$ are expressed as

$$A\left(\mathrm{HB}\right)_{\text{protein-water}} = \frac{N\left(\mathrm{HB}\right)_{\text{protein-water}}}{N\left(\mathrm{H_2O}\right)_{\text{hydration}}}$$

and

$$A\left(\mathrm{HB}\right)_{\text{water-water}} = \frac{N\left(\mathrm{HB}\right)_{\text{water-water}}}{N\left(\mathrm{H_2O}\right)_{\text{hydration}}}$$

where N denotes the number of HB or H_2O molecules.

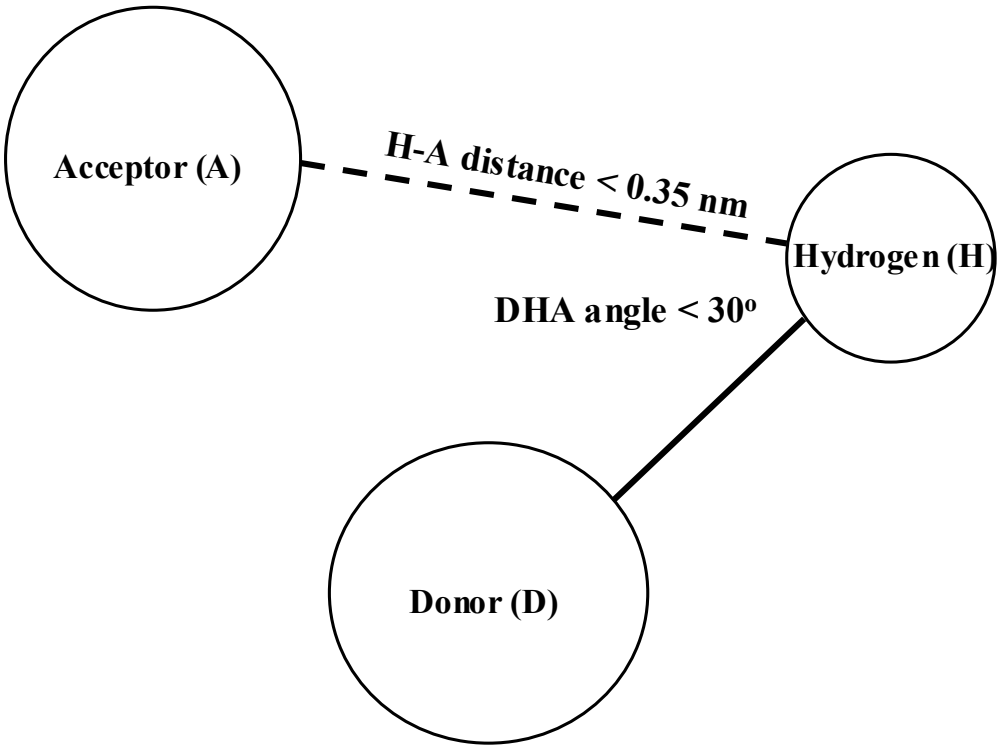

Figure 4.4 Illustration of definition of hydrogen bonds in GROMACS.

Lifetime of HB formed between water molecules or between water and the protein molecules was estimated through the autocorrelations of the existence functions, $h(t)$, which are assigned 1 for bonded pairs and 0 otherwise (Luzar & Chandler, 1996; van der Spoel et al., 2006). The autocorrelation, $c(t)$, is calculated as

$$c(t) = \frac{\langle h(t_0) h(t) \rangle}{\langle h(t) \rangle}$$

where $h(t_0)$ and $h(t)$ represent the values of the existence function at time t_0 and t, respectively, and $\langle h(t) \rangle$ is the average value of the existence function from time t_0 to t. As a result, $c(t)$ is 1 at the beginning of computing where $t_0=t$, and decays as time since the hydrogen bonds are broken with time, and therefore, the lifetime of HB can be measured by evaluating the decay of $c(t)$. Additionally, mobility of water molecules in hydration shells around the protein was also evaluated, which is revealed by the time evolution of the number of the hydrated water molecules (Paradossi, Finelli, Natali, Telling, & Chiessi, 2011). The water molecules in the hydration shells were counted and marked firstly at time t_0, and then those marked water molecules were monitored

and counted again if they were still in the hydration shells until time *t*. The marked water fraction at time *t* was then obtained as $N_t\left(\mathrm{H_2O}\right)/N_{t_0}\left(\mathrm{H_2O}\right)$, and plotted versus time to examine the mobility of the hydration water.

4.4 Particle size measurements

Particle size distributions of samples were determined with a Zetasizer Nano-ZS (Malvern Instruments Ltd, UK) and a Mastersizer 2000 (Malvern Instruments Ltd, UK), as shown in Figure 4.5 and 4.6. The measurement ranges are 3.8 nm – 100 μm for the Zetasizer and 20 nm – 2000 μm for the Mastersizer. Two instruments were involved in the particle size measurements because the Zetasizer provides results with poor quality for the samples with high polydispersity, while the Mastersizer gives biased results for submicron particles (from preliminary experiment and results not shown). Samples were loaded into a cuvette (≈8 mL) for the Zetasizer while for the Mastersizer, samples were added into water (≈800 mL) in the beaker, until the obscuration of the dilution reached ≈5.00. Therefore protein concentration of the samples for a Mastersizer is difficult to specify and in practice, samples with protein concentration of 14% and 16% (w/w) were used for the Mastersizer. As for the Zetasizer, solutions of 1% (w/w) protein concentration were used.

Figure 4.5 Picture of a Zetasizer Nano-ZS.

Figure 4.6 Picture of a Mastersizer 2000.

The Zetasizer and the Mastersizer use light scattering and laser diffraction techniques to measure the particle size distributions, respectively. As shown in Figure 4.7, light scatters when it passes through a particle and the angle and intensity of the

scattered light depends on the size of the particle. Through collecting such information, i.e., the angle and intensity of the scattered light, the scattering pattern is obtained, which is then related to the particle size through the Mie theory (Du, 2004; Wriedt, 2012). As for the Mastersizer, the scattering pattern of the particles is obtained through analyses on the diffraction of the scattered laser, as shown in Figure 4.8.

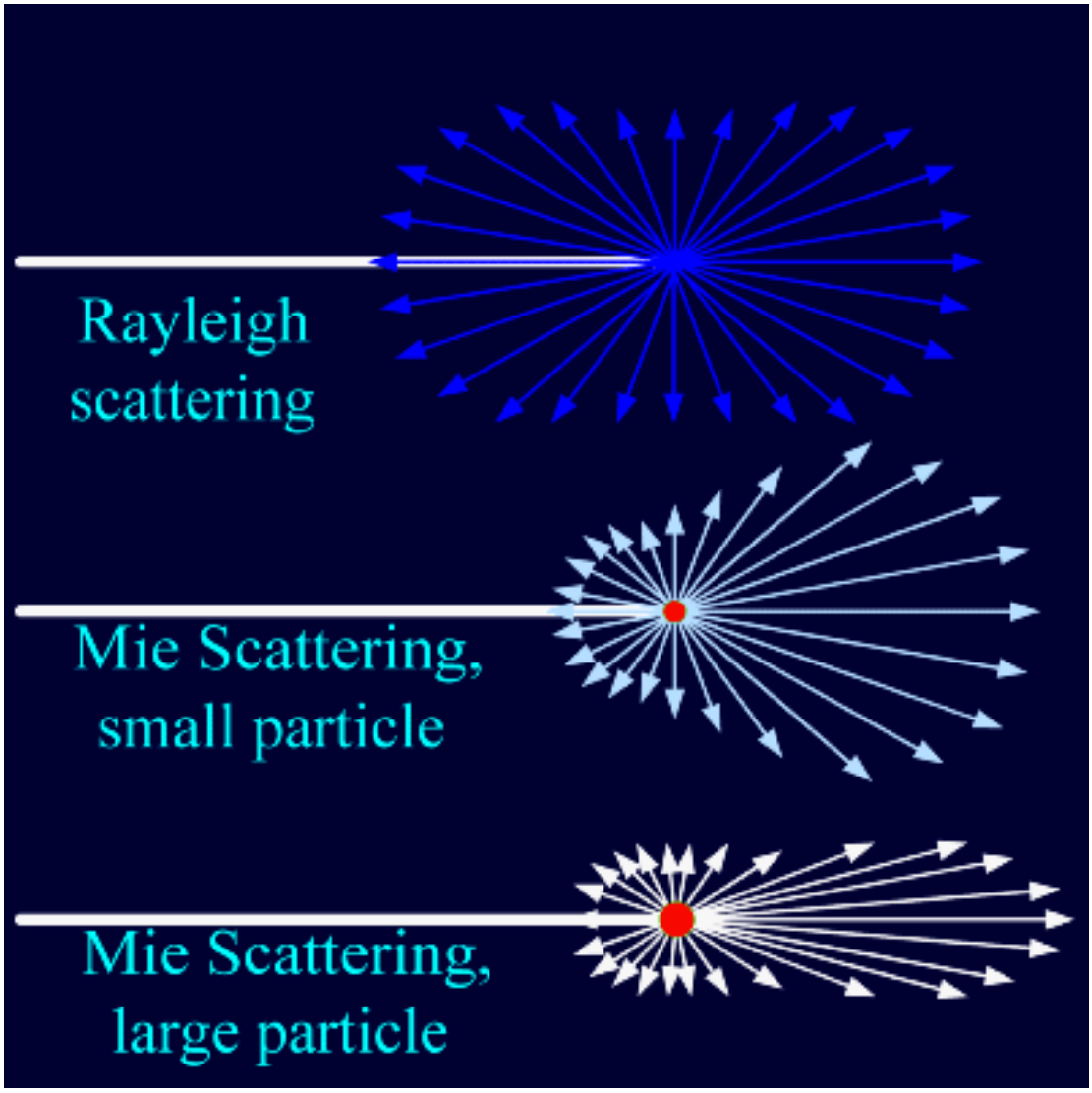

Figure 4.7 Light scattering patterns for different particles (public domain).

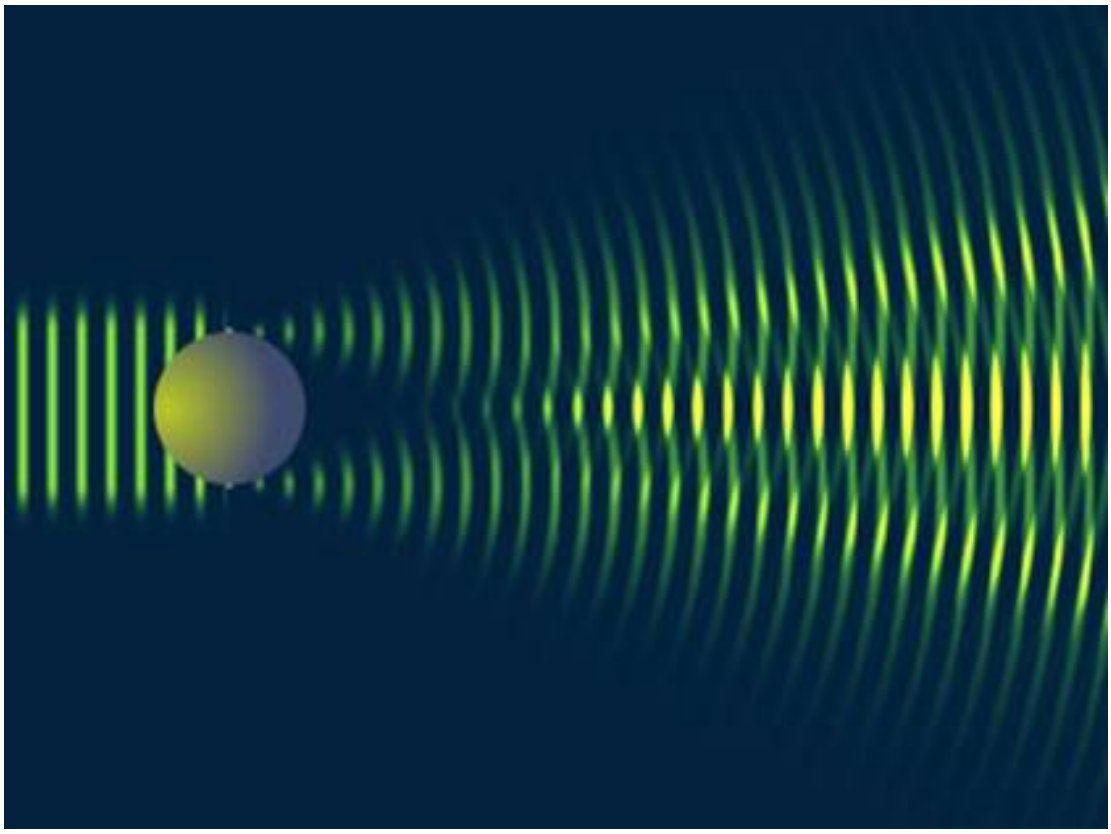

Figure 4.8 Laser diffraction of a spherical particle (public domain).

It should be noted here that the particles are estimated as spheres when the particle sizes, i.e., diameters of the sphere, are measured. The approximate spheres are defined to have the same volume as the particles with irregular shapes. For example, a sphere with the diameter of 39 μm can be used to represent a cylinder with the diameter of 20 μm and the height of 100 μm since they have the same volume as illustrated in Figure 4.9.

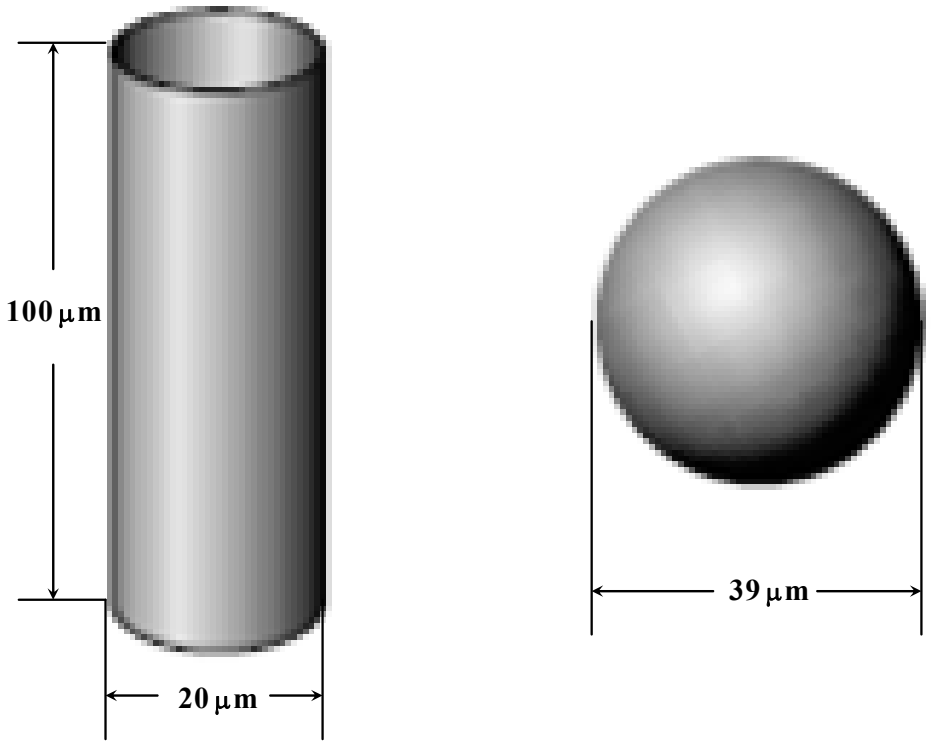

Figure 4.9 An approximate sphere for a cylinder.

4.5 Density measurements

Densities of water and serial dilutions of each protein sample were measured with a PAAR DMA 46 density meter (Anton Paar, UK) as shown in Figure 4.10. In this instrument, a U-tube containing the sample is oscillated by an ultrasonic source (Kayukawa, Hasumoto, & Watanabe, 2003). The resonant frequencies (*f*) of the oscillations for the U-tube with different samples are dependent on the mass of whole system, and thus, the masses and the densities of the samples can be obtained, since the mass and hence the volume of the U-tube is known. From the density results of the serial dilutions of the samples, the partial specific volume of the each sample particle in water was calculated, of which the mathematical detail is illustrated in Section 5.2.5.

Figure 4.10 A picture of a PAAR DMA 46 density meter

4.6 Experimental design

Sequence of all the experiments, including particle size, density and rheology measurements for various samples with different protein concentrations was decided randomly. All the experiments were performed at 20 ^{o}C (unless specified). Every experiment was repeated at least twice and the results with acceptable repeatability were reported.

4.7 Reference

Allen, M.P. (2004). Introduction to molecular dynamics simulation. In D. Frenkel, N. Attig, K. Binder, H. Grubmüller & K. Kremer (Eds.), *Computational Soft Matter: From Synthetic Polymers to Proteins, Lecture Notes* (Vol. 23, pp. 1-28). Jülich, Germany: John von Neumann Institute for Computing.

Berweger, C.D., van Gunsteren, W.F., & Müller-Plathe, F. (1995). Force field parametrization by weak coupling. Re-engineering SPC water. *Chemical Physics Letters, 232*(5-6), 429-436.

Bussi, G., Donadio, D., & Parrinello, M. (2007). Canonical sampling through velocity rescaling. *Journal of Chemical Physics, 126*(1), 014101(014101-014107).

Darden, T., York, D., & Pedersen, L. (1993). Particle mesh Ewald: An *N*.log(*N*) method for Ewald sums in large systems. *Journal of Chemical Physics, 98*(12), 10089-10092.

Du, H. (2004). Mie-scattering calculation. *Applied Optics, 43*(9), 1951-1956.

Essmann, U., Perera, L., Berkowitz, M.L., Darden, T., Lee, H., & Pedersen, L.G. (1995). A smooth particle mesh Ewald method. *Journal of Chemical Physics, 103*(19), 8577-8593.

Gaull, G.E. (1991). Role of micro-particulated protein fat substitutes in food and nutrition. *Annals of the New York Academy of Sciences, 623*(1), 350-355.

Hess, B., Kutzner, C., van der Spoel, D., & Lindahl, E. (2008). Gromacs 4: Algorithms for highly efficient, load-balanced, and scalable molecular simulation. *Journal of Chemical Theory and Computation, 4*(3), 435-477.

Kayukawa, Y., Hasumoto, M., & Watanabe, K. (2003). Rapid density-measurement system with vibrating-tube densimeter. *Review of Scientific Instruments, 74*(9), 4134-4139.

Luzar, A., & Chandler, D. (1996). Hydrogen-bond kinetics in liquid water. *Nature, 379*(4), 55-57.

Maisuradze, G.G., Liwo, A., & Scheraga, H.A. (2009). Principal component analysis for protein folding dynamics. *Journal of Molecular Biology, 385*(1), 312-329.

Maisuradze, G.G., Liwo, A., & Scheraga, H.A. (2010). Relation between free energy landscapes of proteins and dynamics. *Journal of Chemical Theory and Computation, 6*(2), 583-595.

McQuarrie, D.A. (2000). *Statistical Mechanics*. USA: University Science Books.

Oostenbrink, C., Villa, A., Mark, A.E., & van Gunsteren, W.F. (2004). A biomolecular force field based on the free enthalpy of hydration and solvation: The GROMOS force-field parameter sets 53A5 and 53A6. *Journal of Computational Chemistry, 25*(13), 1656-1676.

Paradossi, G., Finelli, I., Natali, F., Telling, M.T.F., & Chiessi, E. (2011). Polymer and water dynamics in poly(vinyl alcohol)/poly(methacrylate) networks. A molecular dynamics simulation and incoherent neutron scattering investigation. *Polymers, 3*, 1805-1832.

Parrinello, M., & Rahman, A. (1981). Polymorphic transitions in single crystals: A new molecular dynamics method. *Journal of Applied Physics, 52*(12), 7182-7190.

Qin, B.Y., Bewley, M.C., Creamer, L.K., Baker, H.M., Baker, E.N., & Jameson, G.B. (1998). Structural basis of the tanford transition of bovine β-lactoglobulin. *Biochemistry, 37*(40), 14014-14023.

van der Spoel, D., van Maaren, P.J., Larsson, P., & Tîmneanu, N. (2006). Thermodynamics of hydrogen bonding in hydrophilic and hydrophobic media. *Journal of Physical Chemistry B, 110*(9), 4393-4398.

Willenbacher, N., & Georgieva, K. (2013). Rheology of disperse systems. In U. Brocke, W. Meier & G. Wagner (Eds.), *Product Design and Engineering: Formulation of Gels and Pastes* (pp. 7-49). Weinheim, Germany: Wiley-VCH Verlag GmbH & Co.

Wriedt, T. (2012). Mie theory: A review. In W. Hergert & T. Wriedt (Eds.), *The Mie*

Theory Basics and Applications (pp. 53-71). New York, USA: Springer-Verlag Berlin Heidelberg.

5 Characterization of protein-based fat replacers: From β-lactoglobulin molecules to particle aggregates

5.1 Introduction

Modifications on whey proteins have been widely employed in food industries to provide new products with innovative functional properties (Kinsella & Whitehead, 1988; Prindiville, Marshall, & Heymann, 2000). One of the important applications of modified whey proteins is to produce protein-based fat replacers (Prindiville et al., 2000; Sandrou & Arvanitoyannis, 2000), of which Simplesse and Hiprotal60 are well known. Rheological properties, such as viscosity and gelation, are very important parameters for evaluations of the fat replacers utilized in food systems, through which the behaviour of the components can be understood and therefore, improvement in processing techniques become feasible. However, characterization of the products, especially the macromolecules, proteins for instance, is of great help in understanding the rheological properties of the fat replacers, especially those based on modified proteins. In this chapter, results for the characterization of the protein materials used in later rheological studies are presented.

In this chapter, a number of techniques are used to characterize the nature of the protein molecules used in this study. This includes molecular dynamics simulation, particle size analysis, scanning electron microscopy and specific volume measurements. The main protein component of whey protein concentrate, β-lactoglobulin, is studied by molecular dynamics computer simulations to understand the protein unfolding and hydration shell changes associated with partial unfolding (B. Hess et al., 2008; van der Spoel et al., 2005). It has been well established that there is one free –SH and two S-S groups buried in the hydrophobic cavity of the native β-lactoglobulin (Cairoli, Iametti, & Bonomi, 1994; Papiz et al., 1986). Upon heating, the β-lactoglobulin molecule unfolds and such five Cys residues expose to the molecular surface of the protein, which favors the formation of intermolecular disulphide bonds through –SH/S-S interchange reactions and thus polymeric aggregates of the proteins (Bryant &

McClements, 1998; Shimada & Cheftel, 1989). Through computer simulations, the exposure of Cys residues of the β-lactoglobulin molecule can be visualized as the polypeptide chain is unfolding, which gives a straightforward view for the possible aggregation of the denatured proteins. Besides the molecular structure, hydration shells of unfolded proteins are also examined, in terms of radial distribution functions, hydrogen bonds forming ability and mobility of the hydrated water molecules, which gives a full map of the unfolding of the β-lactoglobulin.

Beyond the molecular levels, macroscopic properties, such as particle size distribution and structures of protein aggregates are also determined in order to provide foundations for the understandings of the rheological properties of the materials. Moreover, the partial specific volumes of the materials in water solutions are also measured, which are believed to provide useful characteristic parameters for these commercial products.

5.2 Material and methods

5.2.1 Molecular dynamics simulation

Molecular dynamics simulations of β-lactoglobulin were carried out using GROMACS 4.5 MD package (B. Hess et al., 2008). The molecular structure of the protein for the simulations was determined by X-ray diffraction with the PDB code of 3BLG (Qin et al., 1998). A β-lactoglobulin molecule was inserted into a periodic cubic box with the sides 1.0 nm from the surface of the protein molecule in three coordinate directions, which gave a size of 7.0×7.0×7.0 nm for the cubic box. SPC water molecules (Berweger et al., 1995) were filled in the box and the protein molecule is solvated in water with GROMOS96 53A6 force field (Oostenbrink et al., 2004), giving a system of 1 β-lactoglobulin molecule and 11486 water molecules. Since the protein molecule carries a net charge of -9e, 9 Na^+ counter ions were added to neutralize the system. Energy of the neutralized system was minimized with steepest descent algorithm. Electrostatic interactions were modeled with particle mesh Ewald method (Darden et al., 1993; Essmann et al., 1995). Temperature was controlled by coupling the system to a velocity-rescale thermostat (Bussi et al., 2007), and Parrinello-Rahman

pressure coupling barostat (Parrinello & Rahman, 1981) was employed for NPT equilibrations.

The β-lactoglobulin molecules were solvated in SPC water at 300 K and 500 K for 100 ns to obtain the native and unfolded protein molecules, respectively. Heat treatment at 500 K is performed on the protein molecule in the simulations because that high temperature efficiently reduced the unfolding time for β-lactoglobulin and had no different effects on the protein unfolding compared with the protein denaturation temperature, i.e., 350 K ~ 400 K (Euston, 2013). According to the displacements of the backbone of the heated protein molecule compared with the non-heated one, five metastable states were selected from the heated molecule to mimic different stages of protein denaturation and quenched to 300 K for 100 ns, respectively. It should be clear that there could be many stages of protein denaturation and that the five states are selected arbitrarily and may not be fully representative of the ensemble of possible unfolded states. Further analyses were carried out on the six different protein molecules, i.e., one for native and five for quenched β-lactoglobulins. Representative structures were firstly obtained through free energy landscape (FEL) (Maisuradze et al., 2009, 2010). Hydrogen bonds formed between water of hydration shells and the protein and the hydration water molecules themselves were measured using the instantaneous system of each representative protein stricture, while the other parameters, such as solvent accessible surface and radial distribution of water molecules were calculated as the time average for 20 ns after each representative protein structure. The time dependent parameters, i.e., the correlation function of protein-water hydrogen bonds and the number of water molecules in the hydration shells for each protein molecule were also determined for 20 ns starting from the representative protein structure.

5.2.2 Particle size distribution

Particle size distributions of whey protein concentrate, i.e., Lacptodan87 (Arla Foods Ingredients, Denmark), and protein-based fat replacers, i.e., Simplesse® 100[E] (CP Kelco UK Limited, UK) and a series of Hiprotal60 products (Friesland Foods, the

Netherland) in water solutions were determined. A Zetasizer Nano-ZS (Malvern Instruments Ltd, UK) was used to determine the particle size distributions for solutions of Lacptodan87 and Simplesse with a concentration of 1% (w/w), while the particle size distributions of Hiprotal60 products were measured with a Mastersizer 2000 (Malvern Instruments Ltd, UK). Different instruments were selected because the preliminary experiment (not shown) suggested the Hiprotal60 products were micron particles and too large to be examined in Zetasizer Nano-ZS, while the submicrons in Lacptodan87 and Simplesse were too small for Mastersizer 2000. Since the samples used for Mastersizer 2000 were diluted in a wet dispersion unit Hydro 2000MU (Malvern Instruments Ltd, UK), the concentration of the Hiprotal60 samples was selected as 16% (w/w). The median diameters, D[0.5], of Lacprodan87 and Simplesse and Hiprotal60 products were recalculated with the refractive indices ranging from 1.35 to 1.80 with an interval of 0.05 for optimization (Hayakawa, Nakahira, & Tsubaki, 1995; Saveyn, Mermuys, Thas, & van der Meeren, 2002), and the results of particle size distribution for each protein sample was obtained in terms of the optimized refractive index.

5.2.3 Environmental scanning electron microscope (ESEM)

Environmental scanning electron microscope (Model Quanta 650 FEG) (FEI, USA) was used to provide information on particle aggregates in the protein solutions. Two drops of each protein solution with a concentration of 0.01% (w/w) were loaded on a glass slide (Menzel-Gläser, Germany) and left still for evaporation to dryness. The slices were then applied to ESEM in vacuum to obtain the images of the dry particles.

5.2.4 SDS-PAGE

SDS-PAGE was performed using an XCell SureLock^{TM} Mini-Cell Electrophoresis System (Life Technologies Ltd, UK) with BoltTM Mini Gels (Life Technologies Ltd, UK). The running buffer was a solution of 600 mL with a pH value of 8.3, containing 9 g of Tris (Fisher Scientific UK Limited, UK), 43.2 g of glycine (Sigma-Aldrich Co., USA) and 3 g of SDS (Sigma-Aldrich Co., USA) mixed with deionized water. Tris-Glycine SDS Sample Buffer (Life Technologies Ltd, UK) and Sample Buffer,

Laemmli (Life Technologies Ltd, UK) were mixed with 1% protein solutions with a ratio of 1:1 (v/v) for normal and reduced SDS, respectively. The Sharpe Pre-Stained Protein Standard (Life Technologies Ltd, UK) was used as the marker of the molecular weight.

5.2.5 Partial specific volume

The change in volume of the solution resulting from a unit change in the solute mass is expressed as apparent specific volume of the protein, $\bar{v}$ (Moore, 1976), and defined as

$$\bar{v} \equiv \frac{v - v_0}{cv} \tag{5.1}$$

where v and v_0 are the volumes of the solution and the solvent before the solute is added, and c is the concentration of the solute, or protein, in the solution. With the solution and the solvent densities, ρ and ρ_0, the value of $\bar{v}$ can be calculated as

$$\bar{v} = \frac{1 - (\rho - c)/\rho_0}{c} \tag{5.2}$$

where the expression $(\rho\text{-}c)/\rho_0$ is known as the apparent volumetric fraction of the solvent, and often denoted as Φ_0 (Galema & Hoiland, 1991; Sarvazyan, 1991).

The partial specific volume of the protein molecule in the solution, $\bar{v}^o$, expressing the properties of the ideal isolated protein molecules, where there is no intermolecular interaction, is obtained by extrapolating $\bar{v}$ to the limit of zero protein concentration (Gekko & Noguchi, 1974; Zhang & Scanlon, 2011).

$$\bar{v}^o \equiv \lim_{c \to 0} \bar{v} = \lim_{c \to 0} \frac{1 - \Phi_0}{c} \tag{5.3}$$

The densities, ρ_0 and ρ, were measured with a PAAR DMA 46 density meter (Anton Paar, UK) for water and serial dilutions of each protein sample (protein concentrations, w_p, are 0.4%, 0.8%, 1.2%, 1.5%, 2.3%, 3.0%, 4.6%, 6.0%, 9.0%, 12.0%, and 14.0%). The concentration, c, used for determining the partial specific volumes of the particles were calculated in terms of the total solids in the solution as

$$c = \frac{w_p \times \rho}{x_p}$$

where x_p represents the protein content of the samples, i.e., 87% for Lacprodan87, 53%

for Simplesse, and 60% for Hiprotal60 products, respectively.

5.3 Heat-induced denaturation of β-lactoglobulin

5.3.1 Heat-induced unfolding

It is well known that protein molecules unfold and lose their tertiary structures under heating treatment (Damodaran, 1996b). According to the root mean square deviation (RMSD) of the backbone of unfolded polypeptides from the native one, the extent of heat-induced denaturation of a protein molecule is determined. The RMSD of a β-lactoglobulin molecule simulated in water at high temperature (500 K) is plotted together with that at room temperature (300 K) in Figure 5.1. The backbones of both the molecules, i.e., the native and the unfolded ones, have been fitted to exclude the effects of translation and rotation of the molecule in water and thus, the difference is due to unfolding of the molecular structure. Additionally, it should be noted the RMSD of the molecule at 300 K is supposed to result from molecular vibration of the protein (Chalikian, 2003). Stepwise heat-induced unfolding of the β-lactoglobulin molecule is observed in Figure 5.1, where several meta-stable states can be observed. Five unfolded states, as marked in Figure 5.1, of the protein are selected randomly for subsequent quenching.

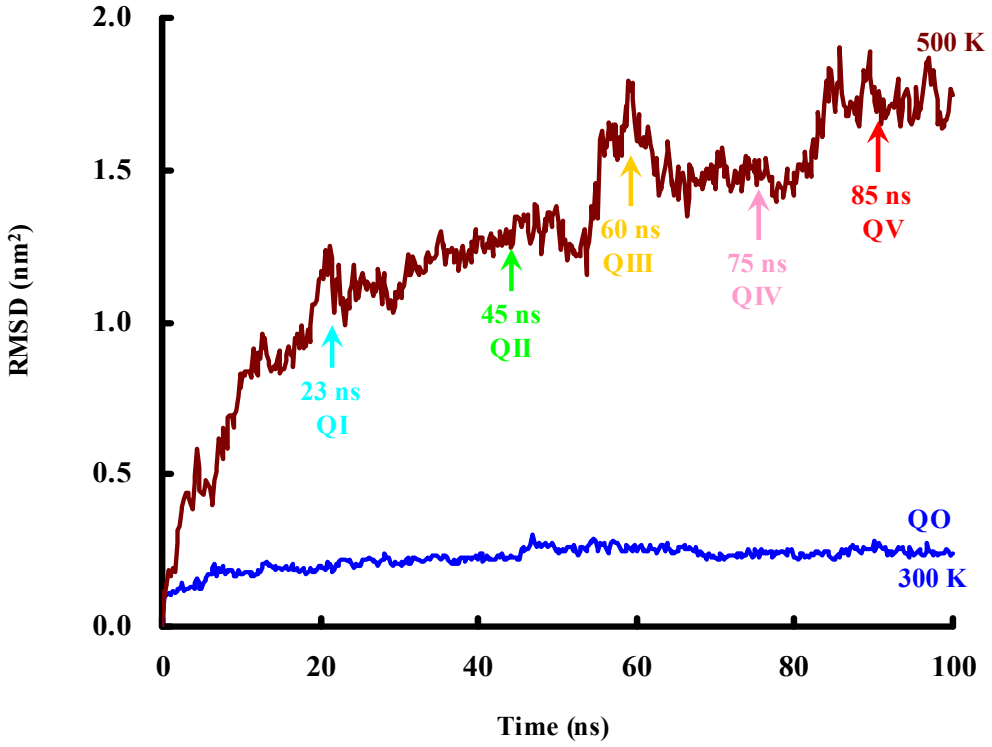

Figure 5.1 Root mean square deviation (RMSD) of native and heated proteins in water.

RMSD of the quenched molecules (QI ~ QV) are shown in Figure 5.2. Compared with Figure 5.1, small fluctuations of RMSD are observed for the quenched molecules, indicating that those molecules preserve their meta-stable structures from further unfolding at room temperature. The state QIII is found to have the largest RMSD, suggesting the most drastic unfolding in the molecular structure. Moreover, it is interesting to find RMSD of the QV state decreases during the first 20 ns of quenching and then remains a constant value similar as that of QIV. That could be due to refolding of the denatured molecule at room temperature (300 K).

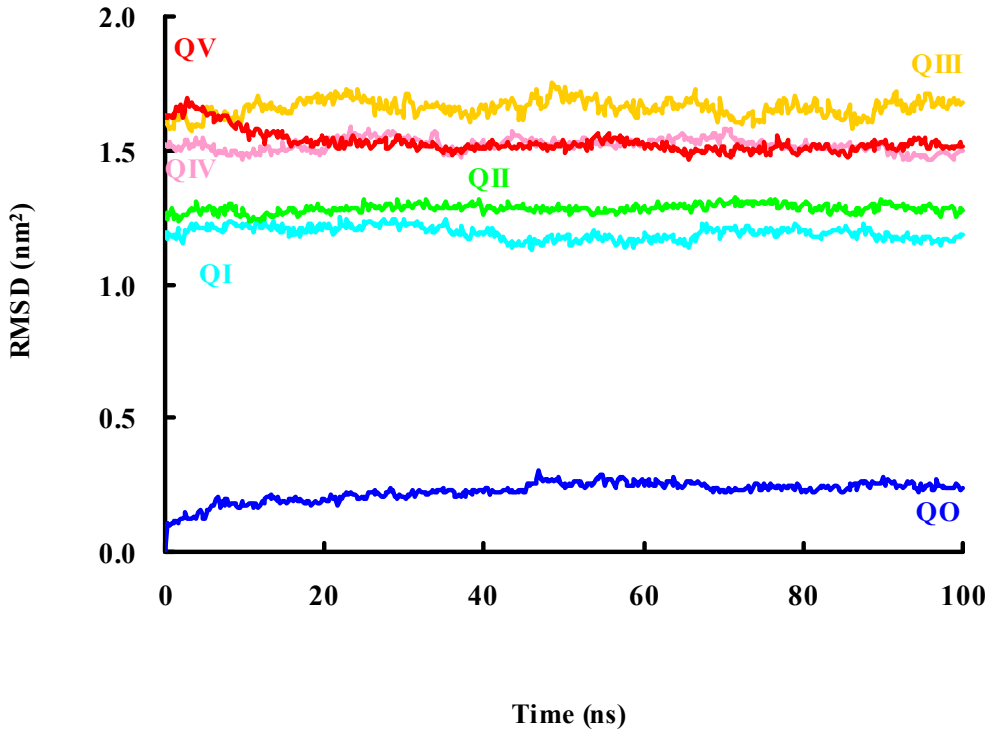

Figure 5.2 Root mean square deviation (RMSD) of native (QO) and different quenched (QI ~ QV) molecules, all the conformations were obtained at 300 K.

5.3.2 Unfolded structure of β-lactoglobulin

Gibbs free energy of each protein molecule was calculated in order to find the representative structure of each protein trajectory according to the Free Energy Landscape (FEL). Two physical parameters (Maisuradze et al., 2010) of the protein molecules, the gyration radius and the root mean square deviation (RMSD) from the crystal structure of β-lactoglobulin, were selected for contour plots as shown in Figure 5.3. The structure of the crystallized protein rather than that of the dissolved one was used as a reference structure here in order to increase the sampling regions. According to the FEL, quenched protein molecules (i.e., QI ~ QV) tended to unfold in water. However, the QII and QIV explored lower Gibbs free energy conformations with folded/refolded conformations. Based on the points with the lowest Gibbs free energies for different proteins, the representative structures for different molecules have been identified. It is noted that five thermodynamically favored conformations exist for the

QV molecule (regions of the lowest Gibbs free energies), which is supposed to result from the high flexibility of the unfolded polypeptide chain. Since hydrophobic surfaces of a protein tend to shrink in water solutions (Damodaran, 1996b), the representative structure for QV molecule is randomly selected from the region with the smallest molecular size (i.e., the lowest gyration radius).

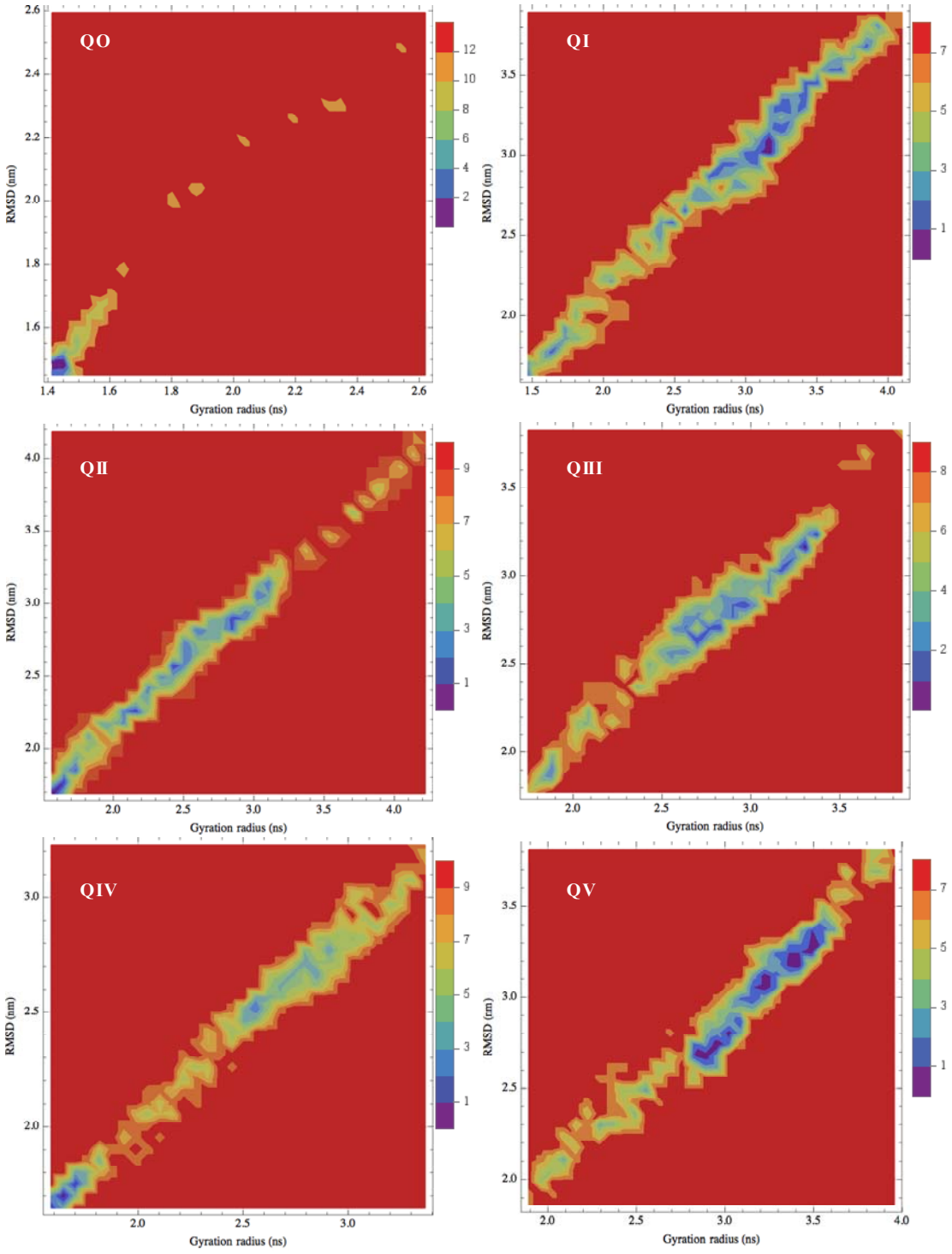

Figure 5.3 Free Energy Landscapes (FEL): Contour plots of Gibbs free energy versus gyration radius and RMSD for different conformations at metastable states.

Representative structures of the quenched molecules obtained from FELs are shown in Figure 5.4. It is found that there are five cysteine (Cys) residues in the polypeptide chain, of which four are connected by two disulphide bonds, i.e., S-S$^{66\text{-}160}$ and S-S$^{106\text{-}119}$. The sulphydryl group of Cys^{121} (i.e., SH^{121}) is a free SH group. Besides, four (Cys^{66}, Cys^{106}, Cys^{119} and Cys^{121}) Cys residues contribute to β-sheet structures in the native protein. As the protein unfolds with heating treatment, its secondary structures melt and the β-sheets turn into turns and coils. As shown in Figure 5.4 from QII to QV, the collapse of secondary structures releases Cys residues from β-sheets into more flexible structures, such as coils and turns. Moreover, it is also found that –SH^{121} and one S-S$^{66\text{-}160}$ are distributed on the opposing ends of the unfolded protein molecules. Such locations of the –SH^{121} and one S-S$^{66\text{-}160}$ and the flexibility of the unfolded structures could favour the intermolecular SH/S-S interchange reactions (Shimada & Cheftel, 1989) and account for the formation of the protein aggregates with a “string-of-beads” structure (Bryant & McClements, 1998).

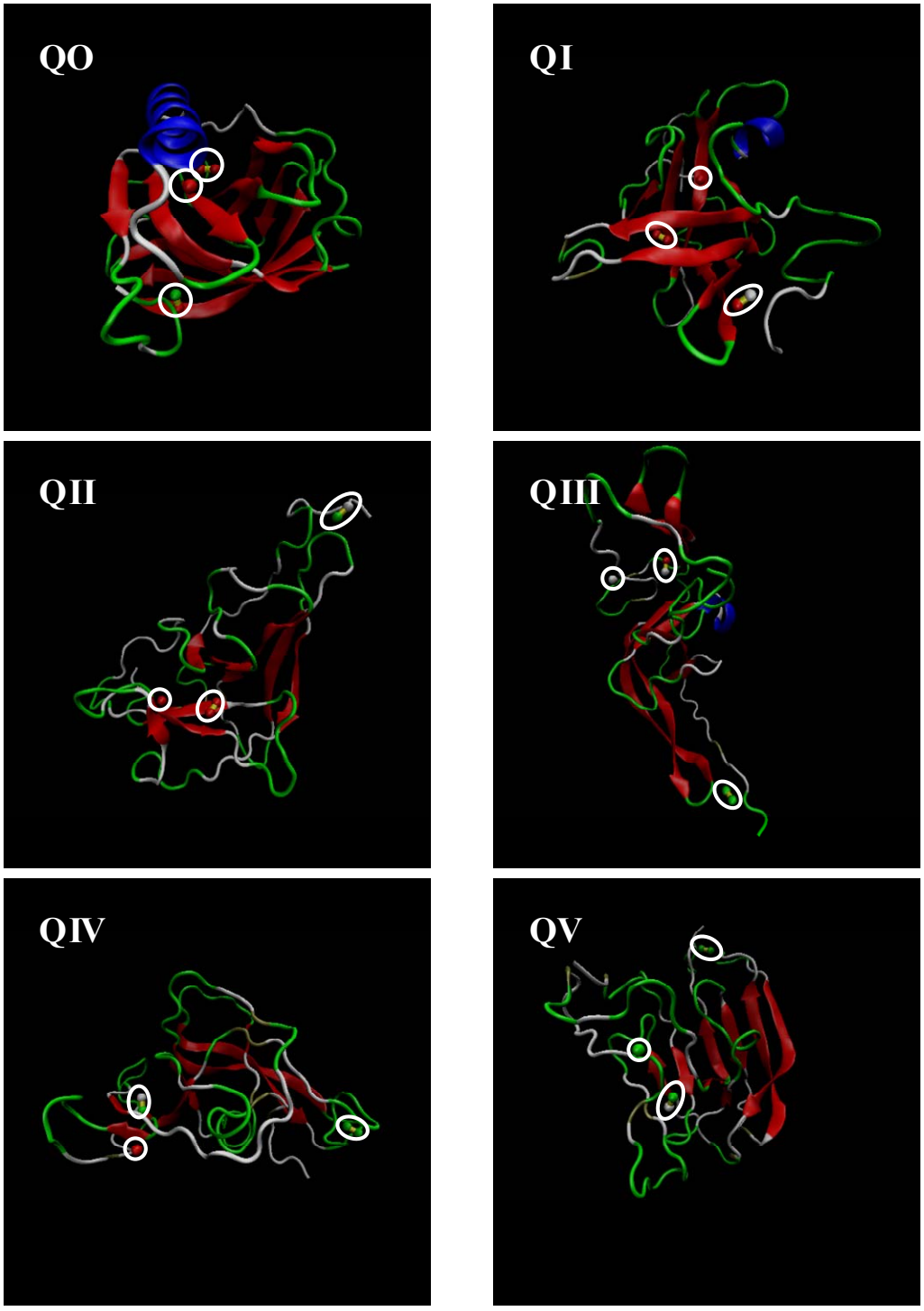

Figure 5.4 Representative structures of proteins with different extent of unfolding (positions of cysteine residues are shown surrounded by white ellipses).

5.3.3 Hydration of β-lactoglobulin

Besides changes in the tertiary and secondary structures, unfolded proteins also modify their hydration shells outside the molecular surfaces (Damodaran, 1996b; Raschke, 2006). It has been believed that hydration waters have very distinct behaviour from bulk water, since the former interact with or are affected by the protein molecular surface (Ball, 2008; Raschke, 2006). Raschke (2006) has concluded that water molecules interact directly with polar groups when they are close, while those close to nonpolar groups prefer interacting with themselves via hydrogen bonds (HB). Accordingly, the solvent accessible surfaces of unfolded proteins are analyzed to estimate the effects of unfolding on the protein hydrations. The time averaged area of solvent accessible surface for each protein (QO ~ QV) is shown in Figure 5.5. It is found that unfolding of proteins increases both the hydrophobic and hydrophilic molecular surfaces. Besides, the QIV molecule is found to have relatively small solvent accessible surface compared with other unfolded structures, which could be due to commencement of protein refolding. In terms of Figure 5.5, QIII and QIV molecules are likely to have more hydration water molecules because of their larger solvent accessible areas.

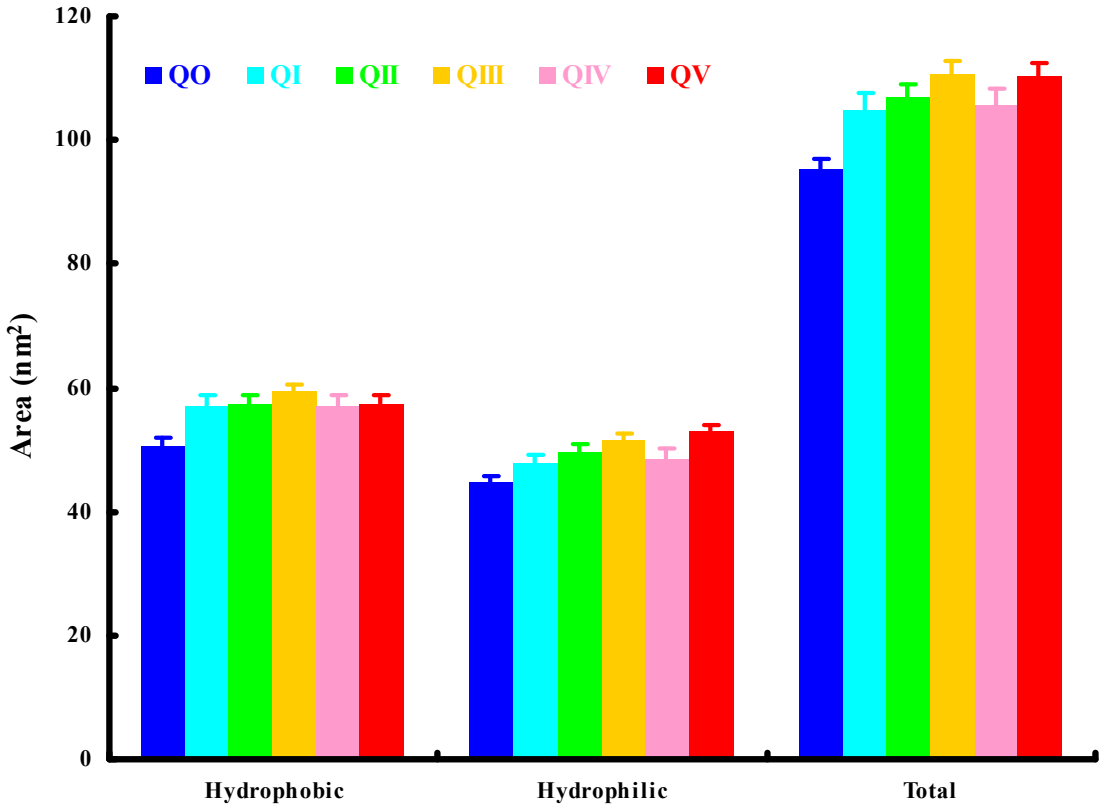

Figure 5.5 Areas of solvent accessible surfaces of different quenched proteins.

The water distributions around the surfaces of the different protein molecules are depicted in Figure 5.6. It is found that there are two hydration shells around the protein molecules, with distances of 0.24 nm and 0.32 nm from the protein surface, respectively. Moreover, the thickness of both the hydration shells are found to be independent of the protein conformations. Due to its more open structure and larger solvent accessible surface as shown in Figure 5.4 and Figure 5.5, respectively, the QIII β-lactoglobulin molecule is observed to have the most hydrations water molecules. Furthermore, it is noted that the hydration shells of the QIII protein start from a much shorter distance than the others. The reason could be more extensive unfolding and loss of the globular structure of the protein molecule. Difference in the distribution of molecules in bulk water is also found for different proteins. However, such results are not sufficient to reveal the effects of protein molecules on bulk water, since the distance, *d*, is measured in terms of the protein surface, and therefore, the effects of protein radii are not excluded.

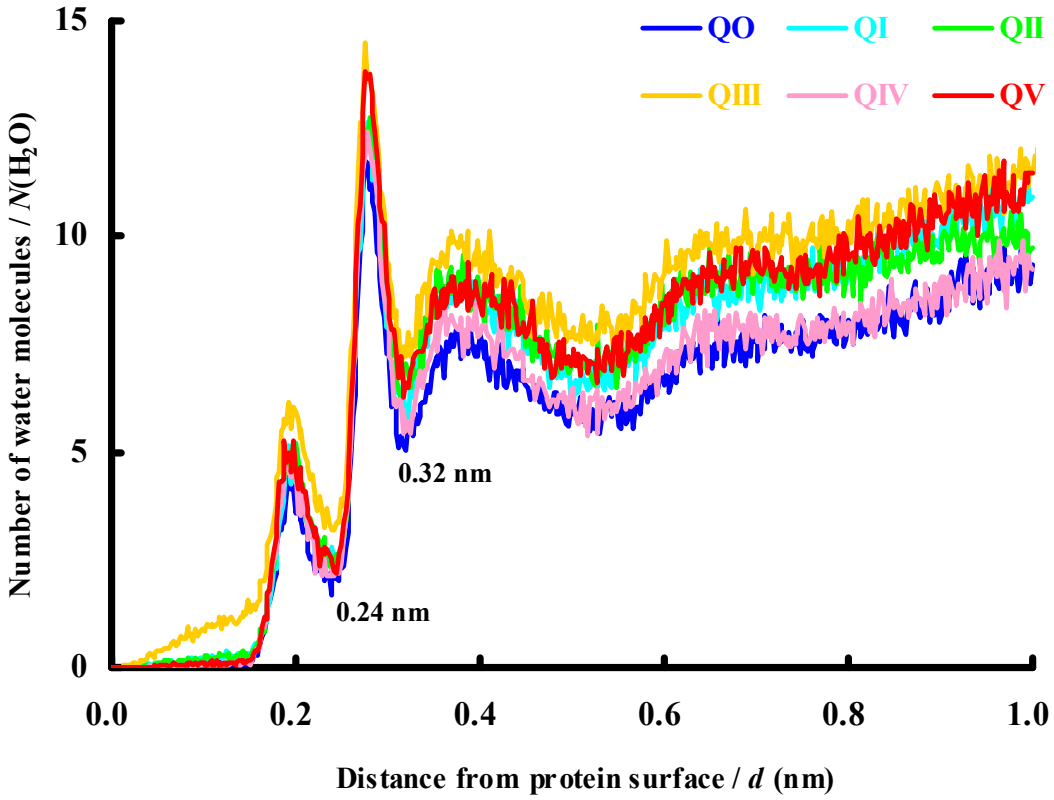

Figure 5.6 Distribution of water molecules, $N(H_2O)$, around protein surface.

Since water molecules in the hydration shells of a protein would form hydrogen bonds with the protein surface or with themselves (Raschke, 2006), the hydrogen bonds formed by water molecules were analyzed. Abilities of different water molecules to form hydrogen bonds are expressed as the ratio of the number of hydrogen bonds, N(HB), to that of water molecules, $N(H_2O)$. Figure 5.7 and Figure 5.8 illustrate the abilities of different hydrated waters to form hydrogen bonds with proteins and water molecules, respectively. It is found in Figure 5.7 that water molecules in the first hydration shell are more inclined to form hydrogen bonds with proteins (W-P HB) than those in the second hydration shell, since the former are closer to the protein surfaces. Besides, hydrophobicity of the protein surfaces seems to be an important factor affecting the hydrogen bond forming ability of water molecules. As shown in Figure 5.7, waters in the hydration shells of QIII protein have the lowest ability to form hydrogen bonds with the protein, which is due to the large number of non-polar groups on the protein surface and therefore, a tendency of waters to form hydrogen bonds with themselves rather than with the protein surface. The preference for water-water

hydrogen bond (W-W HB) formation of hydrated waters is shown in Figure 5.8. It is found that the ability to form W-W HB of hydrated waters around QIII protein is much higher than other proteins, where more hydrophobic molecular surface of the protein is accessible to water molecules. Additionally, unfolded protein structures are found to increase the W-W HB ability of the hydrated waters since there are more non-polar groups exposing to the solvent. The hydrated waters around QIV protein are found to have higher ability to form W-P HB but lower one for W-W HB. This results from the melting secondary structures, mainly β-sheets, and the increased flexibility of the polypeptide chain, which allows some non-polar side chains to head towards the interior of the protein molecule. However, more hydrophobic cavities of the molecule collapse as the QV molecule further unfold, and thus more non-polar groups become water accessible to increase the W-W HB formation, especially in the first hydration shell.

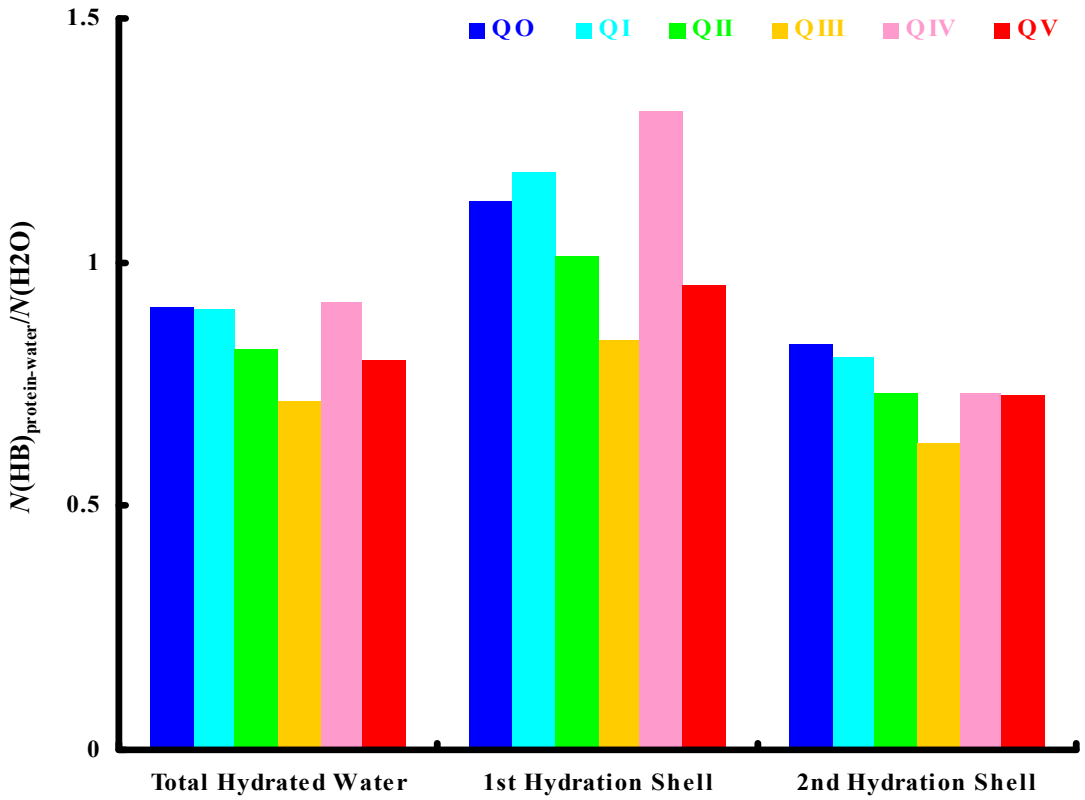

Figure 5.7 Abilities of different hydrated waters to form hydrogen bonds with protein molecules.

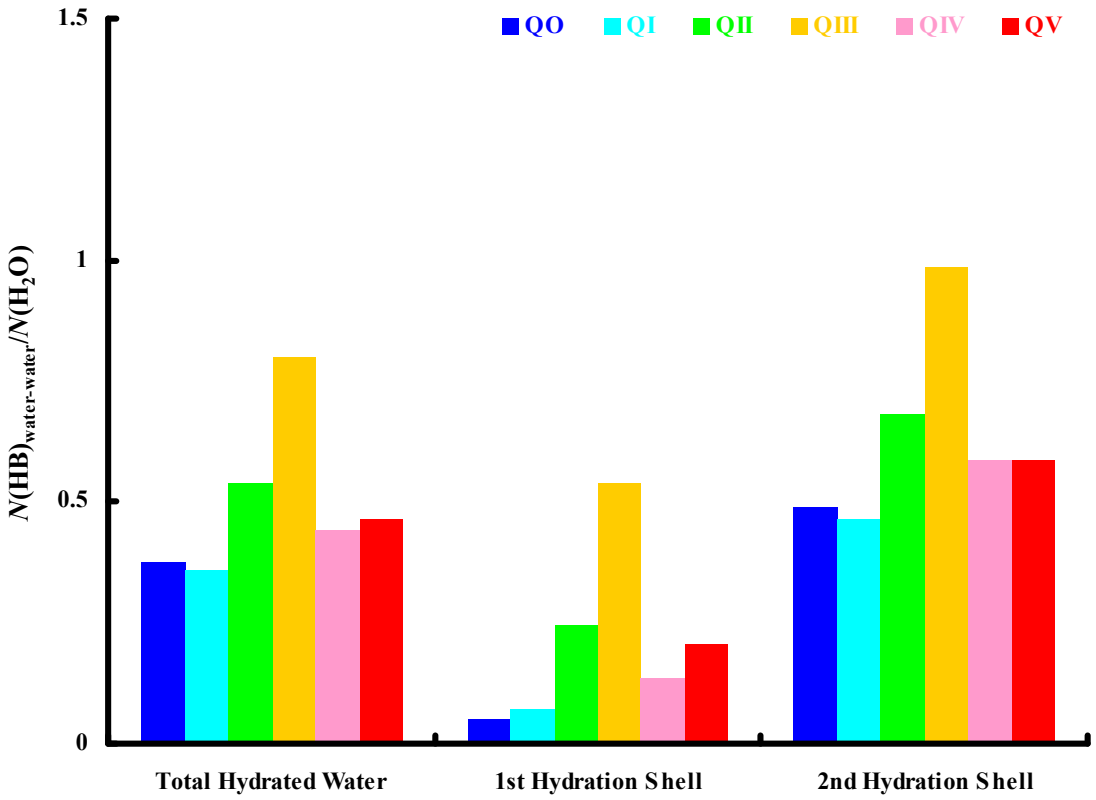

Figure 5.8 Abilities of different hydrated waters to form hydrogen bonds with water molecules.

Lifetime of the hydrogen bonds can be revealed through their autocorrelation functions (Luzar & Chandler, 1996; van der Spoel et al., 2006). The autocorrelation functions of the hydrogen bonds formed by water and the different unfolded β-lactoglobulin molecules are plotted in Figure 5.9. It is found there is no effect of unfolding on the decay time of the protein-water hydrogen bonds. However, the mobility of hydrated water is found to depend on the protein structure, as shown in Figure 5.10, where the fraction of remaining water molecules in the hydration shells was plotted versus time (Paradossi et al., 2011). It is observed that the hydrated water molecules around QI and QIV proteins diffuse more slowly than those around the native structure, i.e., QO, protein molecule, indicating that the P-W HB significantly freeze hydrated water molecules. It is also found that the unfolded proteins (i.e., QI ~ QV) tend to have more hydrated water molecules left in their hydration shells than the native state (i.e., QO). That could be due to the larger molecular sizes of the former, which increase the possibility for the unfolded protein molecules to meet more water molecules in the solutions.

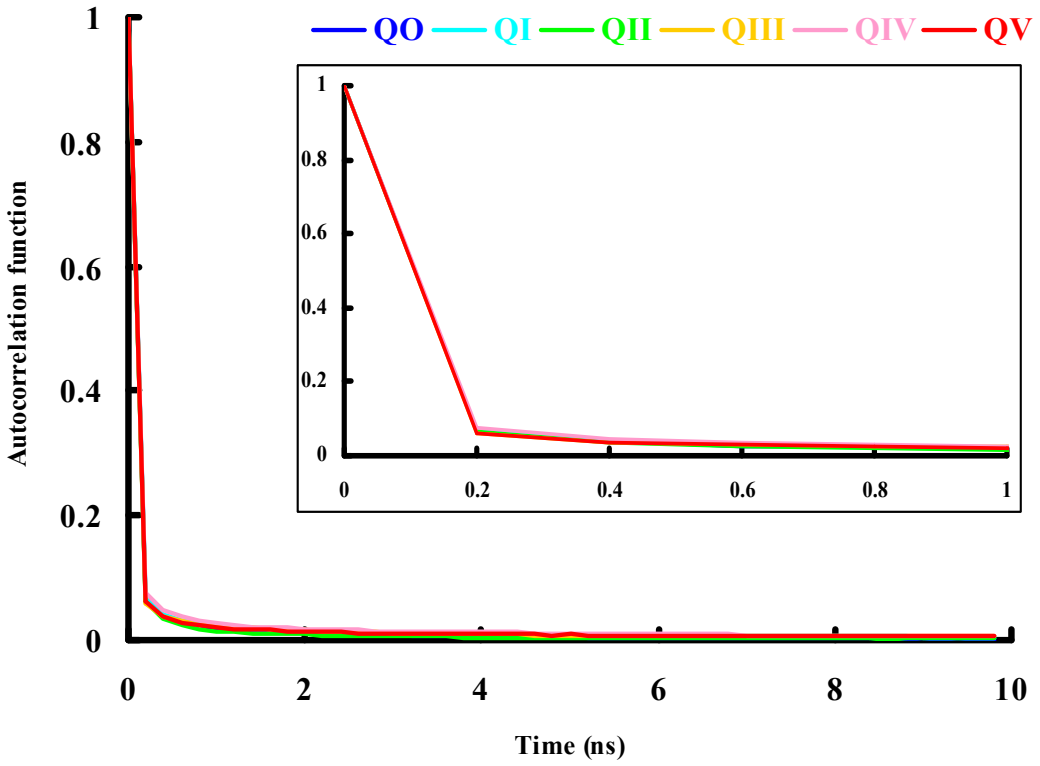

Figure 5.9 Autocorrelation functions of hydrogen bonds formed by water and protein molecules.

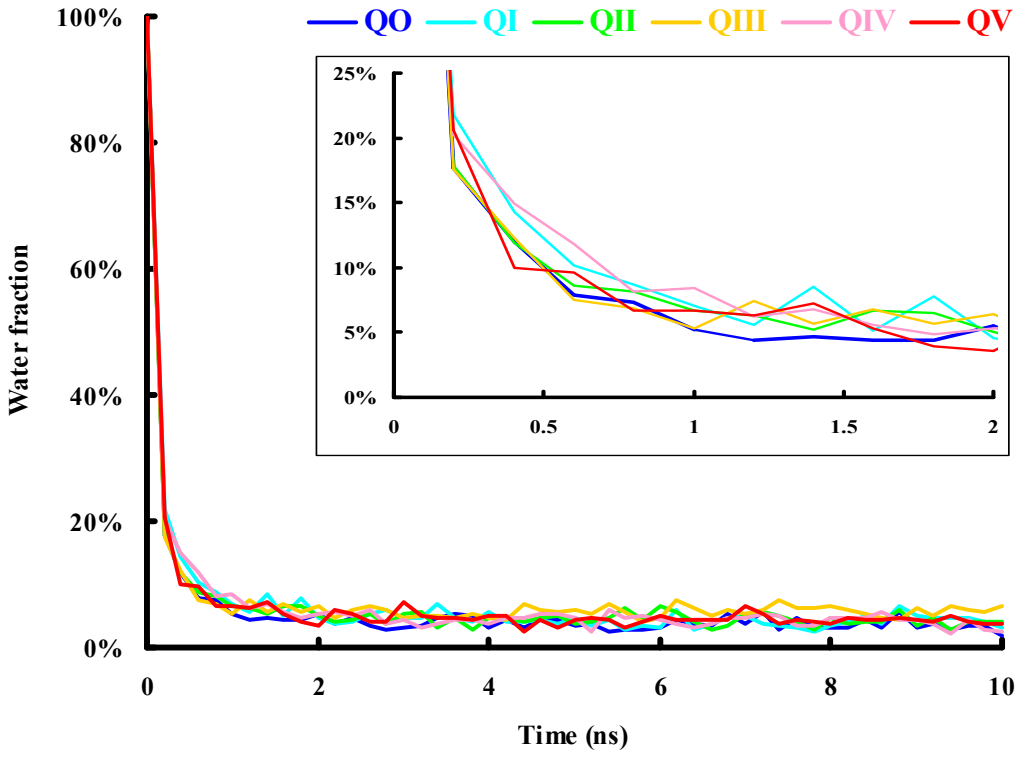

Figure 5.10 Water mobility expressed as time functions of the remaining fraction of hydrated water in the hydration shells.

5.4 Particle size of protein-based fat replacers

5.4.1 Optimization of refractive index

The particle size of the fat replacer material was measured by laser diffraction, where the refractive index of the particle is required for the conversion from the diffraction pattern of a particle to its particle size distribution through the Mie theory (Du, 2004; Wriedt, 2012). There have been several studies focusing on the refractive indices of whey proteins, which reported values of refractive indices of 1.615 for α-lactoglobulin, 1.594 for β-lactoglobulin, and 1.606 for bovine serum albumin (McMeekin, Groves, & Hipp, 1964). However, none of these reported values is considered to be accurate for the particle size measurement of the protein and fat replacer materials here. First of all, the samples in current project are mixtures and thus, are more complicated than pure protein powders. Additionally, the optimized refractive indices, and therefore the particle size distributions, also depend on the equipment employed (Hayakawa et al., 1995). As a result, optimization of the refractive index has been performed to ensure that the correct value can be used to derive particle size data. Optimization of refractive indices for whey protein concentrate (i.e., Lacprodan87) and protein-based fat replacer (i.e., Simplesse and Hiprotal60 products) samples are performed following the method proposed by Hayakawa et al. (1995). The median diameter, D[0.5], of different samples are plotted against refractive indices in Figure 5.11. It is found that values of D[0.5] for all the samples increase with refractive indices up to a certain refractive index value and then keep constant or decrease. Such observations coincide with the results from Hayakawa et al. (1995) and Saveyn et al. (2002). According to these authors, the refractive index corresponding to the first peak of the particle size is considered to be optimized for calculating the particle size distribution. The optimized refractive index for each sample is listed in Table 5.1.

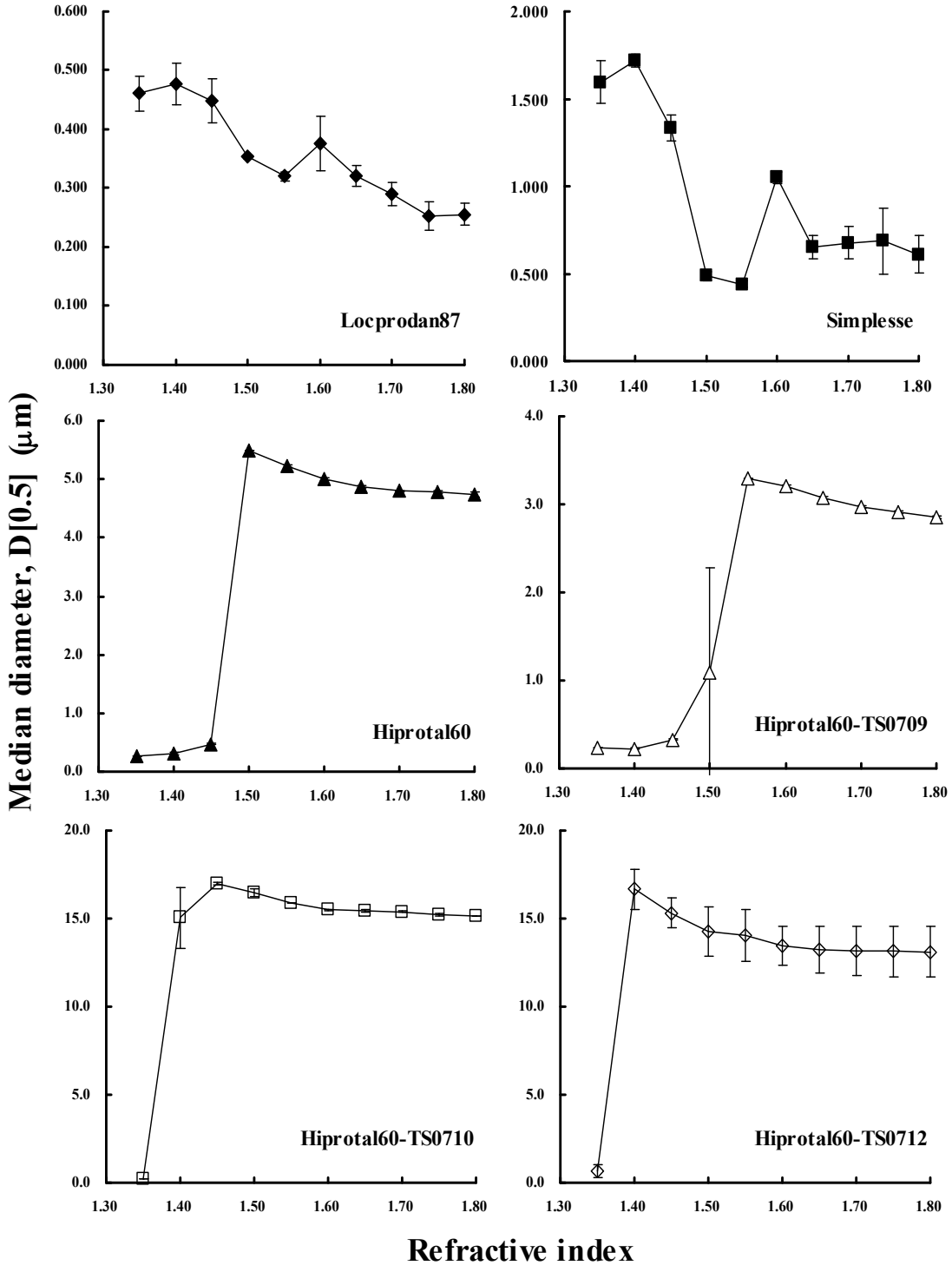

Figure 5.11 Refractive index dependence of the median diameter, D[0.5], for Lacprodan87 (◆), Simplesse (■), Hiprotal60 (▲), Hiprotal60-TS0709 (△), Hirpotal60-TS0710 (□), and Hiprotal60-TS0712 (◇).

Table 5.1 Optimized refractive indices and the corresponding median diameter, D[0.5] of different samples.

Sample	Optimized Refractive Index	Median Diameter / D[0.5] (μm)
Lacprodan87	1.40	0.48 ± 0.04
Simplesse	1.40	1.72 ± 0.04
Hiptotal60	1.50	5.484 ± 0.001
Hiptotal60-TS0709	1.55	3.296 ± 0.001
Hiptotal60-TS0710	1.45	17.00 ± 0.07
Hiptotal60-TS0712	1.40	17 ± 1

5.4.2 Particle size distribution

Particle size distributions of Lacotprodan87 and Simplesse and Hiprotal60 products are calculated with the optimized refractive indices as listed in Table 5.1, and the results are illustrated in Figure 5.12 and 5.13, respectively. It is found that Lacprodan87 particles, are submicrons in water solutions with two peaks in the particle size distribution, concentrating around 0.1 ~ 0.2 μm and 0.6 ~ 0.7 μm, respectively. The first peak (the smaller one) reveals that the proteins, mainly β-lactoglobulins, form small dispersed aggregates in solutions (Ryan, Zhong, & Foegeding, 2013), while the larger particles are supposed to result from aggregation of the proteins during the processing of these whey protein concentrate products (de la Fuente, Hemar, Tamehana, Munro, & Singh, 2002). As for Simplesse, three peaks in the particle size distribution are observed, concentrating around 0.2 μm, 0.9 ~ 1.0 μm and 5 ~ 6 μm, respectively. The smallest peak is supposed to correspond to the dispersed aggregates formed by the proteins as in Lacprodan87, and the main peak, i.e., the second peak, indicate the particle size of the functional components in Simplesse. A narrow distribution for the largest particles is found in Simplesse, which may be a result of flocculation of the particles.

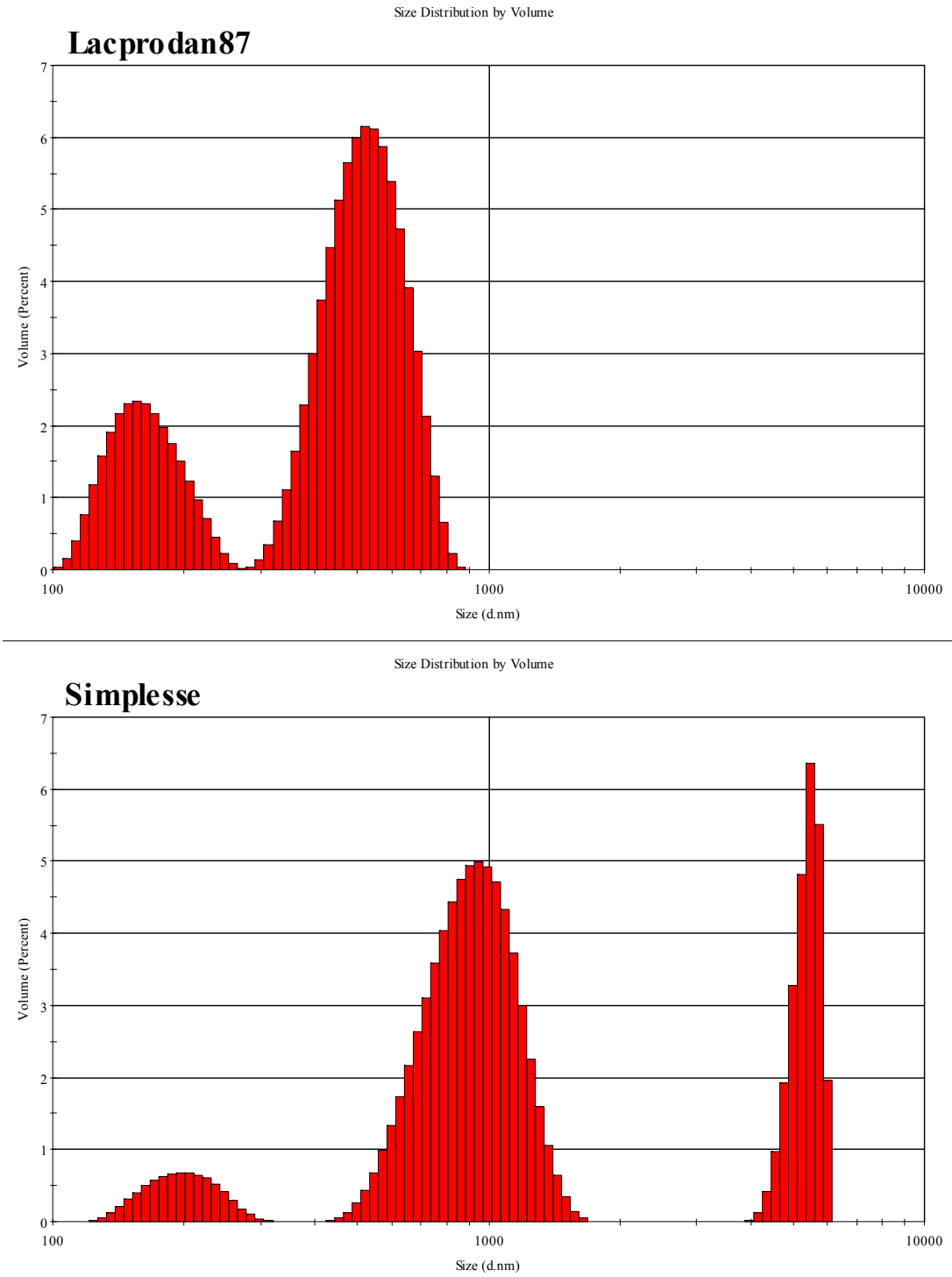

Figure 5.12 Particle size distribution of Lacprodan87 and Simplesse measured from a Malvern Zetasizer.

All the Hiprotal60 products are found to be micron particles as shown in Figure 5.13, indicating all these partial denatured protein products form aggregates in water solutions. It is observed that Hiprotal60 tends to possess larger particles and a wider distribution in water solutions than Hiprotal60-TS0709, while the latter material

exhibit larger aggregates with a particle size of the order of 10 μm, as suggested by its secondary peak. Hiprotal60-TS0710 and –TS0712 are found to have similar diameters and particle size distributions in water solutions, as illustrated in Table 5.1 and Figure 5.13. The large particle size and wide (around 2 orders) distribution reveal that proteins in such materials form large aggregates, which are preserved in water solutions. According to Bryant and McClements (1998), such large aggregates are assumed to be formed by β-lactoglobulins and have a "string-of-beads" structure favored by intermolecular SH/S-S interchange reactions.

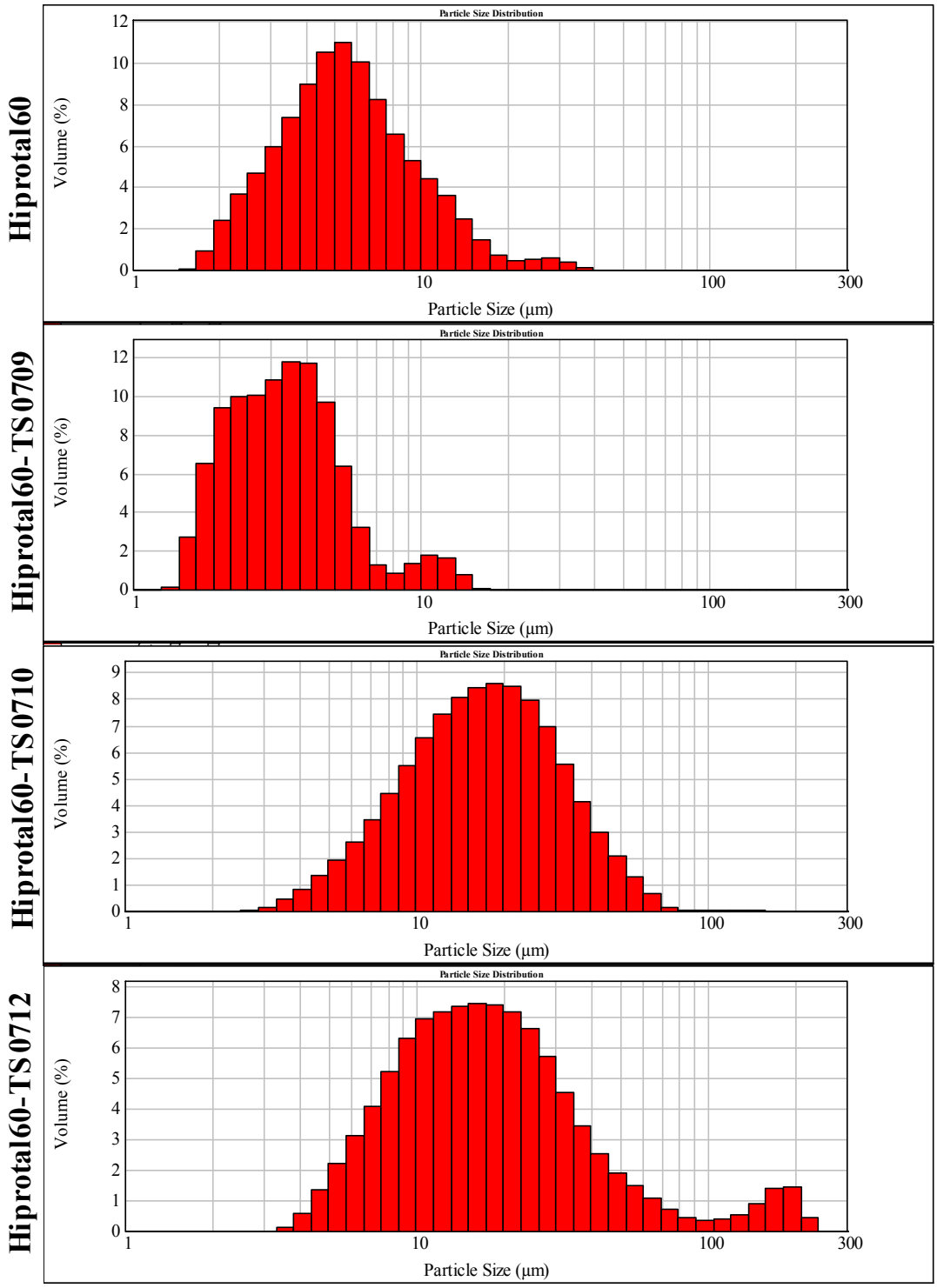

Figure 5.13 Particle size distribution of Hiprotal60 products measured from Malvern Mastersizer.

5.5 Aggregation of proteins in fat replacers

In order to understand the aggregates of the proteins in the samples, especially in the protein-based fat replacers, Environmental scanning electron microscope (ESEM) is employed to image the materials. The electron micrographs of different samples are shown in Figure 5.14 to 5.19. It is found that proteins in Lacprodan87 are barely visible, indicating very small sizes of the particles. Simplesse is observed to behave as globule-like micron sized particles which are formed through aggregation of small granules. Hiprotal60 exhibits large particles formed from smaller aggregates, which is similar to Simplesse, but with more severe aggregation. As for Hiprotal60-TS0709, however, the structure is very different from Simplesse and Hiprotal60, where rod-like aggregates formed by small granules are observed. Despite similar particle size distributions, the large particles in Hiprotal60-TS0710 and –TS0712 are found to have very different structures. Microparticulates are observed in Hiprotal60-TS0710, while large strands are found in Hiprotal60-TS0712. It should be noted that it is unadvisable to relate the particle size results in Figure 5.12 and 5.13 with the images obtained from ESEM, since the former are determined in water solutions while the latter is photographed in vacuum. It is difficult to exclude the effects of water evaporation on protein aggregates. However, some important information is still provided from ESEM. For instance, as shown in Figure 5.19 the large strands observed in Hiportal60-TS0712 reveal the highly elongated aggregation of the proteins and could predict strong gels formed by such material (Stading & Hermansson, 1990; Stading, Langton, & Hermansson, 1992). The results of SDS-PAGE of Lacprodan87 and protein-based fat replacers are shown in Figure 5.20. No difference is found between Lacprodan87 and the fat replacers in both non-reduced and reduced SDS-PAGE, indicating that the aggregates of the modified proteins found in Figure 5.14 to 5.19 are not stabilized by intermolecular disulfide bonds. According to Section 5.3.2, such observations illustrate that the proteins in the fat replacers are not completely unfolded, where the $-SH^{121}$ and one $S\text{-}S^{66\text{-}160}$ are inaccessible to solvent molecules. Therefore, the large particles in the fat replacers, especially those in Hiprotal60-TS0710 and -TS0712, are believed to arise from hydrophobic aggregations of the partial denatured proteins.

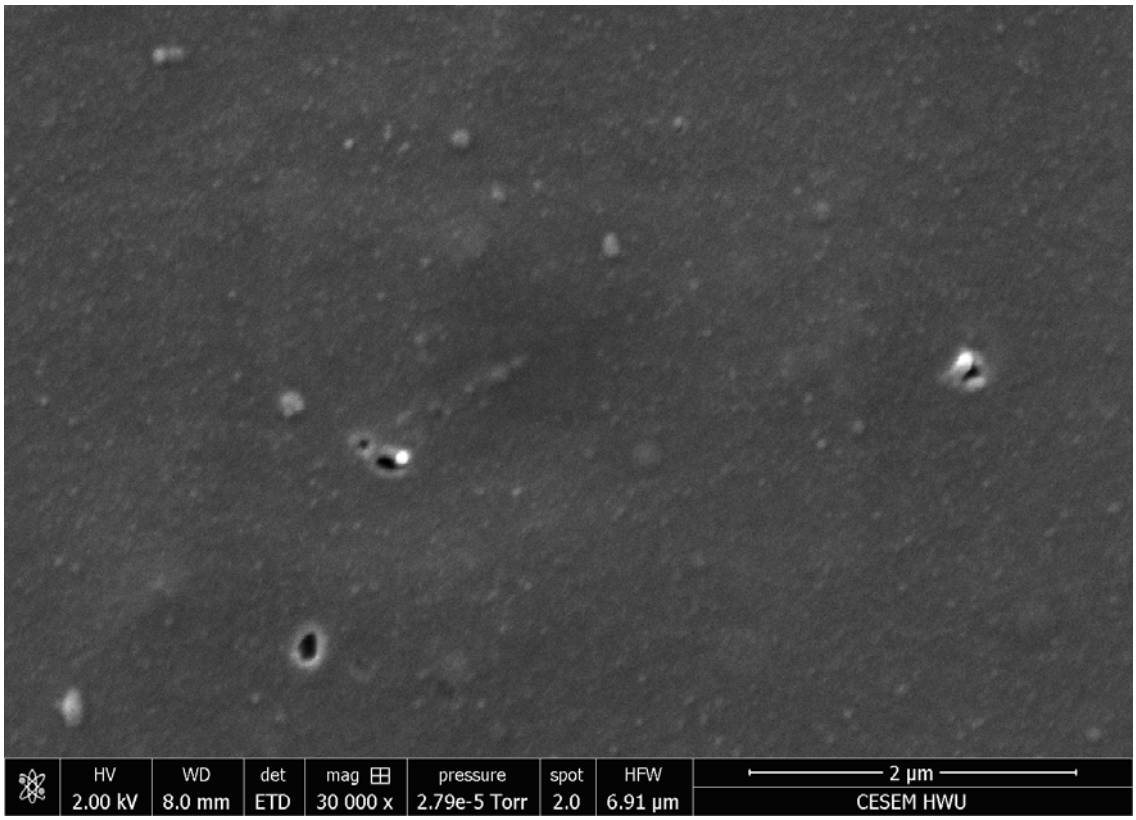

Figure 5.14 Electron micrograph of Lacprodan87 with a magnitude of 30000.

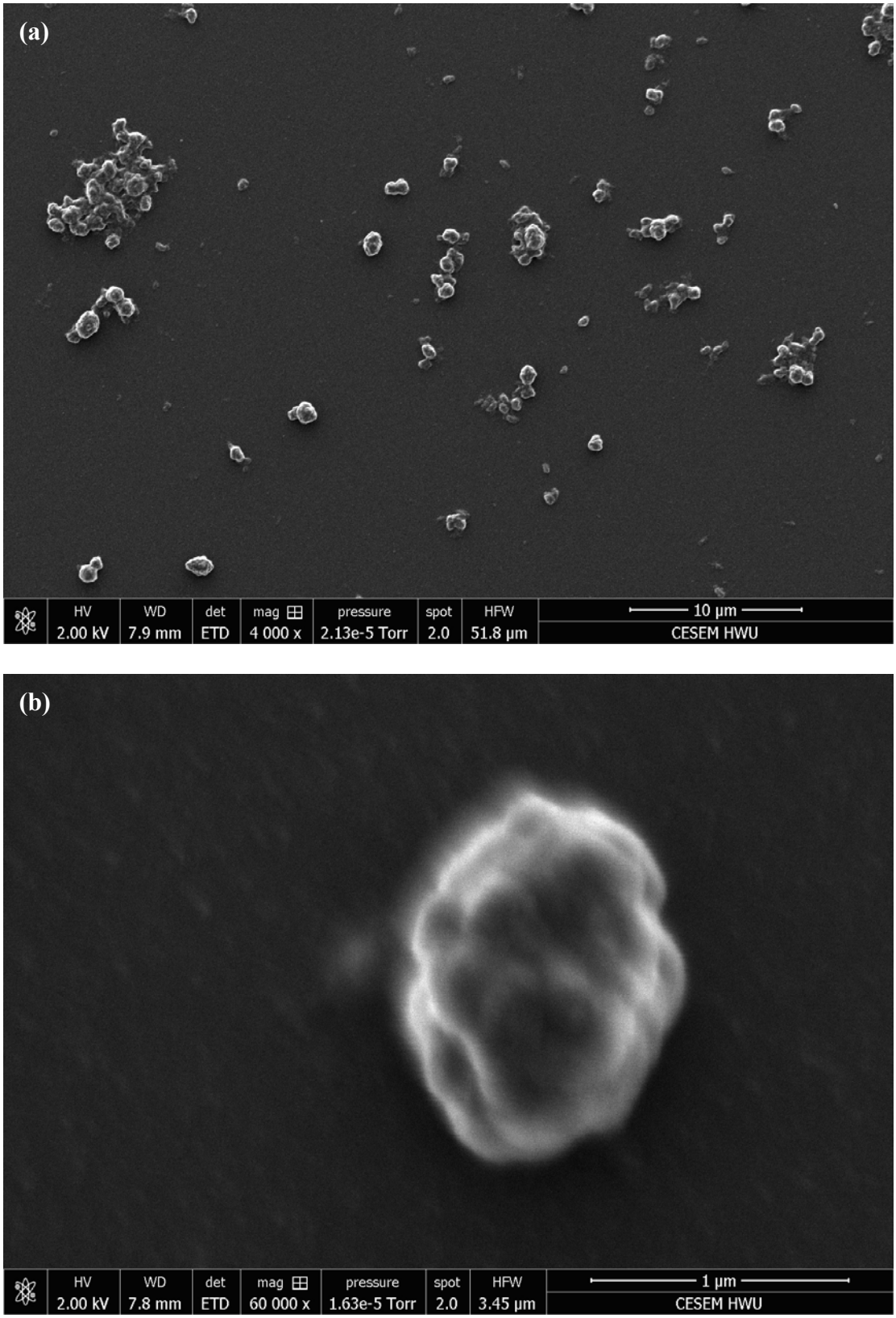

Figure 5.15 Electron micrograph of Simplesse with a magnitude of (a) 4000 and (b) 60000.

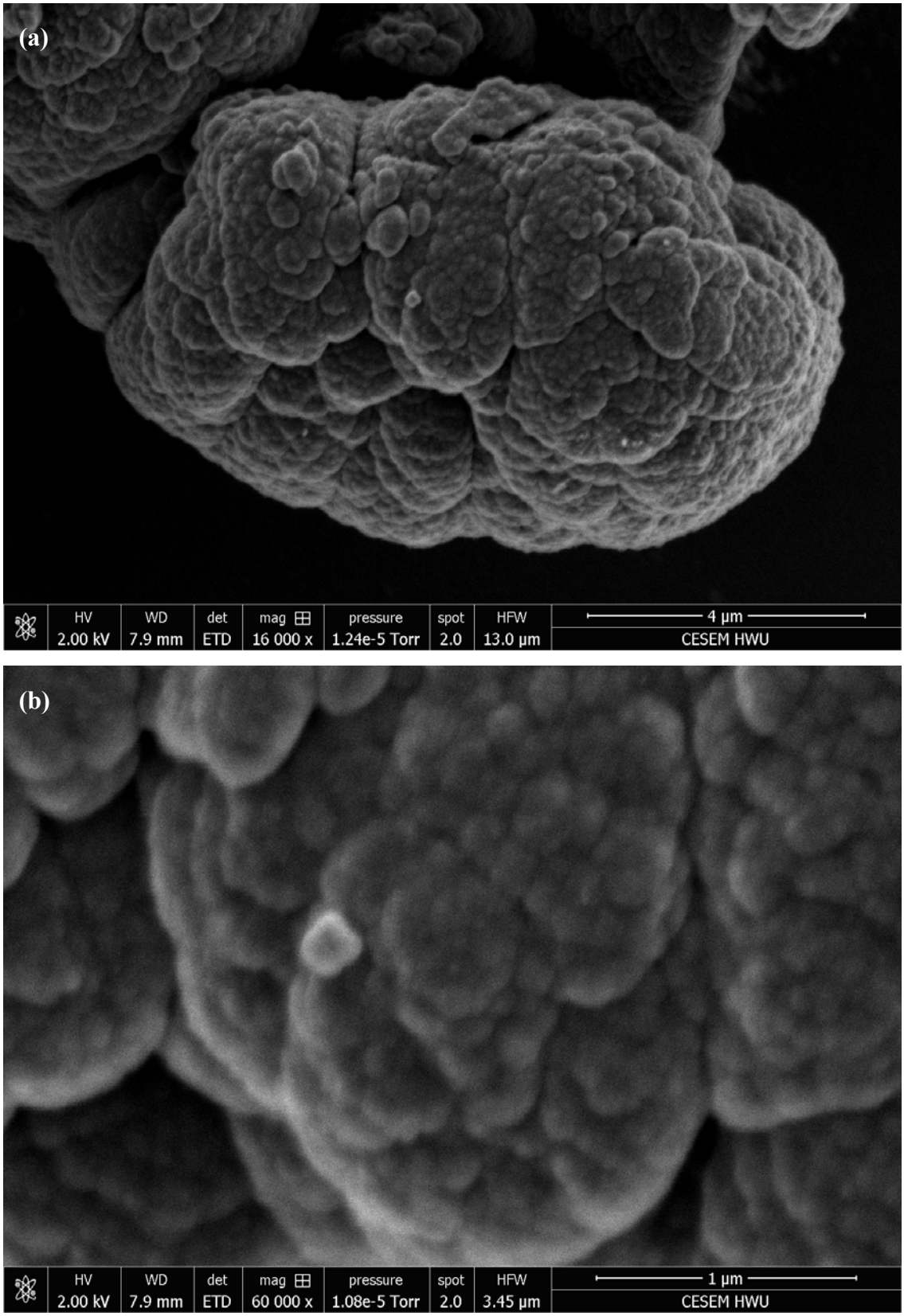

Figure 5.16 Electron micrograph of Hiprotal60 with a magnitude of (a) 16000 and (b) 60000.

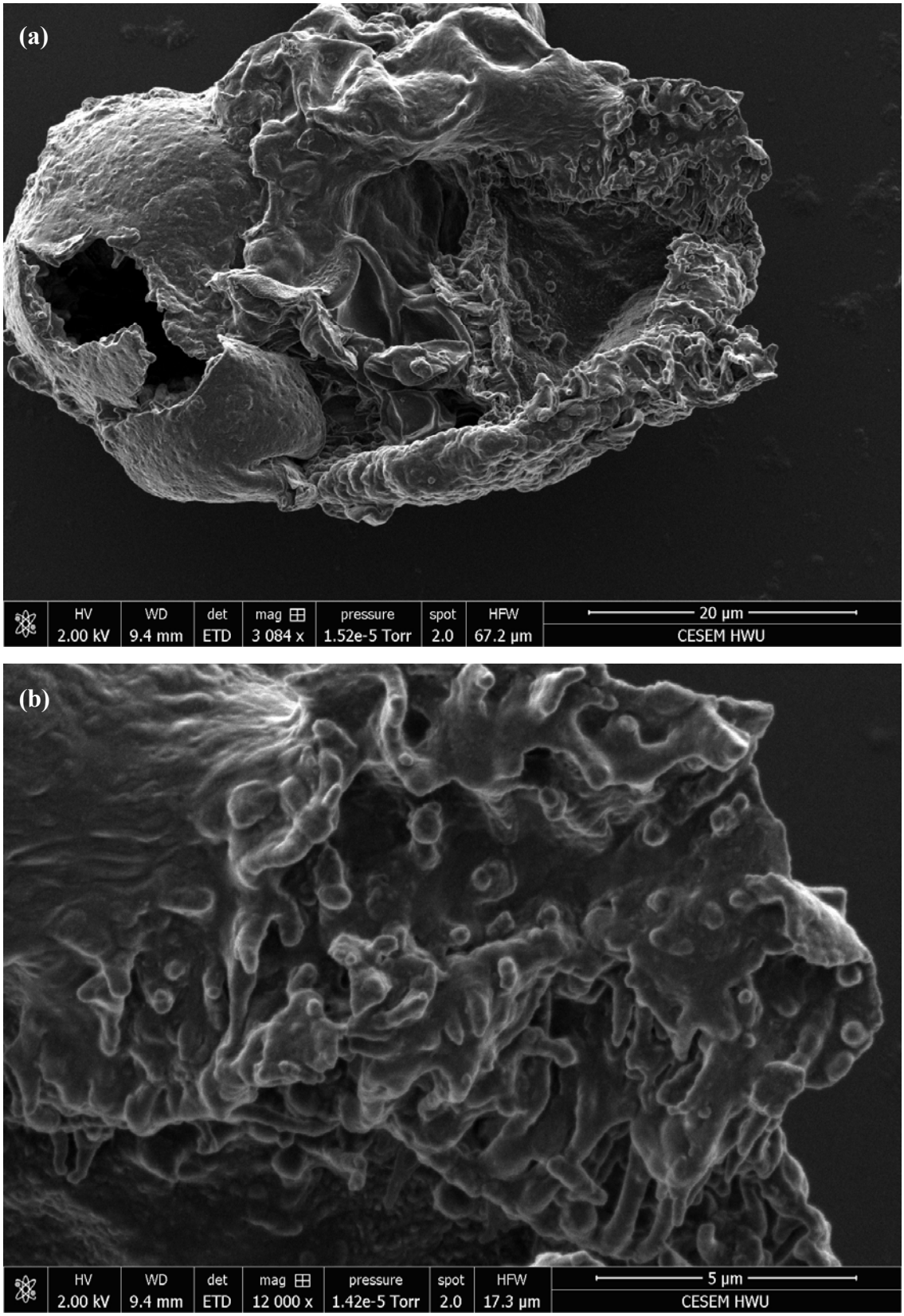

Figure 5.17 Electron micrograph of Hiprotal60-TS0709 with a magnitude of (a) 3084 and (b) 12000.

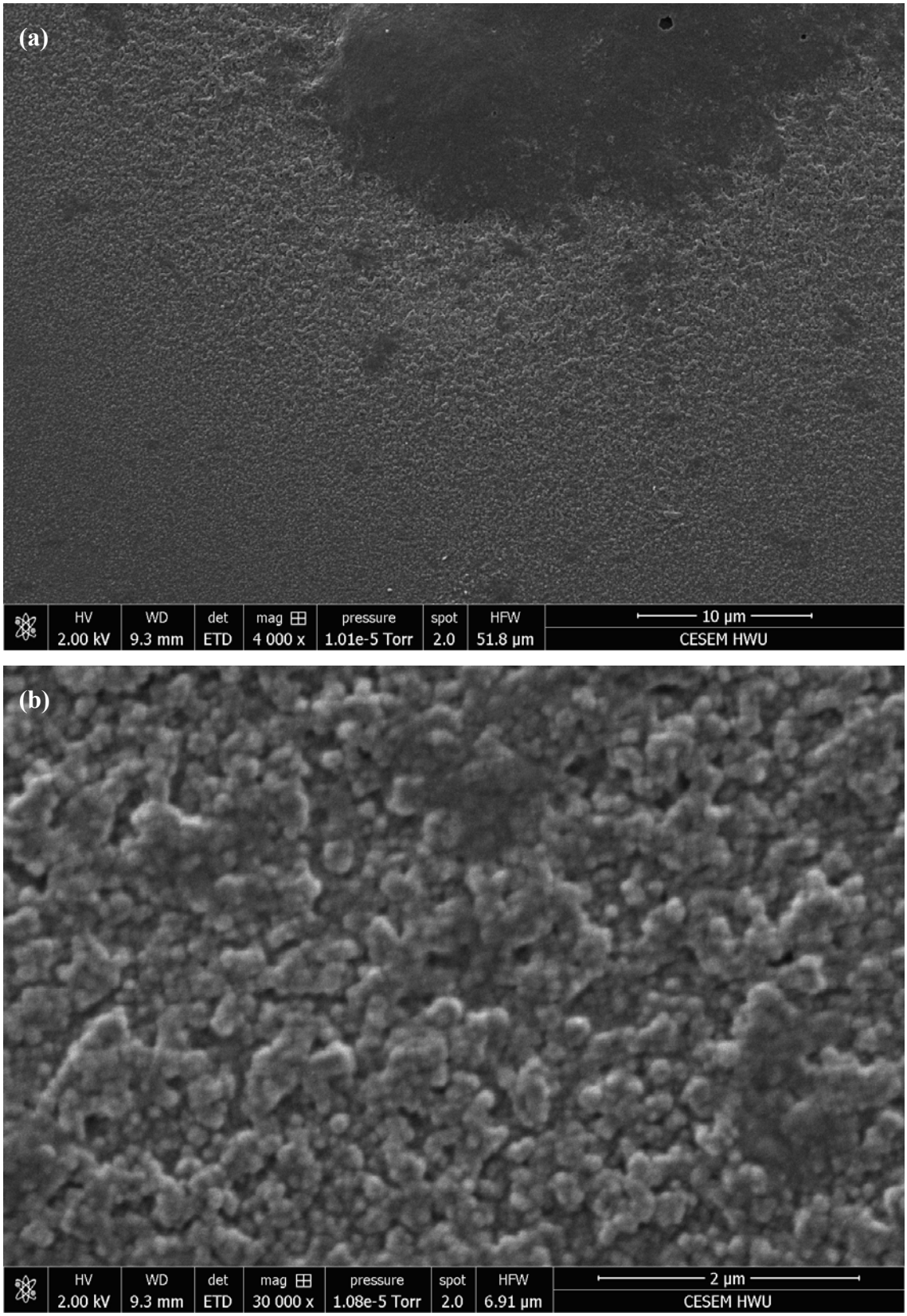

Figure 5.18 Electron micrograph of Hiprotal60-TS0710 with a magnitude of (a) 4000 and (b) 30000.

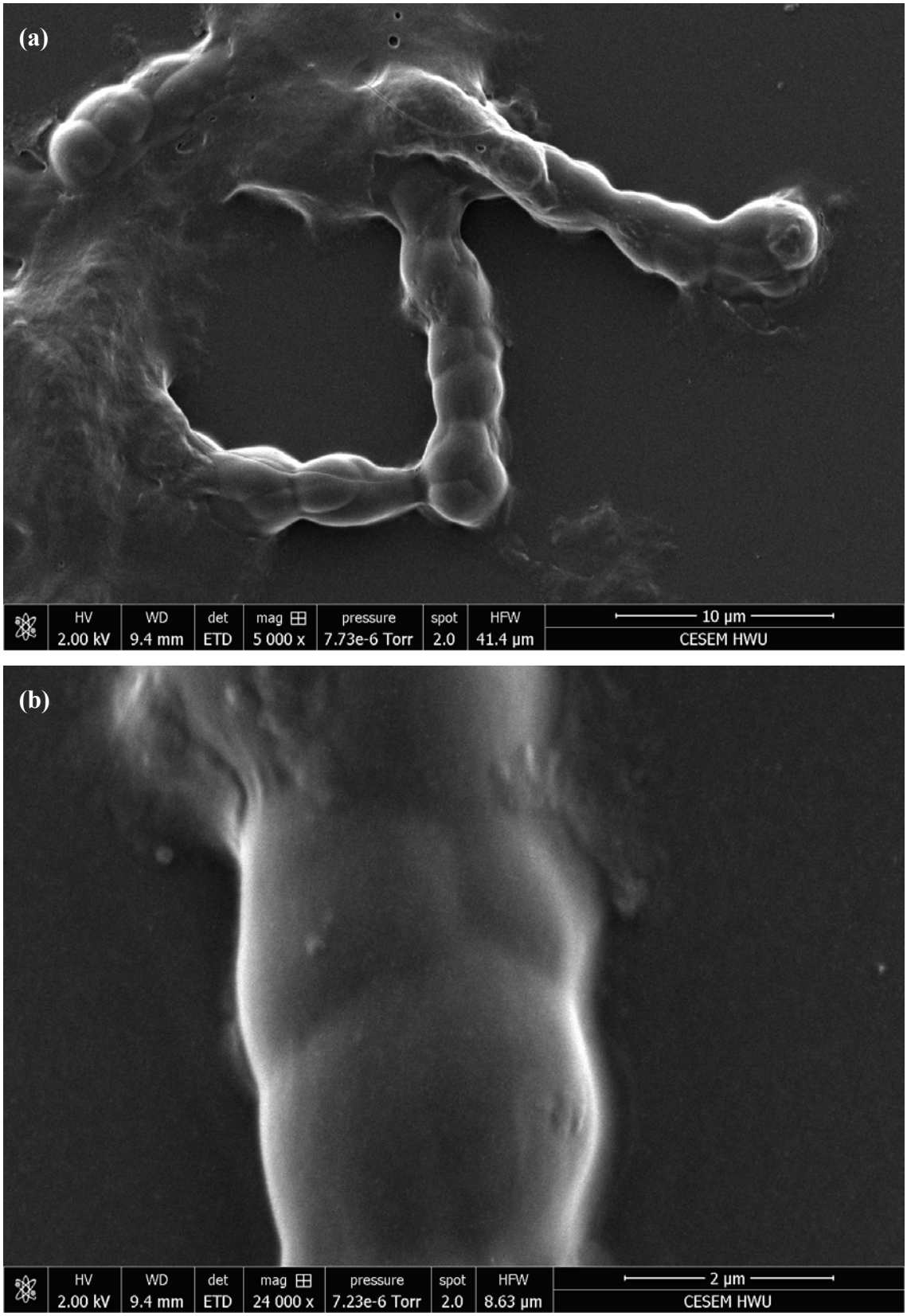

Figure 5.19 Electron micrograph of Hiprotal60-TS0710 with a magnitude of (a) 5000 and (b) 24000.

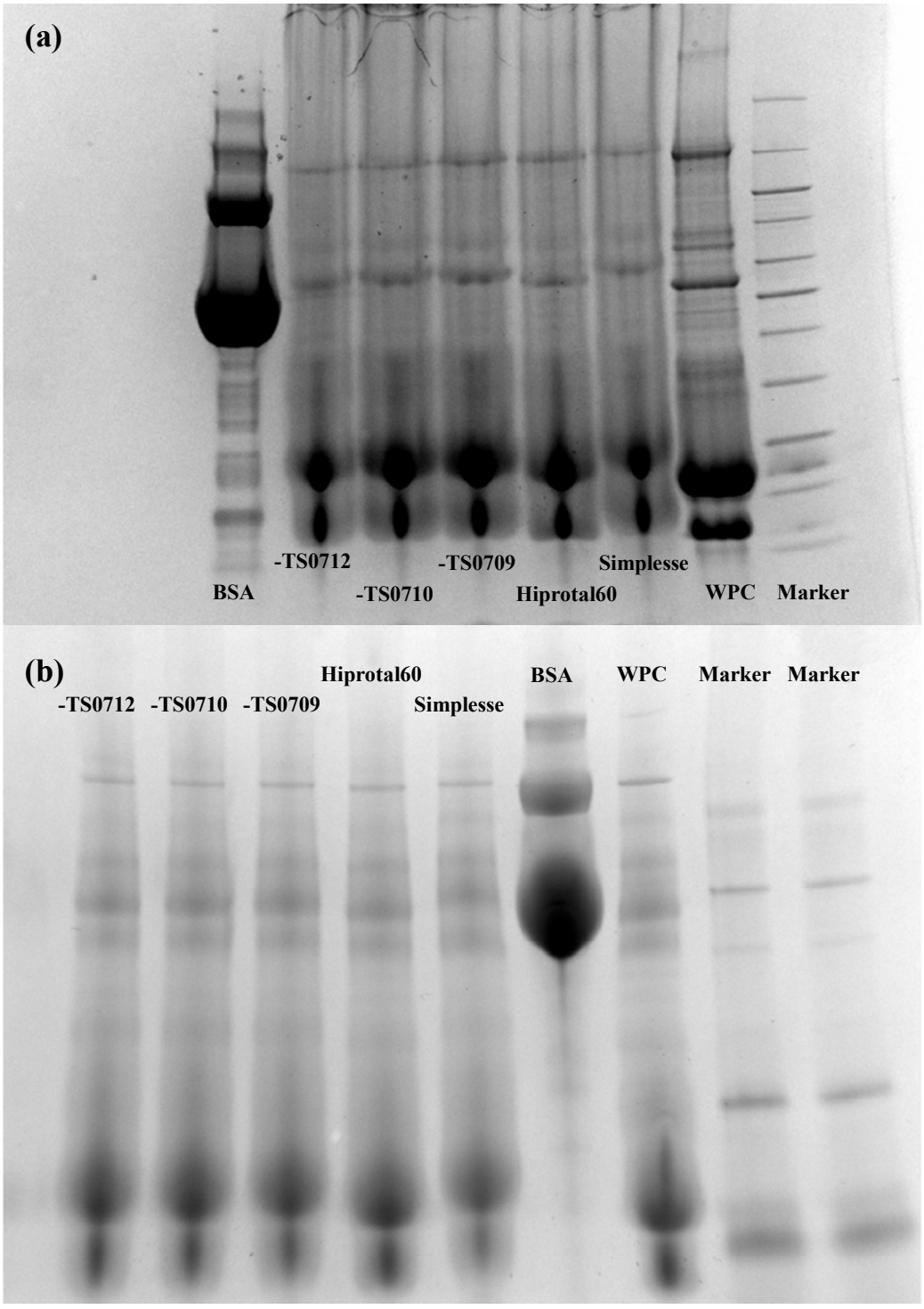

Figure 5.20 Non-reduced (a) and reduced (b) SDS-PAGE of WPC (Lacprodan87), BSA (bovine serum albumin), Simplesse and Hiprotal60 products.

5.6 Partial specific volume

5.6.1 Density of solutions

Like the definition of specific viscosity (Moore, 1976; Zhang & Scanlon, 2011), the concept of specific density, ρ_{sp}, is employed here to express the changes in density of the protein solutions,

$$\rho_{sp} = \frac{\rho}{\rho_0} - 1 \tag{5.4}$$

where ρ represents the absolute density value and the subscript $_0$ indicates properties of the solvent, i.e., water here. The specific density of different serial dilutions of whey protein concentrate (WPC) and modified whey proteins, i.e., Simpless and Hiprotal60 products are plotted versus total solid concentration in Figure 5.21. It is found that the specific density, ρ_{sp}, has good a linear relationships ($R^2 > 0.998$) with the total solid concentration of the serial dilutions. It should be noted that the intercepts of the regression lines of ρ_{sp} in Figure 5.21 are set to be 0 according to the definition of specific density, and thus, the linearity of the density with the concentration of solutions is expected to be better. As expected, the density of the solution increases with the addition of proteins, and the concentration dependences of specific density, $d\rho_{sp}/dw$, numerically equal to the slopes, $[\rho]_{sp}$, of the curves in Figure 5.21, are shown in Tables 5.2. From Figure 5.21 and Table 5.2, it is found that the modified protein products are denser than WPC samples, which is supposed to result from more non-protein materials in the formers. As shown in Section 5.2.5, the volumetric fraction, φ=1-Φ_0, of the total solids in the serial dilutions are calculated and plotted versus the total solid content in Figure 5.22. Similarly as with ρ, a linear relationship is also observed between φ and w.

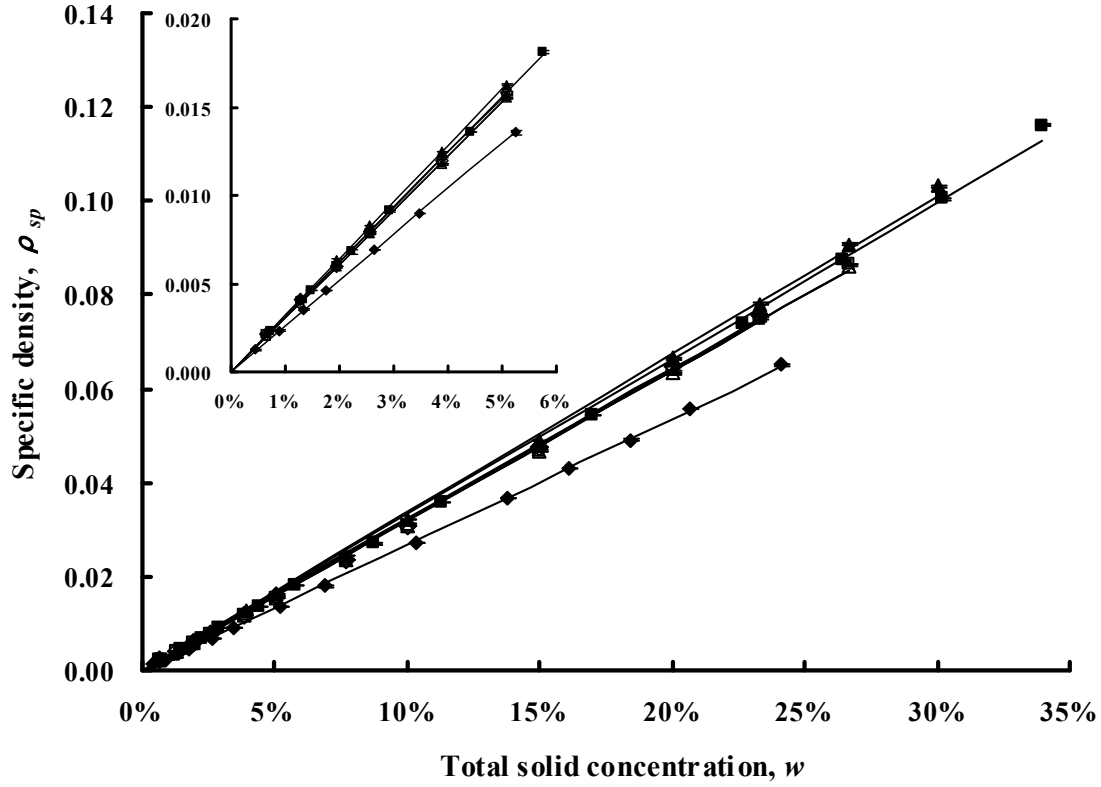

Figure 5.21 Specific density, ρ_{sp}, of serial dilutions of Lacprodan87 (◆), Simplesse (■), Hiprotal60 (▲), Hiprotal60-TS0709 (△), Hirpotal60-TS0710 (□), and Hiprotal60-TS0712 (◇).

Table 5.2 Concentration dependence of specific density, ρ_{sp}, of different proteins products.

	Protein content (%)	$[\rho]_{sp}$	R^2
Lacprotan87 (WPC)	87	0.2676	0.9998
Simplesse	53	0.3319	0.9986
Hiprotal60	60	0.3368	0.9990
Hiprotal60-TS0709	60	0.3194	0.9993
Hiprotal60-TS0710	60	0.3195	0.9994
Hiprotal60-TS0712	60	0.3205	0.9993

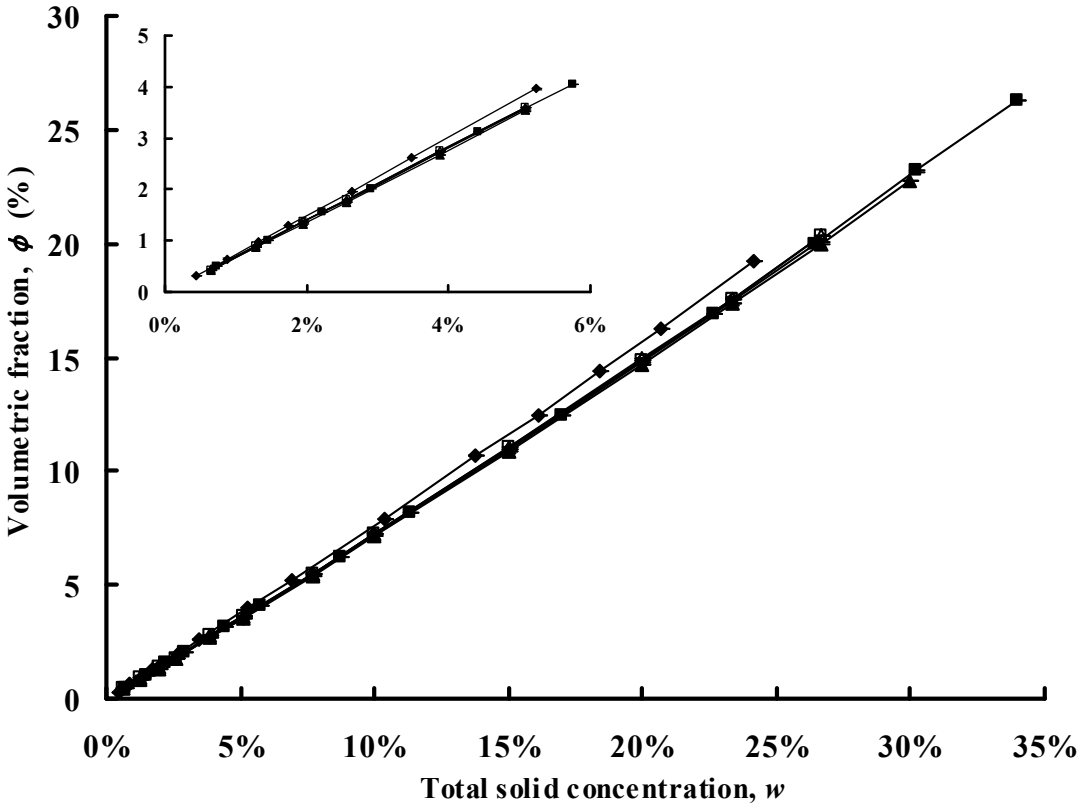

Figure 5.22 Volumetric fraction, φ, of serial dilutions of Lacprodan87 (◆), Simplesse (■), Hiprotal60 (▲), Hiprotal60-TS0709 (△), Hipotal60-TS0710 (□), and Hiprotal60-TS0712 (◇).

5.6.2 Specific Volume of particles

The apparent specific volume of matter in solutions, $\bar{v}$, is calculated from the density and the solute concentration of the solutions as Equation 5.1, where the solute concentration, c (in mg/ml), is calculated from the density, ρ, and the total solid content, w (in %), as $c = \rho \times w$. Values of the apparent specific volume, $\bar{v}$, of WPC and the protein-based fat replacers are plotted in Figure 5.23. According to Figure 5.23, the modified whey proteins are found to have smaller specific volume than the fat replacers, which is supposed to be due to unfolding of the polypeptide chains and loss of the void hydrodynamic core of the protein molecules (Chalikian, 2003). Since the concentration could influence the specific volume of proteins due to protein-protein interactions, the partial specific volume, $\bar{v}^0$, is commonly employed to investigate the

molecular structure of individual proteins (Sarvazyan, 1991).

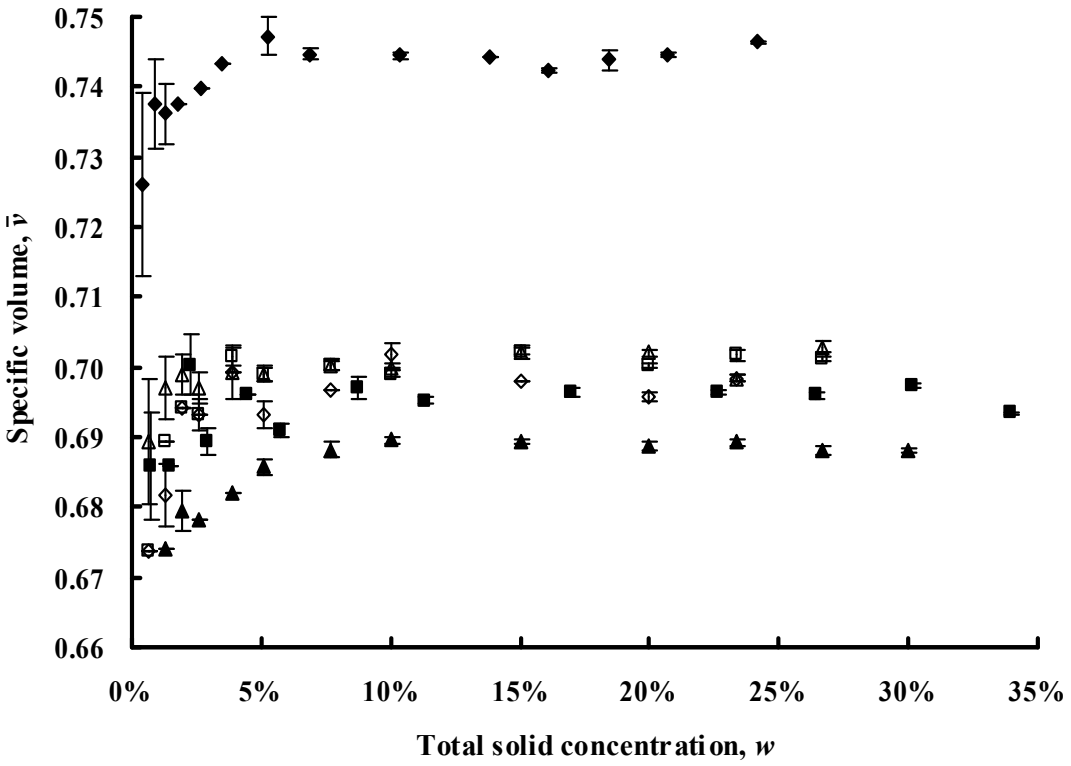

Figure 5.23 Apparent specific volume, $\bar{v}$, of Lacprodan87 (◆), Simplesse (■), Hiprotal60 (▲), Hiprotal60-TS0709 (△), Hirpotal60-TS0710 (□), and Hiprotal60-TS0712 (◇).

It is observed that the values of $\bar{v}$ for all the samples fluctuate and tend to increase at low concentrations (< 6%), while the values are approximately constant at high concentrations (> 6%). Such increasing tendency at low concentrations could reveal more collisions between the molecules as the amount of the proteins is increasing. Therefore, the dilutions with the concentrations lower than 6% are considered as ideal solutions (Pavlovskaya, McClements, & Povey, 1992) and the zero extrapolation for the partial specific volume of the proteins is performed with the values of $\bar{v}$ for these dilute solutions (< 6%).

Values of the partial specific volume, $\bar{v}^0$, of WPC and modified proteins are shown in Table 5.3. Such properties provide the information on the protein structure at the molecular levels (Chalikian, 2001; Chalikian, Totrov, Abagyan, & Breslauer, 1996). It is found the value of $\bar{v}^0$ for Lacprodan87 is smaller than those of β-lactoglobulin

and bovine serum albumin, which have been reported to range from 0.734 ~ 0.751 cm^3/g and 0.736 cm^3/g by Valdez, Le Huérou, Gindre, Urbach, and Waks (2001) and Bernhardt and Pauly (1975), respectively. The impurity of the protein samples, such as lactose and salts are supposed to account for such discrepancy. As for the modified whey proteins, i.e., Simplesse and Hiprotal60 products, the values of $\bar{v}^0$ are even smaller than that of Lacprodan87, which mainly result from more small molecules in the samples, as indicated by the protein contents of these samples.

Table 5.3 Partial specific volume, $\bar{v}^0$, of different protein products.

	$\bar{v}^0$ (cm^3/g)
Lacprotan87 (WPC)	0.723 ± 0.006
Simplesse	0.685 ± 0.004
Hiprotal60	0.664 ± 0.001
Hiprotal60-TS0709	0.684 ± 0.007
Hiprotal60-TS0710	0.683 ± 0.006
Hiprotal60-TS0712	0.680 ± 0.002

5.7 Other components

As discussed in Section 5.6.2, the partial specific volumes of Lacprodan87, Simplesse, and Hiprotal60 products are found to be smaller than, β-lactoglobulin and bovine serum albumin, which is believed to result from non-protein components in these materials. Such components are mainly lactose, which has been reported to inhibit thermal gelation of whey proteins (Garrett, Stairs, & Annett, 1988; Tang, McCarthy, & Munro, 1994). However, thermal gelation properties of fat replacers are out of the scope of this thesis. Moreover, ions, for instance Ca^{2+}, are also supposed to be present, which reduce the electrostatic interactions between proteins by screening effects (Tang et al., 1994). Since the molecular sizes of non-protein components are much smaller than those of proteins, the rheological properties of the materials are believed to be determined mainly by the protein molecules.

5.8 Conclusion

Whey protein concentrate (Lacprodan87) and protein-based fat replacers (Simplesse and Hiprotal60 products) were comprehensively characterized. The characterization was carried out at the molecular level of the β-lactoglobulin, which is the main component of whey proteins. Effects of heat-induced denaturation on the structure and hydration properties of the β-lactoglobulin were determined, which revealed the ability of the unfolded polypeptides to form 'sting-of-bead-like' polymers through –SH/S-S interchange reactions. Ability of the protein molecule to form hydrogen bonds with its hydrated water molecules was weakened by denaturation, while the hydrogen bonds between these water molecules were found strengthened by protein unfolding. From the particle size distributions, the fat replacer samples are characterized in terms of the extent of protein aggregation, i.e., low aggregation for Simplesse, Hiprotal60 and –TS0709 and highly aggregated particles for Hiprotal60-TS0710 and –TS0712. Images obtained from ESEM provided some information on the protein aggregation for different samples, especially for Hiprotal60-TS0710 and –TS0712, of which the former exhibited particulated aggregates while the latter behaved like 'string-of-bead' polymers. However, such information was limited by the fact that the proteins examined were in a dry condition not in solutions. However, no disulphide bond was found in these aggregate according to normal and reduced SDS-PAGE, indicating that the large particles were a result of hydrophobic interactions between the partial denatured protein molecules. In terms of the finding in particle size distributions and the images from ESEM, Simplesse, Hiprotal60 and –TS0709, and Hiprotal60-TS0710 and –TS0712 are characterized as microparticulated, low aggregated and highly aggregated proteins, respectively. Finally, partial specific volume of each sample illustrated that there are denser material in those WPC and fat replacers. Main components of these denser materials are supposed to be lactose and ions, which are believed to have little effects on the rheological properties of the solutions of the whey proteins and the fat replacers.

5.9 References

Ball, P. (2008). Water as an active constituent in cell biology. *Chemical Reviews, 108*(1), 74-108.

Bernhardt, J., & Pauly, H. (1975). Partial specific volumes in highly concentrated protein solutions. I. Water-bovine serum albumin and water-bovine hemoglobin. *The Journal ot Physical Chemistry, 79*(6).

Berweger, C.D., van Gunsteren, W.F., & Müller-Plathe, F. (1995). Force field parametrization by weak coupling. Re-engineering SPC water. *Chemical Physics Letters, 232*(5-6), 429-436.

Bryant, C.M., & McClements, D.J. (1998). Molecular basis of protein functionality with special consideration of cold-set gels derived from heat-denatured whey. *Trends in Food Science & Technology, 9*(4), 143-151.

Bussi, G., Donadio, D., & Parrinello, M. (2007). Canonical sampling through velocity rescaling. *Journal of Chemical Physics, 126*(1), 014101(014101-014107).

Cairoli, S., Iametti, S., & Bonomi, F. (1994). Reversible and irreversible modifications of β-lactoglobulin upon exposure to heat. *Journal of Protein Chemistry, 13*(3), 347-354.

Chalikian, T.V. (2001). Structural thermodynamics of hydration. *Journal of Chemical Physics, 105*(50), 12566-12578.

Chalikian, T.V. (2003). Volumetric properties of proteins. *Annual Review of Biophysics and Biomolecular Structure, 32*, 207-235.

Chalikian, T.V., Totrov, M., Abagyan, R., & Breslauer, K.J. (1996). The hydration of globular proteins as derived from volume and compressibility measurement: Cross correlating thermodynamic and structural data. *Journal of Molecular Biology, 260*(4), 588-603.

Damodaran, S. (1996). Amino acids, peptides, and proteins. In O. R. Fennema (Ed.), *Food Chemistry* (3rd ed., pp. 321-429). New York, USA.: Marcel Dekker.

Darden, T., York, D., & Pedersen, L. (1993). Particle mesh Ewald: An *N*.log(*N*) method for Ewald sums in large systems. *Journal of Chemical Physics, 98*(12), 10089-10092.

de la Fuente, M.A., Hemar, Y., Tamehana, M., Munro, P.A., & Singh, H. (2002). Process-induced changes in whey proteins during the manufacture of whey protein concentrates. *International Dairy Journal, 12*(4), 361-369.

Du, H. (2004). Mie-scattering calculation. *Applied Optics, 43*(9), 1951-1956.

Essmann, U., Perera, L., Berkowitz, M.L., Darden, T., Lee, H., & Pedersen, L.G. (1995). A smooth particle mesh Ewald method. *Journal of Chemical Physics, 103*(19), 8577-8593.

Euston, S.R. (2013). Molecular dynamics simulation of the effect of heat on the conformation of bovine β-lactoglobulin A: A comparison of conventional and accelerated methods. *Food Hydrocolloids, 30*(2), 519-530.

Galema, S.A., & Hoiland, H. (1991). Stereochemical aspects of hydration of carbohydrates in aqueous-solutions. 3. Density and ultrasound measurements. *Journal of Physical Chemistry, 95*(13), 5321-5326.

Garrett, J.M., Stairs, R.A., & Annett, R.G. (1988). Thermal denaturation and

coagulation of whey proteins: Effect of sugars. *Journal of Dairy Science, 71*(1), 10-16.

Gekko, K., & Noguchi, H. (1974). Hydration behaviour of ionic dextran derivatives. *Macromolecules, 7*(2), 224-229.

Hayakawa, O., Nakahira, K., & Tsubaki, J.I. (1995). Estimation of the optimum refractive index by the laser diffraction and scattering method-On the raw material of fine ceramics. *Advanced Powder Technology, 6*(1), 47-61.

Hess, B., Kutzner, C., van der Spoel, D., & Lindahl, E. (2008). Gromacs 4: Algorithms for highly efficient, load-balanced, and scalable molecular simulation. *Journal of Chemical Theory and Computation, 4*(3), 435-477.

Kinsella, J.E., & Whitehead, D.M. (1988). Proteins in whey: Chemical, physical, and functional properties. *Advances in Food and Nutrition Research, 33*, 343-438.

Luzar, A., & Chandler, D. (1996). Hydrogen-bond kinetics in liquid water. *Nature, 379*(4), 55-57.

Maisuradze, G.G., Liwo, A., & Scheraga, H.A. (2009). Principal component analysis for protein folding dynamics. *Journal of Molecular Biology, 385*(1), 312-329.

Maisuradze, G.G., Liwo, A., & Scheraga, H.A. (2010). Relation between free energy landscapes of proteins and dynamics. *Journal of Chemical Theory and Computation, 6*(2), 583-595.

McMeekin, T.L., Groves, M.L., & Hipp, N.J. (1964). Refractive indices of amino acids, proteins, and related substances. In J. A. Stekol (Ed.), *Amino Acids and Serum Proteins* (Vol. 44). Washington, DC, USA: American Chemical Society.

Moore, W.J. (1976). *Physical Chemistry* (5th ed.). London, UK.: Longman Group Limited.

Oostenbrink, C., Villa, A., Mark, A.E., & van Gunsteren, W.F. (2004). A biomolecular force field based on the free enthalpy of hydration and solvation: The GROMOS force-field parameter sets 53A5 and 53A6. *Journal of Computational Chemistry, 25*(13), 1656-1676.

Papiz, M.Z., Sawyer, L., Eliopoulos, E.E., North, A.C., Findlay, J.B., Sivaprasadarao, R., et al. (1986). The structure of β-lactoglobulin and its similarity to plasma retinol-binding protein. *Nature, 324*(6095), 383-385.

Paradossi, G., Finelli, I., Natali, F., Telling, M.T.F., & Chiessi, E. (2011). Polymer and water dynamics in poly(vinyl alcohol)/poly(methacrylate) networks. A molecular dynamics simulation and incoherent neutron scattering investigation. *Polymers, 3*, 1805-1832.

Parrinello, M., & Rahman, A. (1981). Polymorphic transitions in single crystals: A new molecular dynamics method. *Journal of Applied Physics, 52*(12), 7182-7190.

Pavlovskaya, G., McClements, D.J., & Povey, M.J.W. (1992). Ultrasonic investigation of aqueous solutions of globular protein. *Food Hydrocolloids, 6*(3), 253-262.

Prindiville, E.A., Marshall, R.T., & Heymann, H. (2000). Effect of milk fat, cocoa butter, and whey protein fat replacers on the sensory properties of lowfat and nonfat chocolate ice cream. *Journal of Dairy Science, 83*(10), 2216-2223.

Qin, B.Y., Bewley, M.C., Creamer, L.K., Baker, H.M., Baker, E.N., & Jameson, G.B. (1998). Structural basis of the tanford transition of bovine β-lactoglobulin. *Biochemistry, 37*(40), 14014-14023.

Raschke, T.M. (2006). Water structure and interactions with protein surfaces. *Current*

Opinion in Structural Biology, 16(2), 152-159.

Ryan, K.N., Zhong, Q., & Foegeding, E.A. (2013). Use of whey protein soluble aggregates for thermal stability - A hypothesis paper. *Journal of Food Science, 78*(8), R1105-R1115.

Sandrou, D.K., & Arvanitoyannis, I.S. (2000). Low-fat/calorie foods: Current state and perspectives. *Critical Reviews in Food Science and Nutrition, 40*(5), 427-447.

Sarvazyan, A.P. (1991). Ultrasonic velocimetry of biological compounds. *Annual Reviews of Biophysics and Biophysical Chemistry, 20*, 321-342.

Saveyn, H., Mermuys, D., Thas, O., & van der Meeren, P. (2002). Determination of the refractive index of water-dispersible granules for use in laser diffraction experiments. *Particle & Particle Systems Characterization, 19*(6), 426-432.

Shimada, K., & Cheftel, J.C. (1989). Sulfhydryl group/disulfide bond interchange reactions during heat-induced gelation of whey protein isolate. *Journal of Agricultural & Food Chemistry, 37*(1), 161-168.

Stading, M., & Hermansson, A. (1990). Viscoelastic behaviour of β-lactoglobulin gel structures. *Food Hydrocolloids, 4*(2), 121-135.

Stading, M., Langton, M., & Hermansson, A. (1992). Inhomogeneous fine-stranded β-lactoglobulin gels. *Food Hydrocolloids, 6*(5), 455-470.

Tang, Q., McCarthy, O.J., & Munro, P.A. (1994). Oscillatory rheological comparison of the gelling characteristics of egg white, whey protein concentrates, whey protein isolate, and β-lactoglobulin. *Journal of Agricultural & Food Chemistry, 42*(10), 2126-2130.

Valdez, D., Le Huérou, J.Y. , Gindre, M., Urbach, W., & Waks, M. (2001). Hydration and protein folding in water and in reverse micelles: Compressibility and volume changes. *Biophysical Journal, 80*(6), 2751-2760.

van der Spoel, D., Lindahl, E., Hess, B., Groenhof, G., Mark, A.E., & Berendsen, H.J.C. (2005). Gromacs: Fast, flexible, and free. *Journal of Computational Chemistry, 26*(16), 1701-1718.

van der Spoel, D., van Maaren, P.J., Larsson, P., & Tîmneanu, N. (2006). Thermodynamics of hydrogen bonding in hydrophilic and hydrophobic media. *Journal of Physical Chemistry B, 110*(9), 4393-4398.

Wriedt, T. (2012). Mie theory: A review. In W. Hergert & T. Wriedt (Eds.), *The Mie Theory Basics and Applications* (pp. 53-71). New York, USA: Springer-Verlag Berlin Heidelberg.

Zhang, Z., & Scanlon, M.G. (2011). Solvent effects on the molecular structures of crude gliadins as revealed by density and ultrasound velocity measurements. *Journal of Cereal Science, 54*(2), 181-186.

6 Flow behaviour of microparticulated and partial denatured proteins

6.1 Introduction

Whey proteins are widely used as ingredients in various foods because of their unsurpassed nutritional quality (Harper, 2004; Madureira et al., 2007; Séverina & Xia, 2005). In addition, whey proteins are also valuable functional ingredients in foods as emulsifiers, foaming agents and gelling agents. As gelling agents whey proteins are able to aggregate and form gels that improve the textural properties of food products (Kinsella & Whitehead, 1988; Lizarraga et al., 2006). Properties of whey protein concentrates (WPC) solutions, including their rheological behaviour, have been extensively investigated to understand the effects of factors such as protein concentration, temperature, pH and ionic strength on the molecular functionality (Hermansson, 1975; McDonough, Hargrove, Mattingly, Posati, & Alford, 1974; Pradipasena & Rha, 1977a, 1977b; Tang, Munro, & McCarthy, 1993). Modifications, such as heat induced aggregations, of whey proteins have been found to improve the functionality of the proteins (Bryant & McClements, 1998; Foegeding et al., 2011; Hudson et al., 2000; Jeurnink & De Kruif, 1993; Resch & Daubert, 2002). Such improvements have been applied industrially to produce texturisers and thickener for foods, especially those with low content of fat, and therefore, whey proteins are regards as a good source of fat replacers (Sandrou & Arvanitoyannis, 2000). Various fat replacers based on proteins are now available in market, such as Simplesse and Hiprotal, which are microparticulated and aggregated partially denatured proteins, respectively (Prindiville et al., 2000; Renard et al., 1999; Sandrou & Arvanitoyannis, 2000). Different functionalities can be obtained from such products due to their modified structures, and thus, studies on the flow behavior and deduction of the structure-functionality relationship of different fat replacers are of great value for improvement of reduced-fat products.

In this chapter the effects of protein concentration on flow behavior, including shear thinning and thixotropy properties, of partially denatured WPC fat replacers are determined and the interactions and aggregations of modified protein molecules are

discussed. The flow behavior of Simplesse, a microparticulated WPC and non-denatured WPC are also studied for comparison purposes. We hope this will provide a reference for improvement of available protein-based fat replacers or even for invention of new products.

6.2 Material and methods

6.2.1 Protein solutions

Lacptodan87 (Arla Foods Ingredients, Denmark), Simplesse® 100[E] (CP Kelco UK Limited, UK) and a series of Hiprotal60 products, i.e., Hiprotal60, Hiprotal60-TS0709, Hiprotal60-TS0710, and Hiprotal60-TS0712 (Friesland Foods, the Netherland) were dissolved in deionized distilled water at 20~23 °C to make solutions with protein concentrations of 6%, 9%,12%, 14%, 16%, 18% and 21% (w/w). The solutions were stirred gently for at least 1 h to allow full hydration of the proteins.

6.2.2 Rheology measurement

All rheological measurements were performed using a Gemini controlled stress rheometer (Bohlin Instruments, UK), with 4°/40 mm cone and plate at a temperature of 20 °C. The solution samples were loaded onto the surface of the plate and then the cone was set to position with a gap of 150 μm above the plate surface.

Steady viscosity of solutions was determined from ultralow (~10^{-4} s^{-1}) to intermediate (~100 s^{-1}) shear rates. Measuring time changed from 15 min to 5 min when the shear rate exceeded 0.1 s^{-1}, where equilibrium of the flows is easier to achieve. Thixotropy properties were measured through shear-rate sweep tests, where a range of shear rates from ~10^{-3} s^{-1} to ~100 s^{-1} were employed in an up-to-down circular mode. The area between the ascending and descending curves was calculated with the software Bohlin R6.50.5.7 (Bohlin Instruments, UK) and this was reported as the thixotropy.

6.3 Results and Discussion

6.3.1 Concentration dependence

In solution interactions between protein and water molecules and interactions between the proteins themselves give rise to the viscosity of the protein solutions (Barnes et al., 1989; Damodaran, 1996a; Rao, 2007). The protein-protein interactions, which result in an increase in the viscosity of the solution, mainly depend on the size of the protein molecules, and thus, the volume fraction occupied by the protein molecule (Macosko, 1994). Accordingly, dependence of flow behavior on weight concentration of a protein solution reveals the interactions between molecules in the system, based on the assumption of proportionality of volume fraction with weight fraction at moderate concentrations (Pradipasena & Rha, 1977a; Tang et al., 1993) and the fact as indicated in Figure 5.16.

The dependences of the apparent viscosities at the shear rate of 100 s^{-1} on the weight concentration of protein for different samples are shown in Figure 6.1. The viscosity of whey protein solutions has been observed to increase with protein concentration in an exponential pattern (Hermansson, 1975; McDonough et al., 1974; Tang et al., 1993). As shown in Figure 6.1, exponential relationship (R^2>0.95) is also observed from all the solutions. A smaller value of R^2 (around 0.92) for WPC solutions at low concentrations (around 10%, i.e., 6%, 9% and 12%) was observed compared with other samples, which is due to the inclusion of the solutions in the regression process, which have been reported to stay in the linear region (Pradipasena & Rha, 1977a). This hypothesis could be proven to be correct by a higher value of R^2 (>0.95) for a linear regression for dilute WPC solutions.

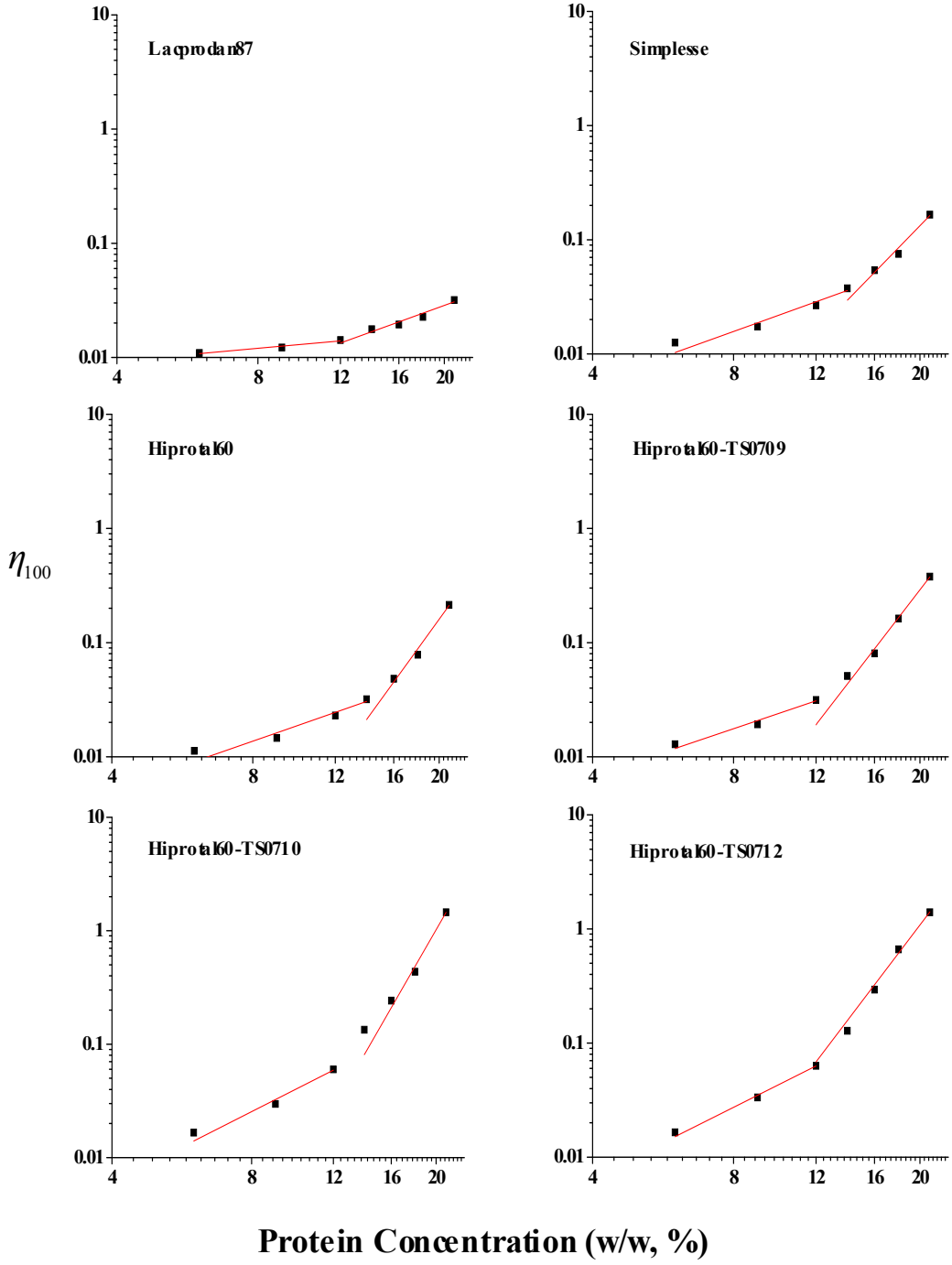

Figure 6.1 Concentration dependence of the apparent viscosity at 100 s^{-1}.

It is found that there are two concentration dependences of viscosity for the WPC solutions. It is found that the viscosity of the dilute solutions tended to increase with concentration linearly in dilute solutions (<12%), while an exponential concentration dependence is observed for concentrated solutions (>12%). Exponential relationship reveals the existence of protein-protein interactions, which grow with the number of

protein molecules and raise the viscosity of the solution (Lizarraga et al., 2006; Macosko, 1994; Pradipasena & Rha, 1977b; Tang et al., 1993). Similarly, two concentration regimes were also observed for other samples, both of the microparticulated (i.e., Simplesse) and partially denatured (i.e., Hiprotal60 products) proteins. However, there was no linear dependence on concentration observed and the viscosities for all the solutions were found to increase exponentially with protein concentrations. Such change in viscosity dependence reveals a transition of the solutions from a 'semi-dilute' behaviour to a 'concentrated' one, where the protein concentration is high enough for some structure formation (Dickinson & Stainsby, 1982; Tang et al., 1993). This is often termed the crossover concentration.

The boundary of the concentration regimes and concentration dependence of viscosity, i.e., the slope of the $\mathbf{log}\,\eta$ v.s. $\mathbf{log}\,w$ (w is concentration in %) plots of each sample are listed in Table 6.1. There was no concentration dependence of viscosity for dilute WPC solutions reported because it is supposed to be a linear relationship between protein concentration and viscosity. It is found that the concentration dependence of WPC at high concentrations (>12%) are similar to those of modified proteins at low concentrations, suggesting that such increase in viscosities were due to hydrodynamic interactions between proteins. Hydrodynamic interactions are significant when the concentration of WPC exceeds 10% but for those modified protein samples, hydrodynamic interactions appear at much lower concentrations (i.e., 6%) due to their large particle sizes. As the concentration increases, the concentration dependences of viscosity of modified proteins are much larger than that of the WPC, indicating that there are stronger intermolecular interactions existing between those modified protein molecules than WPC, and such forces, for instance, hydrogen bonds, hydrophobic interactions and disulphide bridges, facilitate the structure formation in the modified proteins (Elofsson et al., 1997; Ju & Kilara, 1998).

It is also found that the increased rate of viscosity change with concentration for Simplesse solutions in the 'semi-dilute' regime (i.e., Regime 1 in Table 6.1) is similar to those of the partially denatured proteins with small aggregates (i.e., Hiprotal60 and Hiprotal60-TS0709) and WPC, but smaller than those of the partially denatured

proteins with large aggregates (i.e., Hiprotal60-TS0710 and -TS0712). This suggests that microparticulated proteins (i.e., Simplesse) and Hiprotal60 products with a low degree of aggregation have similar hydrodynamic interactions between molecules with the absence of structure formation at high shear rate, while the highly aggregated partially denatured proteins exhibit stronger resistance to flows, perhaps due to their large particle sizes and more hydrophobic interactions of long polymeric chains. Furthermore, microparticulated proteins are found to possess an increased concentration dependence of viscosity at the 'concentrated' regime (i.e., Regime 2 in Table 6.1), but smaller than the partially denatured protein aggregates. This could be because the microparticulated proteins formed flocs at high concentrations. These flocs increased the resistance to flow through the repulsions from stronger electrostatic interactions and from hydration shells at high concentrations but not through aggregation (Ikeda & Nishinari, 2000, 2001; Renard et al., 1999). On the other hand, short rods tend to aggregate due to hydrophobic interactions and form networks with relatively long polymeric chains, which are able to survive at high shear rates. Therefore, the concentration dependence of viscosity in the 'concentrated' regime of the partially denatured proteins with small aggregates approached that of the partially denatured proteins with large aggregates, which may form networks due to hydrophobic interactions and entanglement of the longer chains formed in these products. Similar conclusions could be deduced from the higher crossover concentration of Simplesse compared to Hiprotal60 products, since the compact microparticulated structures allow more particles to flocculate before the flocs feel the short-ranged repulsions from hydration shells (Bryant & McClements, 1998; Ikeda & Nishinari, 2000, 2001), while the entanglements of longer polymeric proteins and long-ranged hydrophobic interactions are more sensitive to protein concentration (Bryant & McClements, 1998). It is also noted that the concentration dependence of viscosity for Hiprotal60-TS0712 at high concentrations is smaller than that of Hiprotal60-TS0710 but similar to those of Hiprotal60 products with lower aggregations, indicating weaker structure of the networks formed by Hiprotal60-TS0710 than that formed by Hiprotal60-TS0712.

Table 6.1 Crossover concentrations and concentration dependence of viscosity of each sample.

	Crossover concentration (%, w/w)	Concentration dependence	
		Regime 1	Regime 2
Lacoprodan87	12	-	1.48
Simplesse	14~16	1.48	4.21
Hiprotal60	14~16	1.43	5.68
Hiprotal60-TS0709	12~14	1.39	5.33
Hiprotal60-TS0710	12~14	2.08	7.11
Hiprotal60-TS0712	12~14	2.05	5.41

6.3.2 Shear rate dependence

The effects of shear rate on viscosity of different samples are shown in Figure 6.2 to 6.7. It is found that all the samples exhibit shear-thinning behaviour, which contradicts the results of previous studies, especially those on β-lactoglobulin (Pradipasena & Rha, 1977a) and WPC (Tang et al., 1993) solutions. With Lacprodan87 (unmodified WPC) we would expect errors in viscosity measurement to be relatively high at small shear stresses, since these are close to the lower sensitivity limits of the instrument using this geometry. In addition, for proteins with small particle size and low viscosity a low Péclet number (*equation 2.42* in *Section 2.6.2*) is found which is supposed to account for such unexpected flowing behaviour, especially that measured at low shear rates (Goodwin & Hughes, 2008; Macosko, 1994). According to M. A. Tung (1978), shear thinning behavior of protein dispersions results from alignment of the polypeptide chains under shear flows, during which the interactions, such as hydrogen bonds and electrostatic interactions, between the randomly oriented molecules are disrupted and new orientations of the protein molecules along shear planes with lower resistance to flows are established. For the solutions of Lacprodan87, however, *Pe* values are very small at low shear rates, suggesting that the shear thinning behaviour of the WPC solutions were mainly due to the orientations of protein molecules by overcoming their Brownian motions, rather than intermolecular interactions (Foss & Brady, 2000; Goodwin & Hughes, 2008; Macosko, 1994).

In Figure 6.2, solutions of WPC (Lacprodan87) are found to have low viscosity and no shear thinning behavior at large *Pe* values (>10), indicating weak interactions

between the protein molecules, which had similar scales as the effects of Brownian motions on the random orientations of the polypeptide chains. Therefore, the increase in viscosity of solutions with protein concentration is believed to result from higher resistance to shear flow due to a greater number density of protein molecules and stronger hydrodynamic interactions between protein molecules as they approach each other (M. A. Tung, 1978). Moreover, WPC solutions are also found to display shear-thickening behaviour at high shear rate (100 s^{-1}), especially for those with protein concentration larger than 14%. Such dilatant behaviour could be due to unfolding of the polypeptide chains caused by high shear rates, i.e., shear stresses, which increase the hydrodynamic interactions and entanglement between the proteins (Pradipasena & Rha, 1977b).

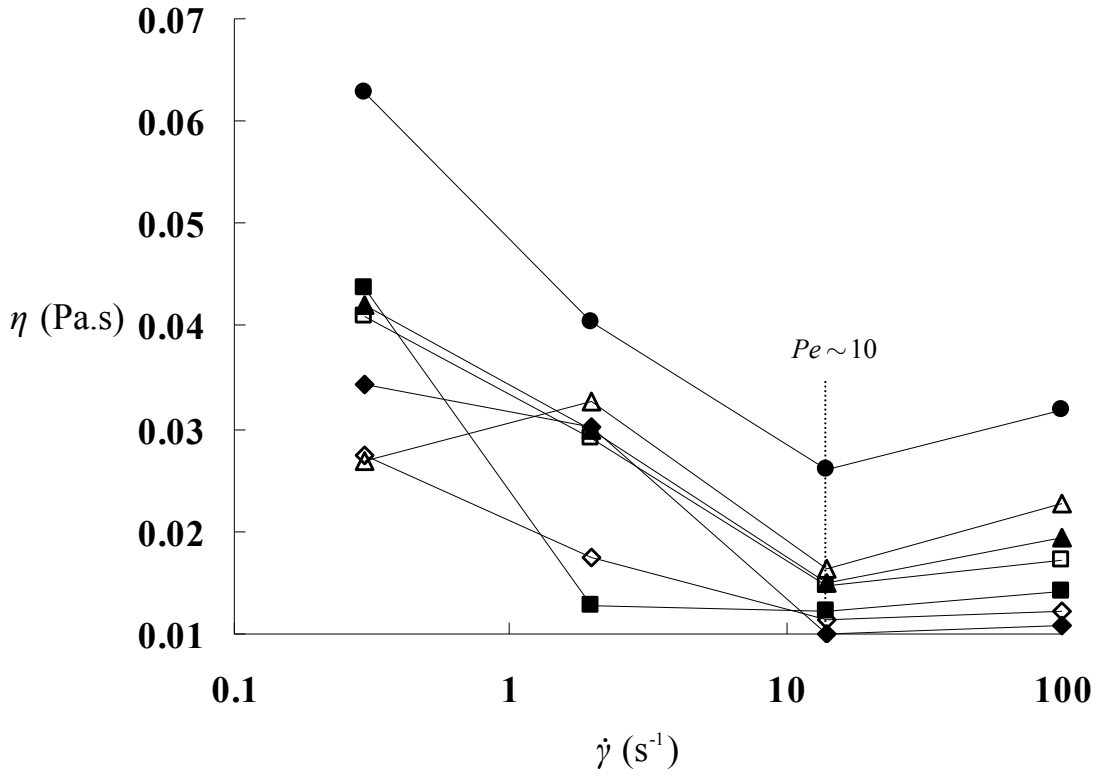

Figure 6.2 Shear dependence of viscosity of Lacprodan87 with 6% (◆), 9% (◇), 12% (■), 14% (□), 16% (▲), 18% (△), and 21% (●) protein concentrations (w/w).

Shear dependence of viscosity for miroparticulated protein (i.e., Simplesse) solutions is demonstrated in Figure 6.3, where the *Pe* values are observed to be larger

than those of WPC, since the former possesses larger particle size and higher viscosity (Goodwin & Hughes, 2008; Macosko, 1994). Shear thinning behaviour was observed in all the solutions of microparticulated proteins with large *Pe* (>10), indicating it is intermolecular interactions that determine the flow behaviour of the proteins other than Brownian motions (Barnes et al., 1989; Rao, 2007; M. A. Tung, 1978). Besides, Newtonian plateaus at high shear rate (100 s^{-1}) are observed in solutions with protein concentrations of less than 16% (w/w), suggesting that the intermolecular interactions between the microparticulates were completely disrupted by high shear stress (Barnes et al., 1989; Rao, 2007; M. A. Tung, 1978). According to Renard et al. (1999), such intermolecular interactions occur by flocculation of the microparticles formed in the solution at rest and at low shear rates. The large flocs are disrupted into small microparticles and thus, give constant viscosity at high shear rates. However, Newtonian plateaus at high shear rates disappear in concentrated solutions (>16% (w/w), Figure 6.3). This could be due to the occurrence of repulsive forces between the hydration shells and the increase in electrostatic interactions of the microparticles, which are short-ranged interactions and increase the resistance of the particles to flow (Bryant & McClements, 1998). Such observations coincide with those shown in Table 6.1, where the concentrated solutions of Simplesse were found to have large increases in the viscosity at a large shear rate (100 s^{-1}).

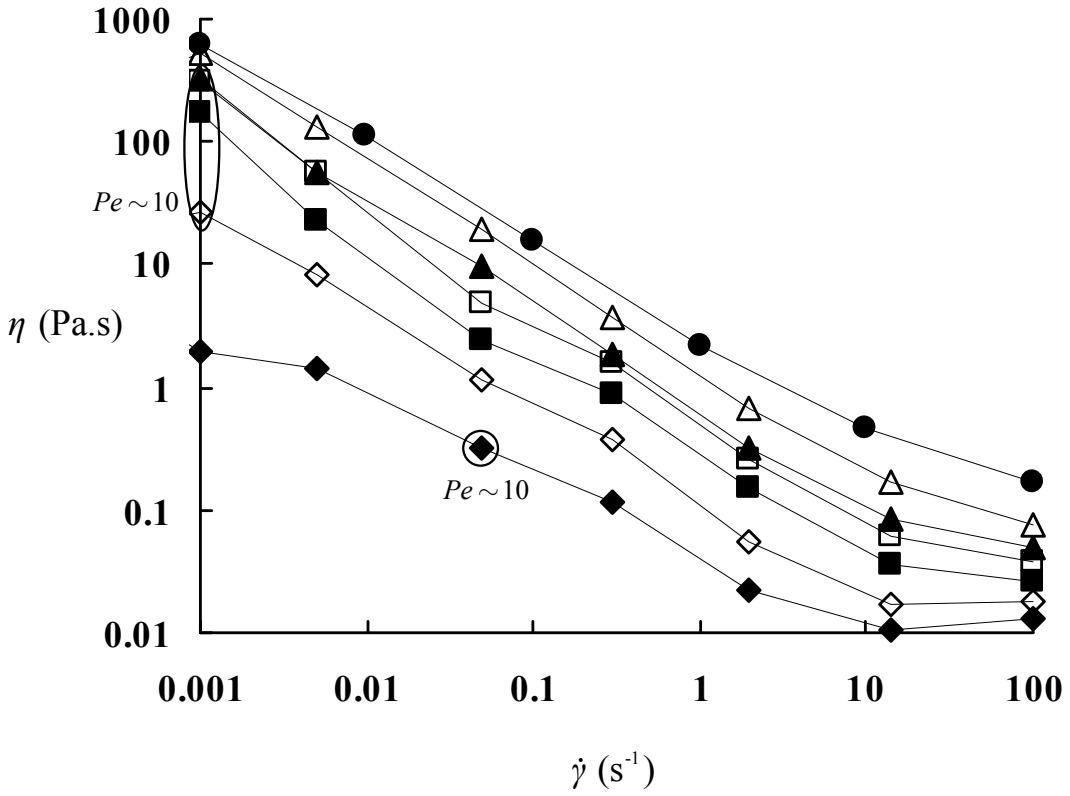

Figure 6.3 Shear dependence of viscosity of Simplesse with 6% (◆), 9% (◇), 12% (■), 14% (□), 16% (▲), 18% (△), and 21% (●) protein concentrations (w/w).

Flowing behaviour of solutions of partially denatured proteins with a low degree of aggregation (i.e., Hiprotal60 and Hiprotal60-TS0709) are shown in Figure 6.4 and 6.5. The *Pe* values of such solutions were smaller than those of microparticulated proteins (i.e., Simplesse as shown in Figure 6.3) due to their smaller particle size and lower viscosity, especially at low concentrations. On the other hand, the *Pe* values of these modified protein solutions are much larger than those of WPC (i.e., Lacprodan87) and Simplesse as shown in Figure 6.2 and 6.3, because of the larger viscosity and larger particle size of the former. Shear thinning properties with the absence of Newtonian plateaus at high shear rates were observed around 16%~18% and 14%~16% of protein concentrations for Hiprotal60 and Hiprotal60-TS0709 as shown in Figure 6.4 and 6.5, respectively, indicating strong aggregated structures are form and dissociated by high shear rates at such protein concentrations, which is in accordance with Table 6.1. It is also found that slight shear-thickening behaviour at low shear rate occurred in concentrated solutions for Hiprotal60 (21%) and Hiprotal60-TS0709 (18%), respectively. This could be because the alignment of the small protein aggregates at

low shear rates favored the growth of the polymeric chain and initialized the structure build-up. Similar building-up effects of low shear rates on native ovalbumin and microparticulated milk protein solutions were also observed by Matsumoto and Chiba (1990) and Renard et al. (1999), respectively.

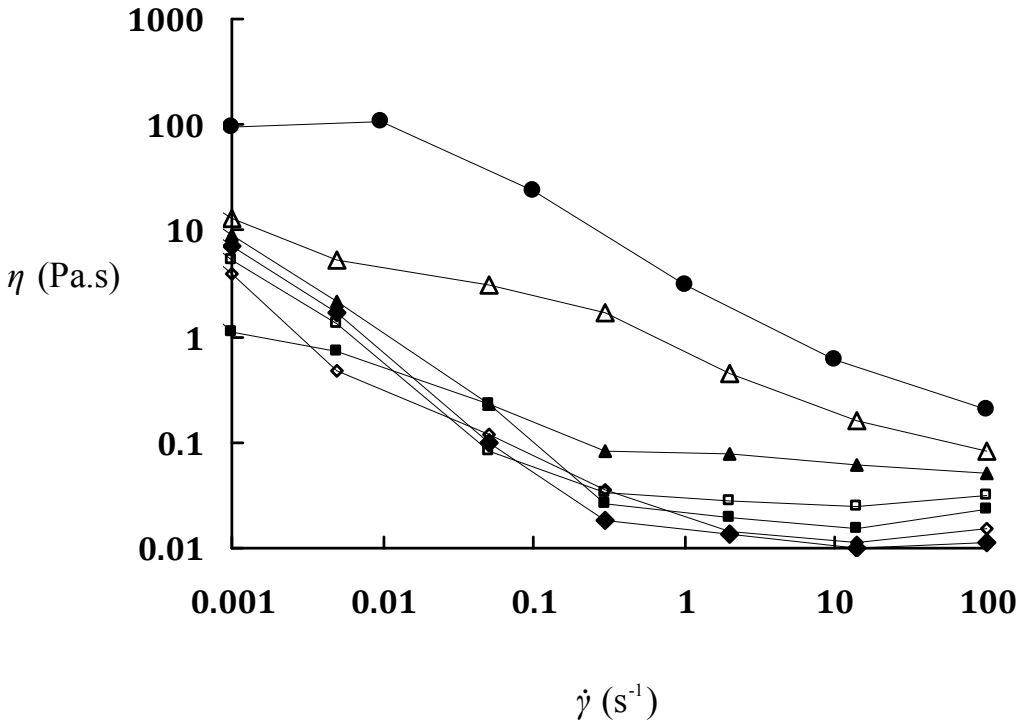

Figure 6.4 Shear dependence of viscosity of Hiprotal60 with 6% (◆), 9% (◇), 12% (■), 14% (□), 16% (▲), 18% (△), and 21% (●) protein concentrations (w/w).

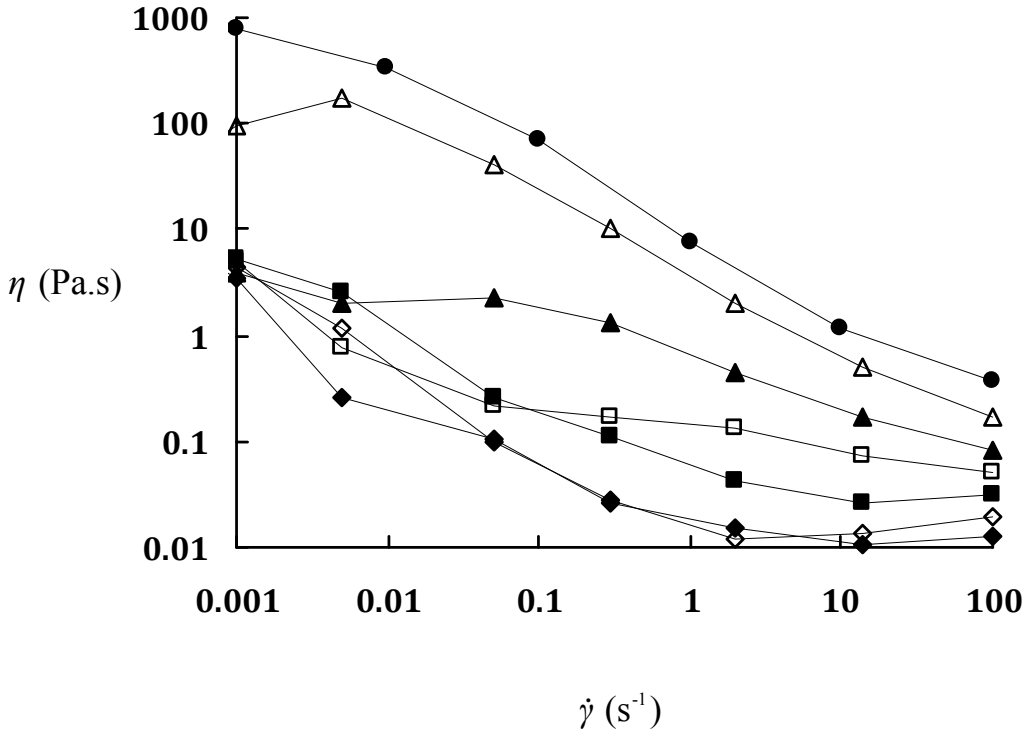

Figure 6.5 Shear dependence of viscosity of Hiprotal60-TS0709 with 6% (◆), 9% (◇), 12% (■), 14% (□), 16% (▲), 18% (△), and 21% (●) protein concentrations (w/w).

The *Pe* values are large (>10,000) for all the solutions of Hiprotal60-TS0710 and Hiprotal60-TS0712 due to their large particle size (as shown in Table 5.1). Therefore, effects of Brownian motions on the viscosity are very small and shear thinning behaviour of the solutions can be attributed to disruption of intermolecular forces between the protein molecules (Foss & Brady, 2000; Macosko, 1994). Shear thinning behavior at low shear rates and Newtonian plateaus at high shear rates were observed in dilute solutions (<12%) of these modified proteins as shown in Figure 6.6 and 6.7. It is also found in these dilute solutions that shear thinning behavior ceased at relatively low shear rates (~1 s^{-1}), indicating that there are no aggregates formed in such dilute solutions, and the polymeric chains completely align along the shear planes around the shear rate ~1 s^{-1} and above. Large increases in viscosity, especially at high shear rates, were observed in the solutions with intermediate (~12%) and high (>12%) concentrations for both of the modified proteins. The Newtonian plateaus observed at high shear rates for the lower protein concentration solutions tend to disappear in the

solutions of 12% protein concentration and above. Such changes could be due to the strong aggregated structures formed by the long polymeric chains of proteins that are broken down by drastic shears (Matveenko & Kirsanov, 2011; M. A. Tung, 1978), which has also been seen in Table 6.1. Similar to the small protein aggregates (i.e., Hiprotal60 and Hiprotal60-TS0709 as shown in Figure 6.4 and 6.5, respectively), build-up of structures is also found in the highly aggregated proteins, at low shear rates, but with lower concentrations (~14%).

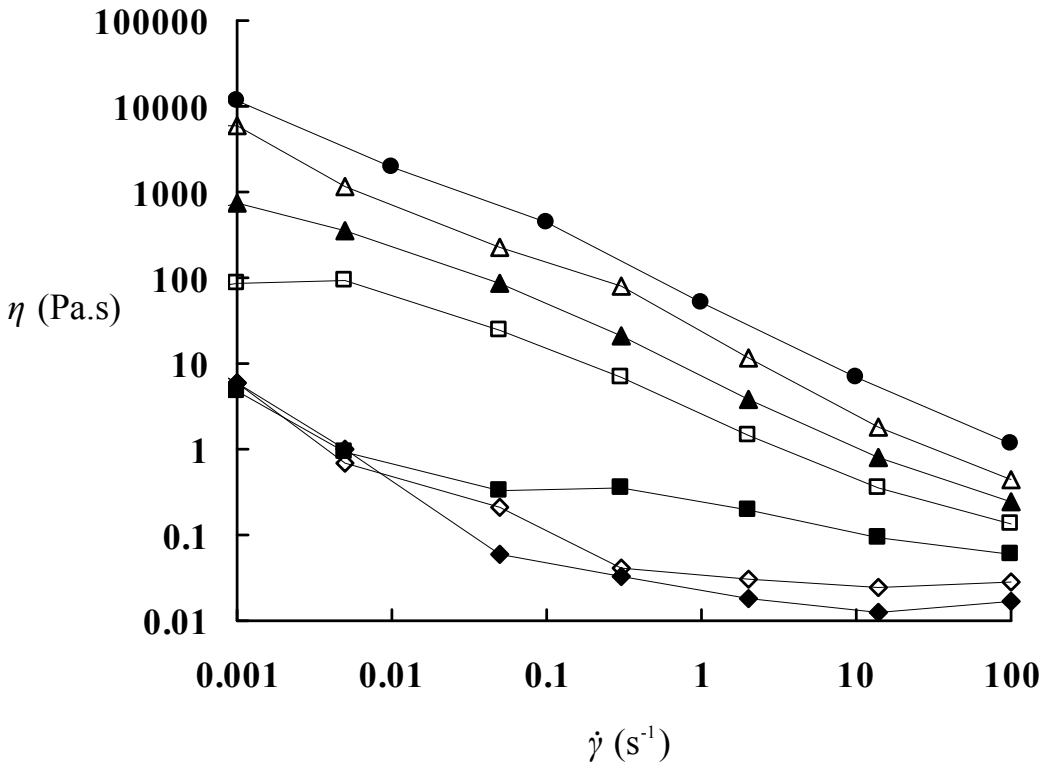

Figure 6.6 Shear dependence of viscosity of Hiprotal60-TS0710 with 6% (◆), 9% (◇), 12% (■), 14% (□), 16% (▲), 18% (△), and 21% (●) protein concentrations (w/w).

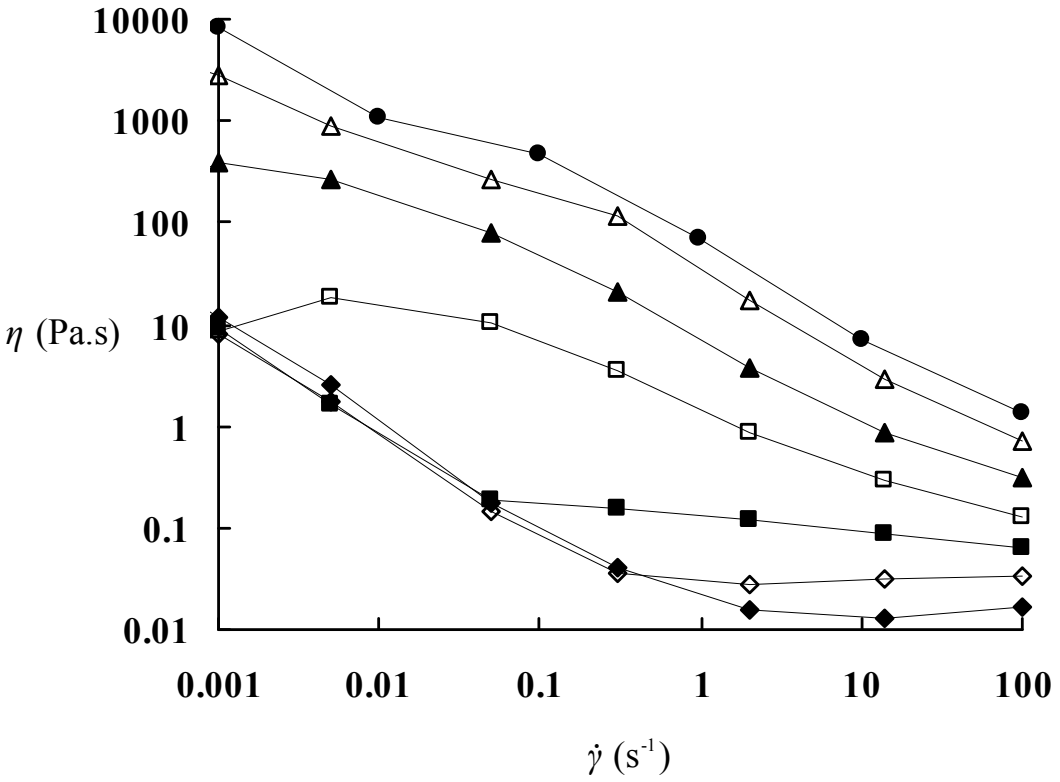

Figure 6.7 Shear dependence of viscosity of Hiprotal60-TS0712 with 6% (◆), 9% (◇), 12% (■), 14% (□), 16% (▲), 18% (△), and 21% (●) protein concentrations (w/w).

As shown from Figure 6.2 to 6.7, modified proteins and WPC had similar viscous behavior in their dilute solutions at high shear rates, indicating the protein molecules had similar hydrodynamic interaction when their intermolecular interactions were not significant, i.e., the protein clusters were completely broken down, and when they were completely aligned along the shear planes (Matveenko & Kirsanov, 2011; M. A. Tung, 1978). In concentrated solutions, however, modified proteins exhibited higher resistance to flows than WPC even at high shear rates, indicating strong intermolecular interactions between the former. Newtonian plateaus at high shear rates were absent in concentrated solutions of modified proteins, suggesting the interactions between the flowing units prevented them from achieving complete alignment.

6.3.3 Thixotropy

Hysteresis loops were first proposed by Green and Weltmann (1943) for studies on thixotropy properties of materials. As shown in Figure 6.8 to 6.13, shear stresses under consecutively increasing and decreasing shear rates were plotted versus shear rates, and the deviation of the two curves from each other revealed thixotropy properties (Green & Weltmann, 1943; Mewis, 1979; Mewis & Wagner, 2009). It is found that all modified proteins, i.e., both microparticulated and partially denatured ones, displayed thixotropic behaviour in concentrated solutions, but that the WPC solutions did not. Moreover, ascending shear stresses were observed to be larger than descending ones for all the thixotropic samples, indicating that aggregates formed from proteins at rest in such concentrated solutions was disrupted by strong shear flows, and that disrupted aggregates could not recover immediately (M. A. Tung, 1978). The hysteresis phenomenon results from the retarded Brownian motions caused by large viscosity, and therefore, it can take a long time for the aligned flowing units, such as protein molecules or small protein aggregates, to recover their random orientations or reform the aggregation structures (Mewis, 1979; M. A. Tung, 1978). It should be noted that the thixotropic properties of microparticulated proteins conflict with the observations of Renard et al. (1999), who found that microparticulated proteins exhibit anti-thixotropic behaviour. The contradiction could be because Renard and his colleague used increased ionic strength in their Simplesse solutions (they were suspended in 0.1 M NaCl) whilst our measurements were carried out in the absence of NaCl. Since electrostatic repulsions are shielded by ions in the solution (Bryant & McClements, 1998; Renard et al., 1999), it is much easier for microparticulated proteins to approach each other and flocculate again with the presence of salt.

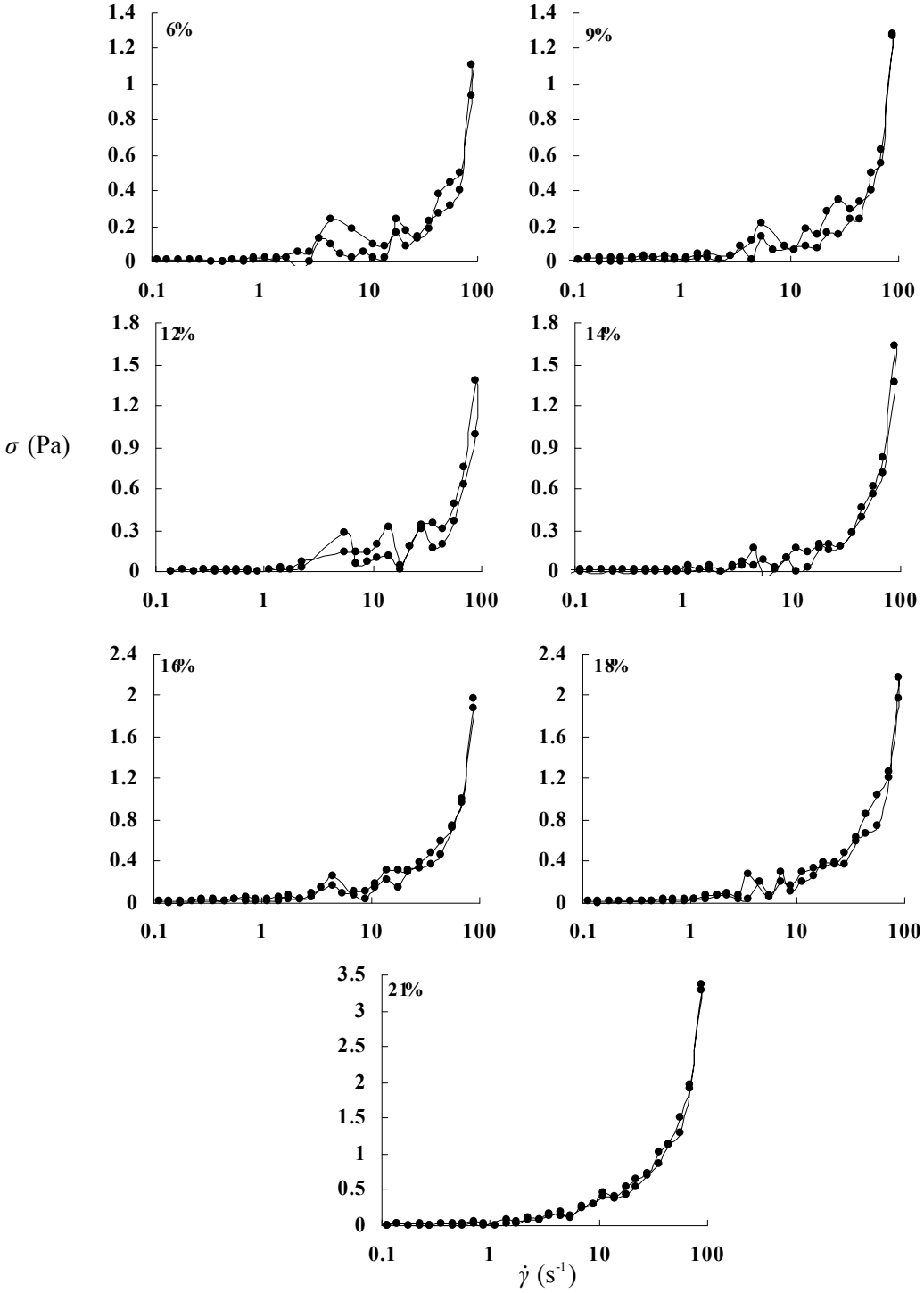

Figure 6.8 Hysteresis loops of Lacprodan87.

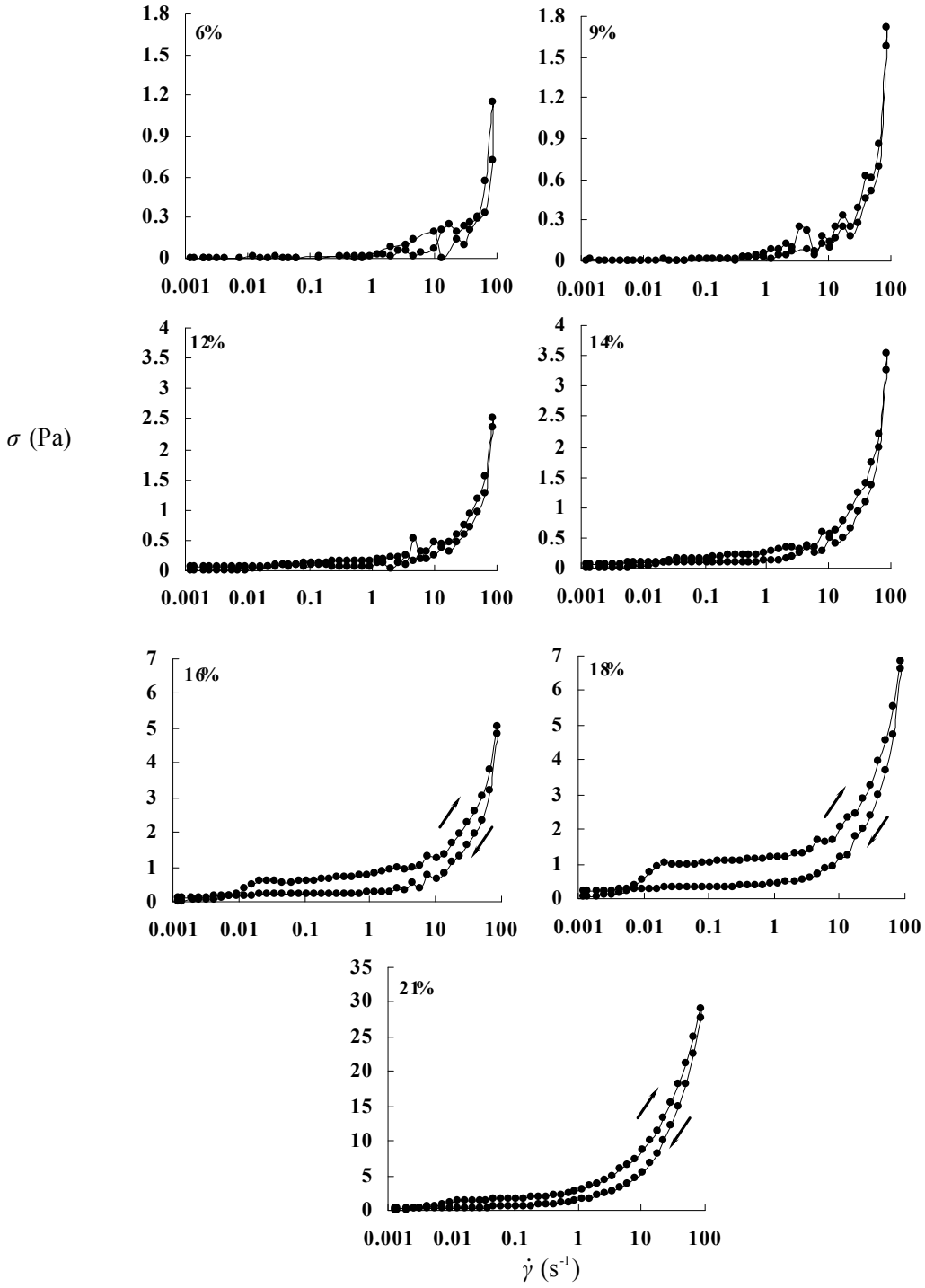

Figure 6.9 Hysteresis loops of Simplesse.

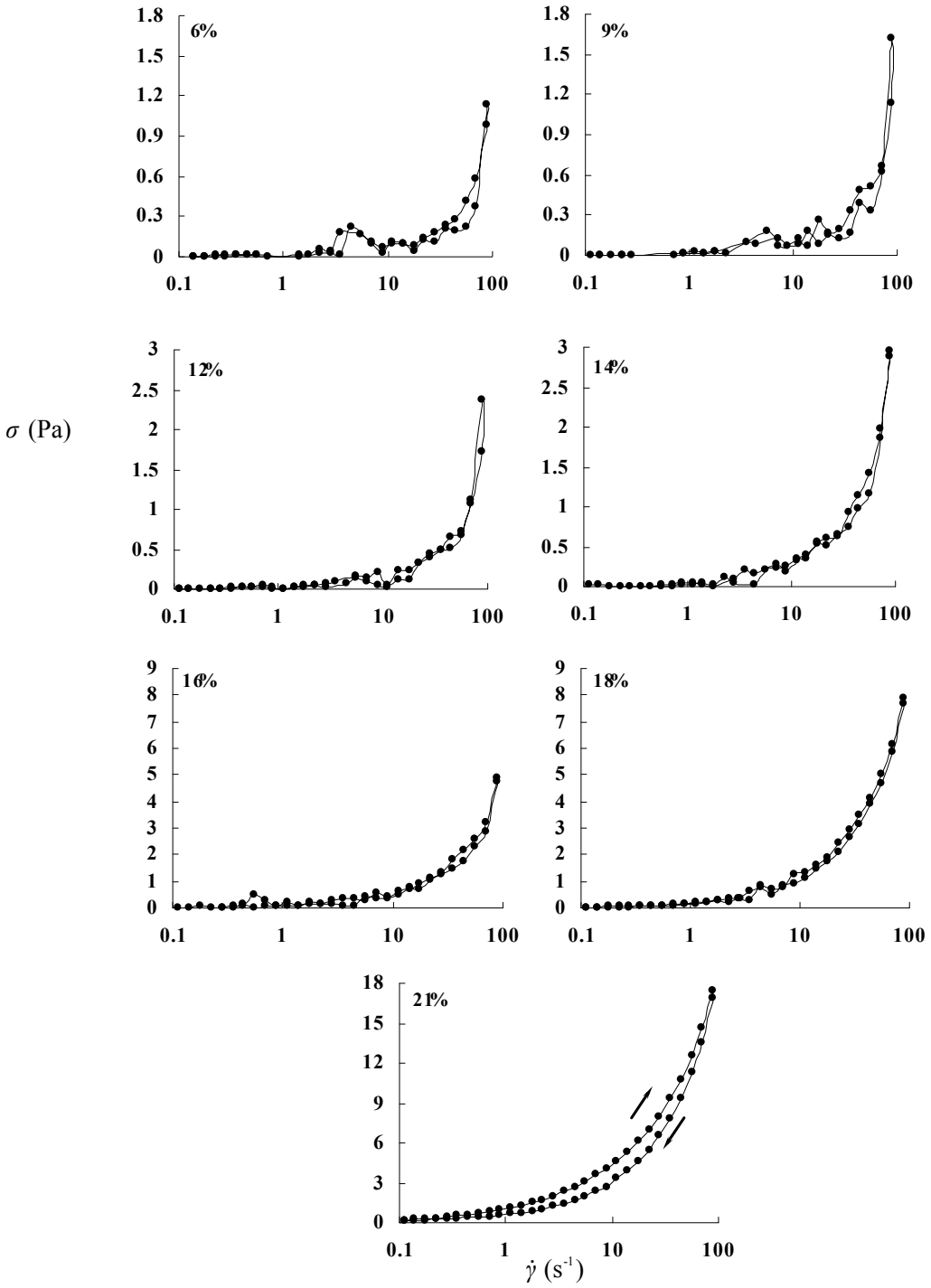

Figure 6.10 Hysteresis loops of Hiprotal60.

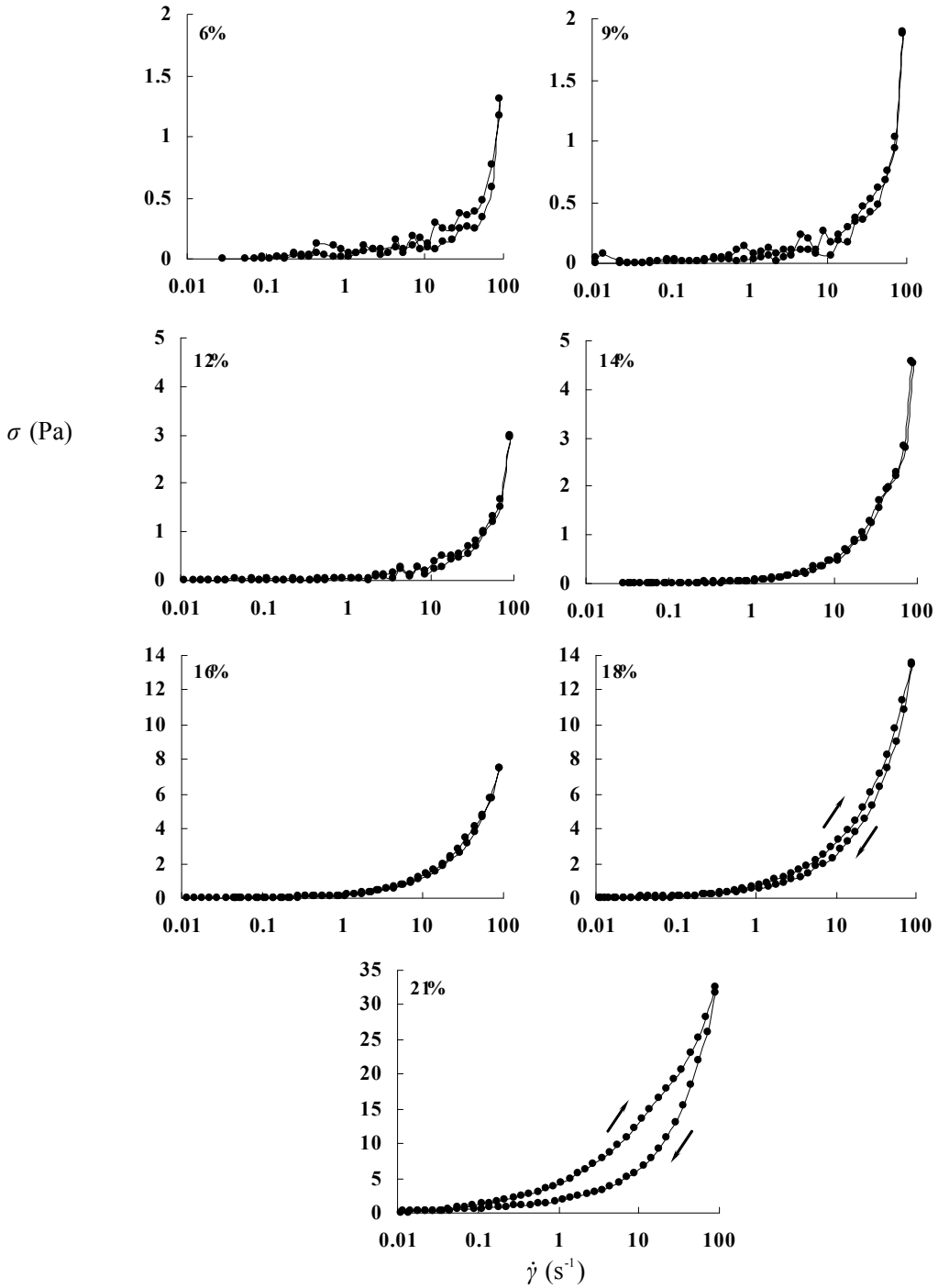

Figure 6.11 Hysteresis loops of Hiprotal60-TS0709.

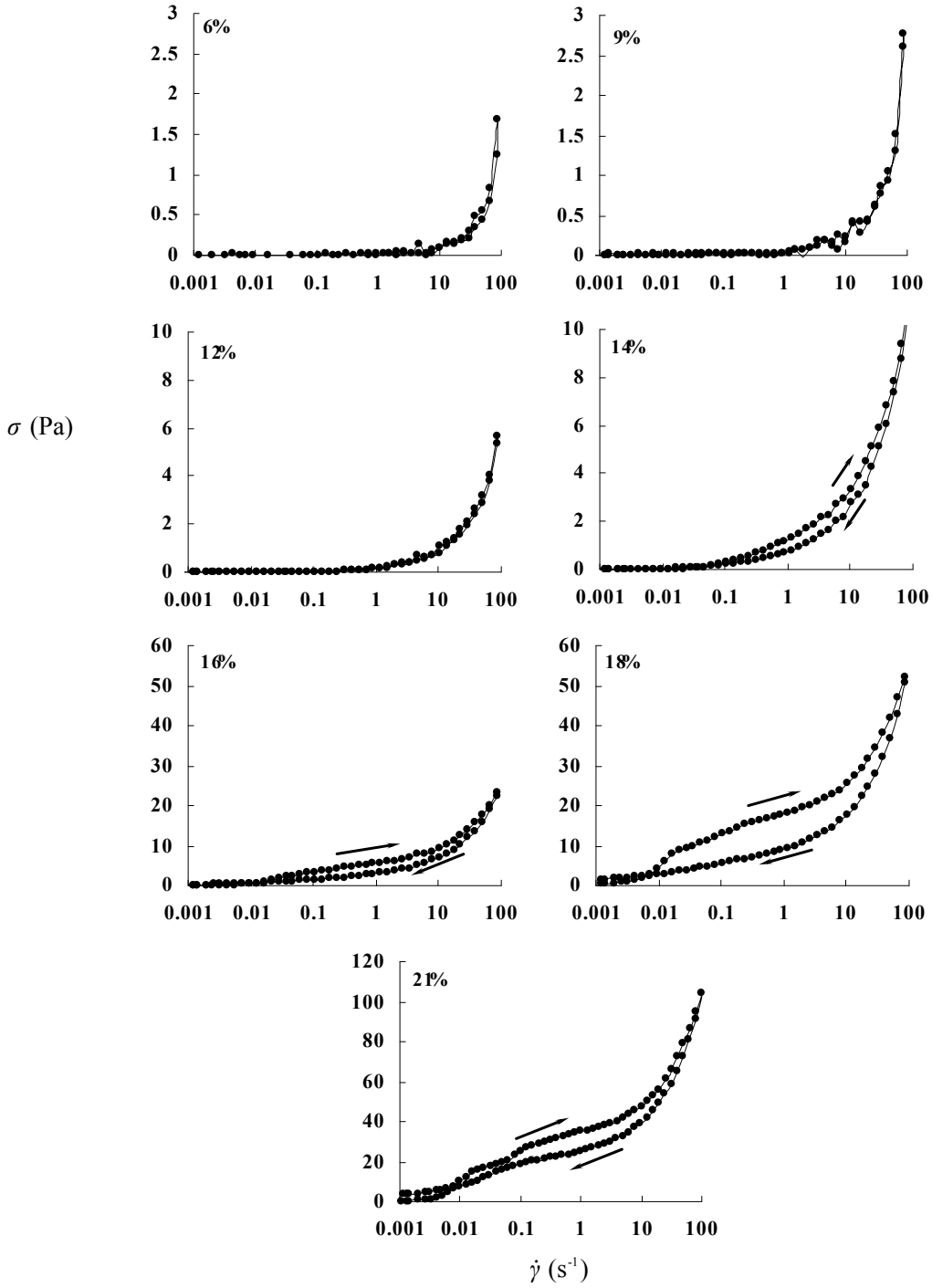

Figure 6.12 Hysteresis loops of Hiprotal60-TS0710.

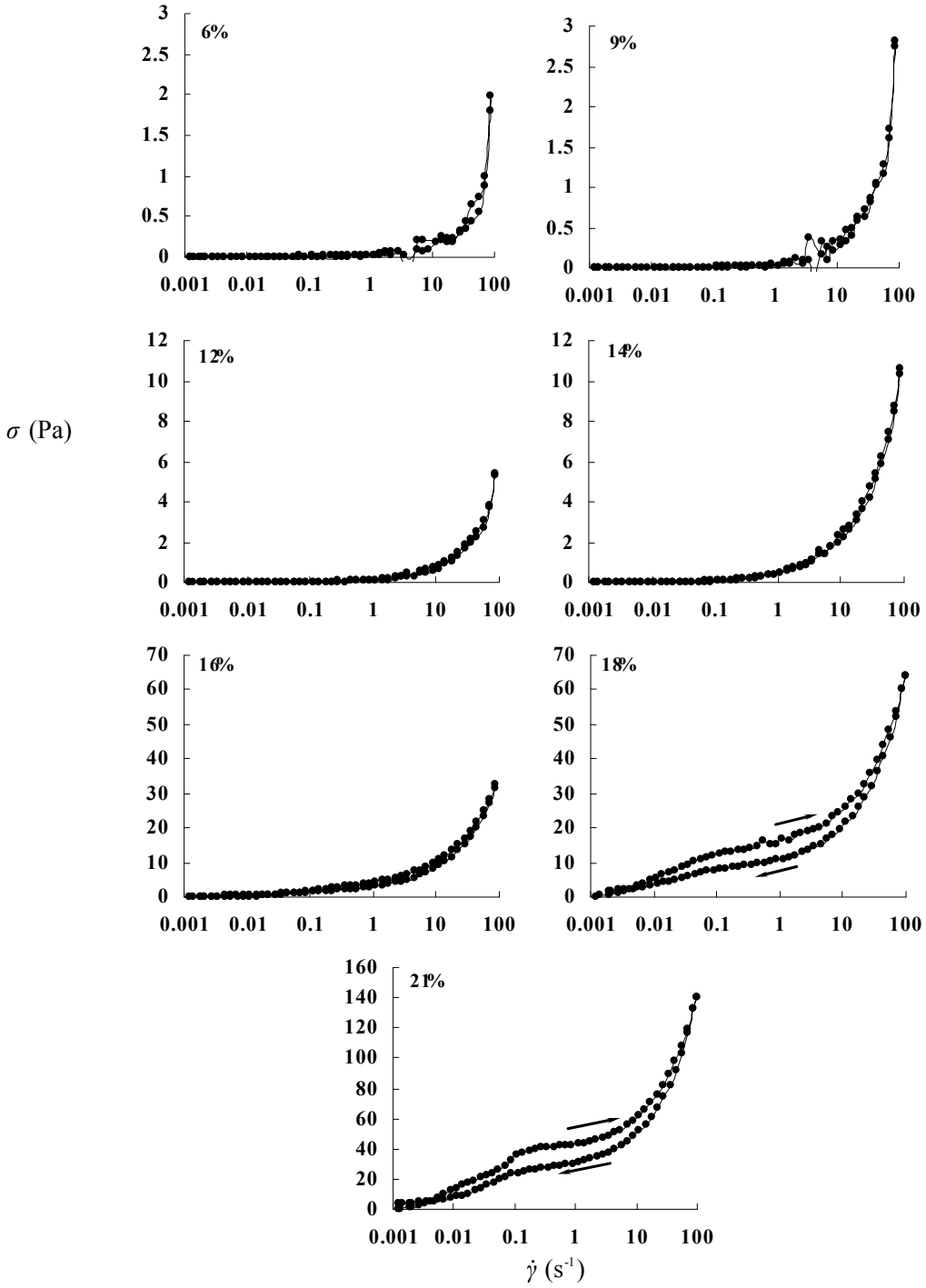

Figure 6.13 Hysteresis loops of Hiprotal60-TS0712.

The surface area of the hysteresis loops, which represented the difference of the speed of energy density dissipation between ascending and descending flows (Kirsanov, Remizov, Novoselova, & Matveenko, 2007; Matveenko & Kirsanov, 2011), is often used to evaluate the degree of thixotropy (Green & Weltmann, 1943; Mewis, 1979; Mewis & Wagner, 2009). Accordingly, the difference of the dissipated energy density,

ΔE, between the two flows, i.e., the product of the area of the hysteresis loops and the time of the test, could be estimated as shown in Figure 6.14. Small changes in ΔE were observed for solutions of Lacprodan87 with different concentrations, indicating that the thixotropy behaviour was mainly due to slow recovery of random orientations of the aligned protein molecules, as well as experimental errors (as discussed earlier). Similar behavior is observed in the dilute solutions of modified (microparticulated and partially denatured) proteins. However, large increases in ΔE (~10^4 Pa or more) were found in concentrated solutions of the modified proteins, where an aggregated structure of the protein molecules is expected to be attained (M. A. Tung, 1978).

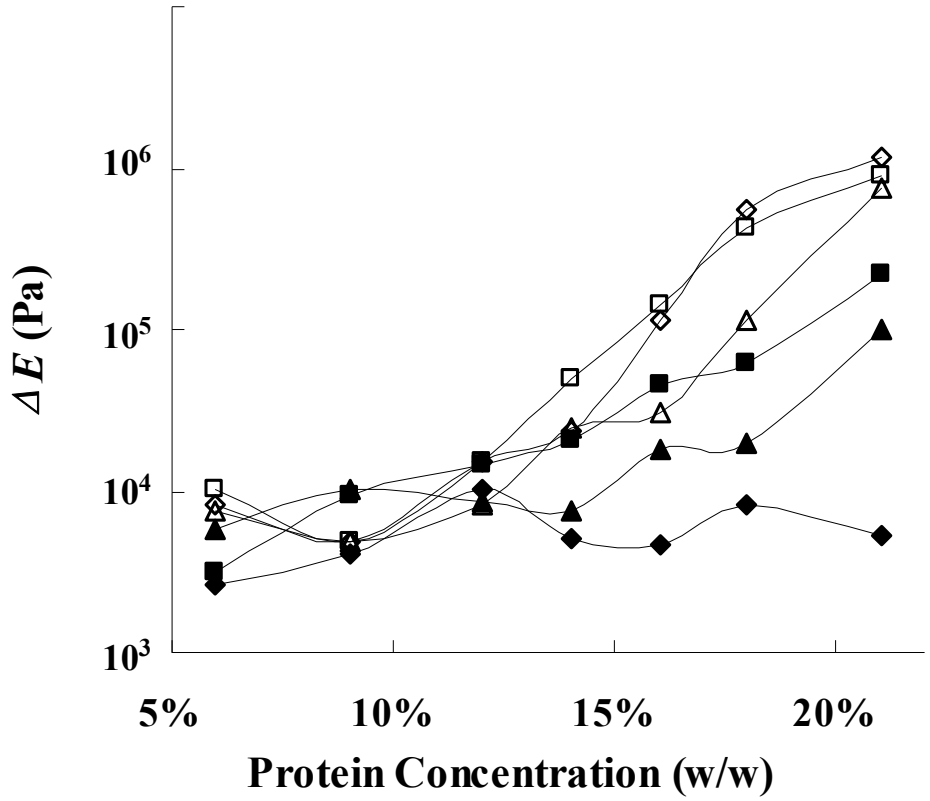

Figure 6.14 Difference of the dissipated energy density between ascending and descending flows of Lacprodan87 (◆), Simplesse (■), Hiprotal60 (▲), Hiprotal60-TS0709 (△), Hiprotal60-TS0710 (□), Hiprotal60-TS0712 (◇).

The critical concentrations of the protein solutions at which ΔE starts to increase rapidly are listed in Table 6.2. It is found that the large aggregated proteins formed structures at lower concentrations, while microparticulated and small aggregated proteins need higher concentrations for aggregation. Such findings were consistent

with what had been concluded in Table 6.1. Flocs rather than network structure formed by microparticulated proteins would account for the difference between Simplesse and Hiprotal60 products, while different lengths of the polymeric chains would explain the differences in the Hiprotal60 products.

Table 6.2 Critical concentrations for large increases in dissipated energy density differences.

	Protein concentration (%, w/w)	Increase in ΔE ($\times 10^4$ Pa)
Lacprdan87	-	-
Simplesse	14~16	2.47
Hiprotal60	14~16	1.03
Hiprotal60-TS0709	12~14	1.62
Hiprotal60-TS0710	9~12	1.05
Hiprotal60-TS0712	9~12	1.07

6.4 Conclusion

Viscous properties of native and commercial microparticulated and partially denatured whey protein concentrates in aqueous solutions have been determined. Exponential increases in viscosity with protein concentration were observed in the solutions with protein concentrations from 6% to 21% for all the samples except for WPC that exhibit linearity between viscosities and protein concentrations in dilute solutions. Such exponential dependence indicates that hydrodynamic and protein-protein interactions exist between the molecules. For solutions of modified proteins, higher exponential dependence of viscosity on protein concentrations was observed, suggesting that aggregated structures formed between modified protein molecules in the solutions. Shear thinning behavior and thixotropy properties, as well as the concentration dependence of viscosity revealed modification of whey protein concentrates could dramatically improve the structuring properties of proteins, and thus, increase the viscosity. Microparticulated proteins were found to require more protein molecules to aggregate due to their flocculated structures. As for partially denatured proteins, those with a large degree of aggregation, i.e., Hiprotal60-TS0710 and Hiprotal60-TS0712, were found to have greater structuring properties, such as lower concentration for a given viscosity and stronger network structures. It is

suggested that partially denatured proteins could provide similar or even better thickening effects in food systems compared with microparticulated proteins. They also offer the opportunity for viscosity and structure control if the extent of denaturation and aggregation is properly controlled.

6.5 Reference

Barnes, H.A., Hutton, J.F., & Walters, K. (1989). *An introduction to rheology*. Amsterdam, The Netherlands: Elsevier.

Bryant, C.M., & McClements, D.J. (1998). Molecular basis of protein functionality with special consideration of cold-set gels derived from heat-denatured whey. *Trends in Food Science & Technology, 9*(4), 143-151.

Damodaran, S. (1996). Amino Acids, Peptides, and Proteins. In O. R. Fennema (Ed.), *Food Chemistry* (3rd ed.). New York, US: Marcel Dekker, Inc.

Dickinson, E., & Stainsby, G. (1982). *Colloids in Food*. London, United Kingdom: Applied Science.

Elofsson, C., Dejmek, P., Paulsson, M., & Burling, H. (1997). Characterization of a cold-gelling whey protein concentrate. *International Dairy Journal, 7*(8-9), 601-608.

Foegeding, E.A., Vardhanabhuti, B., & Yang, X. (2011). Dairy Systems. In I. T. Norton, F. Spyropoulos & P. Cox (Eds.), *Practical food rheology: An interpretive approach*: Wiley-Blackwell.

Foss, D.R., & Brady, J.F. (2000). Structure, diffusion and rheology of Brownian suspensions by Stokesian Dynamics simulation. *Journal of Fluid Mechanics, 407*, 167-200.

Goodwin, J.W., & Hughes, R.W. (2008). *Rheology for Chemists-An Introduction* (2 ed.). Cambridge, UK: The Royal Society of Chemistry.

Green, H., & Weltmann, R.N. (1943). Analysis of the thixotropy of pigment-vehicle suspensions Basic principles of the hysteresis loop. *Industrial and Engineering Chemistry Analytical Edition, 15*(3), 201-206.

Harper, W.J. (2004). *Biological properties of whey components : a review : update 2004*. Elmhurst, IL, US: American Dairy Products Institute.

Hermansson, A.-M. (1975). Functional properties of proteins for foods-flow properties. *Journal of Texture Studies, 5*(4), 425-439.

Hudson, H.M., Daubert, C.R., & Foegeding, E.A. (2000). Rheological and physical properties of derivitized whey protein isolate powders. *Journal of Agricultural and Food Chemistry, 48*(8), 3112-3119.

Ikeda, S., & Nishinari, K. (2000). Intermolecular forces in bovine serum albumin solutions exhibiting solidlike mechanical behaviors. *Biomacromolecules, 7*(4), 757-763.

Ikeda, S., & Nishinari, K. (2001). On solid-like rheological behaviors of globular protein solutions. *Food Hydrocolloids, 15*, 401-406.

Jeurnink, T.J.M., & De Kruif, K.G. (1993). Changes in milk on heating: viscosity

measurements. *Journal of Dairy Research, 60*, 130-150.
Ju, Z.Y., & Kilara, A. (1998). Textural properties of cold-set gels induced from heat-denatured whey protein isolates. *Journal of Food Science, 63*(2), 288-292.
Kinsella, J.E., & Whitehead, D.M. (1988). Proteins in whey: Chemical, physical, and functional properties. *Advances in Food and Nutrition Research, 33*, 343-438.
Kirsanov, E.A., Remizov, S.V., Novoselova, N.V., & Matveenko, V.N. (2007). Physical meaning of the rheological coefficients in the generalized Casson model. *Moscow University Chemistry Bulletin, 62*(1), 18-21.
Lizarraga, M.S., De Piante Vicin, D., González, R., Rubiolo, A., & Santiago, L.G. (2006). Rheological behaviour of whey protein concentrate and λ-carrageenan aqueous mixtures. *Food Hydrocolloids, 20*(5), 740-748.
Macosko, C.W. (1994). *Rheology: Principles, Measurements, and Applications*. New York, USA: Wiley-VCH, Inc.
Madureira, A.R., Pereira, C.I., Gomes, A.M.P., Pintado, M.E., & Xavier Malcata, F. (2007). Bovine whey proteins - Overview on their main biological properties. *Food Research International, 40*(10), 1197-1211.
Matsumoto, T., & Chiba, J. (1990). Rheological and small-angle X-ray scattering investigations on the shape and ordered arrangement of native ovalbumin molecules in aqueous colloids. *Journal of the Chemical Society, Faraday Transactions, 86*(16), 2877-2882.
Matveenko, V.N., & Kirsanov, E.A. (2011). The viscosity and structure of dispersed systems. *Moscow University Chemistry Bulletin, 66*(4), 199-228.
McDonough, F.E., Hargrove, R.E., Mattingly, W.A., Posati, L.P., & Alford, J.A. (1974). Composition and properties of whey protein concentrates from ultrafiltration. *Journal of Dairy Science, 57*(12), 1438-1443.
Mewis, J. (1979). Thixotropy - A general review. *Journal of Non-Newtonian Fluid Mechanics, 6*(1), 1-20.
Mewis, J., & Wagner, N.J. (2009). Thixotropy. *Advances in Colloid and Interface Science, 147-148*, 214-227.
Pradipasena, P., & Rha, C. (1977a). Effect of concentration on apparent viscosity of a globular protein solution. *Polymer Engineering and Science, 17*(12), 861-864.
Pradipasena, P., & Rha, C. (1977b). Pseudoplastic and rheopectic properties of a globular protein (β-lactoglobulin) solution. *Journal of Texture Studies, 8*(3), 311-325.
Prindiville, E.A., Marshall, R.T., & Heymann, H. (2000). Effect of milk fat, cocoa butter, and whey protein fat replacers on the sensory properties of lowfat and nonfat chocolate ice cream. *Journal of Dairy Science, 83*(10), 2216-2223.
Rao, M.A. (2007). *Rheology of Fluid and Semisolid Foods Principles and Applications*. New York, USA: Springer Science+Business Media.
Renard, D., Robert, P., Faucheron, S., & Sanchez, C. (1999). Rheological properties of mixed gels made of microparticulated whey proteins and β-lactoglobulin. *Colloids and Surfaces B: Biointerfaces, 12*, 113-121.
Resch, J.J., & Daubert, C.R. (2002). Rheological and physicochemical properties of derivatized whey protein concentrate powders. *International Journal of Food Properties, 5*(2), 419-434.
Séverina, S., & Xia, W. . (2005). Milk biologically active components as nutraceuticals:

Review. *Critical Reviews in Food Science and Nutrition, 45*(7-8), 645-656.
Sandrou, D.K., & Arvanitoyannis, I.S. (2000). Low-fat/calorie foods: Current state and perspectives. *Critical Reviews in Food Science and Nutrition, 40*(5), 427-447.
Tang, Q., Munro, P.A., & McCarthy, O.J. (1993). Rheology of whey protein concentrate solutions as a function of concentration, temperature, pH and salt concentration. *Journal of Dairy Research, 60*, 349-361.
Tung, M.A. (1978). Rheology of protein dispersions. *Journal of Texture Studies, 9*(1-2), 3-31.

7 Viscoelasticity of microparticulated and partial denatured proteins

7.1 Introduction

Enhanced intermolecular forces were observed for the modified proteins molecules as revealed by viscosity in Chapter 6. Detailed studies on the protein-protein interactions and the aggregating structures of the proteins molecules were performed. Interactions between protein molecules, such as hydrophobic and electrostatic interactions, van der Waals attractions and hydrogen bonding and covalent disulphide bonds, depend on their structures and conformations (Bryant & McClements, 1998; Damodaran, 1996b; Griffin, Griffin, Martin, & Price, 1993; Ross-Murphy, 1995). Ikeda and Nishinari (2001) proposed that globular proteins behaved as colloidal crystals with lattice-like structures stabilized by repulsions from net charges and hydration shells of the proteins. However, once the polypeptide chains are unfolded, the interior non-polar regions and sulfhydryl groups are exposed to the solvent accessible surfaces, and the attractions between molecules, mainly due to hydrophobic interactions and possible disulphide bonds, could dominate over the repulsions, and result in very significant protein aggregations (Elofsson et al., 1997; Ju & Kilara, 1998). It has been widely reported that whey proteins that are partially denatured with pre-heat treatment at low ionic strength exhibit gelling properties at room temperature and thus are defined as cold-gelling WPC's (McClements & Keogh, 1995). The cold-setting gelation could be of great value in the food industry, which would meet the thickening requirement for some special foods that are not suitable for heat processing.

Oscillatory measurements in the linear viscoelastic region are often employed for the investigations on gel systems, since the solid and liquid responses to shear stress can be distinguished (Clark et al., 2001; Ikeda & Nishinari, 2001). By comparing the storage (*G'*) and loss (*G"*) moduli with each other, the conditions under which a system can be considered as having solid-like (*G'>G"*), liquid-like (*G'<G"*), or critical gel (*G'=G"*) behavior (Barnes, 2000; Barnes et al., 1989; Goodwin & Hughes, 2008;

Macosko, 1994; Morrison, 2001). Moreover, the relationship between the dynamic moduli (*G'*, *G"*) and the observation time, (represented experimentally as the frequency, ω, of oscillation) reveals the structure of the gels. Vilgis and Winter (1988), proposed a power law for self-similar or fractal structures for chemical gels, which has been proved to be valid for physical gels (Miyoshi & Nishinari, 1999).

7.2 Material and methods

7.2.1 Protein solutions

Lacptodan87 (Arla Foods Ingredients, Denmark), Simplesse® 100[E] (CP Kelco UK Limited, UK) and a series of Hiprotal60 products, i.e., Hiprotal60, Hiprotal60-TS0709, Hiprotal60-TS0710, and Hiprotal60-TS0712 (Friesland Foods, the Netherland) were dissolved in deionized distilled water at 20~23 °C to make solutions with protein concentrations of 6%, 9%,12%, 14%, 16%, 18% and 21% (w/w). The solutions were stirred gently for at least 1 h to allow full hydration for the proteins. The same procedure was repeated for 21% (w/w) protein solutions, except that acetic acid (≥99.7 w/w %) (Fisher Scientific, USA) was added to adjust the pH to 4.5 during the last 10 min of stirring.

7.2.2 Oscillatory measurements

Oscillation measurements were performed with controlled stress mode using a Gemini advanced rheometer (Bohlin Instruments, UK), with 4°/40 mm cone and plate at a temperature of 20 °C. The solution samples were spread onto the surface of the plate and then the cone was set to its position with a gap of 150 μm above the plate surface. The linear viscoelastic region was found by amplitude sweep measurements taken at a frequency of 1 Hz. From the results of the amplitude sweep, the linear viscoelastic region (if it exists) was obtained up to around a strain of 0.1. A stress/strain combination in the linear viscoelastic region was chosen to use for the frequency sweep measurements. For all systems strains in the range of 0.02-0.05 were selected for frequency sweep measurements.

Frequency sweep measurements were performed in the range of frequencies from 0.001 Hz to 15 Hz, so that the largest angular frequency, ω, is of the order of 100 rad/s. Storage (*G'*) and loss (*G"*) moduli which describe the elastic and viscous properties of samples are obtained directly and the relevant parameters, the complex modulus (G^*) and complex viscosity (η^*) are defined and calculated according to equations 7.1. and 7.2 (Barnes, 2000; Barnes et al., 1989; Blom et al., 1984; Goodwin & Hughes, 2008; Macosko, 1994; Meyers & Chawla, 2009; Morrison, 2001).

$$|G^*| = \frac{\sigma}{\gamma} = \sqrt{\left(G'\right)^2 + \left(G''\right)^2} \tag{7.1}$$

$$|\eta^*| = \frac{\sigma}{\omega} = \sqrt{\left(\frac{G'}{\omega}\right)^2 + \left(\frac{G''}{\omega}\right)^2} \tag{7.2}$$

7.3 Results and discussion

7.3.1 Linear viscoelasticity

In order to obtain the dynamic viscoelastic properties, the linear viscoelastic region of a material must be obtained first, i.e., where linearity between strain and stress is observed (Barnes, 2000; Barnes et al., 1989; Goodwin & Hughes, 2008; Macosko, 1994; Morrison, 2001). Practically, the linear viscoelastic region is constrained to a small range of strains/stresses, so that the spring and the piston of the dashpot in the viscoelastic model remain in the Hookean limit and Newtonian oil, respectively, (Goodwin & Hughes, 2008; Macosko, 1994). Experimentally, this linear viscoelatic range is obtained from strain sweep measurements (Ikeda & Nishinari, 2001). The strain amplitude dependence of viscoelastic behaviour of different protein samples are shown in Figures 7.1 to 7.6.

It was observed that the shear stress, σ, increased linearly with small strain amplitudes. For WPC solutions, i.e., Lacprodan87, the linear region extended to large strain for all the concentrations as illustrated in Figure 7.1. According to equation 7.1 and 7.2, linearity of σ with γ is due to the consistency of the value of the complex modulus, G^*. It was also found that the loss modulus, *G"*, is relatively constant and

larger compared with the storage modulus, *G'*, of the solutions, illustrating that the system mainly dissipated the external energy by viscous flows rather than storing it through inter-particle interactions (Goodwin & Hughes, 2008; Macosko, 1994; Morrison, 2001). It was noted that *G'* was greater than *G"* at small strains, which could be due to the fluctuations of the *G'* resulting from experimental errors since the stresses applied are very close to the instrumental limitation at such small strain. Besides, no linear region of the storage modulus, *G'*, was observed in all the solutions in Figure 7.1, illustrating weak interactions, such as repulsive electrostatic and attractive van der Waals forces, between the dispersed protein molecules, even at high concentrations (~21%, w/w).

Similar behaviour was observed for modified (both the microparticulated and partially denatured) WPC proteins in dilute solutions, indicating weak inter-particle forces between protein molecules at low concentrations. However, a linear region of the storage modulus, *G'*, occurred as the protein concentration increased in the modified protein solutions, as shown in Figure 7.2 to Figure 7.6. Meanwhile, both the loss, *G"*, and storage, *G'*, moduli were found to increase with protein concentrations, indicating that both the hydrodynamic and intermolecular forces increased with protein concentrations, leading to viscous and elastic behaviour of the protein solutions, respectively. It was also found that viscous flows dominated the energy dissipation for the Hiprotal60 solutions even at high concentrations, while for the other modified proteins (Hiprotal60-TS07XX and Simplesse), more viscoelastic properties were observed as *G'* approached *G"* at high concentrations. For those proteins with large particle size (Hiprotal60-TS0710 and –TS0712) elastic responses predominated over the viscous ones as the protein concentration reached 18% (w/w). Such significant elastic behaviour revealed strong protein-protein interactions probably resulting from protein aggregation in these solutions (Ikeda & Nishinari, 2001; Xu et al., 2013).

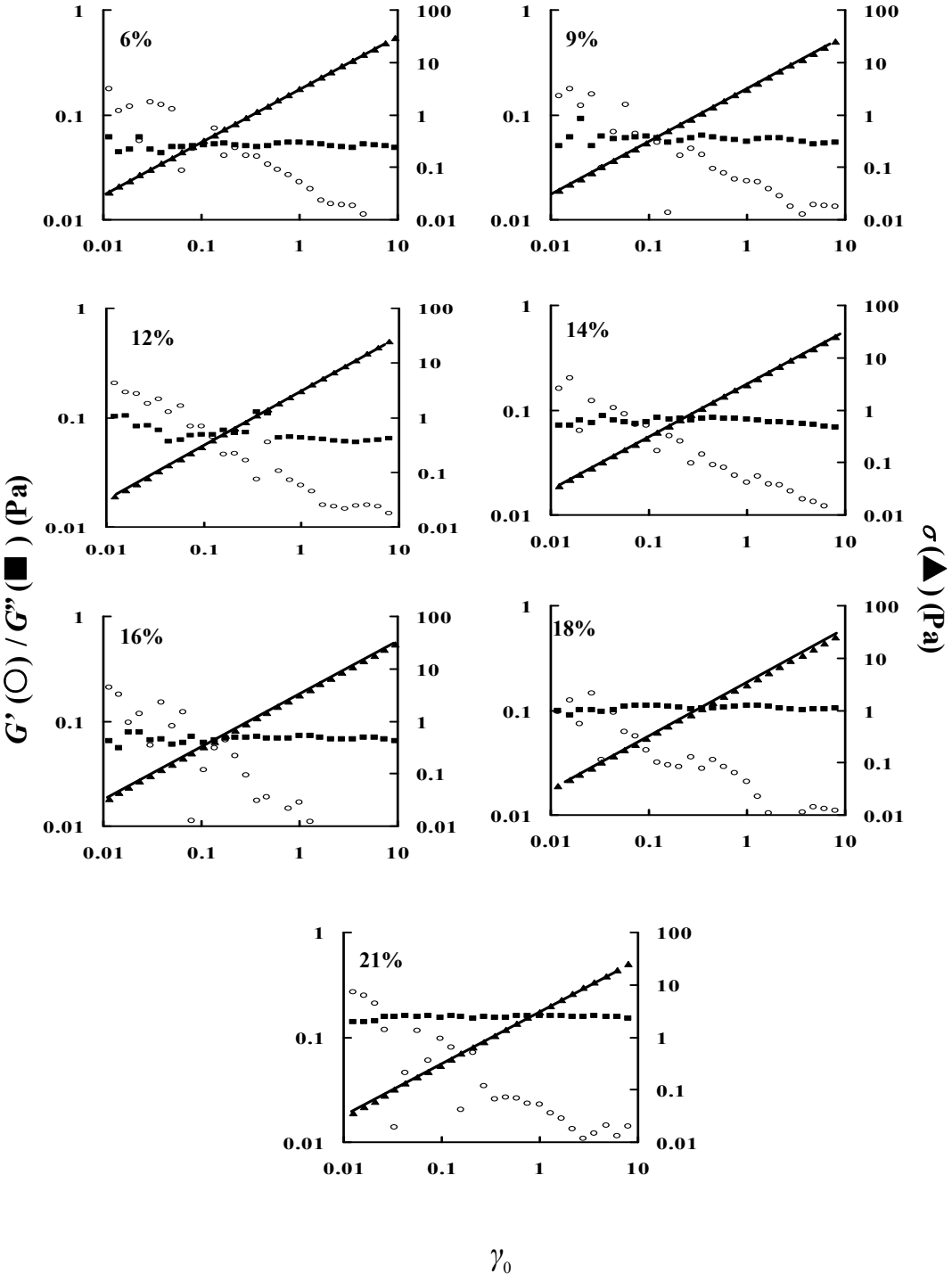

Figure 7.1 Strain amplitude dependence measured at 1 Hz of elastic, *G'* (○), and viscous, *G"* (■) moduli, and shear stress, (▲), of Lacprodan87 solutions with different concentration.

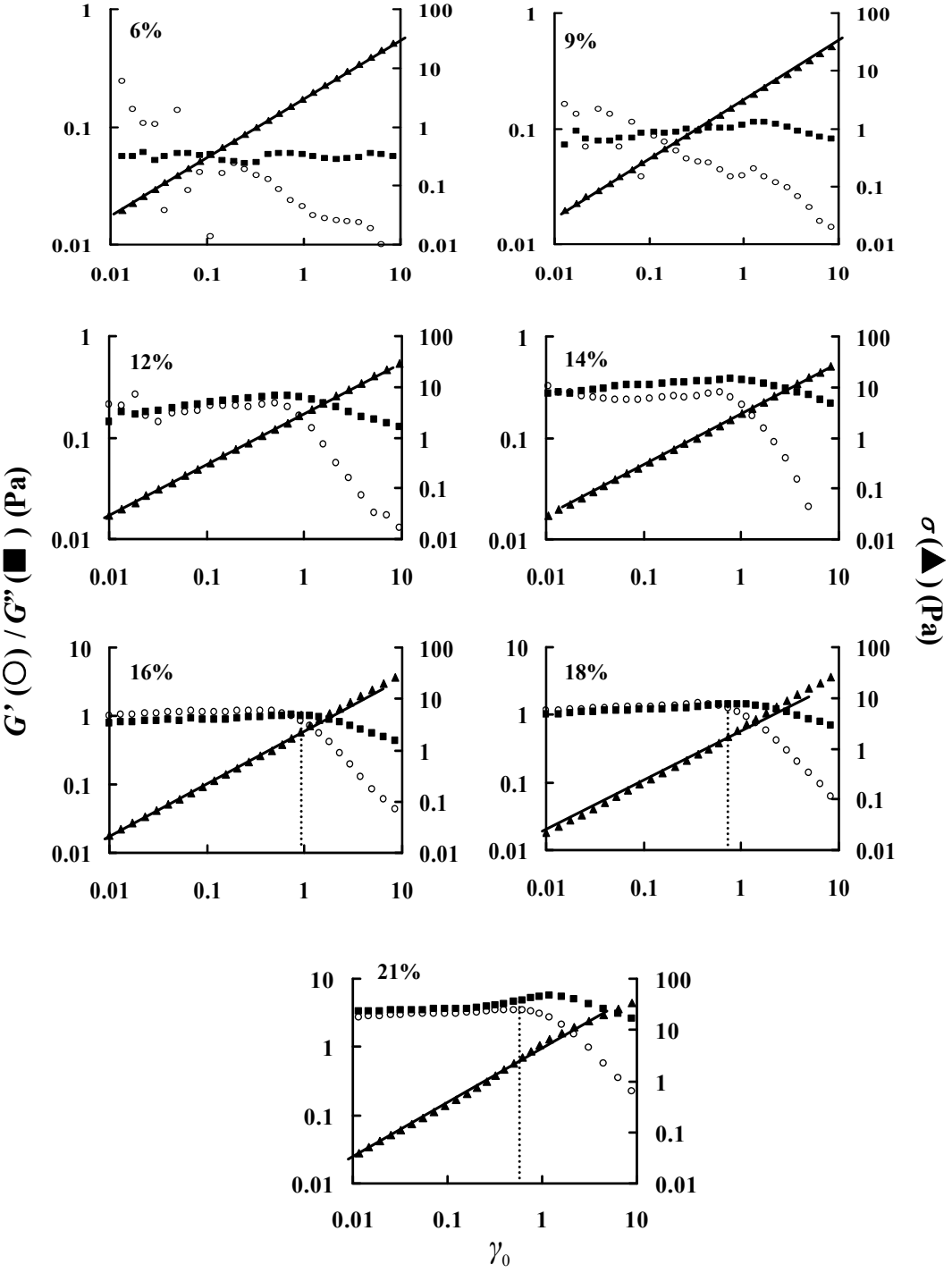

Figure 7.2 Strain amplitude dependence measured at 1 Hz of elastic, *G'* (○), and viscous, *G"* (■) moduli, and shear stress, (▲), of Simplesse solutions with different concentration.

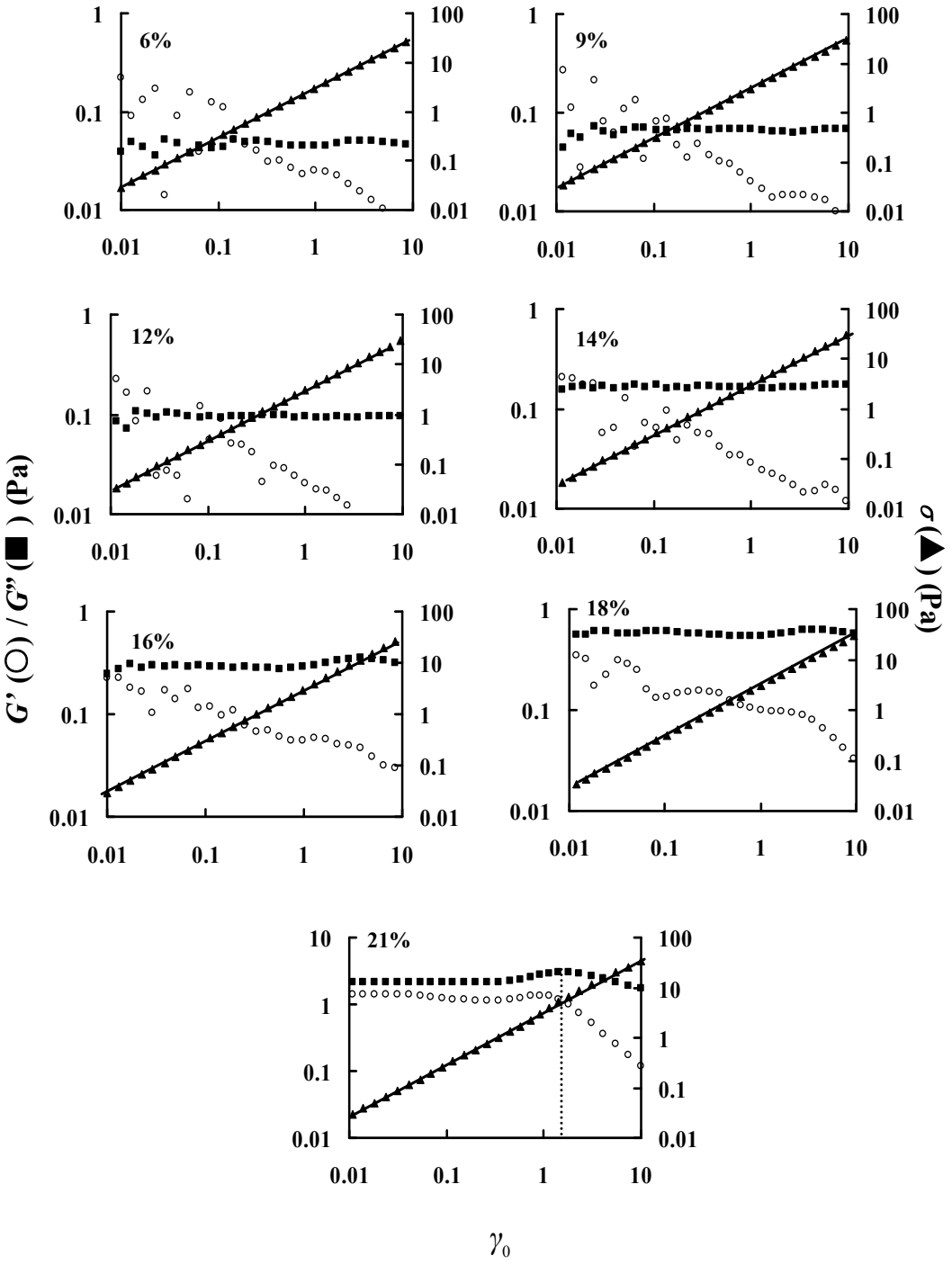

Figure 7.3 Strain amplitude dependence measured at 1 Hz of elastic, *G'* (○), and viscous, *G"* (■) moduli, and shear stress, (▲), of Hiprotal60 solutions with different concentration.

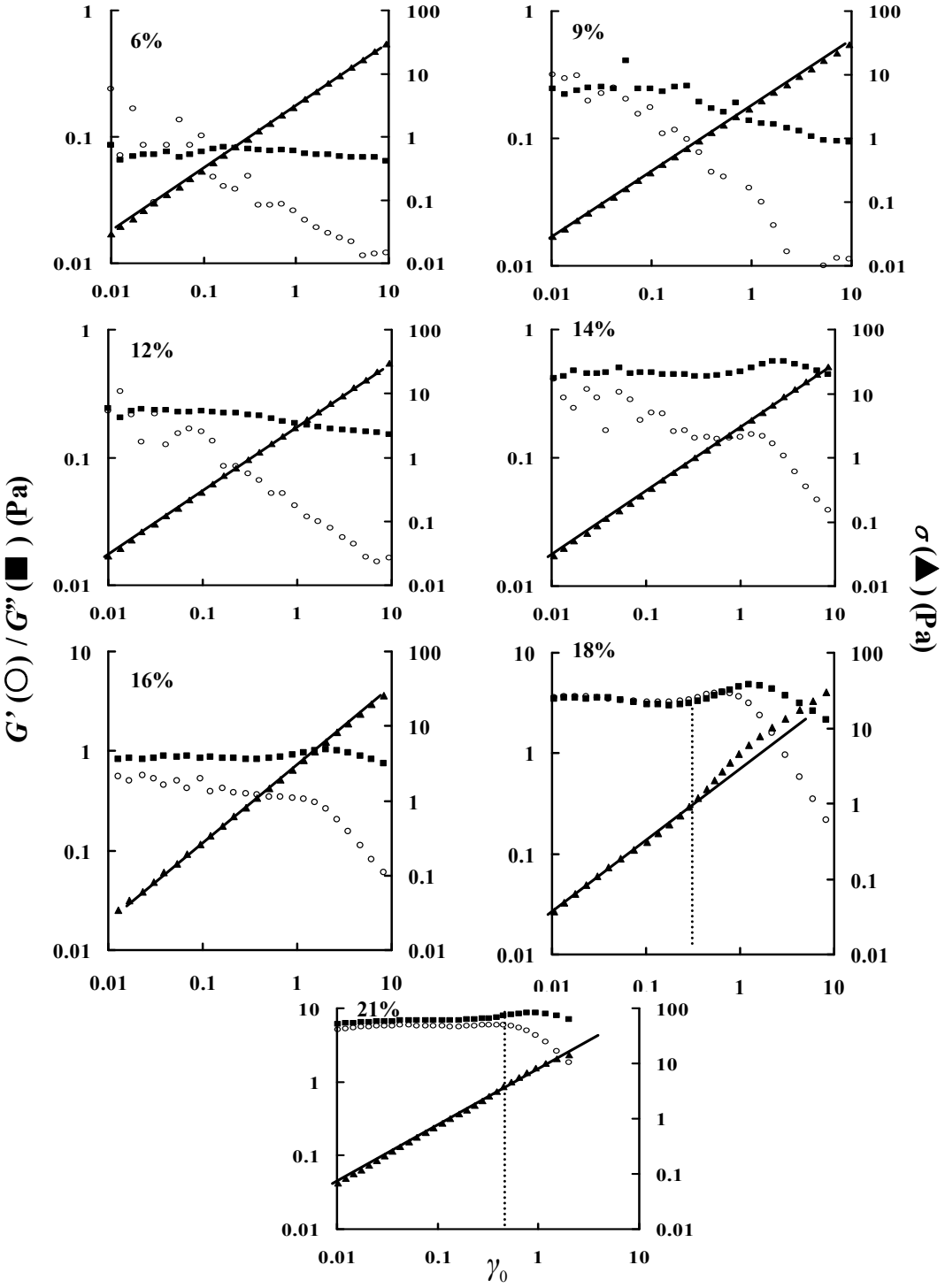

Figure 7.4 Strain amplitude dependence measured at 1 Hz of elastic, *G'* (○), and viscous, *G"* (■) moduli, and shear stress, (▲), of Hiprotal60-TS0709 solutions with different concentration.

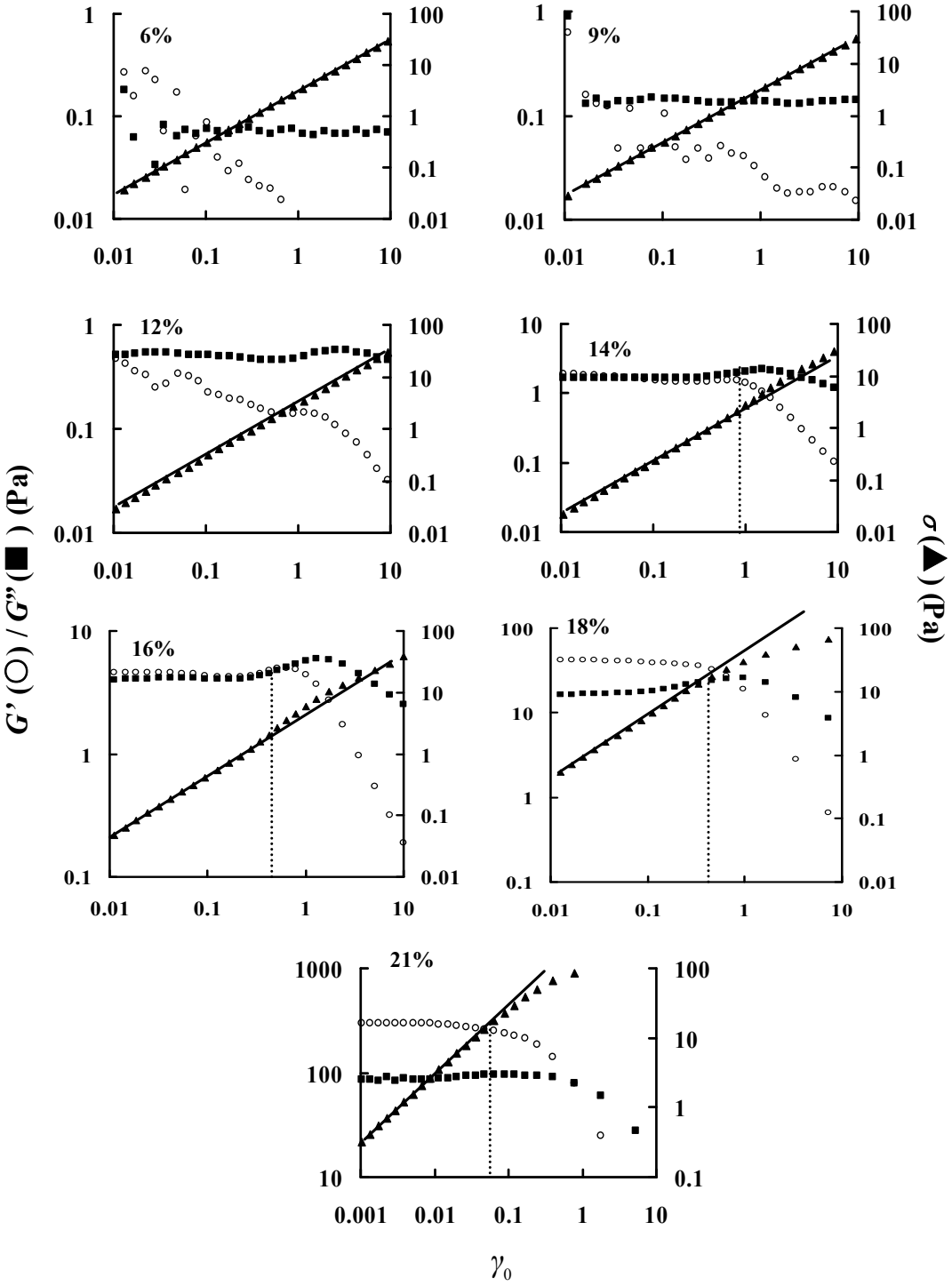

Figure 7.5 Strain amplitude dependence measured at 1 Hz of elastic, *G'* (○), and viscous, *G"* (■) moduli, and shear stress, (▲), of Hiprotal60-TS0710 solutions with different concentration.

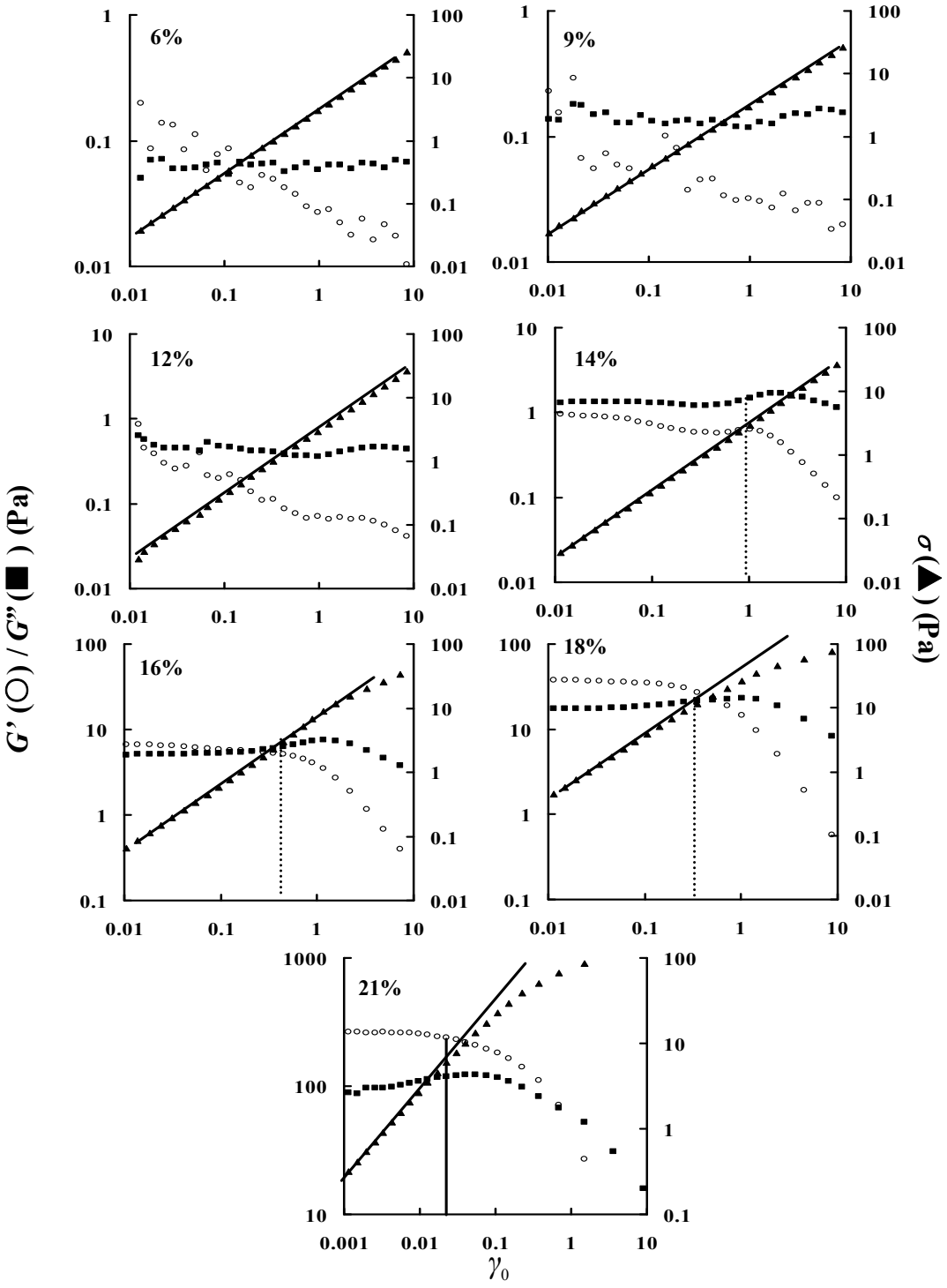

Figure 7.6 Strain amplitude dependence measured at 1 Hz of elastic, *G'* (○), and viscous, *G"* (■) moduli, and shear stress, (▲), of Hiprotal60-TS0712 solutions with different concentration.

The concentration dependence of storage modulus, *G'*, in the linear viscoelastic region for different protein solutions is shown in Figure 7.7. Since the linear regions (if there was one) of *G'* were found to be in the range of strain smaller than 0.1, the values of *G'* for all the samples were estimated/calculated as the average of the observations from 0.015 to 0.055 strain.

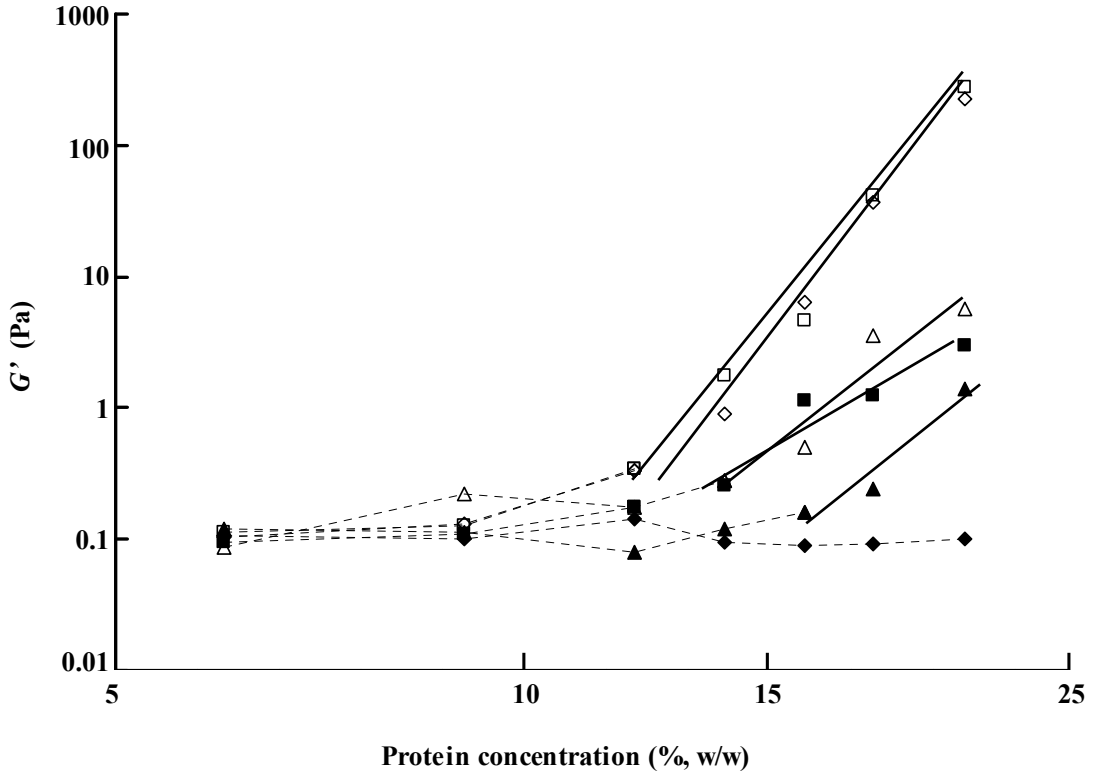

Figure 7.7 Concentration dependence of storage modulus, *G'*, measured at 1 Hz for solutions of Lacprodan87 (◆), Simplesse (■), Hiprotal60 (▲), Hiprotal60-TS0709 (△), Hiprotal60-TS0710 (□), Hiprotal60-TS0712 (◇).

The values of *G'* for WPC (Lacprodan87) solutions were observed to be independent of protein concentrations, which was consistent with the findings of Lizarraga et al. (2006) and the results in the viscosity, η_{100}, of WPC as shown in Figure 6.1 and Table 6.1, where η_{100} exhibited only one concentration dependence, indicating the absence of significant inter-particle forces in such solutions (Ikeda & Nishinari, 2000, 2001). Concentration independence of *G'* was also found in dilute solutions of the modified proteins. As the protein concentration increased, however, the storage modulus, *G'*, started to increase and follow a power law dependence, i.e., $G' \propto w^m$,

where ^{m} represents the slopes of the solid lines in Figure 7.7. Such power law trends at high protein concentrations suggest increased interactions between protein molecules. It was also found that the concentration dependence, i.e., the values of ^{m}, as shown in Table 7.1, of Simplesse and Hiprotal60 and Hiprotal60-TS0709 were much smaller than those of the highly aggregated denatured proteins (i.e., Hiprotal60-TS0710 and –TS0712), suggesting weaker structure formed by the former, while much stronger aggregates, such as network or physical gel existed in the latter (Xu et al., 2013).

Table 7.1 Concentration dependence, ^{m}, of *G'* for different protein samples.

	Concentration dependence (^{m})
Lacoprodan87	-
Simplesse	5.27
Hiprotal60	8.10
Hiprotal60-TS0709	8.15
Hiprotal60-TS0710	12.03
Hiprotal60-TS0712	12.19

7.3.2 Oscillation responses

Since the elastic responses to oscillations in dilute protein solutions were not obvious, as shown from Figure 7.1 to Figure 7.7, frequency sweep measurements were employed to those concentrated (from ~14%) solutions from which elastic behavior increases significantly as shown in Figure 7.7. Cox-Merz plots of different protein solutions are shown in Figures 7.8 to 7.12. From those results, the viscosity of the solutions was found to increase with protein concentration for both steady and dynamic flows, indicating increasing interactions between protein molecules. However, the flowing behavior of proteins could be differentiated individually according to the details of their structures.

It is found that the storage modulus, *G'* was always larger than the loss modulus, *G"*, in all the concentrated Simplesse solutions for the whole frequency range, suggesting the formation of a solid-like structure of the microparticulated proteins

(Ikeda & Nishinari, 2001). Besides, violation of the empirical Cox-Merz rule (Cox & Merz, 1958) is observed for the solutions where the amplitude of the complex viscosity, η^*, was always greater than the steady viscosity, η, indicating that the solid-like structure was susceptible to large strains (Ikeda & Nishinari, 2001; Lizarraga et al., 2006). Increases in the steady viscosity at low shear rates followed by shear thinning behaviour were observed for the solutions. Renard et al. (1999) observed similar phenomenon in Simplesse and suggested that it was due to flocculation of the microparticulated proteins at low shear stresses and disruption of these flocs by large shear stresses and strains. Moreover, the dynamic moduli, i.e., *G'* and *G"*, were found to increase slowly with concentration (also as shown in Figure 7.7), suggesting the flocs could not extend to infinite size as the development of a network or gel of proteins.

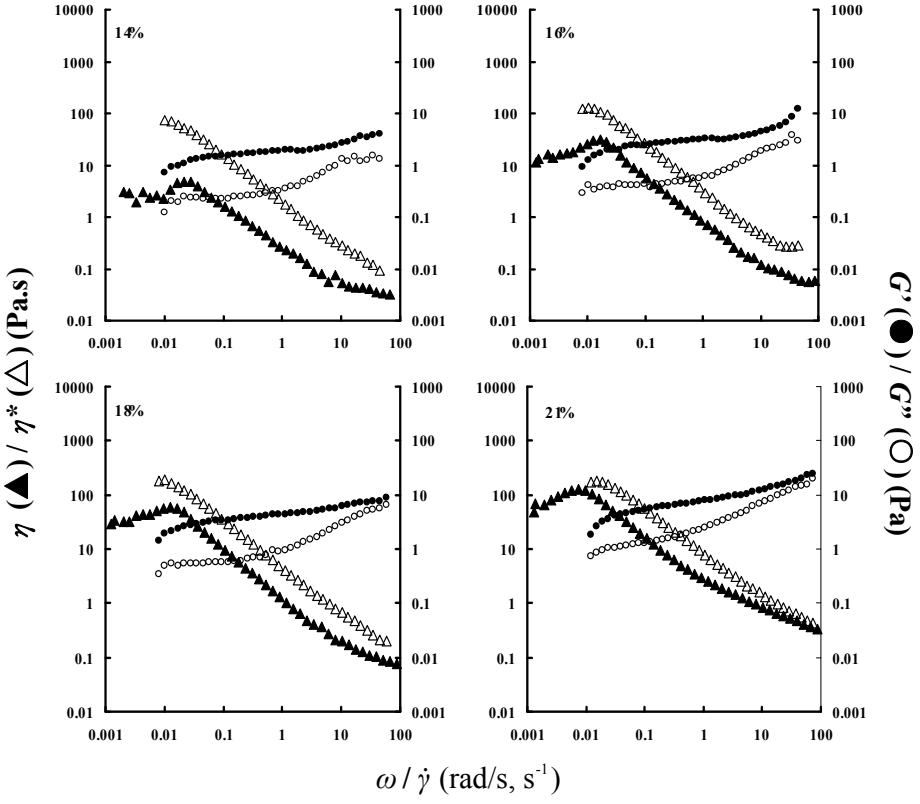

Figure 7.8 Cox-Merz plots of concentrated Simplesse solutions.

The complex viscosity, η^*, of Hiprotal60 solutions was found to be close to their steady viscosity, η, for all the concentrations as shown in Figure 7.9, indicating that

these solutions followed the Cox-Merz rule and thus, aggregation of proteins was absent. The storage modulus, *G'* was smaller than the loss modulus, *G"*, suggesting liquid-like behaviour of the proteins in the solutions. Similar observations such as the liquid-like behaviour and the Cox-Merz rule were also found in Hiprotal60-TS079 solutions with relatively low concentrations (<18%), suggesting no aggregated structures form by the proteins. However, as protein concentration increased to 21% and 18% for Hiprotal60 and Hiprotal60-TS079, respectively, the solutions tended to exhibit viscoelastic properties as *G'* approached *G"*, and the flow behaviour tended to violate the Cox-Merz rule. It is interesting to find that the curves of η^* and η diverged at low angular frequencies and shear rates, but tended to converge as the angular frequency and shear rate increased. Such deviation from the Cox-Merz rule could be due to aggregation of proteins driven by small shear stresses but disrupted by large stresses. Similarly, with Simplesse, shear thickening regions at low shear rates were observed in concentrated Hiprotal60 (~21%) and Hiprotal60-TS709 (>18%) solutions, indicating aggregation or flocculation of protein molecules in these solutions (Renard et al., 1999). There seems to be two opposite effects of steady shears on the aggregation of the low aggregated partial denatured proteins. Alignment of protein molecules at low shear rates contributes to flocculation while large strains tend to break up the structure. Therefore, aggregated structure of protein molecules is inclined to form at small strains with low shear, i.e., under the oscillation conditions within the linear viscoelastic region at small frequencies. As the frequency increases, however, the fragile intermolecular forces are overcome by large stresses and thus, the protein molecules flow individually as the same as in steady flow, even though the shear stress and strain are still constrained in the linear region. Besides, it was also noted that the values of *G'*, *G"*, and η^* of Hiprotal60, are significantly smaller than those of Hiprotal60-TS0709 and other samples, even at a high concentration (~21%), which could verify weak protein-protein interactions and absence of aggregated structures formed by the former.

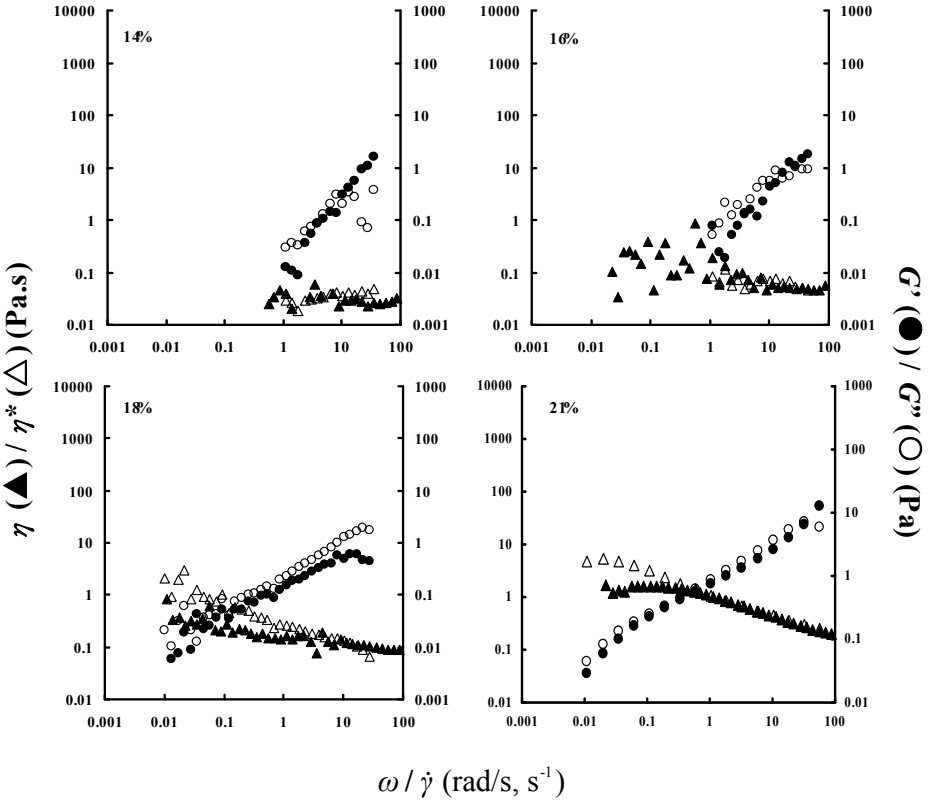

Figure 7.9 Cox-Merz plots of concentrated Hiprotal60 solutions.

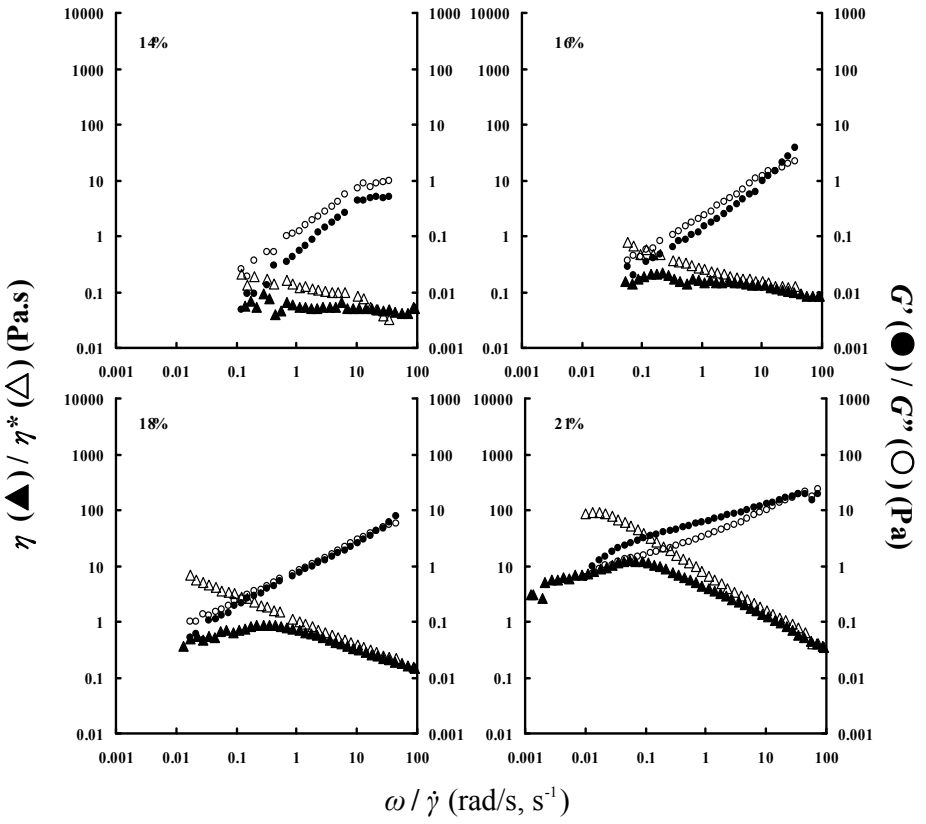

Figure 7.10 Cox-Merz plots of concentrated Hiprotal60-TS0709 solutions.

Similar Cox-Merz behavior to that of the low aggregated partial denatured proteins was observed for those with a high extent of aggregation, i.e., Hiprotal60-TS0710 and Hiprotal60-TS0712, at low (<18%) concentrations, indicating weak interparticle forces and thus fragile aggregates of proteins existing in these solutions. However, *G'* and η^* were found to significantly exceed *G"*, and η as the concentration increases above 18%, suggesting the occurrence of strong interparticle forces and formation of solid aggregates of protein molecules in these solutions. Shear thickening behaviour was also present in the solutions with steady shear at low shear rates, indicating that alignment of the polymeric 'strings' contributed to their aggregation (Renard et al., 1999). Drastic increases were observed in *G'*, *G"*, and η^* for the concentrated (>18%) solutions, which were much larger than those of microparticulated and lowly aggregated denatured proteins, suggesting strong network or physical gel formed by the polymeric protein aggregated chains. Such aggregation of protein could be explained based on the viscoelasticity of the concentrated protein solutions.

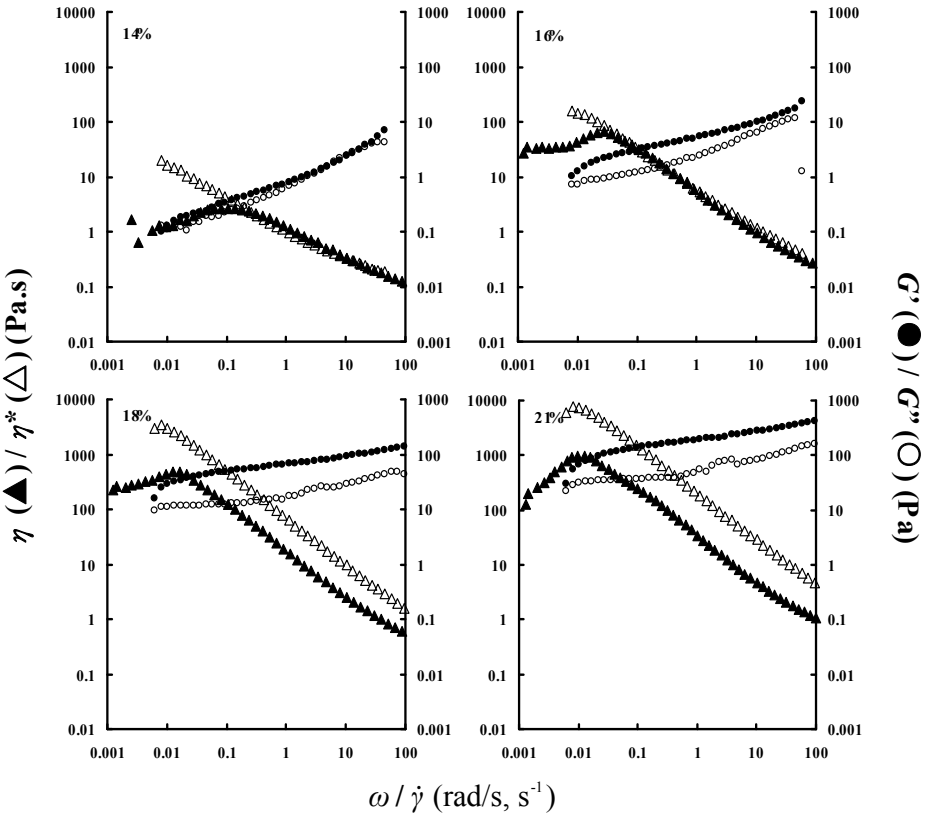

Figure 7.11 Cox-Merz plots of concentrated Hiprotal60-TS0710 solutions.

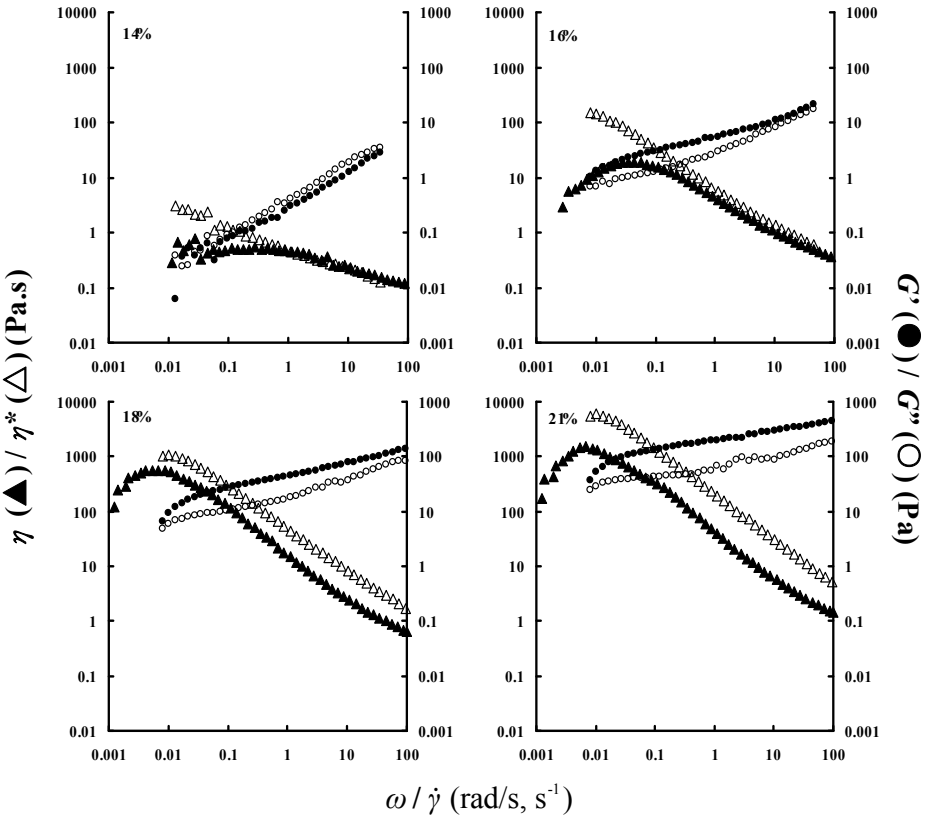

Figure 7.12 Cox-Merz plots of concentrated Hiprotal60-TS0712 solutions.

7.3.3 Aggregation of proteins

The viscoelastic properties of the different protein products in the solutions with a concentration of 21% are plotted in Figure 7.13. The dynamic moduli of Hiprotal60 are much smaller than the other samples, and the loss modulus, *G"* is always lager than *G'*, indicating the absence of aggregation of proteins and liquid-like behaviour of the solution. The viscoelastic behaviours of Simplesse and Hiprotal60-TS0709 were similar to each other. The values of *G'* were larger than those of *G"*, suggesting significant elastic properties of the proteins. Moreover, both *G'* and *G"* of the protein solutions exhibited frequency dependence, indicating the solutions behave like a viscoelastic liquid rather than a solid (Goodwin & Hughes, 2008; Macosko, 1994), which could also be confirmed by visual observations. As indicated in Figure 7.7, concentration dependence and the values of *G'* of Simplesse and Hiprotal60-TS0709 were significantly smaller than those of Hiprotal60-TS0710 and -TS0712, even at the concentration of 21%, where the former exhibit obvious elastic properties, indicating

that these microparticulated and the lowly aggregated denatured proteins form flocs with finite sizes. The viscoelasticity of such protein solutions were supposed to result from the colloidal crystal structures of the flocs stabilized by repulsions between the protein clusters according to Lindsay and Chaikin (1982) and Ikeda and Nishinari (2001).

A strong network appears to form in concentrated (>18%) solutions of polymeric denatured proteins (i.e., Hiprotal60-TS0710 and -TS0712), as indicated by large values and concentration dependence of G' (Xu et al., 2013). In addition, a tendency towards a power law relationship between G', G'' and ω is observed in Figure 7.13, i.e., $G' \sim G'' \sim \omega^n$, suggesting a self-similar or fractal structure of the physical gel formed by the proteins (Ikeda & Nishinari, 2001; Muthukumar, 1989; Vilgis & Winter, 1988). According to percolation theory, the smallest of value of exponents of the power law, i.e., the values of ^{n} should be 0.60, which gives the largest value of fractal dimension $d_f = d = 3$, where d is the Euclidian dimension (Muthukumar, 1989; Vilgis & Winter, 1988). However, the values of such exponent for Hiprotal60-TS0710 and –TS0712 are found to be 0.17±0.02 and 0.19±0.01, respectively. Muthukumar (1989) suggested that the screening of the excluded volume effects due to high concentration of polymers (Doi & Edwards, 1986) accounted for the very small exponent values and proposed that the power law exponent, ^{n}, related the fractal dimension, d_f, of the gel as

$$n = \frac{d \times \left(d + 2 - 2d_f\right)}{2 \times \left(d + 2 - d_f\right)} \tag{7.3}$$

where d is the Euclidian dimension and equals 3 for three dimensional networks. Consequently, the fractal dimension was calculated as 2.3 for the network formed by either Hiprotal60-TS0710 or –TS0712. Winter and Chambon (1986) and Vilgis and Winter (1988) proposed the power law exponent and the fractal dimension for a critical gel where the network expanded to infinite are 0.50 and 2.0, and are larger (0.17 and 0.19) and smaller (2.3) than those of the gel formed by the highly aggregated denatured proteins, respectively, indicating a more rubber-like (Macosko, 1994; Rao, 2007) and denser structure (Ikeda & Nishinari, 2001; Vilgis & Winter, 1988) of the latter. Besides, the fractal dimension of 2.3 was similar to the range of 2.0-2.2, suggesting ordered aggregation of the proteins and presence of linear strand-like structure (Ikeda et al.,

1999), which is consistent with the conclusion from Bryant and McClements (1998) and Chapter 5. Invalidity of the power law was also found at low frequencies for both of Hiprotal60-TS0710 and –TS0712 gels, and thus, the network of the proteins had a finite length scale. According to the interpretation of mechanical spectra by Vilgis and Winter (1988) that the frequency, ω, of the oscillations relate to the length scale, L, of the measurements as $\omega^{-1} \propto t \propto L^{d_w}$, where t is the time for relaxation and the exponent 'd_w' is determined by diffusion of the polymers in solutions, a characteristic frequency, from which power law behavior occurs, could be obtained to reveal the length scale of the fractal structure. The characteristic frequencies for Hiprotal60-TS0710 and –TS0712 were found to be the same at 0.02 rad/s (Figure 7.13), indicating the same length scale of the self-similar network of these two denatured protein solutions.

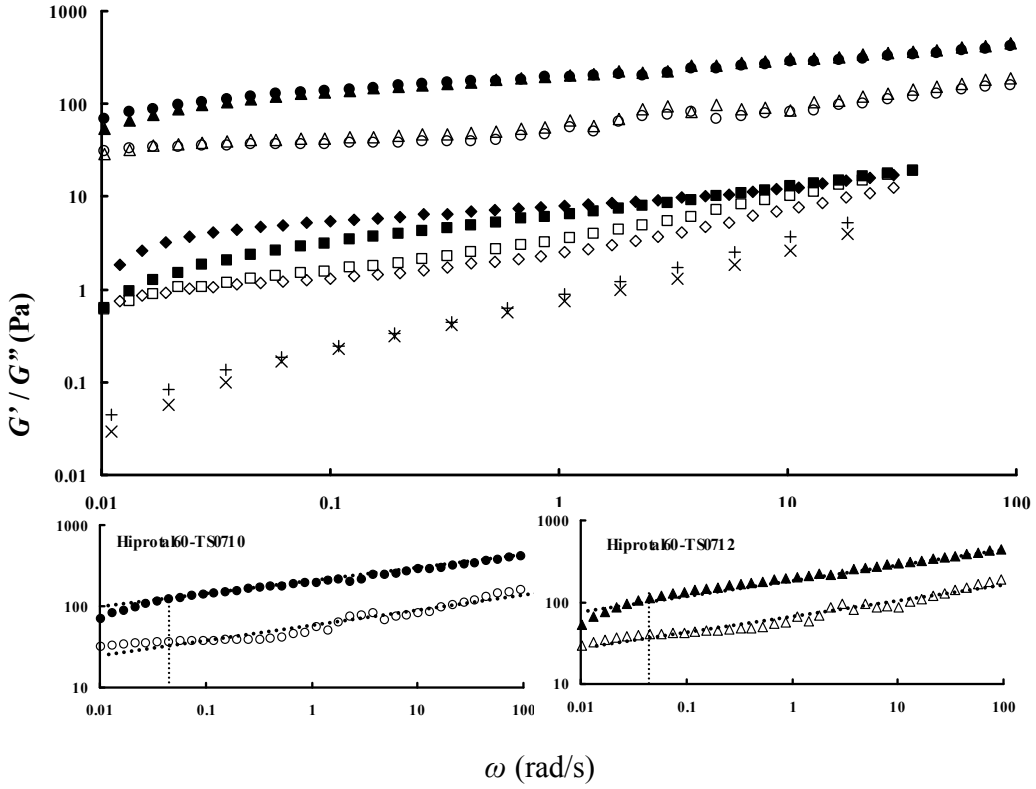

Figure 7.13 Vsicoelasticity *G*'/*G*" of Simplesse (◆/◇), Hiprotal60 (╳/╋), Hiprotal60-TS0709 (■/□), Hiprotal60-TS0710 (●/○), and Hiprotal60-TS0712 (▲/△) solutions with protein concentration of 21% (characteristic frequencies are marked by dash lines).

7.3.4 Effects of low pH

Since WPC is a mixture of proteins containing mainly β-lactoglobulin as well as α-lactalbumin and bovine serum albumin (BSA), each each of which have different isoelectric points (Bryant & McClements, 1998; de Wit & Klarenbeek, 1984; Kinsella & Whitehead, 1988), a definition of the isoelectric point (pI) of WPC is complicated. Marinova et al. (2009) proposed a concept of 'effective' pI for WPC and suggested that it is about 4.2 where the ζ-potential of the proteins is zero. Accordingly, acetic acid was added to the protein solutions to get the pH values to 4.5 in order to approach the pI of proteins and decrease the charges on the protein surface.

The complex viscosity, η^*, of different protein solutions with high concentration (21%) at natural condition (i.e., dissolved in Milli-Q water where the pH of the solutions ranged from 6.2 to 6.7) and solutions adjusted to pH 4.5 are plotted in Figure 7.14. Both η and η^* were found to increase and invalidity of the Cox-Merz rule still held for Simplesse, indicating stronger interfloc forces, and thus, stiffer aggregating structure of those microparticulated proteins at low pH (Macosko, 1994; Rao, 2007). Similar effects of low pH to those on the microparticulated proteins were also observed on low aggregated denatured proteins (i.e., Hiprotal60 and Hiprotal60-TS0709), where η^* was increased by lowering pH. Moreover, more obvious violations against the Cox-Merz rule are seen for the acidic solutions compared to those at natural pH of the protein solution, where the violations are only present at low frequencies and shear rates. Therefore, strain susceptible structure of protein aggregates could be hypothesized to form in the acidic solutions (Ikeda & Nishinari, 2001). The apparent viscosity, η, of the microparticulated and low aggregated denatured proteins were also found to increase at pH of 4.5, suggesting increases in the resistance against alignment of proteins. Since there was no net charge on the protein surfaces at pI, hydrophobic interactions and van der Waals attractions will predominate the electrostatic repulsions between protein molecules and flocs, which causes the further aggregation and flocculation of proteins (Ikeda et al., 1999; Verheul, Pedersen, Roefs, & de Kruif, 1999). Increased hydrodynamic interactions between protein flocs with larger volumes at pH of 4.5 would account for the increases in viscosity of Simplesse and Hiprotal60 and

Hiprotal60-TS0709. Polymeric partial denatured proteins (i.e., Hiprotal60-TS0710 and –TS0712) exhibited larger complex viscosity at pH of 4.5 than at natural pH, while there was no increase in the apparent viscosity, except for at low shear rates, where aggregates of proteins were supposed to be formed and incompletely disrupted (Renard et al., 1999). Such observations suggest that the gel formed by polymeric denatured protein is strengthened at pH 4.5 since the electrostatic repulsions were reduced, but the flowing units remained the same as those at natural pH when the gel structure was disrupted by large strains.

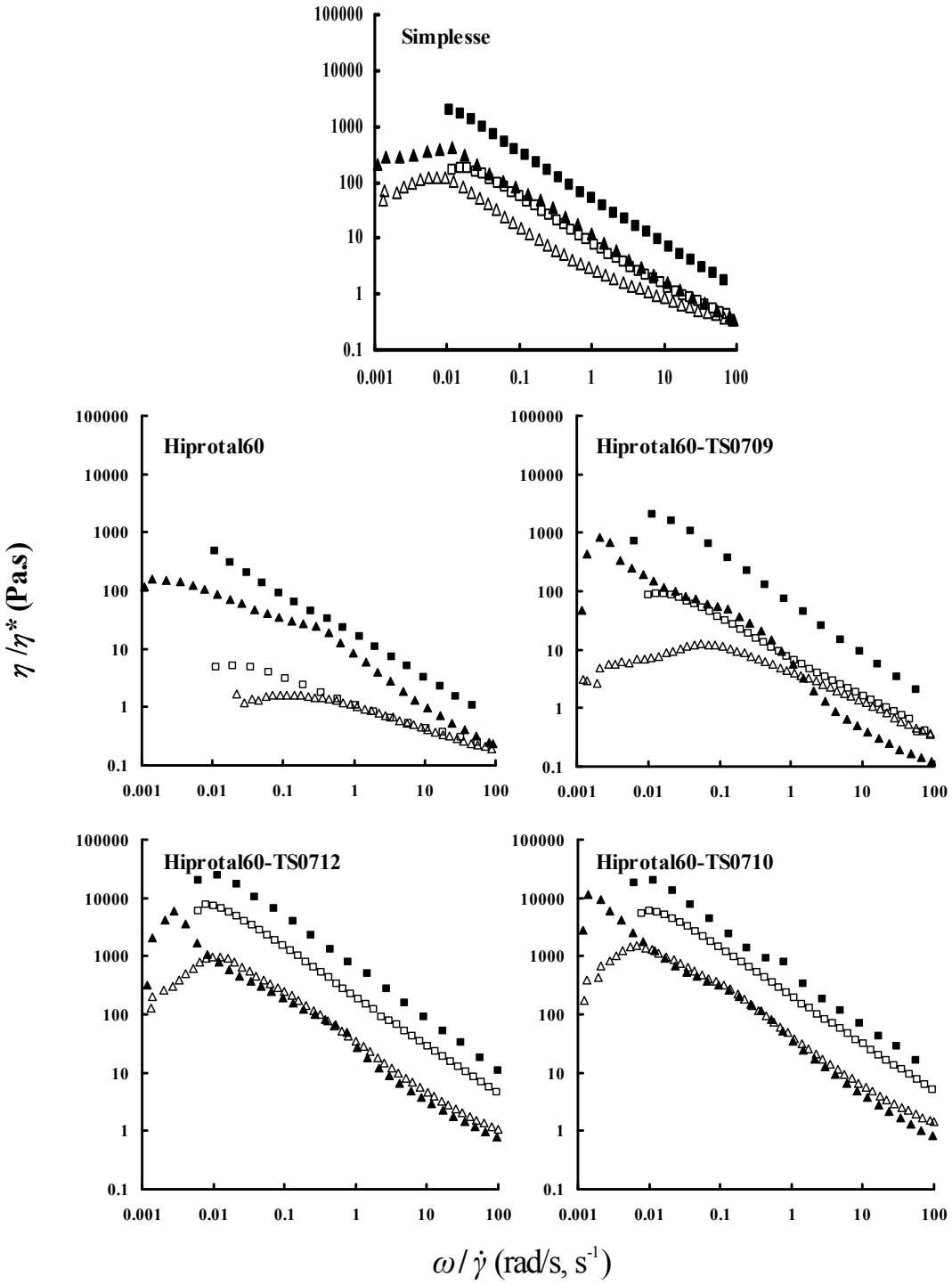

Figure 7.14 Effects of low pH on η/η^* (▲/■) of different protein solutions with the concentration of 21%, where open symbols represent protein solutions of natural pH.

Effects of pH on the dynamic moduli, *G*' and *G*", of different proteins are illustrated in Figure 7.15. All the samples were found to have increased dynamic moduli at pI, suggesting strong association of proteins or flocs. Lager increases in *G*' for microparticulated (Simplesse) and lowly aggregated denatured (Hiprotal60 and

Hiprotal60-TS0709) proteins indicated more significant solid-like behaviour and network or gel structure at ambient temperature rather than the formation of colloidal crystals at the pI (Elofsson et al., 1997; Xu et al., 2013). Power law behavior was not found for Hiprotal60 or Hiprotal60-TS0709, and thus, fractal structures are believed to be absent for the gels formed by lowly aggregated denatured proteins. Besides, *G''* was closer to *G'* for Hiprotal60 than that of Hiprotal60-TS0709, suggesting the former had a weaker gel structure. A tendency of power law was observed for the gel formed by Simplesse with an ^{n} value of 0.20±0.03, indicating a self-similar of fractal structure of the gel, and the fractal dimension was obtained as 2.3 according to equation 7.3 (Muthukumar, 1989).

The increases in *G'* of Hiprotal60-TS0710 and –TS0712 suggested that the gel was strengthened at pI (Elofsson et al., 1997; Goodwin & Hughes, 2008; Ikeda et al., 1999). The thicker structure is believed to result from the reduction or absence of electrostatic repulsions between the protein molecules and the polymeric chains of the aggregates (Goodwin & Hughes, 2008; Ikeda et al., 1999). A power law was found to hold for the gels at pI, but with smaller values of ^{n}, as 0.13±0.00 and 0.15±0.00 for Hiprotal60-TS0710 and –TS0712, respectively. The reduced frequency dependence of *G'* revealed a more solid-like behavior of the gels (Goodwin & Hughes, 2008; Macosko, 1994; Rao, 2007). These more solid-like properties could be due to the denser packing of the polymeric chains in the gels as suggested by the fractal dimension of 2.4 for both the Hiprotal60-TS0710 and –TS0712.

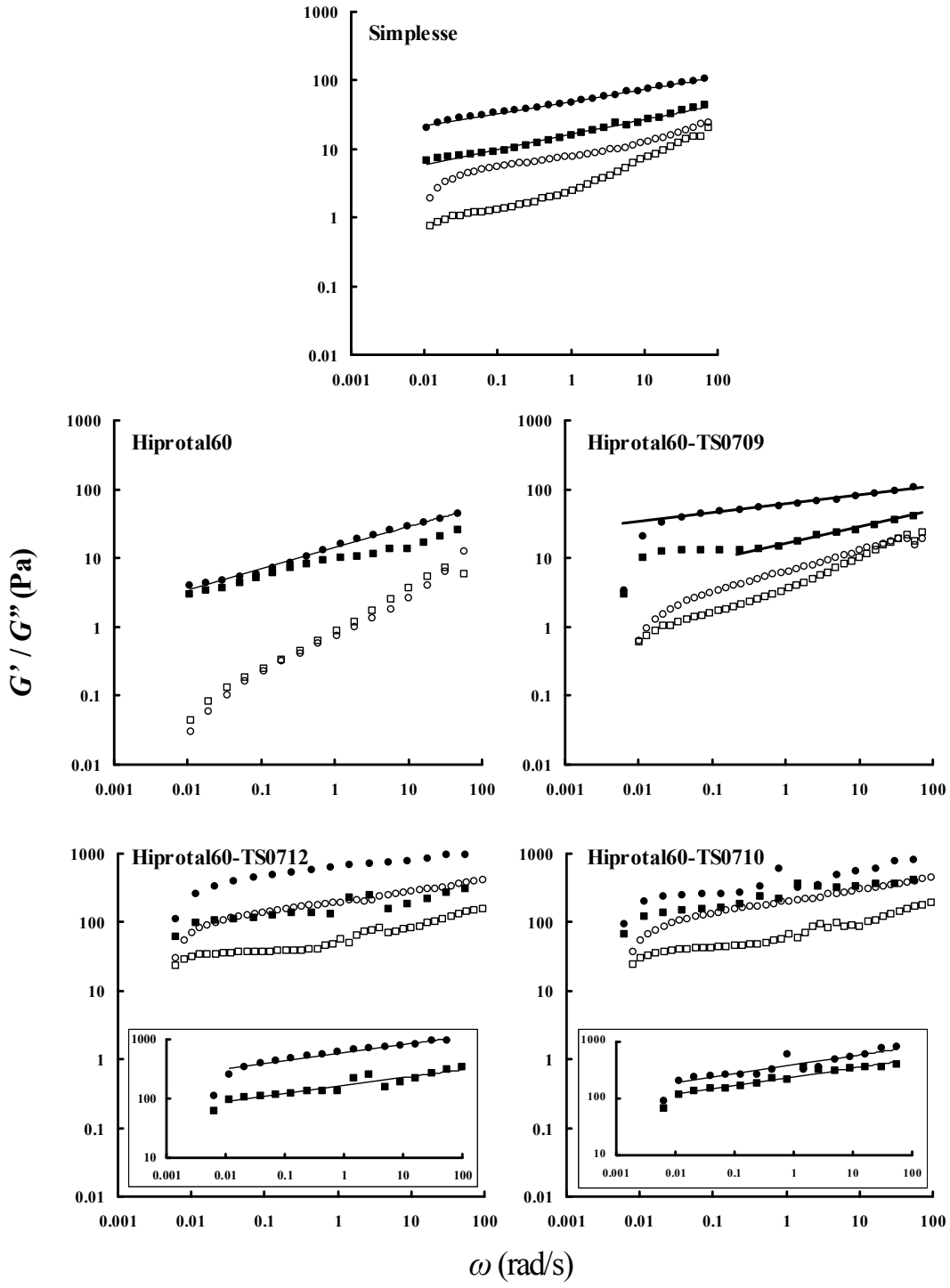

Figure 7.15 Effects of low pH on *G*'/*G*" (●/■) of different protein solutions with the concentration of 21%, where open symbols represent protein solutions of natural pH.

7.4 Conclusion

Aggregation structures were measured through oscillation tests. The solutions of Simplesse exhibited solid-like behaviour at high concentrations, suggesting strong intermolecular or interfloc forces for these microparticulated proteins. Hiprotal60 and Hiprotal60-TS0709 behaved as viscoelastic liquids and the absence of aggregation in these lowly aggregated partial denatured proteins was proposed according to the Cox-Merz rule. Both the solid-like and viscoelastic liquid-like behaviour of the microparticulated and low aggregated partial denatured proteins were believed to result from colloidal crystal structures of the protein molecules and their flocs as suggested by relatively small *G'* values and visual observations. Such lattice-like structures are supposed to be stabilized by electrostatic repulsions. Polymeric denatured proteins (i.e., Hiprotal60-TS0710 and –TS0712) were found to form strong gels with self-similar or fractal structures at high concentrations. Large values of fractal dimensions suggested a dense packing of the polymeric chains in the gels. Cold-setting gelation was found at low pH of the protein solutions for all the modified samples. Fractal structures were proposed in the acid-induced gel of the microparticulated proteins but absent in the low aggregated denatured ones. Besides, the flowing units of the large-strain induced broken aggregates of microparticulated and low aggregated denatured proteins were increased at low pH but remained for the polymeric denatured proteins. Such cold-setting gelation properties of the modified proteins, especially those with partial denaturation and high aggregations would provide a potential of wider applications of the protein-based fat mimetics in food industry.

7.5 Reference

Barnes, H.A. (2000). *Handbook of elementary rheology*. Aberystwyth, UK: Cambrian Printers.

Barnes, H.A., Hutton, J.F., & Walters, K. (1989). *An introduction to rheology*. Amsterdam, The Netherlands: Elsevier.

Blom, C., Mellema, J., Lopulissa, J.S., & Reuvers, A.J. (1984). Frequency dependent linear viscoelastic properties of ordered polystyrene latices. *Colloid & Polymer Science, 262*, 397-402.

Bryant, C.M., & McClements, D.J. (1998). Molecular basis of protein functionality with special consideration of cold-set gels derived from heat-denatured whey. *Trends in Food Science & Technology, 9*(4), 143-151.

Clark, A.H., Kavanagh, G.M., & Ross-Murphy, S.B. (2001). Globular protein gelation-theory and experiment. *Food Hydrocolloids, 15*(4-6), 383-400.

Cox, W.P., & Merz, E.H. (1958). Correlation of dynamic and steady flow viscosities. *Journal of Polymer Science, 28*(118), 619-622.

Damodaran, S. (1996). Amino acids, peptides, and proteins. In O. R. Fennema (Ed.), *Food Chemistry* (3rd ed., pp. 321-429). New York, USA.: Marcel Dekker.

de Wit, J.N., & Klarenbeek, G. (1984). Effects of various heat treatments on structure and solubility of whey proteins. *Journal of Dairy Science, 67*(11), 2701-2710.

Doi, M., & Edwards, S.F. (1986). *The theory of polymer dynamics*. Great Britain: Clarendon Press.

Elofsson, C., Dejmek, P., Paulsson, M., & Burling, H. (1997). Characterization of a cold-gelling whey protein concentrate. *International Dairy Journal, 7*(8-9), 601-608.

Goodwin, J.W., & Hughes, R.W. (2008). *Rheology for Chemists-An Introduction* (2 ed.). Cambridge, UK: The Royal Society of Chemistry.

Griffin, W.G., Griffin, M.C.A., Martin, S.R., & Price, J. (1993). Molecular basis of thermal aggregation of bovine β-lactoglobulin A. *Journal of the Chemical Society, Faraday Transactions, 89*(18), 3395-3406.

Ikeda, S., Foegeding, E.A., & Hagiwara, T. (1999). Rheological study on the fractal nature of the protein gel structure. *Langmuir, 15*(25), 8584-8589.

Ikeda, S., & Nishinari, K. (2000). Intermolecular forces in bovine serum albumin solutions exhibiting solidlike mechanical behaviors. *Biomacromolecules, 7*(4), 757-763.

Ikeda, S., & Nishinari, K. (2001). On solid-like rheological bahaviors of globular protein solutions. *Food Hydrocolloids, 15*, 401-406.

Ju, Z.Y., & Kilara, A. (1998). Textural properties of cold-set gels induced from heat-denatured whey protein isolates. *Journal of Food Science, 63*(2), 288-292.

Kinsella, J.E., & Whitehead, D.M. (1988). Proteins in whey: Chemical, physical, and functional properties. *Advances in Food and Nutrition Research, 33*, 343-438.

Lindsay, H.M., & Chaikin, P.M. (1982). Elastic properties of colloidal crystals and glasses. *Journal of Chemical Physics, 76*(7), 3774-3781.

Lizarraga, M.S., De Piante Vicin, D., González, R., Rubiolo, A., & Santiago, L.G. (2006). Rheological behaviour of whey protein concentrate and λ-carrageenan aqueous mixtures. *Food Hydrocolloids, 20*(5), 740-748.

Macosko, C.W. (1994). *Rheology: Principles, Measurements, and Applications*. New York, USA: Wiley-VCH, Inc.

Marinova, K.G., Basheva, E.S., Nenova, B., Temelska, M., Mirarefi, A.Y., Campbell, B., & Ivanov, I.B. (2009). Physico-chemical factors controlling the foamability and foam stability of milk proteins: Sodium caseinate and whey protein concentrates. *Food Hydrocolloids, 23*(7), 1864-1876.

McClements, D.J., & Keogh, M.K. (1995). Physical properties of cold-setting gels formed from heat-denatured whey protein isolate. *Journal of the Science of Food and Agriculture, 69*(1), 7-14.

Meyers, M.A., & Chawla, K.K. (2009). *Mechanical Behavior of Materials*. New York, US: Cambridge University Press.

Miyoshi, E., & Nishinari, K. (1999). Rheological and thermal properties near the sol-gel transition of gellan gum aqueous solutions. *Progress in Colloid and Polymer Science, 114*, 68-82.

Morrison, F.A. (2001). *Understanding Rheology*. New York, USA: Oxford University Press, Inc.

Muthukumar, M. (1989). Screening effect on viscoelasticity near the gel point. *Macromolecules, 22*(12), 4656-4658.

Rao, M.A. (2007). *Rheology of Fluid and Semisolid Foods Principles and Applications*. New York, USA: Springer Science+Business Media.

Renard, D., Robert, P., Faucheron, S., & Sanchez, C. (1999). Rheological properties of mixed gels made of microparticulated whey proteins and β-lactoglobulin. *Colloids and Surfaces B: Biointerfaces, 12*, 113-121.

Ross-Murphy, S.B. (1995). Structure–property relationships in food biopolymer gels and solutions. *Journal of Rheology, 39*(6), 1451-1463.

Verheul, M., Pedersen, J.S., Roefs, S.P.F.M., & de Kruif, K.G. (1999). Association behavior of native β-lactoglobulin. *Biopolymers, 49*(1), 11-20.

Vilgis, T.A., & Winter, H.H. (1988). Mechanical selfsimilarity of polymers during chemical gelation. *Colloid and Polymer Science, 266*(6), 494-500.

Winter, H.H., & Chambon, F. (1986). Analysis of linear viscoelasticity of a crosslinking polymer at the gel point. *Journal of Rheology, 30*, 367-382.

Xu, J., Inglett, G.E., Chen, D., & Liu, S.X. (2013). Viscoelastic properties of oat β-glucan-rich aqueous dispersions. *Food Chemistry, 138*, 186-191.

8 Protein-based fat replacers in O/W emulsions

8.1 Introduction

Emulsions consist of a dispersed liquid phase evenly distributed within a second liquid phase (Barnes, 1994; Mason, 1999; Walstra, 1996). Oil-in-water (O/W) emulsions, for instance, contain water as the continuous phase with oil droplets distributed inside. Due to the attractions between the droplets in water, the oil will flocculate and phase separation will occur and therefore, emulsifiers are needed to obtain stable emulsions (Damodaran, 1996b; McClements, 2004; Walstra, 1996). Milk proteins have been found to be very good emulsifiers and the emulsions stabilized by these proteins are widely employed in food formulations (Dickinson, 1998, 2001, 2012). Since proteins are also important components in foods, the interactions between proteins and stabilized oil droplets are an interesting area of study, especially for the understanding of mouthfeel and texture of foods.

Proteins are considered as a good emulsifier, not only because they contribute to the formation of small droplets, but also they promote the stability of emulsion droplets. There are four main forms of instability of emulsions, i.e., Ostwald ripening, creaming, coalescence and aggregation (flocculation and coagulation are used for reversible and irreversible aggregation, respectively) as shown in Figure 8.1 (Walstra, 1996). Ostwald ripening as shown in Figure 8.1 is a process where large droplets keep growing while those small ones gradually disappear. Ostwald ripening occurs due to a pressure gradient driven solubilization of the oil phase from small droplets to large droplets. It occurs because oil molecules at the surface of droplets are less energetically favoured than those in the bulk. Small droplets have a large surface area-volume ratio and therefore are less stable than larger droplets. This phenomenon seldom occurs in O/W emulsions because of the low solubility of triacylglycerol oils which are commonly used for O/W emulsions (Walstra, 1996). Creaming results from the upward sedimentation of oil droplets in water due to their low solubility and small density.

Such sedimentation of droplets greatly depends on their particle sizes and the viscosity of the system. However, the emulsion viscosity will decrease during the process of sedimentation and thus increase the rate of the latter (Walstra, 1996). As introduced before that proteins interact with oil and water simultaneously and form a thin layer at the interface of the two phases. However, once the lamella is destroyed, the droplets will immediately flow together and coalescence occurs. Although which is still unknown in coalescence theory, it has been widely agreed that this phenomenon can be reduced by having smaller droplets, thicker protein films and greater interfacial tensions (Walstra, 1996). Aggregation of emulsion droplets is highly dependent on the interactions between them, for instance the van der Waals attractions, electrostatic interactions, steric repulsions and depletion interactions.

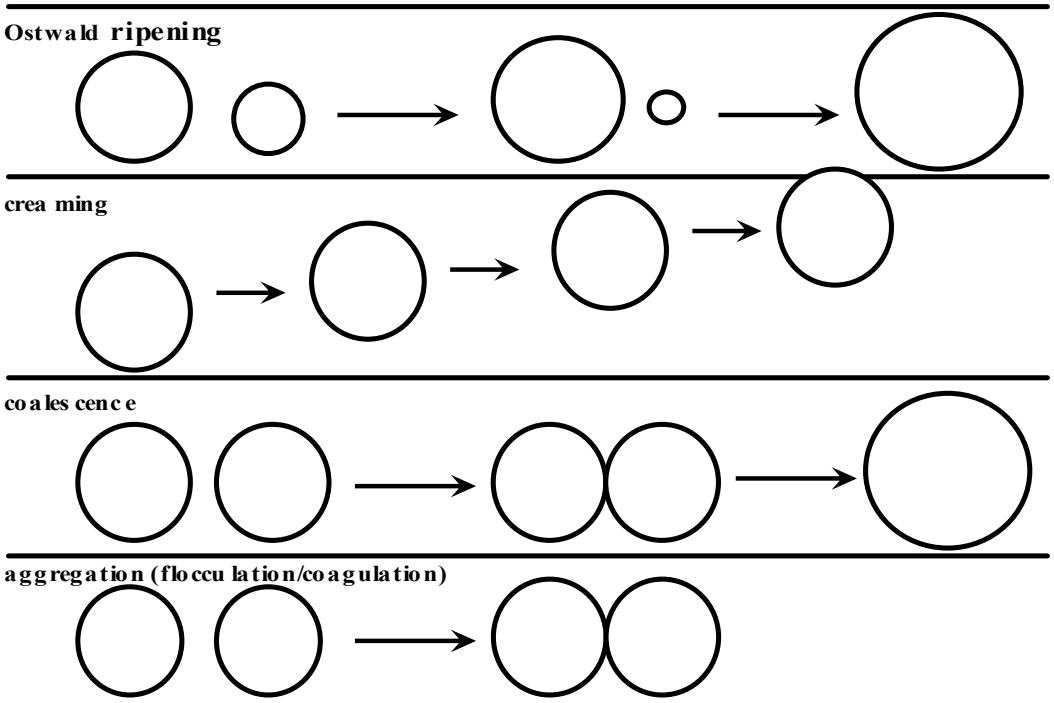

Figure 8.1 Illustration of types of emulsion instability.

It is well known that depletion flocculation of the emulsion droplets occurs with the presence of unabsorbed polymers, such as polysaccharides, in the continuous phase (Barnes, 1994; Dickinson & Golding, 1997; McClements, 2000). The mechanism of depletion flocculation is illustrated in Figure 8.2 (Tadros, 1994): at high concentrations, unabsorbed polymers cannot fit into the gaps between the droplets and the osmotic pressures outside the droplets will increase, which as a result pushes the droplets

towards each other and favours flocculation.

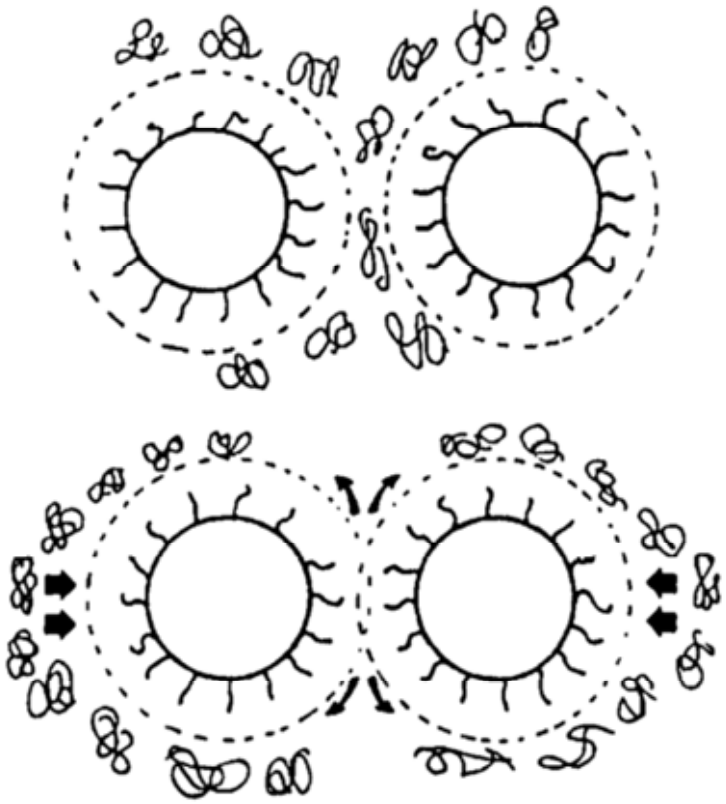

Figure 8.2 Schematic representation of depletion flocculation (Tadros, 1994)

Another important behaviour of emulsions should be the formation of emulsion-filled gels, which has been widely used to form structure in the food, pharmacy and cosmetic industries (Lorenzo et al., 2013). Dickinson and Chen (1999) found that protein-coated droplets were active fillers for heat-set gels of whey protein. Compared with those inactive fillers that only fill the holes on the network, these active ones favour the gel matrix by connecting with the protein molecules. Other than heating, emulsion gels were also obtained by acidification or enzyme treatments (Dickinson, 2012; Dickinson & Yamamoto, 1996; Ye & Taylor, 2009). However, there is a lack of relevant studies on the emulsion droplets effects on cold-set gels at natural conditions. Since the protein-based fat replacers were found to form cold-set gels without the action of heat, acidification or enzyme treatment (Chapter 7), it will be of great value to investigate the interactions between emulsion droplets and those modified proteins, which is also believed to be helpful for applications of such fat replacers in the food industry.

8.2 Material and methods

8.2.1 Protein-stabilized emulsions

Lacptodan87 (Arla Foods Ingredients, Denmark), whey protein concentrate (WPC), was firstly dissolved in water to make a protein solution with a concentration of 1.25% (w/w). Vegetable oil (KTC, purchased from local Tesco supermarket) was weighted and mixed with 1.25% WPC solution with a mass ratio of 20:80. The mixture was homogenized in an APV laboratory homogenizer (Invernsys, Denmark) with the pressure of 200 bar (1 bar = 100,000 Pa) for 5 min. The WPC-stabilized oil emulsion was stored in the fridge at 4 ^{o}C for further use.

8.2.2 Emulsions with added proteins (sol-emulsions)

Lacptodan87 (Arla Foods Ingredients, Denmark), Simplesse® 100[E] (CP Kelco UK Limited, UK) and a series of Hiprotal60 products, i.e., Hiprotal60, Hiprotal60-TS0709, Hiprotal60-TS0710, and Hiprotal60-TS0712 (Friesland Foods, the Netherlands) were dissolved in the protein-stabilized emulsions made as described above. In order to compare the results of the fortified emulsions (sol-emulsions) with those of solutions, protein concentrations of the sol-emulsions are adjusted based on the continuous phase. Since the protein solutions of 21% (w/w) were found to be very viscous and difficult to dissolve in water, the protein concentrations of the sol-emulsions were selected as 6%, 9%,12%, 14%, 16%, and 18% (protein in continuous phase, w/w).

8.2.3 Rheology

Oscillation measurements were performed using a Gemini advanced rheometer (Bohlin Instruments, UK), with 4°/40 mm cone and plate at a temperature of 20 °C. Linear viscoelastic regions were found by amplitude sweep measurements taken at a frequency of 1 Hz. Linear viscoelastic regions (if they existed) were obtained from the results of amplitude sweeps. The strain dependence of the storage (*G'*) and loss (*G"*) moduli of sol-emulsions were similar to those of protein solutions. Therefore, strains of

0.02-0.05 were selected for frequency sweep measurements. Frequency sweep measurements were performed in the range of frequencies from 0.001 Hz to 15 Hz, so that the largest angular frequency, ω, is of the order of 100 rad/s. Complex viscosity (η^*) values were obtained from the storage (*G'*) and loss (*G"*) moduli. Steady viscosity values were measured through shear-rate sweep tests, where a range of shear rates from ~10^{-3} s^{-1} to ~100 s^{-1} were employed.

8.3 Results and discussion

8.3.1 Rheology of the emulsion

First flow properties of the emulsion without extra added proteins were measured. The strain dependence of the viscoelastic properties, i.e., the storage (*G'*) and the loss (*G"*) moduli was depicted in Figure 8.1. It is found that *G"* was independent of strain while *G'* decreased with strain. Small values of both *G'* and *G"* are observed, indicating very low resistance to flow in the emulsions. In addition, *G'* is found to be larger than *G"* at small strains, suggesting weak but significant elasticity existing between droplets, which are disrupted at large strains. Considering the fluctuations resulting from instrumental errors at extremely small strains, a strain of 0.025 was chosen for the frequency sweep measurement of the emulsion in the linear region. The Cox-Merz plot (Cox & Merz, 1958) and the frequency dependence of *G'* and *G"* are shown in Figure 8.3 and Figure 8.4, respectively. It is found that the emulsion obeys the Cox-Merz rule, and thus, no aggregation or strong inter-droplet forces are concluded (Ikeda & Nishinari, 2001; Lizarraga et al., 2006), and therefore, the strain sensitive elasticity could be due to the deformability of the oil droplets (Macosko, 1994). On the other hand, *G'* and *G"* exhibit similar magnitudes and frequency dependence as shown in Figure 8.5, indicating the emulsion behaves as a viscoelastic liquid but with low viscosity.

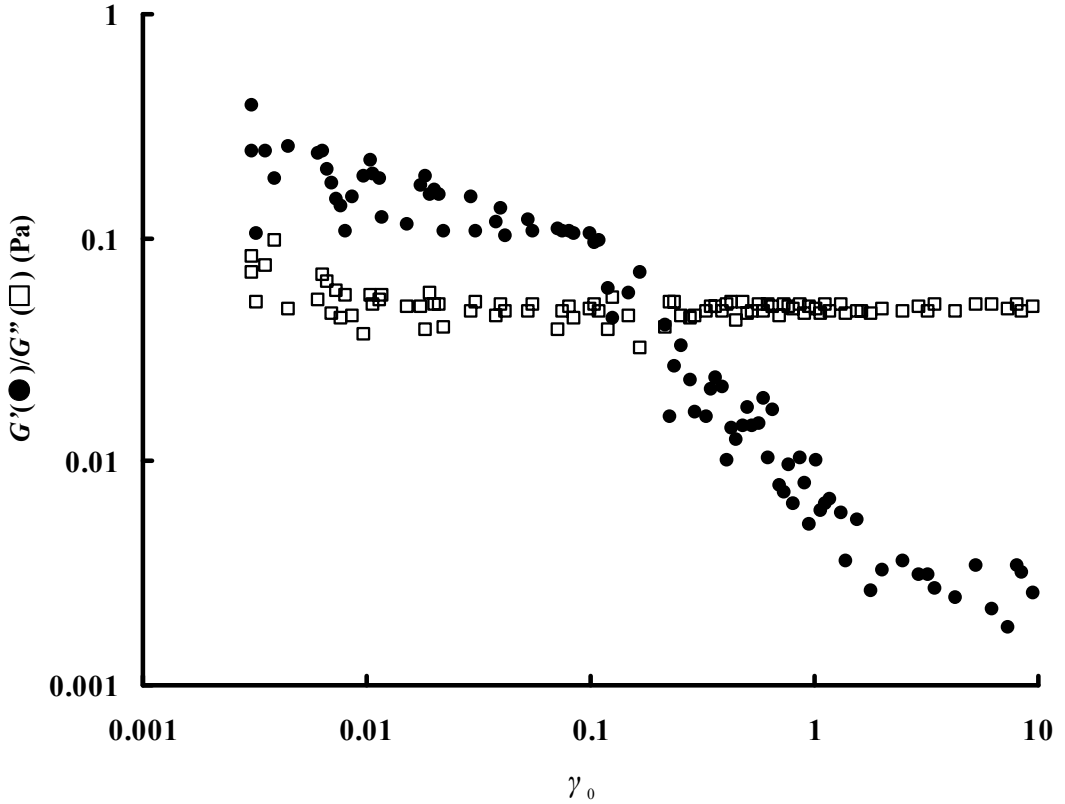

Figure 8.3 Strain amplitude dependence of viscoelasticity measured at 1 Hz of emulsion.

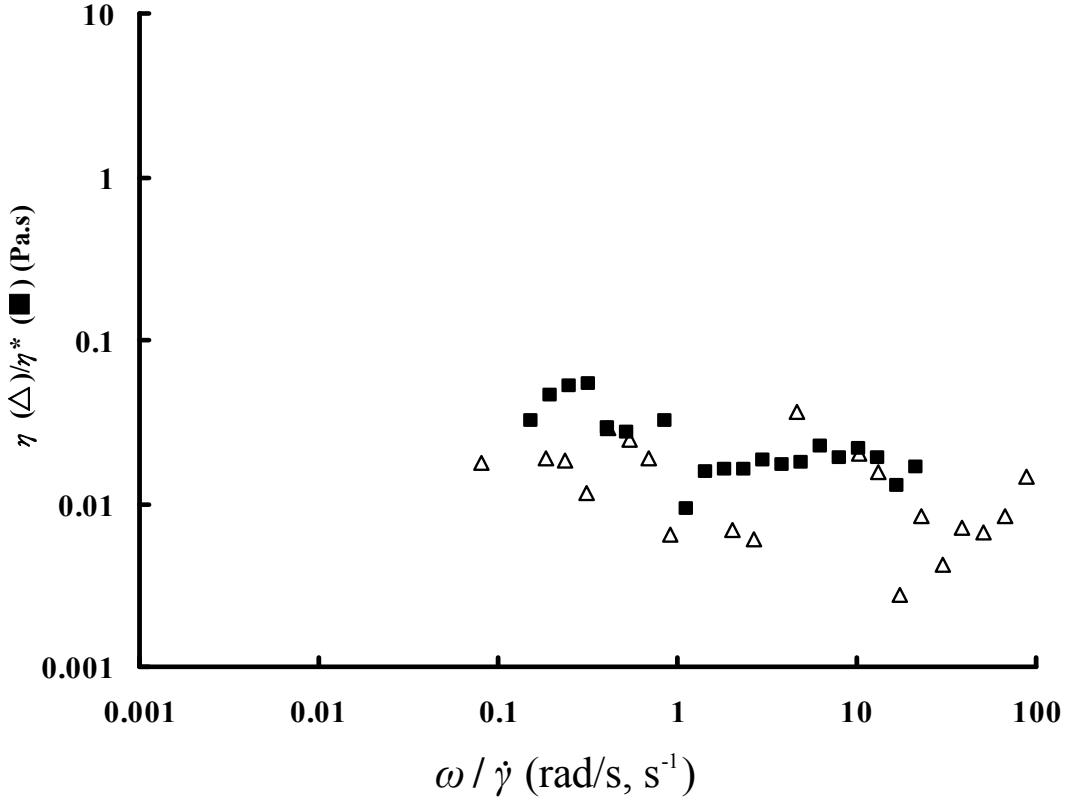

Figure 8.4 Cox-Merz plot of emulsion.

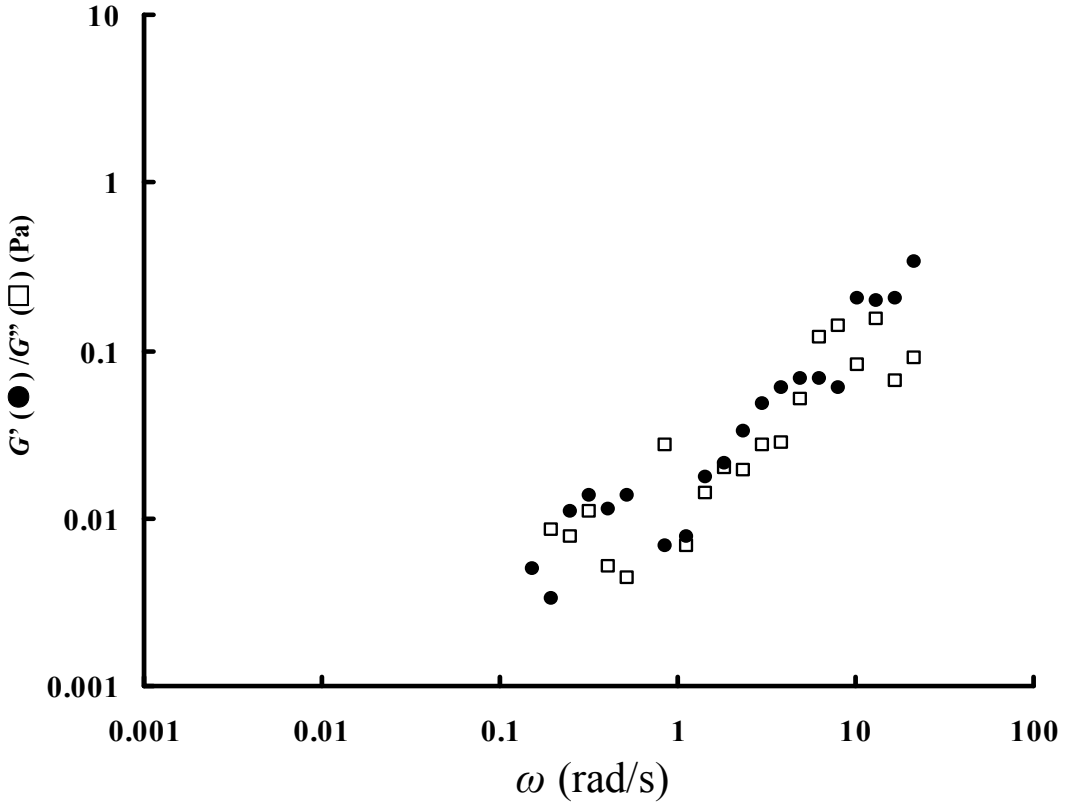

Figure 8.5 Dynamic moduli, *G'* and *G"*, of emulsion.

8.3.2 Linear viscoelasticity of sol-emulsion systems

Amplitude sweep measurements were carried out on the sol-emulsion samples in order to obtain the linear viscoelastic regions. For emulsions with added Lacprodan87 WPC, little effect from the emulsion droplets is found on the viscoelasticity when compared to WPC solutions with no emulsion present, as illustrated in Figure 8.6. The loss modulus, *G"*, of the samples is relatively constant, while the elastic modulus, *G'*, decreased without an obvious linear region, indicating that the system mainly dissipated the external energy by viscous flows rather than storing it through structures formed by proteins or droplets (Goodwin & Hughes, 2008; Macosko, 1994; Morrison, 2001). Proteins dissolved in emulsions are found to give larger *G"* than those in water alone. This could be due to the increased hydrodynamic interactions between the protein molecules dissolved in water and those absorbed on the droplets.

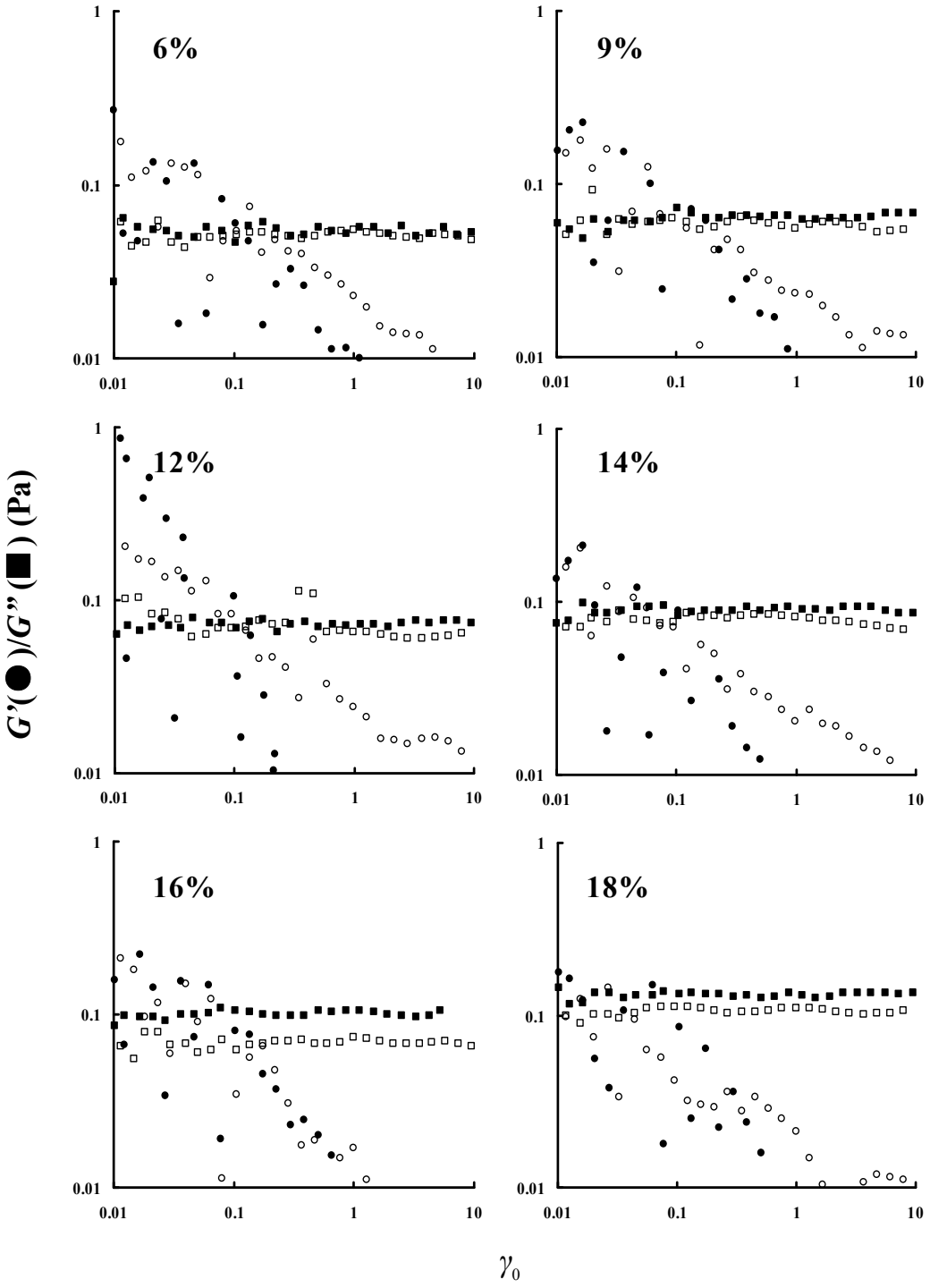

Figure 8.6 Strain amplitude dependence of viscoelasticity measured at 1 Hz of Lacprodan87 dissolved in emulsions and solutions (closed symbols represent presence of emulsion droplets).

Unlike WPC, the microparticualted proteins, i.e., Simplesse, as discussed in Chapter 7, exhibited elastic properties at relatively high concentrations (>12%) in solution due to the electrostatic interactions between the protein molecules and flocs. It

is found in Figure 8.7 that when microparticulated proteins is added to the emulsions, stronger resistance to flows is exhibited as indicated by increased *G'* and *G"*, when the protein concentration is lower than 16%. Such increasing effects, both in elasticity and viscosity, could result from shorter intermolecular distances between the proteins in the emulsions. From this point of view, the motion of the droplets lead to proteins structuring in the aqueous phase, and thus favouring formation of colloidal crystal structures for the proteins (Lindsay & Chaikin, 1982). However, these effects from emulsion droplets disappear when the protein concentration is larger than 16%, indicating that the protein molecules are close enough to each other in the free volume so that the electrostatic interactions are appreciable. There seems to be no interaction between emulsion droplets and Simplesse proteins, but those droplets tend to promote structure in the protein molecules. This hypothesis is supported by the observation that the emulsion droplets increase the protein interactions for dilute solutions (<16%), while they tend to disrupt these interactions for concentrated solutions (>16%).

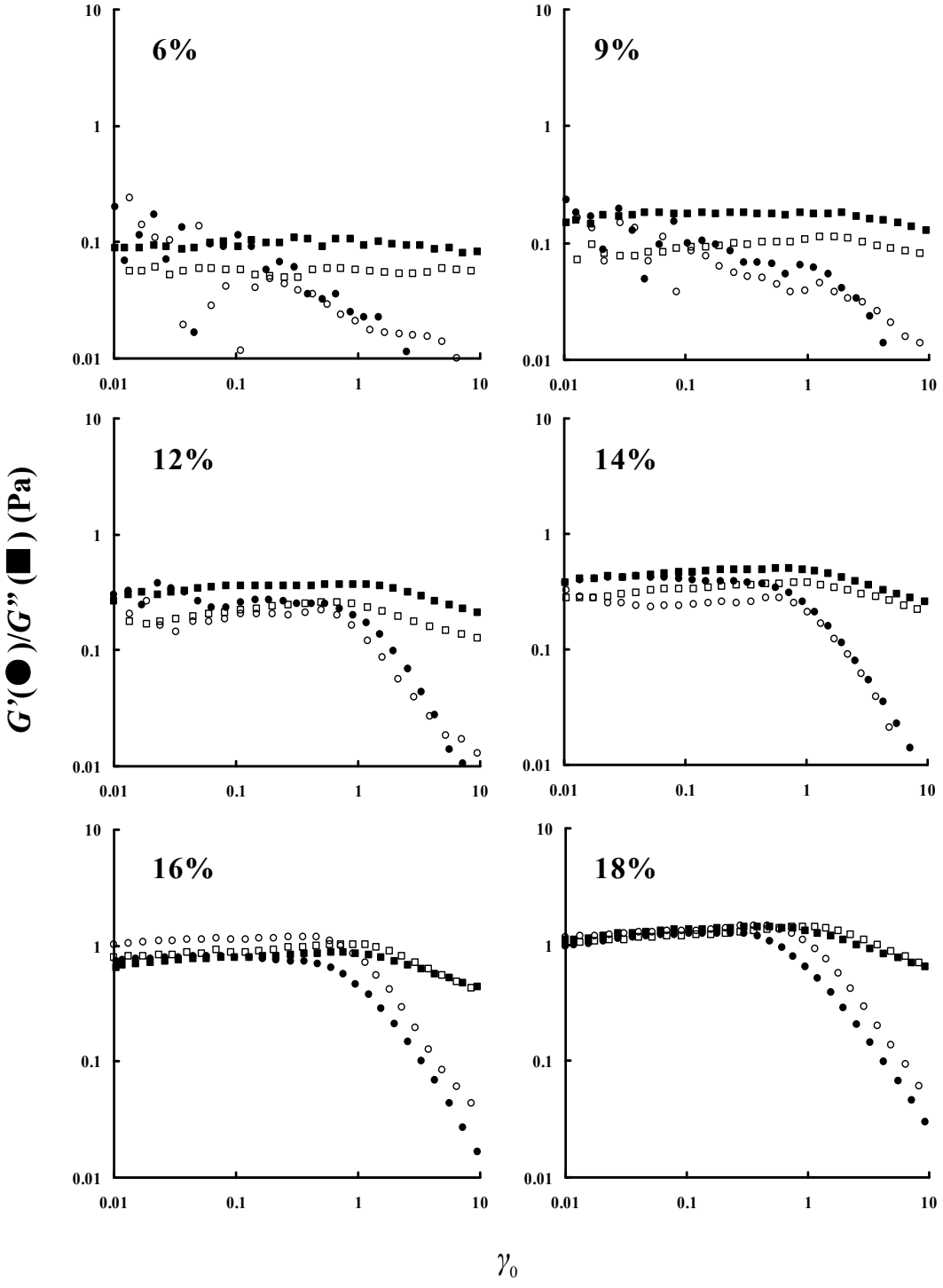

Figure 8.7 Strain amplitude dependence of viscoelasticity measured at 1 Hz of Simplesse dissolved in emulsions and solutions (closed symbols represent presence of emulsion droplets).

Figure 8.8 and 8.9 depict the linear viscoelasticity of the low aggregated partial denatured proteins, i.e., Hiprotal60 and Hiprotal60-TS0709. Although these two proteins, as discussed previously, behave similarly to each other in water, the effects of droplets on the proteins are different. It is found in Figure 8.8 that Hiprotal60 proteins

in emulsions possessed larger values of G' and G" regardless of the protein concentration, while those of Hiprotal60-TS0709 in emulsions, as shown in Figure 8.9, were barely affected by the droplets at concentrations <18%, and exhibiting lower viscosity and elasticity than those in water. Absence of linear region of G' was observed for Hiprotal60-emulsion systems, indicating that there is no or very weak interaction between the protein aggregates and the droplets. Therefore, the increased resistance to flowing is believed to result from a concentration effect leading to reduced volume available for proteins, caused by the volumetric effects from the droplets. Reduction of intermolecular distances between protein molecules will increase the intermolecular repulsions and hydrodynamic interactions, and thus, enhances G' and G", respectively (Macosko, 1994).

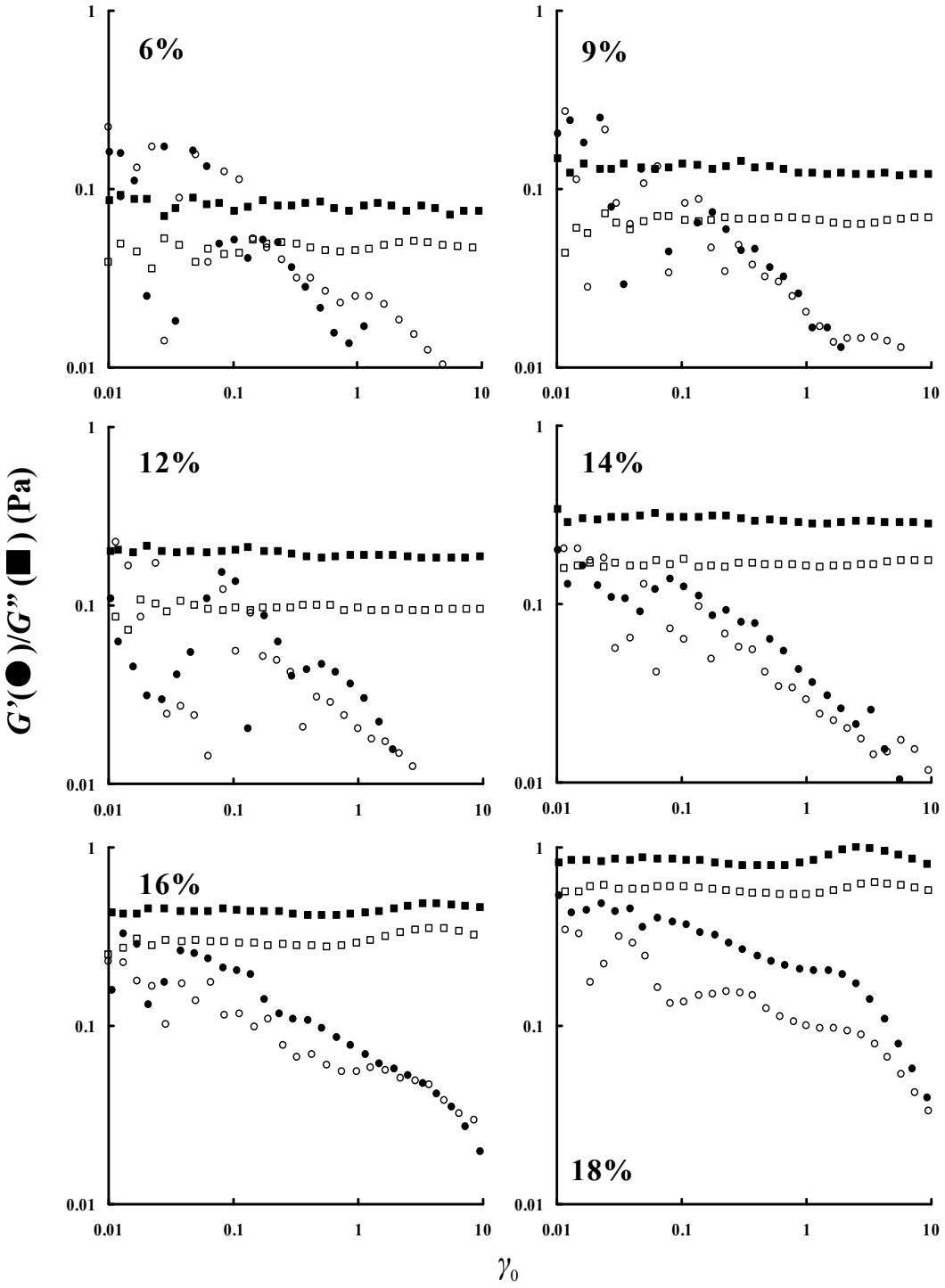

Figure 8.8 Strain amplitude dependence of viscoelasticity measured at 1 Hz of Hiprotal60 dissolved in emulsions and solutions (closed symbols represent presence of emulsion droplets).

For Hiprotal60-TS0709, effects of droplets on the proteins are small at protein concentrations <18%, as shown in Figure 8.9. Moreover, the presence of droplets is found to decrease both the dynamic moduli for the solutions with high concentration (18%). These observations may result from the small particle size of

Hiprotal60-TS0709 proteins, as discussed in Chapter 5, which means that they can fit more easily into the aqueous phase between droplets and that their interactions and motions in free volume are not affected as much by the volume reduction due to droplets. Therefore, values of *G'* and *G"* are not affected by droplets. Increasing protein concentration in the solutions will lead to the interactions between proteins and the formation of protein clusters when the protein content is high enough. These protein clusters exhibit a lattice-like structure and gives a viscoelastic liquid as discussed in Chapter 7. In the protein-fortified emulsions (sol-emulsions), however, it is possible that the growth of these clusters is limited by the available volume, which reduces the viscoelastic of the liquid. In addition, rather than behaving as active fillers, it seems that the emulsion droplets do not crosslink with the proteins in the continuous phase, and even possibly destroy the interactions between the proteins, which gives the result that the dynamic moduli for 18% protein aqueous solution are much larger than those for the sol-emulsion systems with the same concentration of extra added proteins, as shown in Figure 8.9.

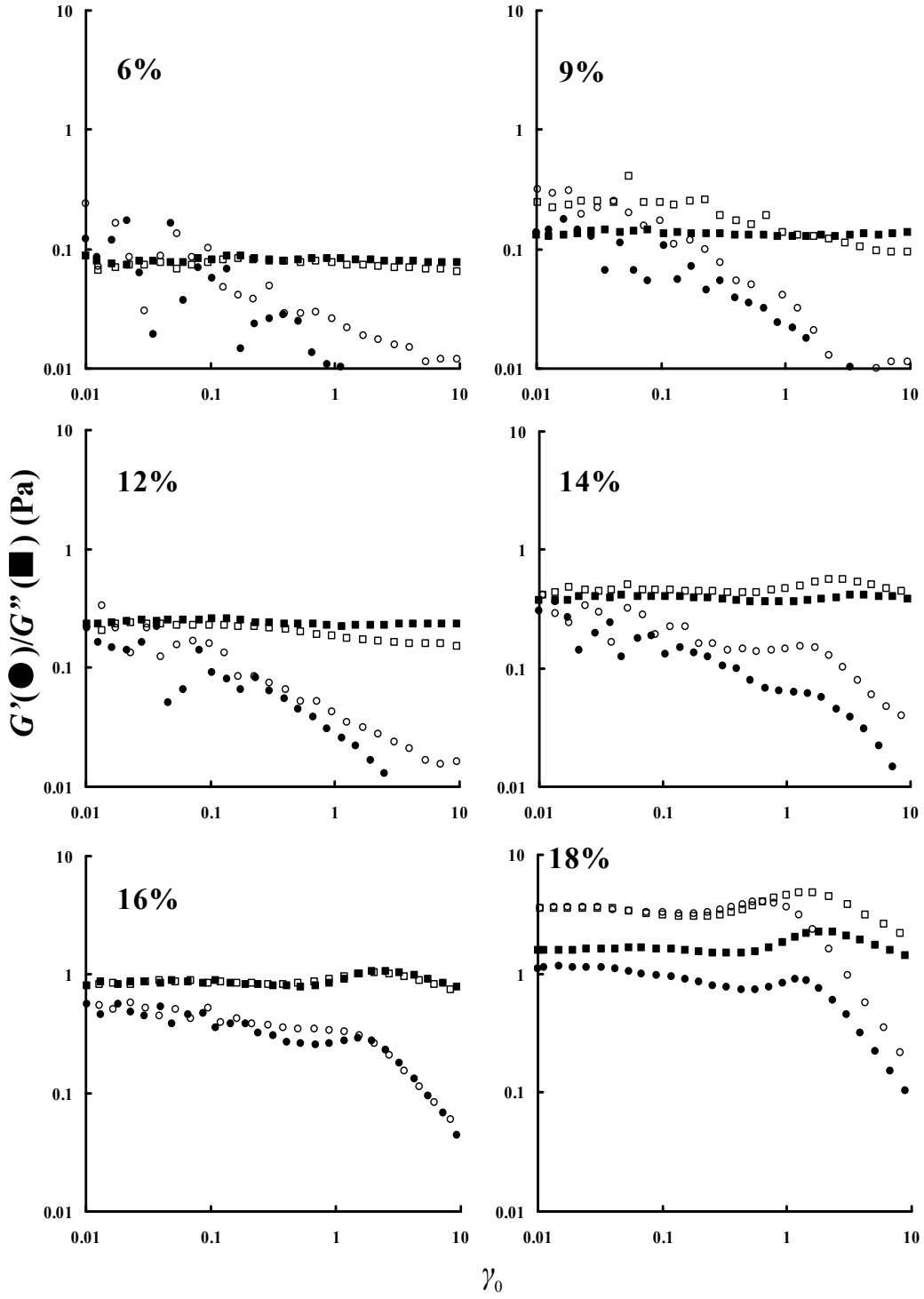

Figure 8.9 Strain amplitude dependence of viscoelasticity measured at 1 Hz of Hiprotal60-TS0709 dissolved in emulsions and solutions (closed symbols represent presence of emulsion droplets).

Strain dependence of the viscoelastic properties of Hiprotal60-TS0710 and Hiprotal60-TS0712 proteins in emulsions are depicted in Figure 8.10 and 8.11, respectively. It is found that droplets have strengthening effects on the gel structures for the proteins with intermediate concentrations (9% ~ 16%), especially for those of

Hiprotal60-TS0710. However, opposite effects of droplets are observed on both of the proteins at the concentration of 18%, where G' and G" of the sol-emulsions are smaller than those of the solutions. Such observations demonstrate that filling effects of emulsion droplets, as reported by Dickinson and Chen (1999) for thermal setting gels, could also exist for the cold setting ones, where droplets could fill the space between the protein aggregates and contribute to the cross-links of these polymeric chains, resulting in increases in the elasticity and viscosity. However, such filling effects of the droplets would prevent denser packing of the protein aggregates since both of G' and G" for the sol-emulsions are found to be smaller than those of the solutions when more proteins were added (18%). Based on the results of amplitude sweep measurements, frequency dependence of dynamic moduli were further determined and analyzed so that more information on the effects of droplets on the proteins could be obtained.

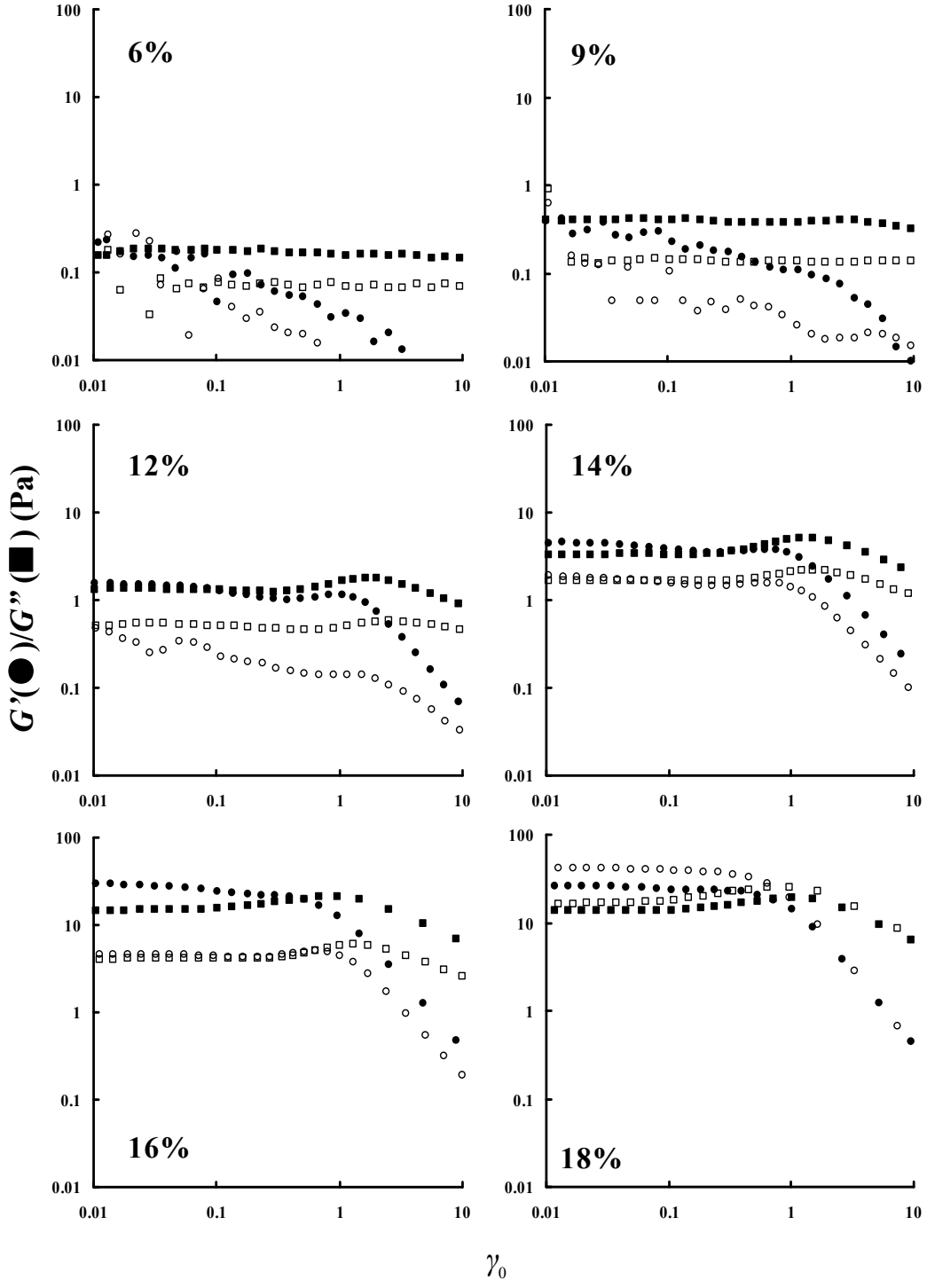

Figure 8.10 Strain amplitude dependence of viscoelasticity measured at 1 Hz of Hiprotal60-TS0710 dissolved in emulsions and solutions (closed symbols represent presence of emulsion droplets).

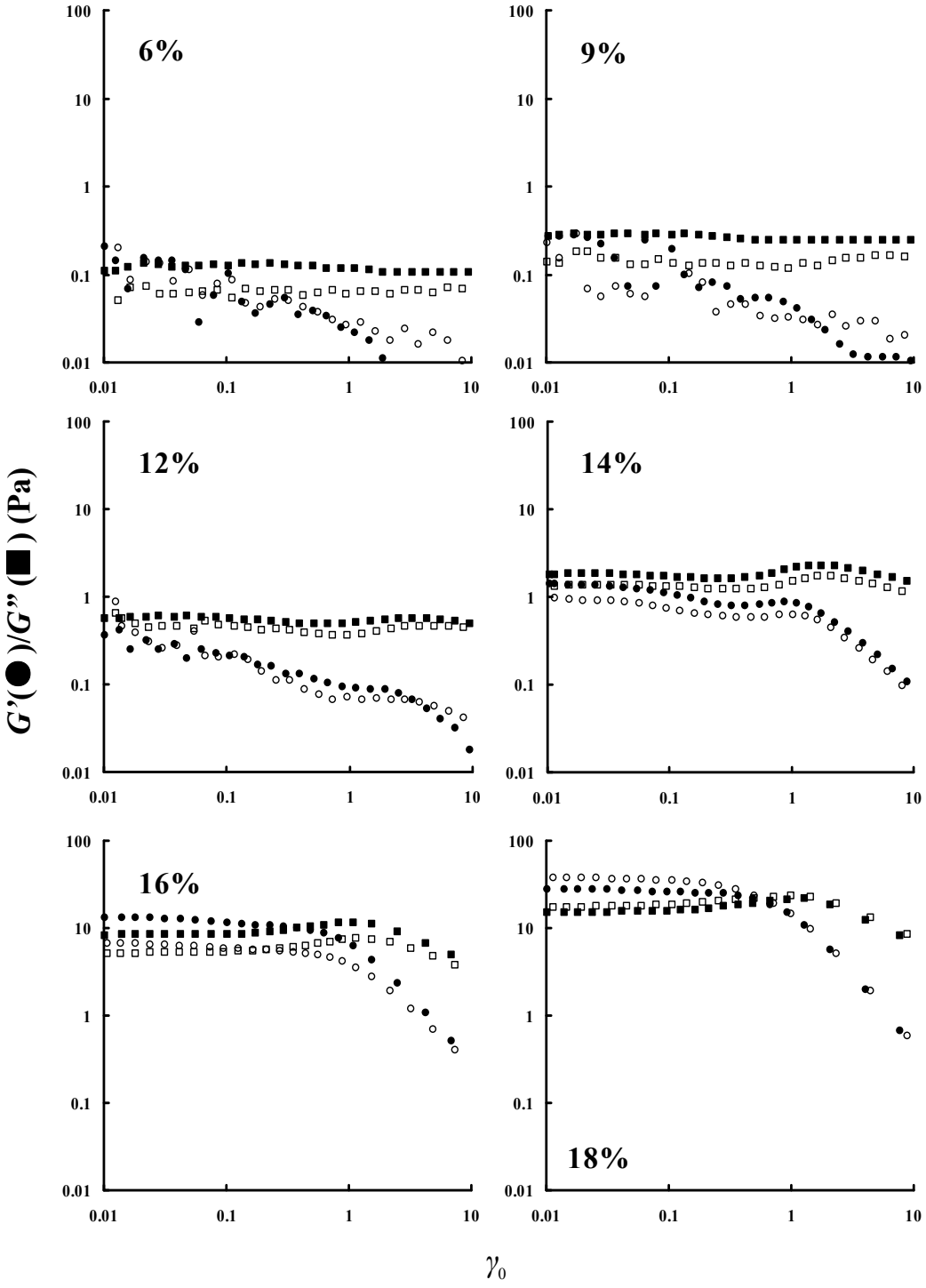

Figure 8.11 Strain amplitude dependence of viscoelasticity measured at 1 Hz of Hiprotal60-TS0712 dissolved in emulsions and solutions (closed symbols represent presence of emulsion droplets).

8.3.3 Effects of droplets on viscosity of protein solutions

Frequency sweep measurements were carried out on the sol-emulsions with relatively high additional protein concentration (from ~12%) where it was easier to identify the linear viscoelastic regions for different proteins. Cox-Merz plots of sol-emulsions with different proteins are shown from Figure 8.12 to Figure 8.16. It is found that different proteins dissolved in emulsions tend to have larger viscous properties, which is supposed to be due to increased hydrodynamic interactions. Shear thinning behaviour was also found for the sol-emulsions, especially for those with high concentrations.

It has been concluded in Chapter 7 that Simplesse proteins in aqueous solutions possess strong intermolecular and interfloc forces and exhibit solid-like behaviour at high concentrations. Similar behaviour is observed for these microparticulated proteins in sol-emulsions. As illustrated in Figure 8.10, the behaviour of Simplesse sol-emulsions violates the empirical Cox-Merz rule (Cox & Merz, 1958). The amplitude of the complex viscosity, η^*, is always greater than the steady viscosity, η, indicating strong interactions between particles and solid-like structures in the system, which is disrupted by large strains (Ikeda & Nishinari, 2001; Lizarraga et al., 2006). It is noted that η^* of solutions is larger than that of sol-emulsions at low angular frequencies, especially for those samples with high concentrations of proteins. Such a finding could be due to the presence of the droplets, which occupy the space between protein molecules and force the proteins to be further apart than those dissolved in water alone. As the frequency increases, the length scale of the measurement is reduced (Vilgis & Winter, 1988), and thus flow behaviour of the local regions only with proteins is detected. For such smaller length scales, the complex viscosity, η^* of the sol-emulsions is the same as that of the protein solutions, indicating that there is no interaction between the droplets and the protein molecules. Unlike η^*, more significant difference is observed in the steady viscosity, η, between Simplesse solutions and its sol-emulsions. It is found that η of the sol-emulsions is larger than that of aqueous solutions of Simplesse at the protein concentrations of 12% and 14%, which is supposed to result from the hydrodynamic interactions between the protein molecules

and the oil droplets. As more proteins are added into the system, however, the protein-protein interactions are disturbed by the droplets, and thus η of the aqueous solutions is larger, as shown in Figure 8.10 for the protein concentration of 18%. Moreover, when the protein-protein interactions are completely disrupted at high shear rate, the hydrodynamic interactions between proteins and droplets again increased η of sol-emulsions over that of protein solutions.

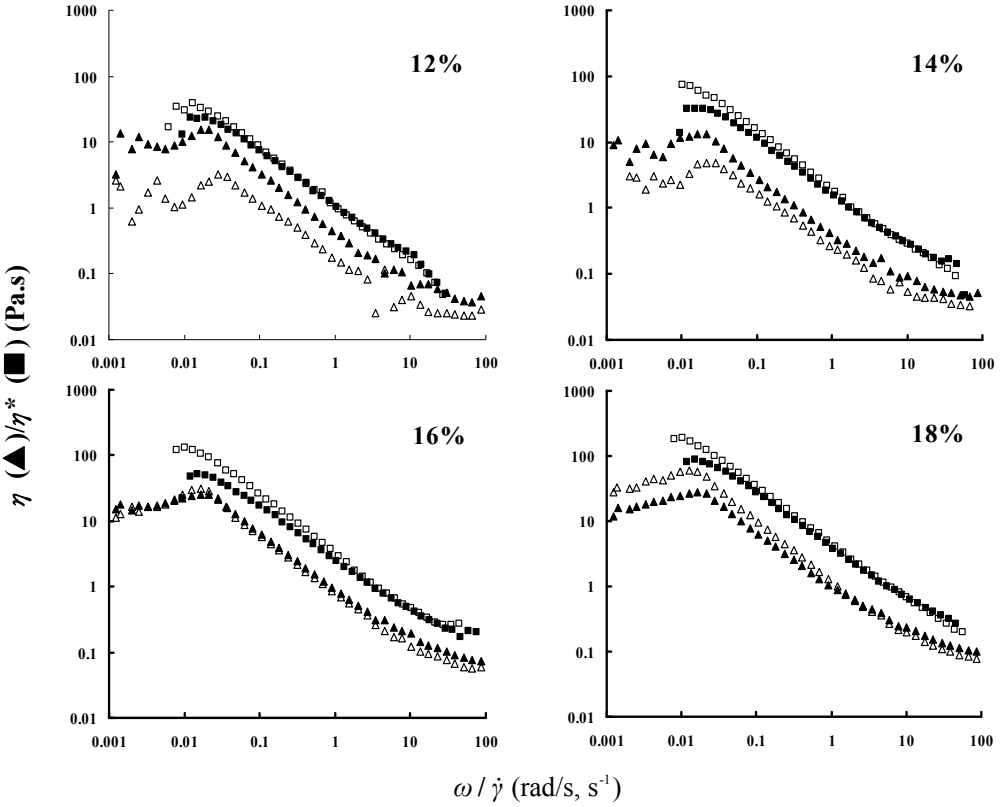

Figure 8.12 Cox-Merz plots of Simplesse dissolved in solutions and emulsions (closed symbols represent presence of emulsion droplets).

It was found in Chapter 7 that Hiprotal60 and Hiprotal60-TS0709 aqueous solutions behaved as viscoelastic liquids with absence of gel-like structures formed by proteins, as indicated by their following the Cox-Merz rule. Validity of the Cox-Merz rule is also observed for the sol-emulsions of Hiprotal60 and Hiprotal60-TS0709 with low protein concentrations (12% and 14%), as shown in Figure 8.13 and 8.14, indicating the proteins in such sol-emulsions behave similarly to those in aqueous solutions. As discussed above, the increases in η^* and η of the sol-emulsions are believed to result from the hydrodynamic interactions between proteins and droplets.

As protein concentration increases to 16% and 18%, however, violation of the Cox-Merz rule is observed. It is very interesting to find that the steady viscosity, η, is larger than the complex viscosity η^*. Similar unusual ($\eta>\eta^*$) results were reported for some polymers (Abdala, Olesen, & Khan, 2003; English, Gulati, Jenkins, & Khan, 1997; English, Raghavan, Jenkins, & Khan, 1999). Based on the transient network theory (Tanaka & Edwards, 1992a, 1992b, 1992c, 1992d), it has been proposed that such unusual behaviour results from the shear-induced structuring of the polymers. However, there is no evidence for the presence of a network formed by proteins in this work (as discussed in Chapter 7), and therefore, aggregations of the oil droplets are believed to account for the observations.

As more proteins are added into the emulsions, the available space between the droplets will decrease and finally it will be insufficient for the proteins to fit in. The protein-free zones result in higher osmotic pressure of the continuous phase, and lead to aggregations of the droplets (Tadros, 1994). It is seen in Figure 8.13 and 8.14 that the steady viscosity, η, is larger than the complex viscosity η^*, for the sol-emulsions of Hiptotal60 and Hiprotal60-TS0709 with protein concentrations of 16% and 18%. Such shear-induced structuring phenomena could be attributed to depletion flocculation of the oil droplets. It seems that larger strains increases the probability for oil droplets to approach and favours the depletion flocculation. Therefore, the values of η are larger than those of η^*. Besides, shear-thinning behaviour is observed for the sol-emulsions of Hiptotal60 and Hiprotal60-TS0709, indicating such flocculation is reversible. It is also found that the depletion flocculation is more significant in sol-emulsions of Hiptotal60 than those of Hiprotal60-TS0709, since the difference between η and η^* is larger for the former. That could be due to the larger particle size of the Hiptotal60 proteins. It has been proposed that polymers with larger particle size create more significant depletion flocculation (McClements, 2000). Accordingly, the absence of depletion flocculation in the sol-emulsions of Simplesse could be attributed to the small particle size of those proteins (as discussed in Chapter 5).

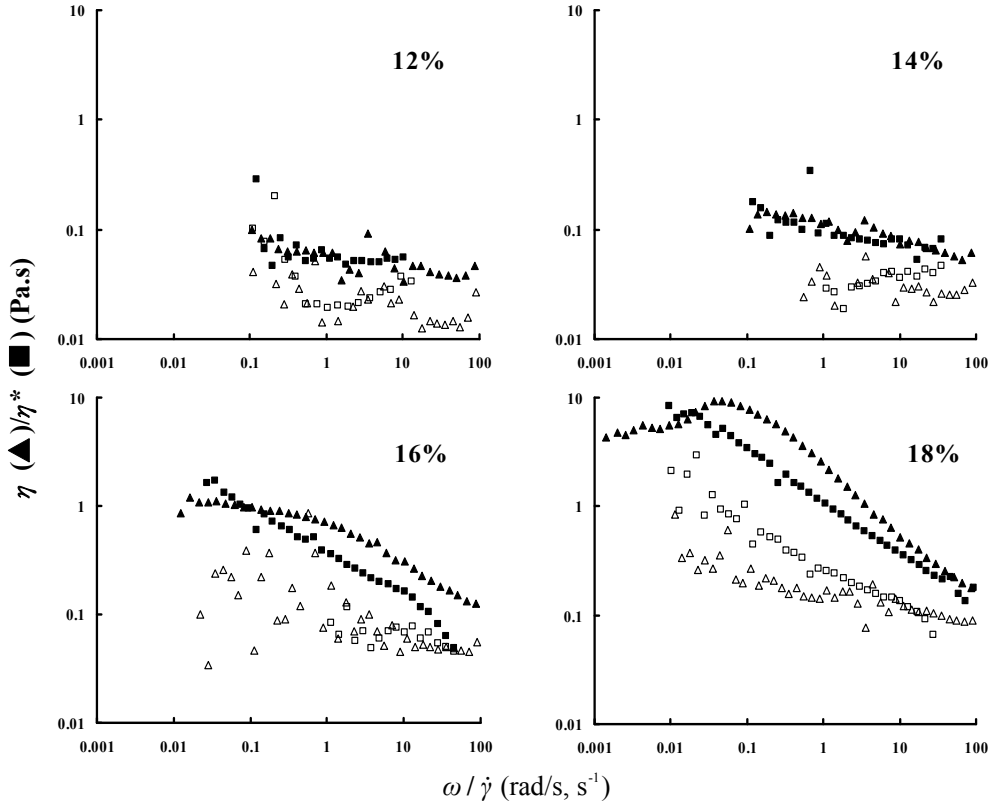

Figure 8.13 Cox-Merz plots of Hiprotal60 dissolved in solutions and emulsions (closed symbols represent presence of emulsion droplets).

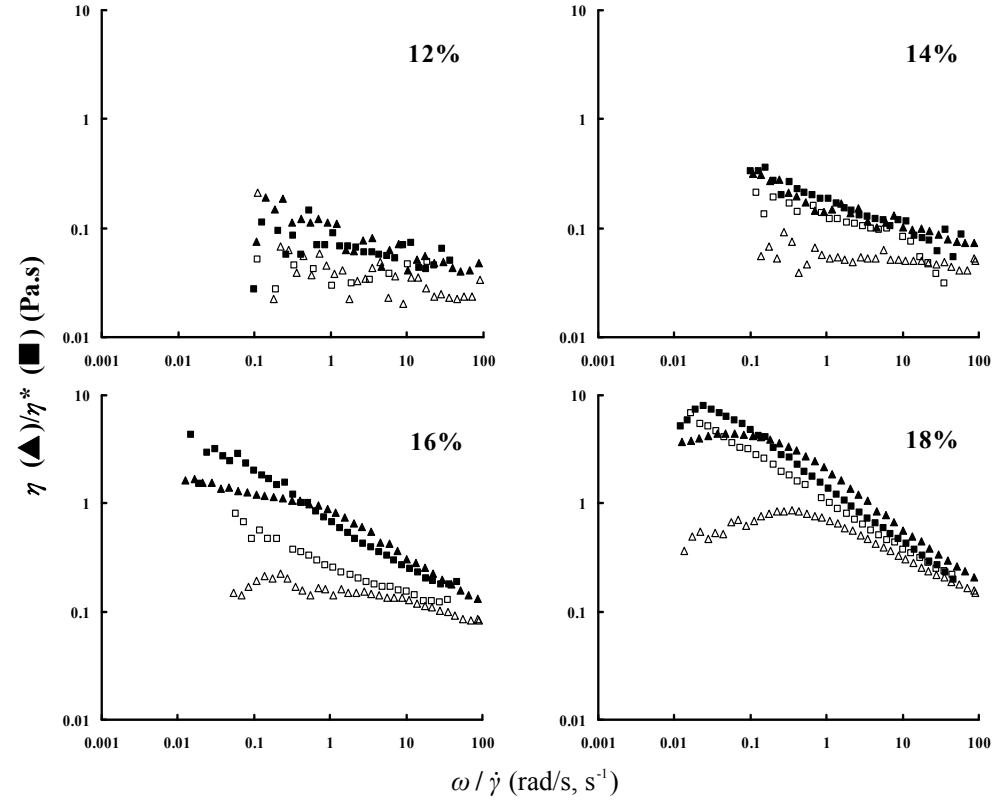

Figure 8.14 Cox-Merz plots of Hiprotal60-TS0709 dissolved in solutions and emulsions closed symbols represent presence of emulsion droplets).

As shown in Figure 8.15 and 8.16, the sol-emulsions of Hiprotal60-TS0710 and –TS0712 have significantly larger η and η^* than their aqueous solutions from low protein concentrations (12%), indicating the occurrence of depletion flocculation of the droplets. It is reasonable that the Hiprotal60-TS0710 and –TS0712 proteins induce depletion flocculation of the oil droplets at lower concentrations than those of Hiprotal60 and Hiprotal60-TS0709, since, as discussed in Chapter 5, the former have larger particle size (McClements, 2000). Moreover, the Cox-Merz rule is found to be valid for sol-emulsions with protein concentrations of 12% and 14% for both the highly aggregated partial denatured proteins. That should be due the large viscosities of the continuous phase, i.e., the protein solutions, which reduce the mobility of the droplets and thus retard the flocculation (McClements, 2000). As the concentrations of the proteins increase, the Cox-Merz law is invalid with $\eta<\eta^*$ for the sol-emulsions, indicating absence of shear-induced flocculation of droplets and presence of strain-induced break up of structure. As discussed in Chapter 7 and previous sections, such strain sensitive structure is found in cold-setting gels formed by proteins and some flocculated oil droplets (Ikeda & Nishinari, 2001; Macosko, 1994; McClements & Keogh, 1995; Rao, 2007). Flocculation of emulsion droplets could be verified by the larger η^* of the sol-emulsion with the protein concentration of 16% for the polymeric denatured proteins. As the protein concentration increases to 18%, however, there is little difference in η^* between the sol-emulsions and the aqueous solutions of the proteins, and flocculation of droplets should be impeded by the immobile gels. Thus, the larger values of η are more likely due to the hydrodynamic interactions between droplets and protein molecules.

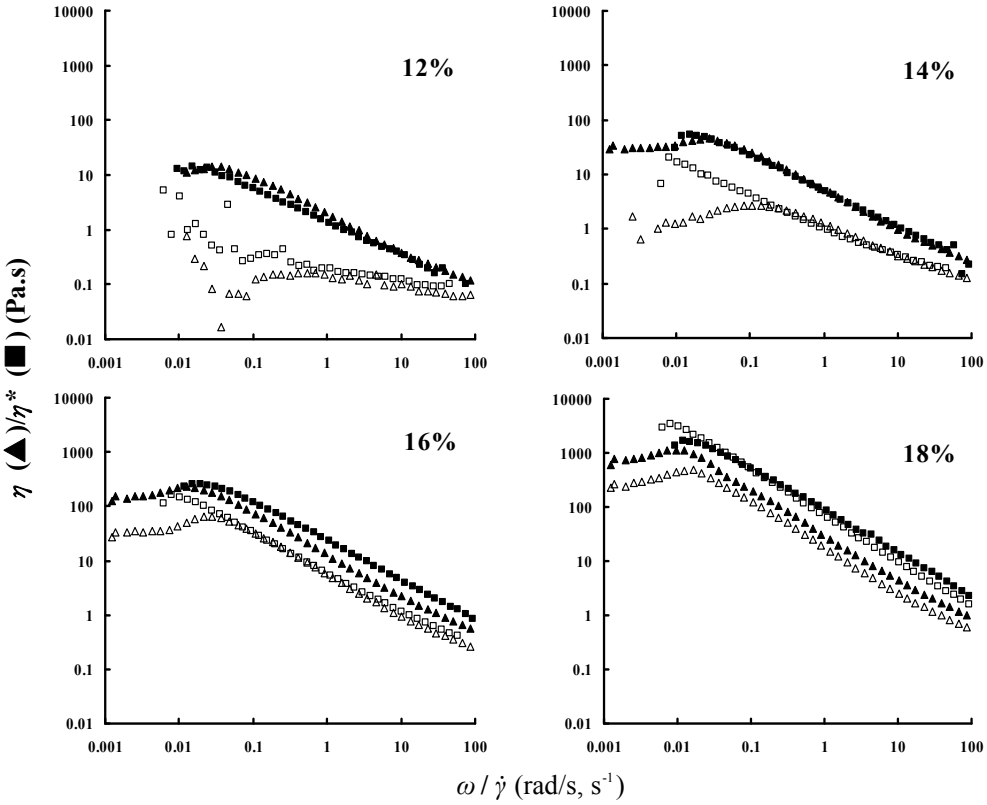

Figure 8.15 Cox-Merz plots of Hiprotal60-TS0710 dissolved in solutions and emulsions (closed symbols represent presence of emulsion droplets).

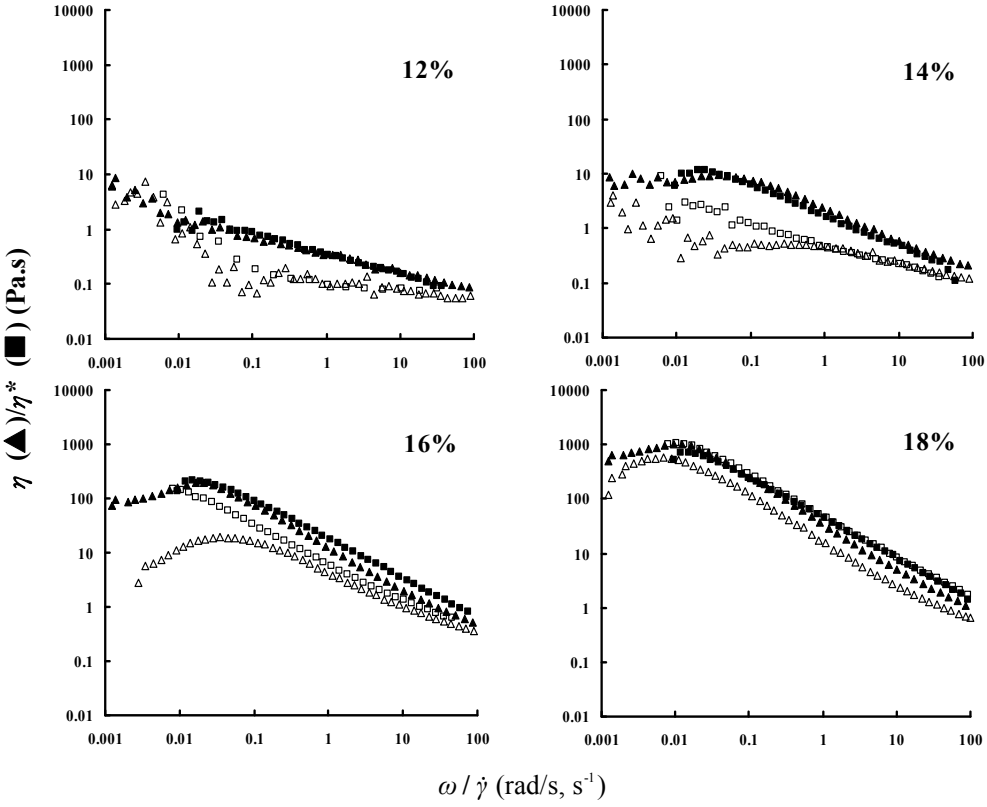

Figure 8.16 Cox-Merz plots of Hiprotal60-TS0712 dissolved in solutions and emulsions (closed symbols represent presence of emulsion droplets).

8.3.4 Effects of droplets on dynamic moduli of protein solutions

In order to obtain the detailed information on the interactions between proteins and droplets, analyses of dynamic moduli, *G'* and *G"*, of the sol-emulsions as functions of oscillation frequencies are performed. Results of sol-emulsions of Simplesse are shown in Figure 8.17. It is found that *G"* tends to be larger for sol-emulsions than that for aqueous solutions, suggesting increased hydrodynamic interactions caused by protein molecules and oil droplets. However, there is no increase in *G'* for sol-emulsions, indicating absence of flocculation of droplets in the emulsions at rest or low shear rates. Conversely, values of *G'* at low angular frequencies for sol-emulsions tend to be smaller than those for aqueous solutions, indicating that the interactions between those microparticulated proteins are disrupted by emulsion droplets.

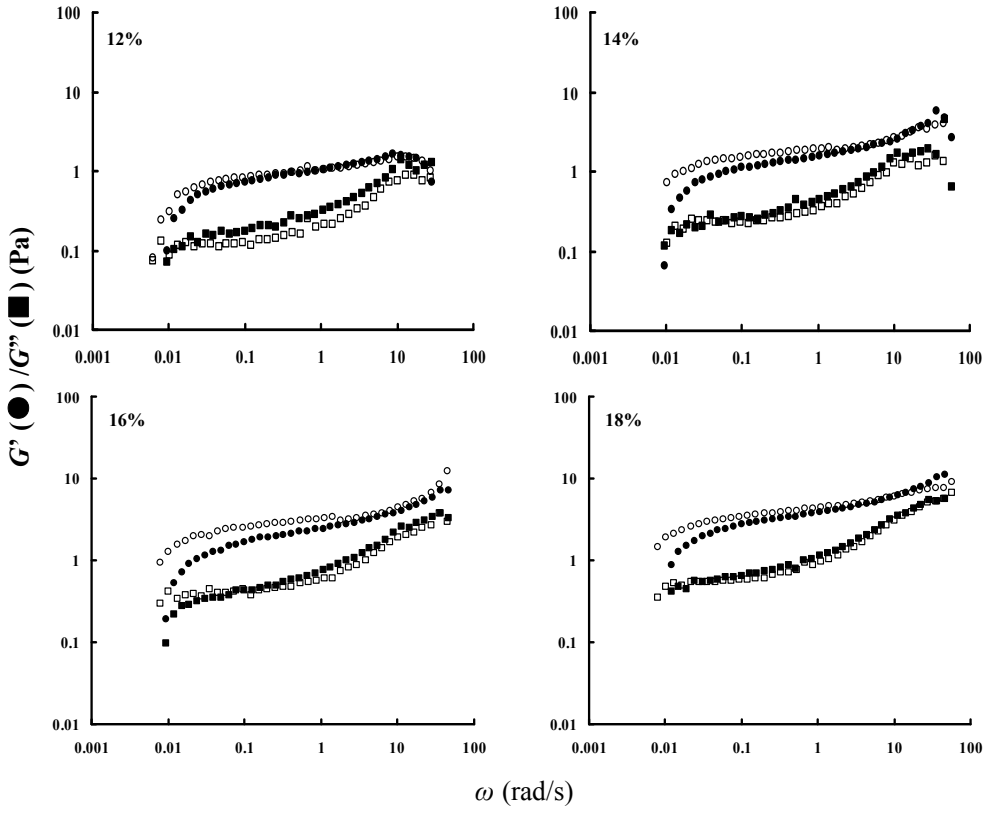

Figure 8.17 Dynamic moduli, *G*' and *G*" of sol-emulsions and aqueous solutions of Simplesse (closed symbols represent presence of emulsion droplets).

Dynamic properties of the low aggregated partial denatured proteins, i.e., Hiprotal60 and Hiprotal60-TS0709, dissolved in emulsions are shown in Figure 8.18 and 8.19. It is found that both *G'* and *G"* are increased by the presence of emulsion droplets. As discussed in Section 8.3.3, such increases are due to depletion flocculation of emulsion droplets. It is also found that the increase in G' and G" for sol-emulsions of Hiprotal60-TS0709 is smaller than that for Hiprotal60, which should be due to smaller particle size of the proteins in the former.

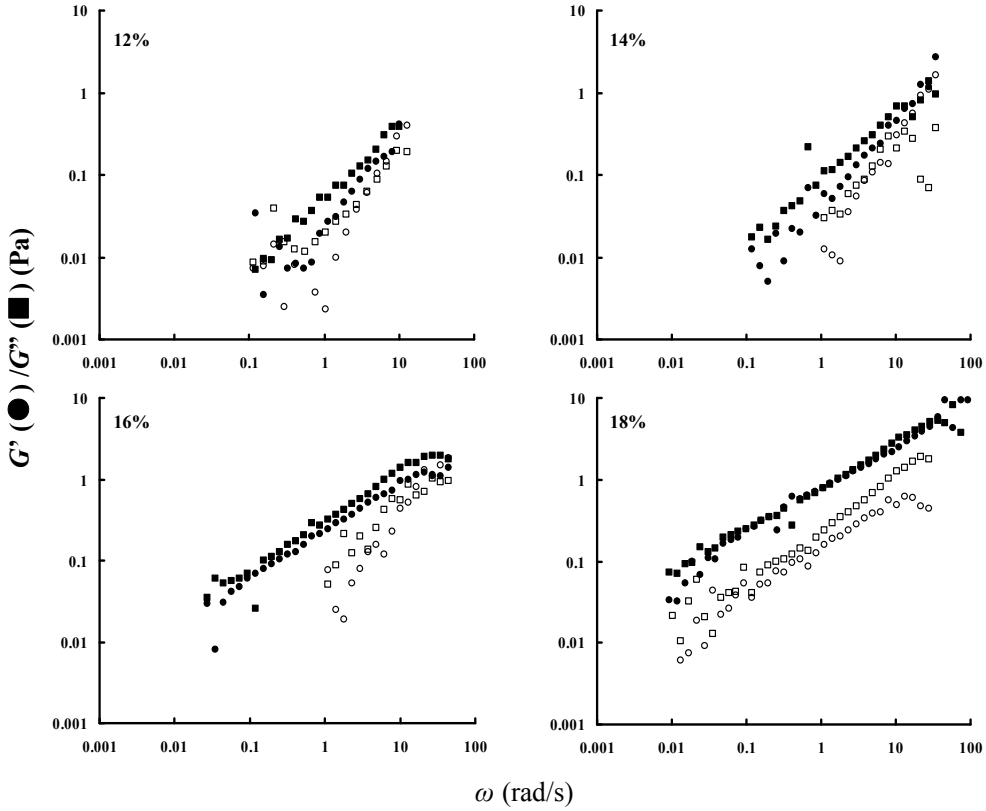

Figure 8.18 Dynamic moduli, *G*' and *G*" of sol-emulsions and aqueous solutions of Hiprotal60 (closed symbols represent presence of emulsion droplets).

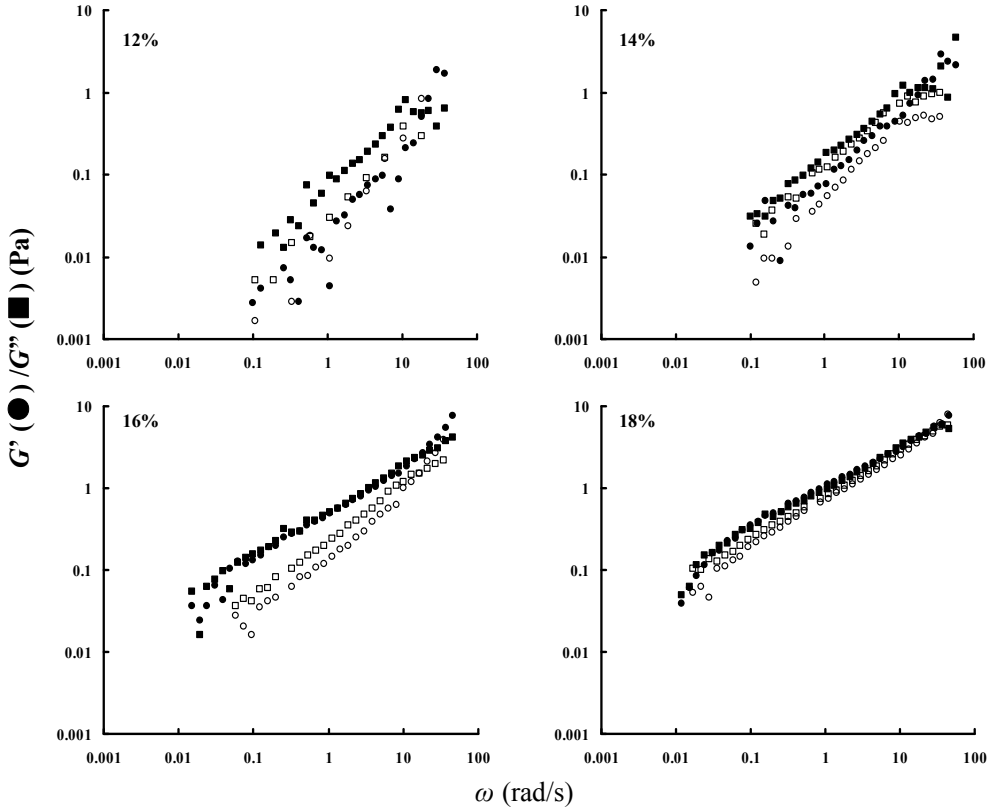

Figure 8.19 Dynamic moduli, *G*' and *G*" of sol-emulsions and aqueous solutions of Hiprotal60-TS0709 (closed symbols represent presence of emulsion droplets).

Values of *G'* and *G"* for sol-emulsions containing Hiprotal60-TS0710 and –TS0712 proteins are shown in Figure 8.20 and 8.21. It is found that the dynamic moduli increase for the sol-emulsions of both the highly aggregated denatured proteins. However, the increases in *G'* and *G"* for sol-emulsions are slower than those of aqueous solutions, and there is a small difference between the two systems (i.e., sol-emulsions and solutions) at the protein concentration of 18%. Such findings indicate that the emulsion droplets alone increase the viscoelastic properties though flocculation, but are not filling the protein gels actively, i.e., they do not interact with the proteins. This conclusion is different from Dickinson and Chen (1999), who reported that protein-coated droplets were active fillers for heat-set gels of whey proteins. One of the reasons for the discrepancy could be the heat treatment in their experiment. Therefore, unfolding of the protein layers should be considered as a crucial factor for the droplets to connect the protein molecules and play a role as active fillers for gels.

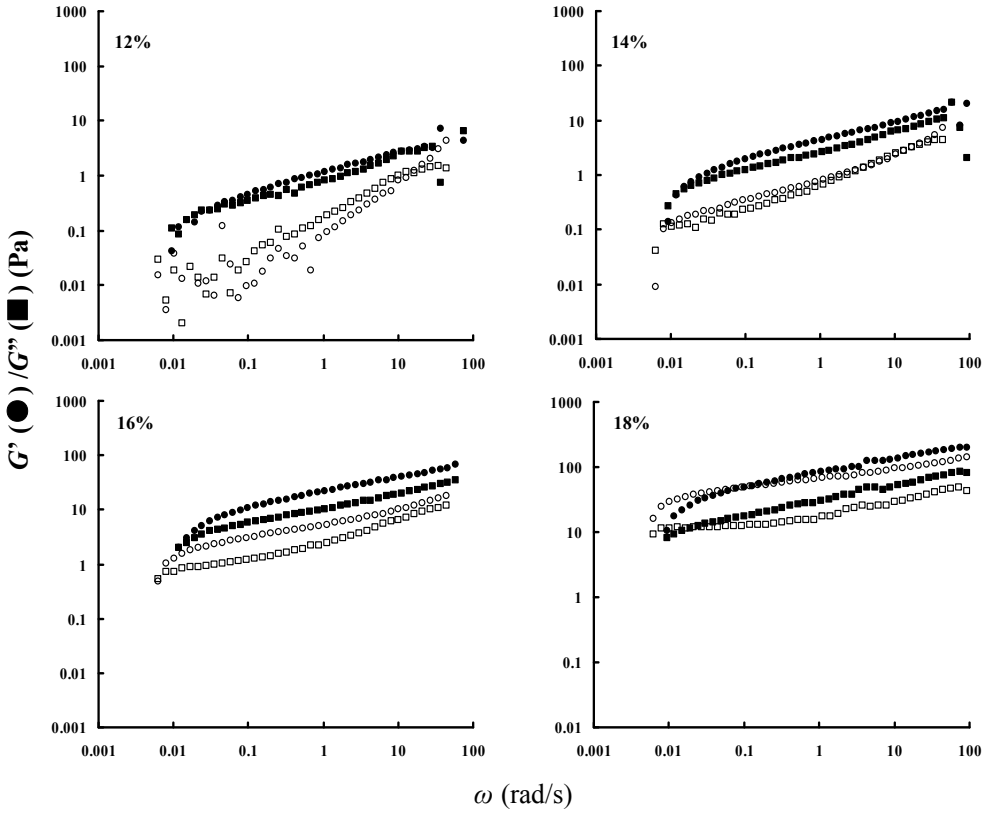

Figure 8.20 Dynamic moduli, *G*' and *G*" of sol-emulsions and aqueous solutions of Hiprotal60-TS0710 (closed symbols represent presence of emulsion droplets).

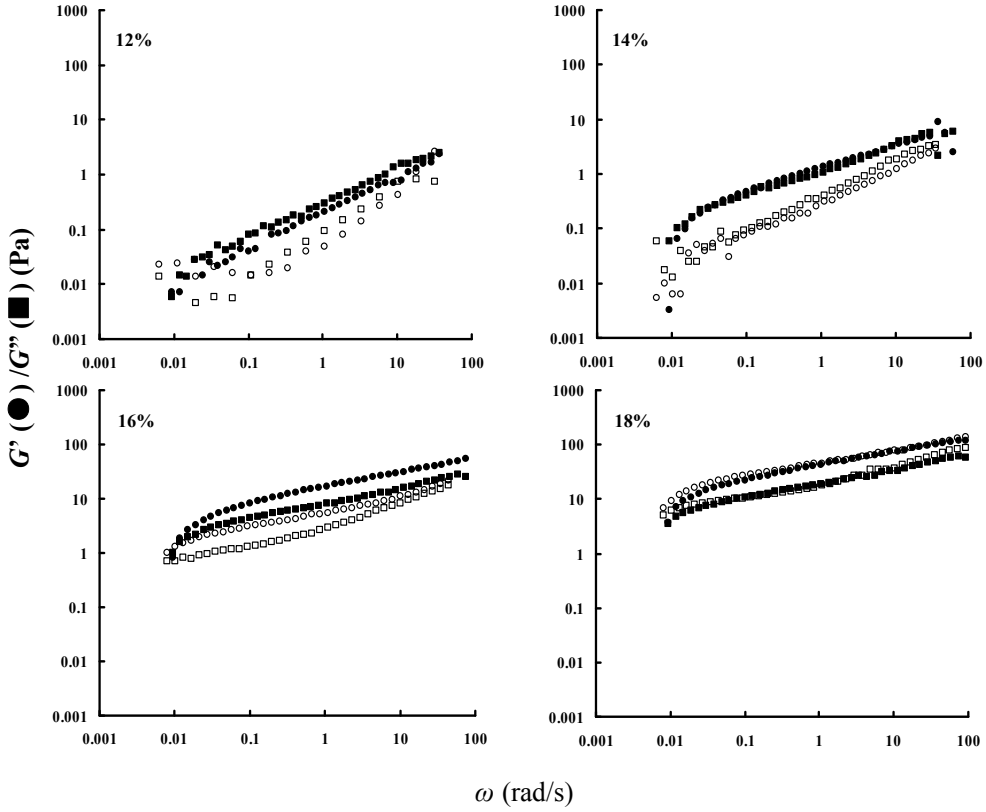

Figure 8.21 Dynamic moduli, *G*' and *G*" of sol-emulsions and aqueous solutions of Hiprotal60-TS0712 (closed symbols represent presence of emulsion droplets).

8.4 Conclusion

Rheological properties of protein based fat replacers dissolved in emulsions were determined in this chapter. Both the viscous and elastic properties were found to increase in the presence of emulsion droplets. For the microparticulated proteins, i.e., Simplesse, the emulsion droplets were found to disrupt the protein interactions as indicated by lower elasticity, while the hydrodynamic interaction between proteins and droplets increased the viscosity of the solution-emulsion systems. The low aggregated partial denatured proteins, i.e., Hiprotal60 and Hiprotal60-TS0709, unlike the Simplesse proteins, were found to induce flocculation of the droplets in emulsions. Such discrepancy is believed to be attributed to the larger particle size of the partial denatured proteins. The depletion flocculation induced by these larger proteins was found to be increased by shear. In the presence of highly aggregated denatured proteins, i.e., Hiprotal60-TS0710 and –TS0712, depletion flocculation of emulsion droplets was

also observed, but not the shear-induced flocculation, which could be attributed to the large viscosity of the continuous phase. Although those polymeric denatured proteins were found to form cold-set gels, there is no active filling effect of protein-coated droplets on the gelling behaviour, indicating that thermal denaturation of the protein layers of the droplets played an important role on their active filling effects.

8.5 Reference

Abdala, A.A., Olesen, K., & Khan, S.A. (2003). Solution rheology of hydrophobically modified associative polymers: Solvent quality and hydrophobic interactions. *Journal of Rheology, 47*(2), 497-511.

Barnes, H.A. (1994). Rheology of emulsions - a review. *Colloids and Surfaces A: Physicochemical and Engineering Aspects, 91*, 89-95.

Cox, W.P., & Merz, E.H. (1958). Correlation of dynamic and steady flow viscosities. *Journal of Polymer Science, 28*(118), 619-622.

Damodaran, S. (1996). Amino acids, peptides, and proteins. In O. R. Fennema (Ed.), *Food Chemistry* (3rd ed., pp. 321-429). New York, USA.: Marcel Dekker.

Dickinson, E. (1998). Proteins at interfaces and in emulsions: Stability, rheology and interactions. *Journal of the Chemical Society, Faraday Transactions, 94*(12), 1657-1669.

Dickinson, E. (2001). Milk protein interfacial layers and the relationship to emulsion stability and rheology. *Colloids and Surfaces B: Biointerfaces, 20*(197-210).

Dickinson, E. (2012). Emulsion gels: The structuring of soft solids with protein-stabilized oil droplets. *Food Hydrocolloids, 2012*, 224-241.

Dickinson, E., & Chen, J. (1999). Heat-set whey protein emulsion gels: Role of active and inactive filler particles. *Journal of Dispersion Science and Technology, 20*(1&2), 197-213.

Dickinson, E., & Golding, M. (1997). Depletion flocculation of emulsions containing unadsorbed sodium caseinate. *Food Hydrocolloids, 11*(1), 13-18.

Dickinson, E., & Yamamoto, Y. (1996). Rheology of milk protein gels and protein-stabilized emulsion gels cross-linked with transglutaminase. *Journal of Agricultural and Food Chemistry, 44*, 1371-1377.

English, R.J., Gulati, H.S., Jenkins, R.D., & Khan, S.A. (1997). Solution rheology of a hydrophobically modified alkali-soluble associative polymer. *Journal of Rheology, 41*(2), 427-444.

English, R.J., Raghavan, S.R., Jenkins, R.D., & Khan, S.A. (1999). Associative polymers bearing n-alkyl hydrophobes: Rheological evidence for microgel-like behavior. *Journal of Rheology, 43*(5), 1175-1194.

Goodwin, J.W., & Hughes, R.W. (2008). *Rheology for Chemists-An Introduction* (2 ed.). Cambridge, UK: The Royal Society of Chemistry.

Ikeda, S., & Nishinari, K. (2001). On solid-like rheological bahaviors of globular protein solutions. *Food Hydrocolloids, 15*, 401-406.

Lindsay, H.M., & Chaikin, P.M. (1982). Elastic properties of colloidal crystals and glasses. *Journal of Chemical Physics, 76*(7), 3774-3781.

Lizarraga, M.S., De Piante Vicin, D., González, R., Rubiolo, A., & Santiago, L.G. (2006). Rheological behaviour of whey protein concentrate and λ-carrageenan aqueous mixtures. *Food Hydrocolloids, 20*(5), 740-748.

Lorenzo, G., Zaritzky, N., & Califano, A. (2013). Rheological analysis of emulsion-filled gels based on high acyl gellan gum. *Food Hydrocolloids, 30*, 672-680.

Macosko, C.W. (1994). *Rheology: Principles, Measurements, and Applications*. New York, USA: Wiley-VCH, Inc.

Mason, T.G. (1999). New fundamental concepts in emulsion rheology. *Current Opinion in Colloid & Interface Science, 4*, 231-238.

McClements, D.J. (2000). Comments on viscosity enhancement and depletion flocculation by polysaccharides. *Food Hydrocolloids, 14*, 173-177.

McClements, D.J. (2004). Protein-stabilized emulsions. *Current Opinion in Colloid & Interface Science, 9*, 305-313.

McClements, D.J., & Keogh, M.K. (1995). Physical properties of cold-setting gels formed from heat-denatured whey protein isolate. *Journal of the Science of Food and Agriculture, 69*(1), 7-14.

Morrison, F.A. (2001). *Understanding Rheology*. New York, USA: Oxford University Press, Inc.

Rao, M.A. (2007). *Rheology of Fluid and Semisolid Foods Principles and Applications*. New York, USA: Springer Science+Business Media.

Tadros, Th.F. (1994). Fundamental principles of emulsion rheology and their applications. *Colloids and Surfaces Physicochemical and Engineering Aspects, 91*, 39-55.

Tanaka, F., & Edwards, S.F. (1992a). Viscoelastic properties of physically cross-linked networks.Transient network theory. *Macromolecules, 25*, 1516-1523.

Tanaka, F., & Edwards, S.F. (1992b). Viscoelastic properties of physically crosslinked networks Part 1. Non-linear stationary viscoelasticity. *Journal of Non-Newtonian Fluid Mechanics, 43*, 247-271.

Tanaka, F., & Edwards, S.F. (1992c). Viscoelastic properties of physically crosslinked networks Part 2. Dynamic mechanical moduli. *Journal of Non-Newtonian Fluid Mechanics, 43*, 273-288.

Tanaka, F., & Edwards, S.F. (1992d). Viscoelastic properties of physically crosslinked networks Part 3. Time-dependent phenomena. *Journal of Non-Newtonian Fluid Mechanics, 43*, 289-309.

Vilgis, T.A., & Winter, H.H. (1988). Mechanical selfsimilarity of polymers during chemical gelation. *Colloid and Polymer Science, 266*(6), 494-500.

Walstra, P. (1996). Dispersed Systems: Basic Considerations. In O. R. Fennema (Ed.), *Food Chemistry* (3rd ed., pp. 96-156). New York, US.: Marcel Dekker, Inc.

Ye, A., & Taylor, S. (2009). Characterization of cold-set gels produced from heated emulsions stabilized by whey protein. *International Dairy Journal, 19*, 721-727.

9 Conclusion

The rheological properties, including viscosity and gelation properties, of whey protein concentrates (WPC), i.e., Lacprodan87, and whey-protein-based fat replacers, i.e., Simplesse and Hiprotal60 products, have been determined and discussed. From the rheology measurements, interactions between different modified protein molecules could be postulated. Moreover, improvements for functionalities of fat replacers based on modified whey proteins could be proposed.

The products from modified whey proteins have been found to exhibit different properties from the whey protein concentrates. The microparticulated proteins, i.e., Simplesse, were found to have particles with a median diameter, D[0.5], of 1.72 ± 0.04 μm, which is larger than the whey protein concentrates with D[0.5] = 0.48 ± 0.04 μm. Various particle size distributions have been obtained for Hiprotal60 products, where the values of D[0.5] were measured as raging from 5.484 ± 0.001 μm and 3.296 ± 0.001 μm for Hiprotal60 and Hiprotal60-TS0709, respectively, to around 17 μm for both of Hiprotal60-TS0710 and Hiprotal60-TS0712. According to the values of D[0.5], those partially denatured proteins were supposed to form polymeric particles with different aggregating degree in the products. Proteins with a low degree of aggregation were postulated in Hiprotal60 and Hiprotal60-TS0709, whilst highly aggregated particles were proposed in Hiprotal60-TS0710 and Hiprotal60-TS0712. Such assumptions have been verified with the observations from ESEM, where Hiprotal60 and Hiprotal60-TS0709 were found to form separate aggregates while the polymeric aggregates formed by Hiprotal60-TS0710 and Hiprotal60-TS0712 were observed to have more continuous structures. Moreover, there was no disulphide bond in the modified proteins, neither the micoroparticulated nor the partially denatured ones, as indicated by the results of normal and reduced SDS-PAGE. Therefore, it can be concluded that the aggregates were formed and stabilized by non-bonded interactions, mainly hydrophobic interactions, between those denatured protein molecules. The partial specific volumes of these protein-based fat replacers were also measured, from

which the modified protein products were observed to be smaller than WPC. Since the modifications, such as denaturation and aggregations, of protein structures were believed to have little effects on the specific volume of a protein, such small values of the protein volume were hypothesized to result from the impurities, such as lactose, of the protein-based fat replacers.

From the flowing properties of the protein-based fat replacers in aqueous solutions, the viscosities of the solutions were observed to exhibit exponential increases in with protein concentrations from 6% to 21% for all the samples, which revealed the hydrodynamic and protein-protein interactions in those solutions. Higher exponential dependence of viscosity on protein concentrations was observed for the modified whey proteins, suggesting stronger interactions between those protein molecules. According to the shear thinning and thixotropic behaviour, the viscosity and the structuring properties in aqueous solutions were found to be drastically increased and improved for the modified whey proteins, compared with the native ones. Protein-based fat replacers had different properties according to the variation in the structures of the protein aggregates. The microparticulated proteins, i.e., Simplesse, were found to require more protein molecules to aggregate for drastic increases in viscosity, while for the partially denatured proteins, i.e., Hiprotal60 products, the flow behavior changed with the extent of the protein denaturation and aggregations. The highly aggregated proteins, i.e., Hiprotal60-TS0710 and Hiprotal60-TS0712 were found to have the best structuring properties with the lowest concentration requirement for viscosity increase and the strongest network structures with the largest viscosities.

More information on the protein aggregates was obtained through oscillation tests. The solutions of Simplesse exhibited solid-like behaviour at high concentrations, suggesting strong intermolecular or interfloc interactions in these microparticulated proteins. The proteins with a low aggregation degree, i.e., Hiprotal60 and Hiprotal60-TS0709 behaved as viscoelatic liquids. The rheological behaviour of these modified proteins was found to obey the Cox-Merz rule, indicating the absence of network formations of these partially denatured proteins or their small aggregated flocs. The solid-like and viscoelastic liquid-like behaviour of the microparticulated and lowly aggregated partially denatured proteins were proposed to result from colloidal crystal

structures of the protein molecules and their flocs since both of them exhibited small values of storage moduli (*G'*). The lattice-like structures of these colloidal crystals were believed to be stabilized by electrostatic repulsions between the proteins. Polymeric denatured proteins, i.e., Hiprotal60-TS0710 and Hiprotal60-TS0712, were found to form strong gels with self-similar or fractal structures at high concentrations. Large values of fractal dimensions suggested a dense packing of the polymeric chains in the gels. Cold-setting gelation was observed for all the modified samples when the pH was close to the pI of the whey proteins. Fractal structures were proposed in the acid-induced gels formed by the microparticulated proteins but not those from the lowly aggregated denatured proteins. Besides, the structure units of the aggregates of microsparticulated and lowly aggregated denatured proteins were increased by lowering the pH to the pI as indicated by increased apparent viscosities, but such effects were not found for the polymeric denatured proteins.

The rheological properties, such as viscosity and elasticity of the modified whey proteins, were found to increase with the presence of emulsion droplets. The emulsion droplets were found to disrupt the interactions of microparticulated proteins, i.e., Simplesse, as indicated by lower elasticity. However, the viscosity of the solution-emulsion systems increased compared with the solution systems, which were proposed to result from the hydrodynamic interaction between the protein particles and oil droplets. Unlike those Simplesse, Hiprotal60 and Hiprotal60-TS0709 were found to induce flocculation of the droplets in the emulsions due to their larger particle sizes. Moreover, shearing was found to have positive effects on such depletion flocculation. Depletion flocculation of emulsion droplets was also observed in the presence of highly aggregated denatured proteins, i.e., Hiprotal60-TS0710 and Hiprotal60-TS0712. However, the shear-induced effect on flocculation was not found, which should be attributed to the large viscosity of the continuous phase. There was no active filling effect of protein-coated droplets on the gelling behaviour of those polymeric denatured proteins, indicating that thermal denaturation of the protein layers of the droplets played an important role in their active filling effects on protein gels.

Molecular dynamics (MD) computer simulations were also performed on β-lactoglobulin proteins in order to understand the thermal effects on the structures,

and thus the functionalities of whey proteins at molecular levels. It was found that the α-helices and β-barrels were lost as the β-lactoglobulin unfolded, giving an open and soft protein molecule. The four cysteine (Cys) residues (Cys^{66}, Cys^{106}, Cys^{119} and Cys^{121}) previously buried in the hydrophobic cavity were exposed to the molecular surface of the protein, which could contribute to the protein-protein interactions and protein functionalities, such as gelation, through –SH/S-S exchange interactions. The ability of the protein molecule to form hydrogen bonds with its hydrated water molecules was weakened by denaturation, which was supposed to decrease the repulsions due to hydration shells between protein molecules. Moreover, the hydrogen bonds between the hydrated water molecules were strengthened by protein unfolding. Such effects on hydrated water molecules were supposed to increase the water holding abilities of the proteins, especially for the gels formed by the denatured proteins.

It has been found that partially denatured proteins could provide similar or even better thickening effects to food systems compared with microparticulated proteins. The functionalities of the protein based fat replacers in food systems could be improved if the extent of denaturation and aggregation of proteins is properly controlled. Cold-setting gelation is observed for the partially denatured proteins, especially those highly aggregated ones. Such functionality would provide a potential of wider applications of the protein-based fat mimetics in food industry, especially for those food products not suitable for heat treatments.

Appendix I A consistent set of parameters

Alphabet

A(HB)	H-bond forming ability
$A(\mathbf{\Gamma})$	an instantaneous state of the system
$\langle A(\mathbf{\Gamma})\rangle_{ens}$	ensemble average
A_{obs}	observed macroscopic property
b	bond length
c	concentration (in mg/mL)
$c(t)$	autocorrelation
D	diffusion coefficient
d	Euclidian dimension
D[0.5]	median diameters
De	Deborah number
d_f	fractal dimension
E	system energy
ΔE	difference of the dissipated energy density during a hysteresis loop
F	external shear force
G	elastic modulus
$G(t)$	shear modulus
G^*	complex modulus

$\|G^*\|$	magnitude of complex modulus
G'	storage modulus
G''	loss modulus
G_{Gibbs}	Gibbs free energy
$\mathscr{H}$	Hamiltonian
$h(r)$	gap between the cone and plate
$h(t)$	autocorrelations of the existence functions
$\langle h(t) \rangle$	average value of the existence function
$\tilde{H}(t)$	conserved effective energy
$J(t)$	compliance
$\mathscr{K}$	kinetic energy
k_B	Boltzmann constant (=1.38062×10−23 J/K)
$\mathscr{L}$	Lagrangian
L	length scale of the measurements
M_D	torque on the cone
m_i	mass of the i-th atom
N	atom number
$N(\mathrm{H_2O})$	number of water molecules
$N(\mathrm{HB})$	number of hydrogen bonds
N_1	1st normal stress difference
N_2	2nd normal stress difference
p	hydrostatic pressure

P	system pressure
Pe	Péclet number
$P_i(X_i^{(1)}, X_i^{(2)})$	paired parameters
$\mathbf{p}^N$	generalized momenta conjugated to molecular coordinates
$\dot{\mathbf{q}}$	velocity
$\ddot{\mathbf{q}}_i$	acceleration of the *i*th atom or molecule
$\mathbf{q}^N$	molecular positions
r_{ij}	distance between the *i*-th and *j*-th atoms
t	observation time
T	absolute temperature (in K)
$\mathscr{T}$	kinetic temperature
u	velocity
$u(r)$	circumferential velocity
$\mathscr{V}$	potential energy
V	system volume
$\bar{v}$	apparent specific volume
$\bar{v}^o$	partial specific volume
w	total solid content (in %)
w_p	protein concentration (in %)
x_p	protein content of samples

Greek

β_T	isothermal compressibility coefficient
γ	strain
$\dot{\gamma}$	shear rate
$\mathbf{\Gamma}$	a single point in the $6N$-dimensional phase space
$\gamma^*(t)$	complex strain
δ	phase difference
η	viscosity
η^*	complex viscosity
η'	dynamic viscosity
η''	out-of-phase component of complex viscosity
η_s	viscosity of solvent
θ	bond angle
λ	rescaling factor
μ	chemical potential
Π	total stress tensor
ρ	solution density
ρ_0	solvent density
ρ_{sp}	specific density
σ	shear stress
$\sigma^*(t)$	complex stress
τ	relaxation time

φ	volume fraction
Φ	dihedral angle
Φ_0	volumetric fraction of the solvent
Ψ_1	1st normal stress coefficient
Ψ_2	2nd normal stress coefficient
$\Psi_i(X_i^{(1)}, X_i^{(2)})$	thermodynamic potential
ω	radial frequency
$\Omega(\mathbf{\Gamma})$	number of possible systems in an ensemble